2007:05

DOCTORAL THESIS

Exotic Phases of Matter in Compact Stars

Fredrik Sandin

Luleå University of Technology
Department of Applied Physics and Mechanical Engineering
Division of Physics

2007:05 | ISSN: 1402-1544 | ISRN: LTU-DT -- 07/05 -- SE

Doctoral Thesis in Physics

Exotic Phases of Matter in Compact Stars

Jan Fredrik Sandin
from Östavall

Division of Physics
Luleå University of Technology
SE-971 87 Luleå
Sweden

To my parents,
for giving me a curious character

ABSTRACT

This doctoral thesis in physics at Luleå University of Technology is devoted to the phenomenology of compact stars, and theoretical models of their interior. Particle physics has provided fundamental concepts and details needed to develop a description of matter and the evolution of the universe. It is, however, difficult to obtain information about the properties of matter at low temperature and high density from such experiments. In this context, astrophysical observations constitute an important source of information, thanks to the high resolution of present and near-future terrestrial and space-based observatories. The density of matter in neutron stars exceeds that in atomic nuclei, and little is known about the nature of their interior. It is clear that the interaction between the smallest observed building blocks of atomic nuclei, the quarks, becomes weaker with increasing density. Matter should therefore dissolve into a state of nearly free quarks at high densities, and models of classical superconductivity advocate that this state is a superconductor. The argument for this is simple: a low-temperature Fermi system with a weak attractive interaction is unstable with respect to formation of Cooper pairs. It is not known if this state of matter exists in neutron stars, but models suggest that it is possible. The major part of the work summarised in this thesis is the development of a model of superconducting quark matter, and its consequences for the phenomenology of neutron stars and their formation in the collapse of massive stars. It is a Nambu–Jona-Lasinio model with self-consistently calculated quark masses and pairing gaps, which properly accounts for the β-equilibrium and/or charge neutrality constraints in compact stars and heavy-ion collisions. Phase diagrams and equations of state of superconducting quark matter are presented, and the influence of different assumptions about the effective quark interaction is investigated. The effect of neutrino untrapping in hypothetical quark cores of newborn neutron stars is investigated, and phase diagrams for quark matter with trapped neutrinos are presented. While no evidence for the presence of quark matter in neutron stars exists, it is explicitly shown that observations do not contradict this possibility. On the contrary, the presence of a quark matter core in neutron stars can overcome problems with hadronic equations of state. In contrast to the expectation from more simple model calculations, the results presented here suggest that strange quarks do not play a significant role in the physics of compact stars. While there is some room for bare strange stars, such models suffer from low maximum masses, and the presence of a hadronic shell tends to render stars with strange matter cores unstable. Regardless of the nature of mat-

ter in neutron stars, general relativity and the standard model of particle physics limit their density to $\lesssim 10^{16}$ g/cm^3. In the light of established theory, any object with a density exceeding this limit should be a black hole. It is suggested in this thesis that if quarks and leptons are composite objects, as suggested, *e.g.*, by the three particle generations in the standard model, a yet unobserved class of compact objects with extremely high densities could exist. As the hypothetical pre-quark particles are called preons, these objects are named 'preon stars'. The properties of preon stars are estimated, and it is shown that their maximum mass depends on the quark compositeness energy scale. In general, the mass of these objects should not exceed that of the Earth, and their maximum size is of the order of metres. Several methods to observationally detect preon stars are discussed, notably, by gravitational lensing of gamma-ray bursts and by measuring high-frequency gravitational waves from binary systems. To have a realistic detection rate, *i.e.*, to be observable, they must constitute a significant fraction of cold dark matter. This condition could be met if they formed in a primordial phase transition, at a temperature of the order of the quark compositeness energy scale. Some unexplained features observed in spectra of gamma-ray bursts are discussed, as they are similar to the signature expected from a preon-star gravitational lensing event. An observation of objects with these characteristics would be a direct vindication of physics beyond the standard model.

Keywords: *Compact stars – Neutron stars – Quark stars – Hybrid stars – Protoneutron stars – Preon stars – Preons – Compositeness – Colour superconductivity.*

Appended Papers

Paper I

J. Hansson and F. Sandin, "Preon stars: a new class of cosmic compact objects", *Physics Letters* **B616**, 1 (2005); astro-ph/0410417.

Paper II

F. Sandin, "Compact stars in the standard model – and beyond", *The European Physical Journal* **C40** S2, 15 (2005); astro-ph/0410407. Also to appear in *"How and where to go beyond the standard model"*, proceedings of the International School of Subnuclear Physics, Erice, ed. A. Zichichi: World Scientific (2007).

Paper III

D. Blaschke, S. Fredriksson, H. Grigorian, A. M. Öztaş and F. Sandin, "The phase diagram of three-flavor quark matter under compact star constraints", *Physical Review* **D72**, 065020 (2005); hep-ph/0503194.

Paper IV

F. Sandin and A. M. Öztaş, "Condition for gapless color-antitriplet excitations in Nambu–Jona-Lasinio models", *Physical Review* **C73**, 035203 (2006); hep-ph/0512087.

Paper V

T. Klähn, D. Blaschke, F. Sandin, Ch. Fuchs, A. Faessler, H. Grigorian, G. Röpke and J. Trümper, "Modern compact star observations and the quark matter equation of state", submitted to *Physics Letters* **B**; nucl-th/0609067.

Paper VI

F. Sandin and J. Hansson, "The observational legacy of preon stars – probing new physics beyond the LHC", to be submitted; astro-ph/0701768.

Paper VII

F. Sandin and D. Blaschke, "The quark core of protoneutron stars in the phase diagram of quark matter", submitted to *Physical Review* **D**; astro-ph/0701772.

Other Publications

Articles in popular magazines

J. Hansson and F. Sandin, "Preonstjärnor - en ny sorts himlakropp?", *Populär Astronomi* **4**, 8 (2005).

J. Hansson and F. Sandin, "Stor som en kula men tyngre än jorden", *Forskning och Framsteg* **7**, 40 (2005).

Numerical software

F. Sandin, "On-line 3-flavour colour superconductivity calculator", http://3fcs.dyndns.org.

F. Sandin, "On-line gravitational femtolensing calculator", http://femtolensing.dyndns.org.

Preface

This thesis is devoted to the physics of compact stars and some exotic phases of matter that could exist in these fascinating objects. By tradition, it consists of an introduction and appended research papers. The former provides some essential background needed to grasp the content of the papers. As the physics of compact stars is a multi-diciplinary field, a proper introduction is beyond the scope of this thesis. I therefore focus on essential topics, in particular technical aspects applied in the theoretical derivations and numerical calculations. References are given to textbooks and research papers that cover some complementary topics.

I am pleased by the combination of main-stream research and investigations on topics of more hypothetical nature that underlays this thesis. The former constitutes a basis for the scientific content of the work, and has been performed in a highly active field of physics in collaboration with leading experts in an international context. This work has resulted in useful experiences, four completed papers and about an equal amount of present projects. The numerical software developed in this work is partially available on-line for cross-checking, and for others to use. The work on preon stars is of more hypothetical nature and have resulted in valuable experiences. It is clear that theoretical physics needs both "good" and "bad" new ideas, as it is notoriously difficult to correctly judge the value of a new idea at an early stage in its development. Nevertheless, it takes courage and a sensible type of confidence to develop them, and that need some trial and error. The preon star hypothesis has been awarded with a prize on suggestion by Gerard 't Hooft and Antonino Zichichi, and it has resulted in three scientific papers. Preon stars have been recognised also in several popular magazines, and the first publication was on Science Direct's top-25 list of most read (downloaded) articles. It is a great joy to see that the work has stimulated others to consider the idea.

The research presented in this thesis has been performed in collaboration, mainly with David Blaschke, Sverker Fredriksson, Hovik Grigorian, Johan Hansson, Thomas Klähn, and Ahmet Öztaş, and to some extent also with Amand Faessler, Christian Fuchs, Gerd Röpke, and Joachim Trümper. I thank David Blaschke for his hospitality during my visits to Rostock and Dubna, for his guidance and support in the daily work, and for introducing me in a group of great people and a fruitful collaboration. I would also like to express my gratitude to Mark Alford, Jens

Berdermann, Michael Buballa, Mike Cruise, Ed Fenimore, Huben Ganev, Achim Geiser, Jeremy Goodman, Pawel Haensel, Abuki Hiroaki, Gerard 't Hooft, Henning Knutsen, Kostas Kokkotas, John Ralston, Sanjay Reddy, Avetis Sadoyan, Igor Shovkovy, Andrew Steiner, and Stefan Typel for useful discussions, and for their helpful and inspiring attitude. The numerical results presented in the appended papers were calculated on a local FreeBSD computer cluster that belongs to Hans Weber, I am most grateful to him for giving me unlimited access to his computers, and for useful discussions on classical superconductivity and statistical physics. It is a pleasure to acknowledge the influence of my supervisor, Sverker Fredriksson, who is a great mentor. He has supported me since I was an undergraduate student attending his lectures in particle physics, on a journey from a curious student to a nearly independent researcher and teacher, in a professional and mature manner. Thanks to him, I got useful experiences from research projects and teaching, as a lecturer in mechanics, already as an undergraduate student. He helped me to find a diploma work at CERN and to get a Ph.D. position. I thank my co-supervisor, Johan Hansson, for his support and for his ingenious ideas, which have inspired me to learn new aspects of physics. The work on preon stars would not have been realised without him. I am grateful to my office-mate, Erik Elfgren, for our daily discussions on interesting topics. I thank him and Tiia Grenman for their help with practical issues. I acknowledge support from the Swedish Graduate School of Space Technology and the Royal Swedish Academy of Sciences.

Finally, I am grateful to my family for their support, in particular to Maria for taking care of our little son while I have been busy completing this work.

Luleå in February 2007,

Fredrik Sandin

Acronyms

2SC	2-flavour Colour Superconducting (phase)
BNL	Brookhaven National Laboratory
CERN	European Organisation for Nuclear Research (in French)
CFL	Colour-Flavour Locked (phase)
E(s)oS	Equation(s) of State
GRB	Gamma-Ray Burst
HS	Hubbard-Stratonovich (transformation)
LHC	Large Hadron Collider
MF	Mean-Field (approximation)
NJL	Nambu–Jona-Lasinio (model)
NS	Neutron Star
PNS	Protoneutron Star
QCD	Quantum Chromodynamics
QGP	Quark-Gluon Plasma
RHIC	Relativistic Heavy-Ion Collider
SM	Standard Model (of particle physics)
SQM	Strange Quark Matter

Units and Symbols

SI units are used in the Introduction. Unless explicitly stated otherwise, I use natural units, $\hbar = c = k_B = 1$ or Gravitational (geometrized) units, $G = c = 1$, in subsequent chapters, depending on the application. See Appendix A for further information. The Dirac gamma matrices, γ^μ, and the Gell-Mann generators, λ_i, are defined in Appendix B. The Minkowski metric is $\eta^{\mu\nu} = \mathrm{diag}(1, -1, -1, -1)$. Three-vectors are denoted in boldface, *e.g.*, $\mathbf{p}$ has components p_x, p_y and p_z.

Table of Contents

Chapter 1

Introduction

Our universe, as we know it today, was created in the "big bang" about 13.7 billion years ago. In the beginning, space was filled with a hot and dense energy bath, a fluid of radiation that presumably emerged from some type of "quantum fluctuation". The universe has ever since expanded and cooled down. We do not know much about the first 10^{-34} s after the big bang, more than that the universe seems to have undergone a period of extremely rapid expansion, so-called inflation. Inflation is mainly needed to explain the high level of isotropy in the so-called cosmic microwave background, which is the electromagnetic radiation that originates from the time when the universe became transparent to photons.

The first matter particles, the quarks, started to emerge in the radiation fluid already after 10^{-32} s. Quarks are, as far as we know today, the fundamental constituents of a broad range of composite particles, so-called hadrons. The most well-known examples of hadrons are the neutrons and protons, which constitute atomic nuclei. It is believed that one extra quark per $\sim 10^9$ quark-antiquark pairs was created due to an asymmetry. That is why we mainly observe matter in the universe, rather than radiation (created when matter and antimatter annihilate) or antimatter. The creation of particles from "energy" can be qualitatively understood in terms of Einstein's famous equation $E = mc^2$, or as he originally wrote it, $m = E/c^2$. This equation suggests that energy, E, and mass, m, are somehow related, or perhaps are the same thing. The origin of mass is still a great mystery at the conceptual level. The rules of nature for creating massive particles out of energy is, on the other hand, amazingly well understood within the range of energies that has been studied in particle physics experiments.

Hadrons started to form after about one microsecond, when the universe had become sufficiently cold and diluted. About 0.1 milliseconds after the big bang, leptons started to emerge in the matter-radiation fluid. The most well-known example of leptons is the electron, which constitutes the negative charge in atoms. After about one minute, helium nuclei, and a small fraction of deuterium and lithium nuclei, started to form by fusion reactions. A few minutes later, the primordial matter con-

tent of the universe had been created. It consisted of roughly 75% hydrogen nuclei, 25% helium nuclei, and small amounts of deuterium and lithium nuclei. Neutral atoms did not form until several hundred thousand years later, when the universe had cooled down to a temperature of about 3000 K. When that happened, the universe became effectively transparent to photons, and light could then propagate freely in the universe. The light from that time is the cosmic microwave background radiation that we observe in the sky today. Due to the expansion of the universe, *i.e.*, of the space-time fabric, the light waves have been "stretched" (redshifted) on their journey and arrive here at Earth as microwaves, even though they started out in the early universe as visible, mainly orange, light.

As the universe expanded, small density fluctuations in the primordial radiation fluid were enhanced by gravity and eventually gave rise to large clouds of hydrogen and helium, which continued to contract due to gravity and friction. The first stars and galaxies were created in such gas clouds. Even today we observe large clouds of interstellar gas, consisting mostly of molecular hydrogen and helium, and small amounts of dust and heavier elements, which have been created by thermonuclear fusion reactions in stars. The gas clouds range in size from a fraction of a light-year to several hundred light-years, and in mass from about 10 to 10^7 solar masses. Stars more massive than a few solar masses often form in small groups in the densest regions of the clouds. About 60-70% of all stars have a companion star, *i.e.*, half of all stars on the sky are actually "binaries".

1.1 Compact objects

Stars have different sizes, the smallest not even deserving the name, since the pressure and temperature inside them are insufficient to start fusion. Other stars are huge and deplete their energy rapidly. As the thermonuclear fusion reactions diminish in the core of a star, the thermal pressure decreases. Eventually, a critical point is reached: When the force of gravity is no longer balanced by the thermal pressure, the star starts to collapse. What happens after that depends on the mass. If the star is a few times more massive than the Sun, the collapse is eventually halted due to the "degeneracy pressure" of electrons, and a so-called white dwarf forms. If the star is more massive, around ten solar masses, the collapse continues until the atomic nuclei start to "overlap" and the core stabilises as a dense neutron star. The gravitational energy released as the core collapses to a neutron star causes a giant explosion - a supernova - that expels the outer layers of the star, see Figure 1.1. For extremely massive progenitor stars, the collapse is assumed to lead to the formation of black holes.

The endpoint of the thermonuclear processes in the core of ordinary stars depends on their mass. For the progenitors of neutron stars, the mass is sufficiently high for the nuclear burning to continue until a core of iron has formed. Iron has the most

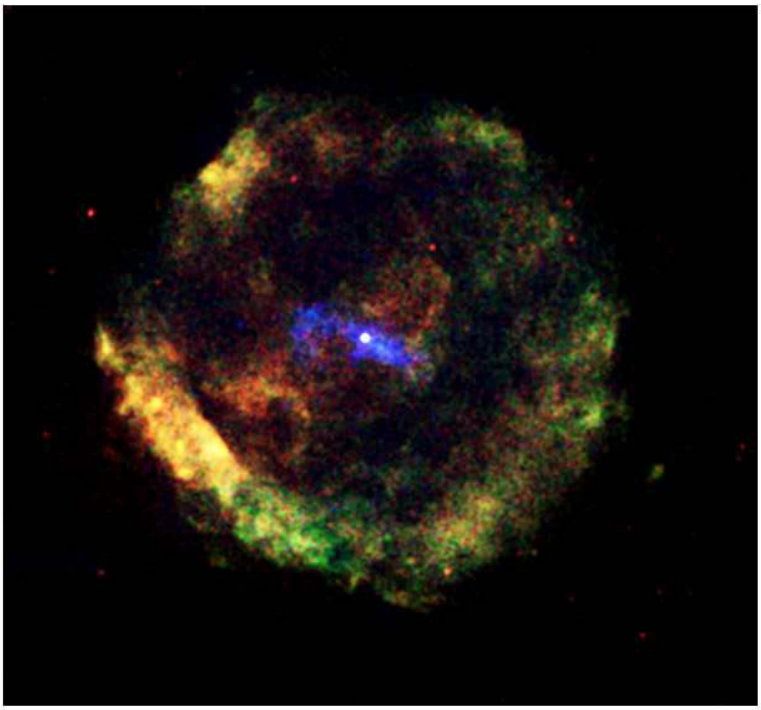

Figure 1.1: G11.2-0.3, the remnant of a massive star that exploded in a supernova about 1600 years ago. This image is a combination of X-ray and radio observations by the space-based Chandra X-ray observatory and the terrestrial Very Large Array observatory. The radio observations are used to measure the remnant's expansion rate, which can be used to calculate how long ago the star exploded. A neutron star and a cigar-shaped cloud of energetic particles, known as a pulsar-wind nebula, are visible in high-energy X-rays (blue). A shell of heated gas from the outer layers of the exploded star surrounds the pulsar and emits lower-energy X-rays (represented in green and red). Credit: NASA/CXC/Eureka Scientific/M. Roberts *et al.*

stable nucleus, and heavier elements are formed only in supernovæ. Consequently, neutron stars have practically identical chemical composition, as they are created in the collapsing iron cores of their progenitor stars. White dwarfs, on the other hand, have varying chemical composition, because their progenitor stars collapse before an iron core has formed. As the chemical composition of neutron stars is unique, so is their equilibrium sequence (see Chapter 2). This is essential in studies of their phenomenology.

White dwarfs, neutron stars and black holes are extremely dense objects, so-called compact objects, which are left behind in the debris when normal stars "die".

That is, when most of the nuclear fuel has been consumed and they collapse under the pull of gravity. With the exception of small black holes, which evaporate quickly due to so-called "Hawking radiation", and accreting neutron stars and white dwarfs, all three types of compact objects are essentially static over the lifetime of the universe and therefore represent the final stage of stellar evolution. Some properties of these objects are presented in Table 1-1. For comparison, the radius of the Sun, which by itself accounts for more than 99% of the solar system's mass, has a radius of about 7×10^5 km. Observe the significant difference between ordinary luminous stars, such as our Sun, and the extremely compact neutron stars, which have masses that typically exceed that of the Sun packed into a region of space about ten kilometres in radius.

Table 1-1: Distinguishing traits of the three different types of compact stellar objects traditionally considered in astrophysics. Here, $\mathrm{M}_\odot \simeq 2 \times 10^{30}$ kg is the mass of the Sun.

Object	Mass	Radius	Mean density
White dwarf	$\lesssim 1.4\ \mathrm{M}_\odot$	$\sim 10^4$ km	$\lesssim 10^8$ g/cm^3
Neutron star	$\sim 1 - 2\ \mathrm{M}_\odot$	~ 10 km	$\lesssim 10^{15}$ g/cm^3
Black hole	Arbitrary	$2GM/c^2$	$\sim M/R^3$

1.2 Neutron stars

Neutron stars are created in the aftermath of some core collapse supernovæ, as was first suggested by Baade and Zwicky already in 1934 [1]. Following the collapse, the core of the star is compressed to a hot protoneutron star (PNS), which cools rapidly due to neutrino emission, leaving a hot neutron star. The neutrinos are created in the collapse by inverse β-decay, *i.e.*, by weak interactions between energetic electrons and protons, which yield neutrons and electron neutrinos. During the collapse, roughly 99% of the gravitational energy is emitted in the form of neutrinos. Only 0.01% of the energy is carried away by photons, still, supernovæ are sufficiently bright to outshine their host galaxies. The remaining gravitational energy ($\sim 1\%$) is converted into the kinetic energy of the expelled crust. Although these numbers are fairly well known, as they can be obtained from observations and basic theoretical estimates, the inner engine of core collapse supernovæ is poorly understood. See Paper VII for further information.

Neutron stars are extremely dense objects. In their interior, one cubic centimetre of matter has a mass of $\sim 10^{12}$ kg. This corresponds to the density of a few thousand oil supertankers compressed into the size of a sugar cube. Due to the high density

and, relatively speaking, low temperature in neutron stars, they are presumably unique astrophysical "laboratories" that can be used to explore the high-density properties of matter. This activity complements, and is intimately connected to particle physics experiments, which yield detailed information about particles and their interactions. In principle, there is hope that the properties of high-density matter in neutron stars can be deduced from the standard model of particle physics. However, it is presently not possible to solve the complex mathematical problem, and the only means to obtain information about their interior is therefore to use approximate effective models in combination with observations. The composition of neutron stars is unknown, and there are many "exotic" possibilities for the nature of their interior, *e.g.*, it could consist of hyperons, superconducting quark-gluon plasma, or crystalline phases of quarks, see Figure 1.2. Consequently, the name

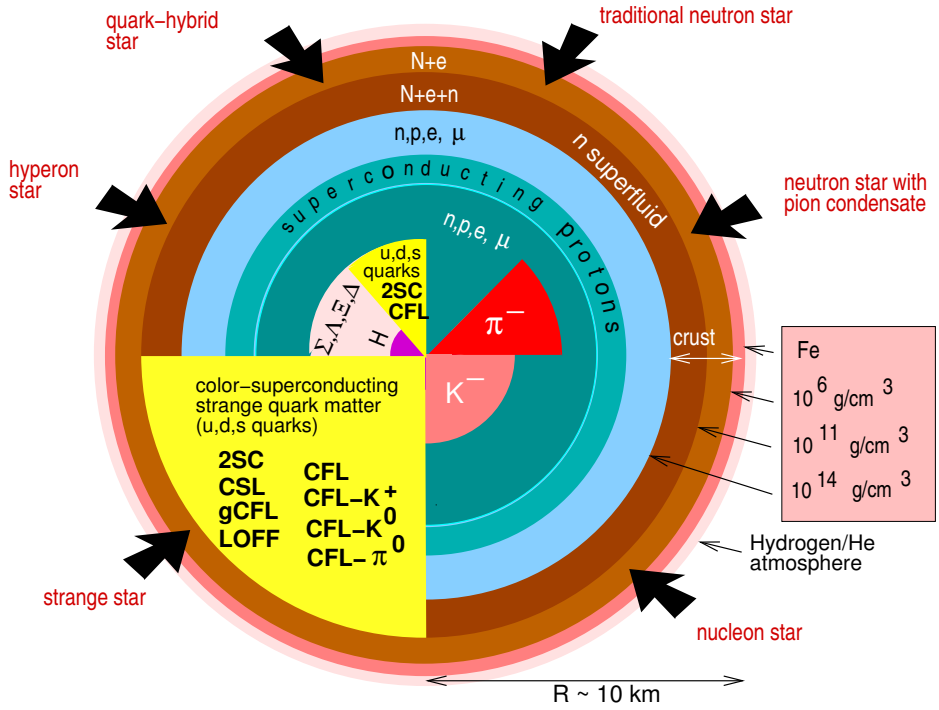

Figure 1.2: Novel phases of subatomic matter in the interior of a neutron star, as suggested by different theories. Reprinted figure with permission from F. Weber, *Prog. Part. Nucl. Phys.* **54**, 193 (2005). Copyright 2004 by Elsevier Ltd.

"neutron star" is presumably a misnomer, but in keeping with tradition, I will refer to these objects as neutron stars. I will, however, distinguish between three different classes of neutron star models in this thesis and in the appended papers. These are

- Traditional neutron stars, which consist of nucleons and leptons.

- Hybrid stars, which have a nuclear-matter shell and a quark-matter core.
- Quark/Strange stars, which consist of (strange) quark matter and have a thin crust, or electrostatic boundary layer.

As indicated in Figure 1.2, also other models of neutron stars exist in the literature, but the discussion here concerns mainly these three classes.

Over the last few years, observations of neutron stars have provided important clues about their properties. In particular, neutron stars with masses ranging from about one solar mass to two solar masses have been observed. This is in contrast to the numerous earlier observations, which all indicated that neutron stars have a mass of ~ 1.4 $M_\odot$. The maximum mass of neutron stars is by itself a key parameter in theoretical models, and in combination with measurements of neutron star radii, it is possible to deduce information about the equation of state (EoS) of high-density matter. For further information about neutron star observations and how they are related to the properties of matter at high density, see Chapter 2 and Paper V.

1.3 Preon stars

Less than 100 years ago, atoms were considered to be a blob of positive charge with embedded, negatively charged electrons. This model, which is known as the plum-pudding model, was proposed in 1906 by Thomson, who discovered the electron a few years earlier. The electrons were free to rotate within the cloud of positive charge, and atomic spectra were thought to be connected to the different energy levels of the orbits. However, Thomson was not very successful in explaining observed spectral lines with his model. A few years later, Geiger, Marsden and Rutherford discovered that atoms have a small positively charged nucleus, and the plum-pudding model was thereby abandoned. The nucleus was revealed by alpha particles sent through a thin sheet of gold, as they were reflected at high angles. Rutherford was astonished by the result:

> *"It was almost as incredible as if you fired a fifteen inch shell at a piece of tissue paper and it came back to hit you."*

As of today, the sub-atomic structure is fairly well understood down to the level of quarks and leptons, and within the resolving power of past and present particle accelerators, there is no evidence for further substructure.

Quarks and leptons are therefore considered to be fundamental entities in the so-called standard model of particle physics (SM). It is clear, however, that the SM is unable to explain the matter content of the universe, especially the vast amounts of so-called dark matter needed to describe, *e.g.*, the observed rotation of galaxies and the evolution of structure in the universe. There seems to be no hope of explaining the abundance of dark matter without introducing new fundamental

particles. The SM is therefore considered to be incomplete. It suffers also from a number of conceptual shortcomings. For example, it does not explain the particle family structure, *i.e.*, why there are six types of quarks and six types of leptons organised into three families. Also, most quarks and leptons are unstable and decay into particles with lower mass. There have been numerous situations in the past when properties like these have turned out to be a result of compositeness, *i.e.*, that the particles are composed of even smaller, and more fundamental particles. The most recent example is the large number of hadrons that puzzled physicists a half-century ago, before the quarks were discovered.

Preons constitute a conjectured, more fundamental level of elementary particles, beneath the quarks and leptons of the SM [2]. If such particles exist, it is possible that a yet unobserved class of compact objects could exist, composed of preons. This possibility is investigated in Paper I, where the properties of such objects – preon stars – are estimated. The idea is further developed in Paper II and Paper VI, where the possibility to detect preon stars is also investigated. In general, we find that the characteristic mass and size of preon stars depend on the compositeness energy scale. For example, assuming that the heaviest quark (the top) is the most weakly bound composite particle of the SM, we get the following estimates for the mass and radius of preon stars

$$M \sim 2 \times 10^{24}\,\mathrm{kg} \left(\frac{\mathrm{TeV}}{\Lambda}\right)^{3/2}, \tag{1.1}$$

$$R \sim 3 \times 10^{-3}\,\mathrm{m} \left(\frac{\mathrm{TeV}}{\Lambda}\right)^{3/2}. \tag{1.2}$$

Here, Λ is the top quark compositeness energy scale. For details, see Paper VI. As $\Lambda <$ a few TeV is ruled out by experiments, it is clear that preon stars, if they exist, are extremely small astrophysical objects, which could have remained unnoticed. They could be detected only if they were created in abundance in the early universe, and constitute a significant fraction of dark matter. Preon stars could be detected, *e.g.*, as gravitational lenses leaving signatures in the spectra of gamma-ray bursts, by the high-frequency gravitational radiation emitted from binary coalescence events, and by the seismic waves emitted as they pass through the Earth or the Moon. A few gamma-ray burst spectra with unexplained features similar to those expected from a preon-star gravitational-lensing event exist, see Paper VI.

Except for a few technical details, described in the references, the discussion of preon stars in the appended papers is rather self-consistent. As the ideas presented in the papers are not restricted to a particular preon model, I will not review specific models here. There are many preon models and a proper discussion is beyond the scope of this thesis. The interested reader is therefore referred to the literature, see, *e.g.*, [2–4] and references therein.

1.4 This thesis

This doctoral thesis treats the phenomenology of compact stars and some theoretical models of their interior. By tradition, it consists of an introduction and appended research papers. The former provides some essential background needed to grasp the content of the papers. In Chapter 2, I introduce the basic theory of compact stars, as applied in the papers. Chapter 3 contains a brief introduction to thermal quantum field theory, which is the theoretical framework used in the derivation and development of the superconducting quark matter model in Paper III, Paper IV, Paper V, and Paper VII. Some basic concepts and models of quark matter are introduced in Chapter 4, and superconducting quark matter is discussed in Chapter 5. The appendices contain some definitions and relations that I find useful in the daily work, and which are referred to in the text.

Chapter 2

Theory of Compact Stars

The physics of compact stars is a multidisciplinary and active field of research. A proper introduction is beyond the scope of this thesis and the interested reader is therefore referred to one of the classical books on the subject [5, 6]. Useful and pedagogical discussions can be found also in [7, 8]. For recent theoretical and observational developments, see, *e.g.*, [9–12] and references therein. The formation and evolution of protoneutron stars are thoroughly discussed in [13, 14]. This list of references serves as a starting point only, as there are literally thousands of papers on the subject. Here I will focus on the essential theory needed to understand the discussions and calculations in the appended papers. It is assumed that the reader has some experience with Einstein's general theory of relativity. The time coordinate is denoted with x^0, and the spatial coordinates are (x^1, x^2, x^3). Indices denoted with Greek letters can have any value in the set $\{0, 1, 2, 3\}$, while the values of Roman indices are limited to the set $\{1, 2, 3\}$, *i.e.*, these indices denote spatial coordinates only. Greek indices should not be confused with the functions $\nu(r)$ and $\lambda(r)$, which enter the metric functions $g_{00}(r)$ and $g_{11}(r)$. The Minkowski metric is defined as $\eta_{\mu\nu} = \mathrm{diag}(1, -1, -1, -1)$. I use the standard notation, R, for the scalar curvature. This quantity should not be confused with the radius R of a star. Gravitational units are used, see Appendix A.2, but G is typically kept explicit in the formulæ to maintain consistency with Newton's theory in the limit of weak gravitational fields.

2.1 Hydrostatic equilibrium

In a static star there is a balance between gravity and pressure. This balance is called hydrostatic equilibrium. Under the assumption that the gravitational field is not too strong, so that Newton's law of gravitation can be applied, the condition for hydrostatic equilibrium is straightforward to derive. Consider a small region dA of a thin spherical shell of thickness Δr, located at radius r. This piece of matter is in

equilibrium if the net force acting on it vanishes

$$\sum F_r = p(r)dA - p(r+\Delta r)dA - \frac{GM(r)\,\rho(r)dA\Delta r}{r^2} = 0. \tag{2.1}$$

Here $p(r)$ is the pressure, $M(r)$ the mass enclosed by the shell at radius r, and $\rho(r)$ the matter density. Rearranging terms and taking the limit $\Delta r \to 0$, the condition for hydrostatic equilibrium becomes

$$\lim_{\Delta r\to 0} \frac{p(r+\Delta r) - p(r)}{\Delta r} \equiv \frac{dp}{dr} = -\frac{GM(r)\,\rho(r)}{r^2}. \tag{2.2}$$

In this Newtonian description the mass enclosed within a spherical shell of radius r can be obtained with a volume integral in Euclidean space

$$M(r) = 4\pi \int_0^r dr\, r'^2 \rho(r'). \tag{2.3}$$

Equations (2.2) and (2.3) are the hydrostatic equations for a non-rotating star in the limit of weak gravitational fields. If the equation of state, $\rho = \rho(p)$, of matter is known, the hydrostatic equations can be integrated for a given value of the central pressure up to the surface of the star, where the pressure vanishes. The radial coordinate, R, where $p(R) = 0$, defines the radius of the star, and $M(R)$ its gravitational mass. For each choice of the central pressure, the solution of the hydrostatic equations describes a star configuration. For any given equation of state, the sequence of possible equilibrium star configurations can therefore be obtained from the solutions of the hydrostatic equations for different values of the central pressure.

The newtonian hydrostatic equations describe the structure of ordinary stars, planets, and white dwarfs. For dense compact stars, such as neutron stars, the curvature of spacetime cannot be neglected and a realistic model of such objects must be based on general relativity, *i.e.*, the generalisations of (2.2) and (2.3) to strong gravitational fields. These equations are derived in Section 2.4, after the discussion of curved spacetime in the next two sections.

2.2 Static isotropic spacetime

In static isotropic regions of spacetime, such as the interior and exterior regions of an isolated static star, the most general form of the line element in spherical coordinates is

$$d\tau^2 = U(r)dt^2 - V(r)dr^2 - W(r)r^2(d\theta^2 + \sin^2\theta\, d\phi^2). \tag{2.4}$$

For simplicity, the radial coordinate, r, is defined such that $W(r) = 1$. Consequently, the line element can be written as

$$d\tau^2 = e^{2\nu(r)}dt^2 - e^{2\lambda(r)}dr^2 - r^2(d\theta^2 + \sin^2\theta\, d\phi^2), \tag{2.5}$$

where $\nu(r)$ and $\lambda(r)$ are functions of r only. The relation between the line element and the metric tensor is $d\tau^2 = g_{\mu\nu}dx^\mu dx^\nu$. By comparing this with (2.5), one finds that

$$g_{\mu\nu} = \begin{bmatrix} e^{2\nu(r)} & 0 & 0 & 0 \\ 0 & -e^{2\lambda(r)} & 0 & 0 \\ 0 & 0 & -r^2 & 0 \\ 0 & 0 & 0 & -r^2\sin^2\theta \end{bmatrix}. \tag{2.6}$$

The functions $\nu(r)$ and $\lambda(r)$ are governed by Einstein's field equation

$$G^{\mu\nu} = \kappa T^{\mu\nu} + \Lambda g^{\mu\nu}. \tag{2.7}$$

Here $G^{\mu\nu}$ is the Einstein curvature tensor, which is a function of the metric. The energy-momentum tensor, $T^{\mu\nu}$, represents the "matter" content of space. Λ is the so-called cosmological constant and κ is a constant that has to be determined in the weak-field limit, where Einstein's field equation should be consistent with Newton's theory. The Λ-term was not present in the original theory, but was added by Einstein to obtain a static cosmology before it was known that the universe is expanding. As of today, it appears to be the best model of dark energy and the expanding universe [15]. It corresponds to a constant energy density of empty space, and a constant negative pressure. Recent measurements of Λ yield a value for the corresponding density of the order 10^{-29} g/cm^3. This tiny "vacuum density" is negligible in models of compact stars, because it is at least 30 orders of magnitude lower than the density at the surface of a neutron star, and about 45 orders of magnitude smaller than their central density. The Λ-term can therefore be omitted in the derivation of the general-relativistic hydrodynamic equations. The situation is different in cosmology where the vacuum density dominates, because at large scales the universe has vast regions of empty space and the corresponding volume compensates for the smallness of Λ.

When Einstein derived the field equation (2.7) he was motivated by Poisson's equation, $\nabla^2\Phi = 4\pi G\rho$, for the gravitational potential, Φ, generated by a field of density ρ in Newton's theory. He was seeking a tensor that is linear in the second-order derivatives of the metric, or quadratic in the first-order derivatives. The only tensor that can be created from the metric, and its first- and second-order derivatives, is the Riemann-Christoffel curvature tensor (hereafter Riemann tensor for short),

$$R^\lambda_{\sigma\mu\nu} = \Gamma^\lambda_{\sigma\nu,\mu} - \Gamma^\lambda_{\sigma\mu,\nu} + \Gamma^\alpha_{\sigma\nu}\Gamma^\lambda_{\alpha\mu} - \Gamma^\alpha_{\sigma\mu}\Gamma^\lambda_{\alpha\nu}, \tag{2.8}$$

where $\Gamma^\lambda_{\mu\nu}$ is the Christoffel symbol,

$$\Gamma^\lambda_{\mu\nu} = \frac{1}{2}g^{\lambda\alpha}\left(g_{\alpha\nu,\mu} + g_{\alpha\mu,\nu} - g_{\mu\nu,\alpha}\right). \tag{2.9}$$

Here I use the standard 'comma subscript' notation for coordinate derivatives, *i.e.*,

$$S_{,\mu} = \frac{\partial S}{\partial x^\mu}. \tag{2.10}$$

The Christoffel symbol is the affine connection of the Riemann manifold, which can be used to define the covariant derivative of a vector field

$$A_{\mu;\nu} = \frac{dA_\mu}{dx^\nu} - \Gamma^\lambda_{\mu\nu} A_\lambda. \tag{2.11}$$

This derivative reduces to ordinary differentiation in inertial frames and, consequently, locally in any gravitational field. Unlike ordinary derivatives, however, the covariant derivative transforms as a second-rank tensor and therefore retains its form under any coordinate transformation and in any gravitational field. This is essential for the formulation of physical laws, as they should be independent of the frame in which they are expressed.

In the special theory of relativity, conservation of energy and momentum requires that the divergence of the energy-momentum tensor vanishes,

$$T^{\mu\nu}{}_{,\nu} = 0. \tag{2.12}$$

This conservation law can be generalised to an arbitrary frame by replacing the ordinary coordinate derivative with a covariant derivative,

$$T^{\mu\nu}{}_{;\nu} = 0. \tag{2.13}$$

Now, consider the Einstein field equation (2.7). The covariant derivative of $\Lambda g^{\mu\nu}$ is zero, because the metric reduces to the Minkowski metric in an inertial frame, which has vanishing derivatives, and this result is by definition independent on the choice of frame. The covariant divergence of the Einstein curvature tensor, $G^{\mu\nu}$, should therefore vanish. The only contraction of the Riemann tensor that has a vanishing covariant derivative is

$$G^{\mu\nu} = R^{\mu\nu} - \frac{1}{2} g^{\mu\nu} R, \tag{2.14}$$

where $R^{\mu\nu}$ is the Ricci tensor and R is the scalar curvature, which are defined by

$$R_{\mu\nu} = R^\lambda_{\mu\nu\lambda}, \tag{2.15}$$

$$R = g^{\mu\nu} R_{\mu\nu}. \tag{2.16}$$

This result follows from the Bianchi identities, which is a set of differential relations for the Riemann tensor. For a discussion about the geometrical meaning of $G^{\mu\nu}{}_{;\nu} = 0$, see Chapter 15 in [8]. Unlike the conservation equation for an inertial system (2.12), the generalisation to arbitrary curvature (2.13) does not ensure that the energy and momentum of matter are conserved. It is the divergence of $G^{\mu\nu} - \kappa T^{\mu\nu}$ that vanishes, so matter and gravitational fields exchange energy and momentum. The gravitational field also interacts with itself, because it has energy and momentum. This is a consequence of Einstein's equation and its non-linear dependence of $g^{\mu\nu}$.

The metric of static isotropic regions of spacetime obeys equations (2.5), (2.7)-(2.9), and (2.14)-(2.16), for a given energy-momentum tensor $T^{\mu\nu}$. The affine connection (2.9) is

$$\begin{aligned}
&\Gamma^1_{00} = \nu' e^{2(\nu-\lambda)}, && \Gamma^0_{10} = \nu', \\
&\Gamma^1_{11} = \lambda', && \Gamma^2_{12} = \Gamma^3_{13} = r^{-1}, \\
&\Gamma^1_{22} = -re^{-2\lambda}, && \Gamma^3_{23} = \cot\theta, \\
&\Gamma^1_{33} = -r\sin^2\theta\, e^{-2\lambda}, && \Gamma^2_{33} = -\sin\theta\,\cos\theta,
\end{aligned} \tag{2.17}$$

where the primes denote differentiation with respect to r, and $\Gamma^\lambda_{\mu\nu} = \Gamma^\lambda_{\nu\mu}$. The Ricci tensor (2.15) can be expressed in the affine connection by a contraction of the Riemann tensor (2.8)

$$R_{\mu\nu} = \Gamma^\alpha_{\mu\alpha,\nu} - \Gamma^\alpha_{\mu\nu,\alpha} + \Gamma^\alpha_{\mu\beta}\Gamma^\beta_{\nu\alpha} - \Gamma^\alpha_{\mu\nu}\Gamma^\beta_{\alpha\beta}. \tag{2.18}$$

It follows from (2.17) that

$$\begin{aligned}
R_{00} &= -\left(\nu'' - \lambda'\nu' + \nu'^2 + \frac{2\nu'}{r}\right) e^{2(\nu-\lambda)}, \\
R_{11} &= \nu'' - \lambda'\nu' + \nu'^2 - \frac{2\lambda'}{r}, \\
R_{22} &= (1 + r\nu' - r\lambda')\, e^{-2\lambda} - 1, \\
R_{33} &= R_{22}\sin^2\theta.
\end{aligned} \tag{2.19}$$

The scalar curvature (2.16) is obtained as a contraction of the Ricci tensor with the metric,

$$R = -\frac{2e^{-2\lambda}}{r^2}\left(r^2\nu'' + r^2\nu'^2 - r^2\nu'\lambda' + 2r\nu' - 2r\lambda' - e^{2\lambda} + 1\right). \tag{2.20}$$

Einstein's curvature tensor (2.14) can now be constructed from the Ricci tensor and the scalar curvature,

$$\begin{aligned}
G^0_0 &= \frac{e^{-2\lambda}}{r^2}\left(1 - 2r\lambda'\right) - \frac{1}{r^2}, \\
G^1_1 &= \frac{e^{-2\lambda}}{r^2}\left(1 + 2r\nu'\right) - \frac{1}{r^2}, \\
G^2_2 &= e^{-2\lambda}\left(\nu'' + \nu'^2 - \nu'\lambda' + \frac{\nu' - \lambda'}{r}\right), \\
G^3_3 &= G^2_2,
\end{aligned} \tag{2.21}$$

where mixed tensors are used as their explicit expressions are relatively short. In the next section, I will derive a particularly simple and important solution for the metric of static isotropic spacetime.

2.3 The Schwarzschild solution

In the empty space outside a static compact star the energy-momentum tensor vanishes, $T^{\mu\nu} = 0$, and the tiny contribution from the cosmological constant, Λ, can be neglected. Einstein's field equation (2.7) therefore reduces to $G^{\mu\nu} = 0$, which implies that

$$R^{\mu\nu} = \frac{1}{2} g^{\mu\nu} R. \tag{2.22}$$

This is a set of differential equations for the functions $\nu(r)$ and $\lambda(r)$. These equations can be further simplified when multiplied with the metric $g_{\sigma\mu}$,

$$R_\sigma^{\ \nu} = \frac{1}{2} \delta_\sigma^{\ \nu} R, \tag{2.23}$$

and contracted for $\sigma = \nu$,

$$R = \frac{1}{2} R \quad \Longrightarrow \quad R = 0. \tag{2.24}$$

Consequently, the vanishing of the Einstein tensor implies that both the scalar curvature and the Ricci tensor vanish. The Riemann tensor, however, vanishes only in the limit $r \to \infty$, where spacetime is flat.

Setting $R_{00} = R_{11} = 0$ in (2.19), it follows that

$$-\left(\frac{2\nu'}{r} + \frac{2\lambda'}{r}\right) e^{2(\nu-\lambda)} = 0 \quad \Longrightarrow \quad \nu' + \lambda' = 0. \tag{2.25}$$

Inserting this result in $R_{22} = 0$, I get an equation for the function $\lambda(r)$,

$$(1 - 2r\lambda')e^{-2\lambda} = 1. \tag{2.26}$$

This differential equation has the solution

$$g_{11} \equiv -e^{2\lambda} = -\left(1 - \frac{C_1}{r}\right)^{-1}, \tag{2.27}$$

for some constant C_1. In the limit $r \to \infty$, spacetime is flat and the metric, $g_{\mu\nu}$, simplifies to the Minkowski metric. This condition is met by the solution (2.27). The integration constant, C_1, is determined such that the solution is consistent with Newton's theory of gravity in the weak-field limit. I will return to this issue later. An equation for $\nu(r)$ can be obtained from (2.25)-(2.27),

$$1 + 2r\nu' = \left(1 - \frac{C_1}{r}\right)^{-1}, \tag{2.28}$$

which has the solution

$$g_{00} \equiv e^{2\nu} = C_2 \left(1 - \frac{C_1}{r}\right). \tag{2.29}$$

The integration constant, C_2, must be unity in order to give the correct limit as $r \to \infty$.

The constant, C_1, can be determined in the following way. Consider the motion of a slowly moving ($v \ll c = 1$) test particle at large r, where gravity is weak. The motion of the particle is governed by the geodesic equation

$$\frac{d^2x^\lambda}{d\tau^2} + \Gamma^\lambda_{\mu\nu}\frac{dx^\mu}{d\tau}\frac{dx^\nu}{d\tau} = 0. \tag{2.30}$$

To leading order, the proper time, τ, is equal to the coordinate time, t, because the particle is moving slowly and $g_{\mu\nu} \simeq \eta_{\mu\nu}$, where $\eta_{\mu\nu}$ is the Minkowski metric of flat spacetime. The geodesic equation therefore simplifies to an expression for the acceleration of the particle,

$$\frac{d^2x^i}{dt^2} \simeq -\Gamma^i_{\mu\nu}\frac{dx^\mu}{d\tau}\frac{dx^\nu}{d\tau}. \tag{2.31}$$

Because the gravitational field is weak, it possible to choose a coordinate system where the metric can be expressed as a perturbed Minkowski metric,

$$g_{\mu\nu} = \eta_{\mu\nu} + h_{\mu\nu}, \tag{2.32}$$

where $h_{\mu\nu}$ is the perturbation. The dominant term in the sum over μ and ν in (2.31) is for $\mu = \nu = 0$, because the other terms are smaller by at least a factor of v. The Christoffel symbol of this term is

$$\Gamma^i_{00} = \frac{1}{2}g^{i\alpha}\left(g_{\alpha 0,0} + g_{\alpha 0,0} - g_{00,\alpha}\right) \simeq \frac{1}{2}\eta^{i\alpha}(2h_{\alpha 0,0} - h_{00,\alpha}). \tag{2.33}$$

The chain rule, $h_{i0,0} \simeq h_{i0,j}\, v^j$, where v^j is the velocity of the test particle, implies that the terms $2h_{\alpha 0,0}$ in (2.33) are negligible for $\alpha \neq 0$. The Christoffel symbol therefore simplifies to

$$\Gamma^i_{00} \simeq \frac{1}{2}h_{00,i}. \tag{2.34}$$

Inserting this result in (2.31), it follows that the acceleration of the test particle is

$$\frac{d^2x^i}{dt^2} \simeq -\frac{1}{2}h_{00,i}. \tag{2.35}$$

This weak-field result should be consistent with the expression for the acceleration of a test particle in Newton's theory,

$$\frac{d^2x^i}{dt^2} = -\Phi_{,i} = -\left(-\frac{GM}{r}\right)_{,i}, \tag{2.36}$$

where Φ is the gravitational potential and M is the mass of the object that generates it. Consequently, $h_{00} = -2GM/r$, and according to (2.32)

$$g_{00} = 1 - \frac{2GM}{r}. \tag{2.37}$$

It follows from (2.29) that the integration constant is

$$C_1 = 2GM. \tag{2.38}$$

This completes the derivation of the metric outside a static spherically symmetric object. The solution is named in honour of Schwarzschild, who found it already in 1916, a few months after Einstein published his general theory of relativity. Later, Birkhoff proved that this is the most general static, spherically symmetric, vacuum solution of Einstein's field equation. The line element of the Schwarzschild solution is

$$d\tau^2 = \left(1 - \frac{2GM}{r}\right) dt^2 - \left(1 - \frac{2GM}{r}\right)^{-1} dr^2 - r^2(d\theta^2 + \sin^2\theta\, d\phi^2), \tag{2.39}$$

and the corresponding diagonal metric is

$$\begin{aligned} g_{00}(r) &= e^{2\nu(r)} = 1 - \frac{2GM}{r}, \\ g_{11}(r) &= -e^{2\lambda(r)} = -\left(1 - \frac{2GM}{r}\right)^{-1}, \\ g_{22}(r) &= -r^2, \\ g_{33}(r,\, \theta) &= -r^2 \sin^2\theta. \end{aligned} \tag{2.40}$$

Observe that the metric is singular at the radius $r = 2M$. This radius is called the Schwarzschild radius, r_S. The singularity can be removed by a change of coordinates and does not correspond to a singularity of spacetime. However, if r_S exceeds the physical radius, R, of an object, it is/becomes a black hole. No particle, nor light, can leave the region $R < r < r_S$, as no future lightcone extends beyond r_S. Observe that the Schwarzschild solution is valid *only* in empty space above the surface of a star. The equations for the interior will be derived in the next section.

2.4 The Tolman-Oppenheimer-Volkoff equations

The general-relativistic hydrostatic equations were derived and applied to models of neutron stars already in 1939 by Tolman, Oppenheimer and Volkoff [16, 17]. These equations are derived from Einstein's field equation under the assumptions that the metric is static and isotropic, and that matter is a perfect fluid. The latter assumption is expected to be a good approximation for the extremely dense interior of a static compact star, because the strong gravitational force is balanced by a huge pressure and rigid-body forces have a negligible effect on the structure. The metric and the corresponding Einstein curvature tensor were derived in Section 2.2. The energy-momentum tensor should be a symmetric second-rank tensor that has a

vanishing covariant divergence (2.13). In a perfect fluid, the pressure is isotropic in the rest frame of a fluid element, and there are no shear stresses. In this local frame the energy-momentum tensor is

$$T'^{\mu\nu} = \begin{bmatrix} \epsilon & 0 & 0 & 0 \\ 0 & p & 0 & 0 \\ 0 & 0 & p & 0 \\ 0 & 0 & 0 & p \end{bmatrix}, \tag{2.41}$$

where ϵ is the energy density and p the pressure. This result can be generalised to any Lorentz frame by a standard coordinate transformation on the form $T^{\mu\nu} = \Lambda_\alpha{}^\mu \Lambda_\beta{}^\mu T'^{\alpha\beta}$. The result for an arbitrary Lorentz frame is

$$T^{\mu\nu} = -p\eta^{\mu\nu} + (p+\epsilon)u^\mu u^\nu, \tag{2.42}$$

where u^μ is the four-velocity of the fluid element. In the rest frame, where $u^0 = 1$ and $u^i = 0$, this expression simplifies to (2.41). The energy-momentum tensor (2.42) can be generalised to an arbitrary gravitational field by the principle of general covariance[1],

$$T^{\mu\nu} = -pg^{\mu\nu} + (p+\epsilon)u^\mu u^\nu. \tag{2.43}$$

The fluid four-velocity satisfies the relation

$$g_{\mu\nu} u^\mu u^\nu = 1, \tag{2.44}$$

because $d\tau^2 = g_{\mu\nu} dx^\mu dx^\nu$ and

$$u^\mu \equiv \frac{dx^\mu}{d\tau}. \tag{2.45}$$

The relation between the pressure and the energy density depends on the microscopic properties of matter and the state of the star, *e.g.*, its temperature. I will return to this issue later.

In a static star, the three-velocity of every fluid element is zero. It then follows from (2.44) that

$$u^0 = {g_{00}}^{-1/2}, \qquad u^i = 0. \tag{2.46}$$

Consequently, in a static star the energy-momentum tensor of a perfect fluid (2.43) simplifies to

$$T_0{}^0 = \epsilon, \qquad T_i{}^i = -p. \tag{2.47}$$

[1]The principle of general covariance states that any law that holds in the special theory of relativity, *i.e.*, in the absence of gravity, can be generalised to an arbitrary gravitational field by replacing the metric $\eta_{\mu\nu}$ with $g_{\mu\nu}$, and replacing coordinate derivatives with covariant derivatives.

Using this expression and the result (2.21), Einstein's field equation (2.7) yields the following set of differential equations for the functions $\nu(r)$ and $\lambda(r)$

$$\frac{e^{-2\lambda(r)}}{r^2}\left[1-2r\lambda'(r)\right]-\frac{1}{r^2}=\kappa\epsilon(r), \tag{2.48}$$

$$\frac{e^{-2\lambda(r)}}{r^2}\left[1+2r\nu'(r)\right]-\frac{1}{r^2}=-\kappa p(r), \tag{2.49}$$

$$e^{-2\lambda(r)}\left[\nu''(r)+\nu'(r)^2-\nu'(r)\lambda'(r)+\frac{\nu'(r)-\lambda'(r)}{r}\right]=-\kappa p(r). \tag{2.50}$$

The first equation (2.48) can be integrated immediately and yields

$$e^{-2\lambda(r)}=1+\frac{\kappa}{r}\int_0^r dr' r'^2\epsilon(r'). \tag{2.51}$$

Here the integration constant has been fixed such that the result is consistent in the vacuum limit, $\epsilon(r)\to 0$. The metric is continuous at the surface of the star. Consequently, this result matches the Schwarzschild solution (2.27) at $r=R$,

$$e^{-2\lambda(R)}=1+\frac{\kappa}{R}\int_0^R dr' r'^2\epsilon(r')=1-\frac{2GM}{R}. \tag{2.52}$$

Comparing terms it follows that the integral over the energy density is proportional to the gravitational mass of the star. It is therefore natural to define the mass, $M(r)$, enclosed within a shell of radius r according to

$$M(r)\equiv 4\pi\int_0^r dr' r'^2\epsilon(r'), \tag{2.53}$$

where the prefactor is defined such that the infinitesimal element represents the volume of the shell at radius r' with thickness dr'. The total mass is $M=M(R)$, and the constant of proportionality in Einstein's field equation (2.7) is

$$\kappa=-8\pi G. \tag{2.54}$$

From these results it follows that

$$g_{11}(r)=-e^{2\lambda(r)}=-\left[1-\frac{2GM(r)}{r}\right]^{-1}, \tag{2.55}$$

which is on the same form as the Schwarzschild result (2.40), with the difference that the metric at r depends only on the mass enclosed within a shell of radius r, and not on the total mass.

With this information the hydrostatic equations can be derived from the differential equations (2.48)-(2.50). Rearranging terms, the first two differential equations can be written

$$2r\lambda'(r) = 1-e^{2\lambda(r)}\left[1+\kappa r^2\epsilon(r)\right], \tag{2.56}$$

$$2r\nu'(r) = -1+e^{2\lambda(r)}\left[1-\kappa r^2 p(r)\right]. \tag{2.57}$$

The derivative of the latter equation is

$$2\nu'(r) + 2r\nu''(r) = \left\{2\lambda'(r)\left[1 - \kappa r^2 p(r)\right] - \kappa\left[2rp(r) + r^2 p'(r)\right]\right\} e^{2\lambda(r)}. \quad (2.58)$$

These three equations can be combined to obtain an expression for $\nu''(r)$,

$$\begin{aligned} 2r^2\nu''(r) &= 1 - \left[2\kappa r^2 p(r) + \kappa r^3 p'(r)\right] e^{2\lambda(r)} \\ &\quad - \left[1 - \kappa r^2 p(r)\right]\left[1 + \kappa r^2 \epsilon(r)\right] e^{4\lambda(r)}. \end{aligned} \quad (2.59)$$

Inserting the expressions for $\lambda'(r)$ (2.56), $\nu'(r)$ (2.57), and $\nu''(r)$ (2.59) in (2.50), and using the physical value (2.54) for κ, the following differential equation for the pressure is obtained

$$\frac{dp}{dr} = -\frac{G[p(r) + \epsilon(r)][M(r) + 4\pi r^3 p(r)]}{r[r - 2GM(r)]}. \quad (2.60)$$

This is the Tolman-Oppenheimer-Volkoff (TOV) equation for hydrostatic equilibrium of a spherically symmetric object. In combination with the expression for the mass (2.53), and a microscopic theory for the relation between the pressure and the energy density, this equation gives the equilibrium solution for the pressure in a compact star. These equations are the generalisations of the newtonian hydrostatic equations (2.2)-(2.3).

If the equation of state, $\epsilon(p)$, of matter is known, the TOV equations can be integrated for a given value of the central pressure up to the surface of the star, where the pressure vanishes[2]. The radial coordinate, R, where $p(R) = 0$, defines the radius of the star, and $M(R)$ its gravitational mass. For each choice of the central pressure, the solution of the TOV equations describes a star configuration. The sequence of possible equilibrium star configurations can therefore be obtained by solving the TOV equations for different values of the central pressure. When solving these equations numerically, it is sometimes convenient to use an adaptive steplength, Δr, that is calculated such that the relative decrease of the pressure per step is constant,

$$\Delta r = \frac{1}{N}\frac{rp(r)[r - 2GM(r)]}{G[p(r) + \epsilon(r)][M(r) + 4\pi r^3 p(r)]}. \quad (2.61)$$

Here, N is a number that roughly determines the number of integration steps needed to reach the surface. The value of Δr should be limited from below by some small

[2] In general, the number of thermodynamic degrees of freedom, N_F, is given by Gibbs phase rule: $N_F = N_C - N_P + 2$, where N_C is the number of distinct compounds not being in thermal equilibrium and N_P is the number of phases. Consequently, even in the simple case of a homogenous star, the equation of state is a function of two variables. Such additional microscopic degrees of freedom can be removed with variational methods, see [18] for an example, or by making some simplifying assumptions about the thermal state of the star. For example, in equilibrium the temperature distribution in a compact star is given by the metric functions, see Section 2.10, and for new-born protoneutron stars the entropy per baryon is roughly constant, see Paper VII.

number, otherwise problems will arise at the surface. More sophisticated adaptive algorithms can be used, but my experience is that the method outlined above is reliable. It is convenient to set $G = 1$ (the speed of light, c, does not enter the formulæ, because it is explicitely set to unity) and measure all quantities in powers of a kilometre. Some useful conversion factors are provided in Appendix A.3.

2.5 Uniform density solution

In general, the the TOV equations, (2.53) and (2.60), have to be integrated numerically. A number of analytic solutions are known, however, and one of them is particularly interesting as it provides a limiting value of M/R that applies to any star in hydrostatic equilibrium. Consider a hypothetical star composed of incompressible matter, *i.e.*, a star with a uniform energy density, $\epsilon(r) = \epsilon_0$. This star has the highest possible value of M/R for a given central density. The equation (2.60) can be written

$$-\frac{dp}{[p(r)+\epsilon_0][3p(r)+\epsilon_0]} = \frac{4\pi G}{3}\frac{r\,dr}{1-8\pi G r^2\epsilon_0/3}. \tag{2.62}$$

This equation can be integrated and has the solution

$$\frac{p(r)+\epsilon_0}{3p(r)+\epsilon_0} = \sqrt{\frac{1-2GM/R}{1-2GMr^2/R^3}}, \tag{2.63}$$

where the boundary condition $p(R) = 0$ is used to determine the integration constant. It follows that

$$p(r) = \epsilon_0\frac{\sqrt{1-2GM/R}-\sqrt{1-2GMr^2/R^3}}{\sqrt{1-2GMr^2/R^3}-3\sqrt{1-2GM/R}}. \tag{2.64}$$

Clearly, the solution for $p(r)$ has a singularity[3] at the radius, $r = r_\infty$, where the denominator of (2.64) vanishes,

$$r_\infty^2 = 9R^2 - \frac{4R^3}{GM}. \tag{2.65}$$

Because the pressure is a scalar, this singularity cannot be removed by a transformation of the coordinates. The singularity is therefore unphysical and must not appear. This implies that r_∞^2 must be negative, which is equivalent to

$$\frac{2GM}{R} < \frac{8}{9}. \tag{2.66}$$

[3]It follows from (2.70) that also the metric is singular at r_∞.

As this condition follows directly from the general relativistic hydrodynamic equations, it applies to all equilibrium compact star configurations. Note that the Schwarzschild radius, $r_S = 2GM$, is less than $8R/9$, so there is no singularity in the interior and exterior solutions for equilibrium star configurations.

It is possible to obtain a more stringent condition on $2GM/R$ of a star with uniform density, as compared to (2.66), under the assumption that $p < \epsilon$. This is believed to be the case, because at low pressure the energy density of matter is dominated by the mass-energy of baryons, so $p < \epsilon$, and if the speed of sound is lower than the speed of light at all pressures it follows that $dp/d\epsilon < 1$. According to (2.63), the central pressure, $p_c = p(0)$, of a uniform density star obeys the relation

$$\frac{2GM}{R} = 1 - \left(\frac{p_c + \epsilon_0}{3p_c + \epsilon_0}\right)^2. \tag{2.67}$$

Assuming that $p < \epsilon$, it follows that

$$\frac{2GM}{R} < \frac{3}{4}. \tag{2.68}$$

This result holds for a uniform-density star, but should not be trusted in more realistic applications. In general, (2.66) is valid and applies to any static model of compact stars.

2.6 Decoupling of matter from gravity

The properties of matter and spacetime are linked by Einstein's field equation. Spacetime is affected by the energy-momentum tensor of the matter fields, and matter is affected by the curvature of spacetime. For example, the Dirac equation contains the scalar product $\gamma_\mu \partial^\mu \equiv g_{\mu\nu}\gamma^\nu \partial^\mu$, which depends on the metric. Solutions of the Dirac equation, or any other relativistic equation depend on the curvature. Consequently, the matter equations can be solved in flat spacetime only if the changes of the metric functions are negligible at distances comparable to the size of the microscopic system. If this condition is met, a local Lorentz frame can be erected for the microscopic system, and the solution obtained in that frame can be generalised to an arbitrary frame by the principle of general covariance. At Earth this is typically the case, and the matter field equations can therefore be solved in flat spacetime. For applications in strong gravitational fields, however, this is not necessarily the case.

The TOV equations depend on the EoS of matter. It is therefore necessary to check whether the EoS used in compact star calculations can be pre-calculated in a Lorentz frame, or if it is necessary to solve the matter equations and the TOV equations self-consistently. Using the expression (2.55) for the metric function $g_{11}(r)$

and the upper limit (2.66) for the compactness of a compact star, it follows that

$$\frac{g_{11}(R)}{g_{11}(0)} = \left(1 - \frac{2GM}{R}\right)^{-1} < \left(1 - \frac{8}{9}\right)^{-1} = 9. \tag{2.69}$$

The metric changes by no more than a factor 9 over the size of a star. For neutron stars, with $R \sim 10\,\mathrm{km}$, the metric changes by a relative fraction $\sim 9{\times}1\,\mathrm{fm}/R \simeq 10^{-18}$ over the spacing of nucleons in the star. The change in the metric is therefore negligible at distances spanning a large number of nucleons, and the error introduced by solving the matter equations in flat spacetime should be negligible.

2.7 Metric functions

In some applications it is useful to have the metric functions $g_{00}(r)$ and $g_{11}(r)$. The radial metric function, $g_{11}(r)$, is given by (2.55). In general, it is not possible to obtain an expression for the time component of the metric, $g_{00}(r)$, because the differential equation for $\nu(r)$ depends on the TOV solutions for $p(r)$ and $M(r)$. Inserting the expression (2.55) for $e^{2\lambda(r)}$ in (2.57), it follows that

$$\frac{d\nu}{dr} = \frac{G[M(r) + 4\pi r^3 p(r)]}{r[r - 2GM(r)]}. \tag{2.70}$$

The metric function, $g_{00} = e^{2\nu(r)}$, is continuous at the surface of the star. The solution for $\nu(r)$ must therefore match the Schwarzschild solution (2.29) at $r = R$. This boundary condition can be met only in hindsight, when the TOV equations have been solved and the total mass of the star is known. However, as the differential equation (2.70) is invariant with respect to a constant shift $\nu(r) \to \nu(r) + C$, any solution for $\nu(r)$ can be rescaled to match the boundary condition. A convenient strategy is therefore to integrate (2.70) in parallel with the TOV equations, with an arbitrary initial value for $\nu(r = 0)$, say zero. Once a solution is obtained, $\nu(r)$ is rescaled to match the Schwarzschild solution at the surface,

$$\nu(r) \longrightarrow \nu(r) - \nu(R) + \frac{1}{2}\ln\left[1 - \frac{2GM(r)}{R}\right], \quad r \le R. \tag{2.71}$$

Using this method, there is no need to store the solutions for $p(r)$ and $M(r)$, and no second integration pass is needed. In the following sections, I will describe some physical applications of the metric functions.

2.8 Surface redshift

The frequency of light is affected by gravitational fields. When a compact star is observed, the light reaching the instrument has escaped the gravitational potential

generated by the mass of the star. It should therefore appear redshifted, as compared to the frequency of the light emitted from the surface of the star. To obtain an expression for the redshift, consider an ideal situation where the observer is located at an infinite distance from the star. An atom at rest on the surface of the star emits a photon in the radial direction, towards the location of the observer. Consider the photon as a wave train, and the successive wave crests as spacetime events. The coordinate time between two neighbouring wave crests is related to the invariant line element by

$$d\tau_e = \sqrt{g_{00}(R)}\, dt, \tag{2.72}$$

where the subscript 'e' indicates that this relation holds as the photon is emitted. The photon then propagates according to the relation

$$d\tau^2 = g_{00}(r)dt^2 - g_{11}(r)dr^2 = 0. \tag{2.73}$$

Here, the metric functions $g_{00}(r)$ and $g_{11}(r)$ are defined by (2.29) and (2.27). It follows that

$$\Delta t = \int_R^\infty dt = \int_R^\infty dr \left[\frac{g_{11}(r)}{g_{00}(r)}\right]^{1/2}, \tag{2.74}$$

where Δt is the coordinate time needed for a wave crest to propagate from $r = R$ to $r = \infty$. Consequently, as the photon travels from the surface of the star towards the observer, the coordinate time between two wave crests is preserved in the rest frame of the compact star. An observer with a fixed position relative the star, *i.e.*, with fixed coordinates r, θ and ϕ, will measure a proper time

$$d\tau_o = \sqrt{g_{00}(\infty)}\, dt, \tag{2.75}$$

which is the analogue of (2.72) at the location of the observer. Because the relation between proper time and coordinate time is different at $r = R$ and $r = \infty$, and the distance in coordinate time between neighbouring wave crests is preserved, the frequency of the wave changes as it propagates. The frequency is proportional to the inverse of the proper time, so the ratio of the observed, ω_o, and emitted, ω_e, frequencies is

$$\frac{\omega_o}{\omega_e} = \left[\frac{g_{00}(R)}{g_{00}(\infty)}\right]^{1/2} = \sqrt{1 - 2GM/R}. \tag{2.76}$$

Conventionally, the redshift, z, is defined as the relative difference between the wavelength, λ, of observed and emitted light,

$$z \equiv \frac{\lambda_o - \lambda_e}{\lambda_e} = \frac{\lambda_o}{\lambda_e} - 1 = \frac{\omega_e}{\omega_o} - 1 = \left(1 - \frac{2GM}{R}\right)^{-1/2} - 1. \tag{2.77}$$

The redshift is a consequence of gravitational time dilation. Time moves slowly in a strong gravitational field, as measured by a remote observer. It follows from the

compactness limit (2.66) that the upper limit for the redshift of any static compact star is

$$z < \left(1 - \frac{8}{9}\right)^{-1/2} - 1 = 2. \tag{2.78}$$

Redshift measurements of neutron stars provide information about M/R. In combination with other observational techniques used to deduce M and/or R, this information can be used to pinpoint the physical compact star sequence in the $M - R$ plane. In addition, high redshifts are difficult to explain with compact star models based on soft EsoS. A measurement of a star with high surface redshift would therefore rule out some microscopic models. In particular, $z \gtrsim 0.5$ could be difficult to explain with hybrid star models, see the discussion on surface redshifts in Paper V. For information about observations of surface redshifts, see [9] and references therein.

2.9 Baryon number

In studies of the evolution of compact stars, such as the effects of cooling and neutrino dissipation, it is necessary to have some invariant quantity that identifies a particular star. The total baryon number of a star is such a quantity, because it is conserved as long as there is no flow of baryons across the boundary, *i.e.*, as long as there are no accretion or evaporation of matter at the surface. The conserved baryon number current, j^μ, is related to the proper baryon number density, n, by

$$n(r) = u_\mu(r) j^\mu(r) = \sqrt{g_{00}(r)}\, j^0(r) = e^{\nu(r)} j^0(r), \tag{2.79}$$

where the fluid four-velocity, u_μ, is given by (2.46). The proper baryon number density, *i.e.*, the baryon number density in a local inertial frame, should be deduced from the microscopic theory used to calculate the EoS. In absence of gravity, the total conserved charge is obtained by integration of j^0 over the volume of the space. In a strong gravitational field, the ordinary volume element has to be replaced with the invariant volume element, $\sqrt{-g}\, d^4x$, where $g = \det(g_{\mu\nu})$ is the determinant of the metric. It follows from (2.6) that

$$\sqrt{-g} = e^{\nu(r)+\lambda(r)} r^2 \sin\theta. \tag{2.80}$$

Consequently, the total baryon number, N, of a star can be obtained by an integral over the volume, V, of the star at definite time,

$$N = \int_V d^3x\, \sqrt{-g} j^0(r) = 4\pi \int_0^R dr\, e^{\nu(r)+\lambda(r)} r^2 j^0(r). \tag{2.81}$$

With the expression for the proper baryon number density (2.79), this integral simplifies to

$$N = 4\pi \int_0^R dr\, e^{\lambda(r)} r^2 n(r) = 4\pi \int_0^R dr\, \left[1 - \frac{2GM(r)}{r}\right]^{-1/2} r^2 n(r), \tag{2.82}$$

where $M(r)$ is defined by (2.53).

In general, it is the baryon current j^μ that is conserved. While the derivation above suggests that this implies that also the total baryon number, N, of a star should be conserved, this could need a formal justification. To this end, the following standard result for the relation between the covariant divergence and the ordinary divergence of a vector field, A^μ, is needed

$$\sqrt{-g}A^\mu{}_{;\mu} = \left(\sqrt{-g}A^\mu\right)_{,\mu}. \tag{2.83}$$

This relation can be obtained from (2.9) and (2.11) through a cofactor expansion of the determinant. Now, if A^μ is a conserved current, it follows that

$$A^\mu{}_{;\mu} = 0 \quad \Longrightarrow \quad \left(\sqrt{-g}A^\mu\right)_{,\mu} = 0. \tag{2.84}$$

Separate the time component from the spatial components,

$$\left(\sqrt{-g}A^0\right)_{,0} = -\left(\sqrt{-g}A^i\right)_{,i}, \tag{2.85}$$

and integrate the result over the volume of the star at definite time,

$$\int_V d^3x \, \left(\sqrt{-g}A^0\right)_{,0} = -\int_V d^3x \, \left(\sqrt{-g}A^i\right)_{,i}. \tag{2.86}$$

The integral on the right-hand side can be transformed into a surface integral with Gauss' theorem,

$$\int_V d^3x \, \left(\sqrt{-g}A^i\right)_{,i} = \int_S \sqrt{-g}\mathbf{A}\cdot d\mathbf{S}, \tag{2.87}$$

where S represents the surface of the star. If there is no three-current, $\sqrt{-g}\mathbf{A}$, crossing the surface of the star, the right-hand side of (2.87) vanishes. Consequently, the integral on the left-hand side of (2.86) vanishes,

$$\begin{aligned} \int_V d^3x \, \left(\sqrt{-g}A^0\right)_{,0} = 0 \quad &\Longrightarrow \quad \frac{\partial}{\partial t}\int_V d^3x \, \sqrt{-g}A^0 = 0 \\ &\Longrightarrow \quad \int_V d^3x \, \sqrt{-g}A^0 = \text{constant}, \end{aligned} \tag{2.88}$$

which means that the total charge of the current A^μ is conserved.

The total baryon number of a star (2.82) is conserved as long as there are no accretion and evaporation of matter at the surface. As mentioned above, it is therefore useful in calculations of compact star evolution. For example, in order to calculate the changes of the mass and the radius of a star as it cools from one temperature, T_1, to a temperature $T_2 < T_1$, one can proceed in the following way. Two EsoS are prepared, one for each temperature. The two compact star sequences corresponding to these two EsoS are calculated, and for each temperature the baryon numbers, N, masses, M, and radii, R, are stored in a table. The result is obtained by comparing

the masses and radii in these two tables, for rows with equal baryon number. For further information and more examples, see Paper III and Paper VII. See also the discussion of thermal equilibrium in the next section. The baryon number can be used also to estimate the gravitational binding energy of a star, since the difference between the gravitational mass, M, and the mass of an equivalent number of neutrons, $M_A = Nm_n$, is essentially due to gravitational binding.

2.10 Equilibrium temperature

Thermodynamic potentials are defined in a local inertial frame for each matter element. How, then, are the thermodynamic equilibrium conditions for the matter elements modified in the presence of a gravitational field? In Section 2.8, the redshift of photons emitted from the surface of a compact star is discussed. Due to gravitational time dilation, which is a consequence of the radial dependence of the metric function g_{00}, two observers located at different distances from the surface measure different frequencies for two identical photons emitted from the star. Now, imagine that two parallel plates are placed at slightly different distances from the surface of a compact star. The plates are heated up and then isolated from the environment. What will the temperature of the two plates be when they are in thermal equilibrium? The plates exchange energy mainly by emission of photons. The photons emitted from the lower (upper) plate are redshifted (blueshifted) on their journey towards the other plate. A vanishing net flow of energy in-between the plates therefore requires that the lower plate has higher temperature than the upper plate. As two systems are in thermal equilibrium only if the net flow of energy in-between them vanishes, the plates must have different temperatures to be in thermal equilibrium. The same applies to matter elements in the interior of a compact star, because the metric varies over the radius of the star. In the following, I will derive an expression for the equilibrium temperature distribution in a compact star.

As this discussion is limited to static stars, it is convenient to consider the equilibrium condition in an external gravitational field, where the metric function $g_{00}(r) = e^{2\nu(r)}$ is given by (2.70)-(2.71). The benefit of this strategy is that one does not have to account for the change in the gravitational field caused by the transfer of energy (or particles) between matter elements. This simplified model is equivalent to an exact formulation if first-order variations are considered only. If second-order variations are needed, *e.g.*, in an investigation of the stability of the equilibrium distribution, it is not possible to formulate the equations in an external field. However, as the goal here is to obtain an expression for the equilibrium temperature, $T(r)$, the external field formulation can be applied.

The energy, E, of a particle in a local inertial frame is related to its energy, E_0, in the rest frame of the compact star by

$$E_0 = \sqrt{g_{00}(r)}\, E = e^{\nu(r)} E. \tag{2.89}$$

If a particle moves in the gravitational field, it is the quantity E_0 that is conserved. The equilibrium condition can be formulated with a standard variational principle: for a given entropy and particle number, the energy of the star should be a minimum. If the energy in an infinitesimal volume of space changes, without any change in the density of particles, n, the temperature is defined by $T = \partial E/\partial S|_n$, where S is the entropy per particle. Denoting the proper volume of a fluid element with $dV = 4\pi e^{\lambda(r)} r^2 dr$, see (2.80), the total energy of all particles is

$$\int_V dV\, E_0 n = \int_V dV\, e^{\nu(r)} E n. \tag{2.90}$$

This expression should be minimised subject to the additional constraint that the total entropy of the star is constant,

$$\int_V dV\, Sn = \text{constant} \quad \Longrightarrow \quad \delta \int_V dV\, Sn = 0. \tag{2.91}$$

Consequently, the equilibrium condition is (the variations of $\nu(r)$ and n vanishes)

$$\begin{aligned} \int_V dV\, n \left(e^{\nu(r)} \delta E - \Lambda \delta S \right) &= \int_V dV\, n \delta S \left(e^{\nu(r)} \frac{\partial E}{\partial S} - \Lambda \right) \\ &= \int_V dV\, n \delta S \left(e^{\nu(r)} T - \Lambda \right) = 0, \end{aligned} \tag{2.92}$$

where Λ is a Lagrange multiplier. It follows that

$$e^{\nu(r)} T(r) = \sqrt{g_{00}(r)}\, T(r) = \Lambda = \text{constant}. \tag{2.93}$$

This expression can be applied in the following way. Consider a compact star with central temperature $T(0)$ that cools slowly by surface emission. If the cooling rate is low and the thermal conductivity is sufficiently high, the matter elements within the star are in thermal (quasi-) equilibrium. According to (2.93), the product $e^{\nu(r)} T(r)$ should therefore be constant inside the star. This leads to an expression for the temperature distribution,

$$T(r) = T(0) e^{\nu(0) - \nu(r)}. \tag{2.94}$$

Observe that this relation holds also when the function $\nu(r)$ is unknown up to a linear transformation. It is therefore not necessary to apply the transformation rule (2.71) before calculating the equilibrium temperature $T(r)$. This simplifies the computational problem considerably, as $T(r)$ can be computed in parallel with the integration of the hydrostatic equations, and the correct EoS can be computed/looked up for each integration step. For more information and further examples on how to model finite temperatures in compact stars, see, *e.g.*, [19, 20], Paper III and Paper VII.

2.11 Limiting mass and stability

Some properties of the general-relativistic hydrostatic equations, (2.53) and (2.60), are not present in the newtonian weak-field analogy, (2.2) and (2.3). In general relativity, all forms of energy contributes to gravity, while in Newton's theory, the strength of the gravitational field depends only on the mass-density. The factor $(p + \epsilon)$ on the right-hand side of (2.60) shows that in general relativity, pressure does not only support a star against gravitational collapse, but it also contributes to the strength of the gravitational force. Consequently, with increasing central pressure, the gradient of the pressure, $-dp/dr$, increases. It is then possible, and this is indeed the case, that for sufficiently high central pressures, the radius decreases with increasing central pressure. The compact star sequence therefore has a maximal mass for some critical value of the central pressure, which depends on the EoS. This maximum mass is referred to as the 'limiting mass' of the compact star sequence. Examples of this feature of the general relativistic hydrostatic equations can be found in all appended papers, except Paper IV and Paper VI.

The solutions of the equations (2.53) and (2.60) represent stellar configurations in hydrostatic equilibrium. However, equilibrium does not assure stability, because it may correspond either to a maximum or to a minimum of the gravitational mass $(= E/c^2)$ of the star. This is analogous with a classical rigid-body pendulum, which has one stable equilibrium position (hanging down) and one unstable equilibrium position (standing up). The details of the stability analysis for compact stars is beyond the scope of this introduction. A pedagogical derivation of the stability equations can be found in Chapter 26 of [8], and a formulation that is convenient to use in practical calculations is provided in [21]. An application of the stability equations can be found in Paper I. In principle, the stability equations are obtained from an analysis of the radial eigenmode vibrations of stellar configurations. An instability is characterised by an eigenmode amplitude that grows (exponentially) in time. The eigenmode equation can be formulated as a Sturm-Liouville boundary value problem. A necessary, but not sufficient, condition for stability is that the gravitational mass is an increasing function of the central density,

$$\left.\frac{\partial M(\epsilon)}{\partial \epsilon}\right|_{r=0} > 0. \tag{2.95}$$

A detailed analysis of the stability equations shows that a compact star sequence can turn from stability to instability, or vice versa, only at values of the central density where the equilibrium mass is stationary,

$$\left.\frac{\partial M(\epsilon)}{\partial \epsilon}\right|_{r=0} = 0. \tag{2.96}$$

Consequently, the maximum mass configuration of a compact star sequence is at the onset of instability. Stability may be restored at higher densities only if the

EoS changes such that the condition (2.95) is satisfied, and the amplitudes of the radial eigenmodes are well-behaved. White dwarf sequences[4] become unstable at the maximum mass configuration, and stability is restored only when the degeneracy pressure of nuclei stabilises a new class of compact stars, the neutron stars. In some particular models of the high-density equation of state, where, *e.g.*, a transition to strange quark matter causes a large discontinuity in the speed of sound, stable stellar configurations with central densities higher than that of the maximum mass neutron/hybrid star exist [22–25], see also Paper III and Paper VII. In Paper I it is suggested that if quarks and leptons are composite particles, a stable sequence of compact stars could exist at still higher density. This hypothesis is further discussed in Paper II and Paper VI.

[4] A white dwarf sequence is not unique, because the EoS depends on the chemical composition of the star. See, *e.g.*, Chapter 3 in [5].

Chapter 3

Thermal Quantum Field Theory

Thermal quantum field theory (or thermal field theory, TFT for short) is extensively used, *e.g.*, in high-energy physics and astrophysics. It is an invaluable tool in the development of models of high-density matter in compact stars. TFT is used to calculate expectation values of physical observables of a quantum field theory (QFT), *e.g.*, pressures, energy densities and particle number densities. The models of colour superconducting quark matter described in Paper III, Paper IV, Paper V, and Paper VII were derived with TFT methods. In this chapter, I will introduce some of the basic concepts needed to follow the discussions in these papers. There are many textbooks on the subject, and a proper review is beyond the scope of this thesis. The interested reader is therefore referred to the literature for further information, *e.g.*, [26], which I find particularly useful. Most concepts discussed in this chapter originates from that book, except the Hubbard-Stratonovich transformations derived in Section 3.7. A number of different formulations of TFT exist, *e.g.*, the method of second quantisation, which is the customary approach to non-relativistic many-body theory, the imaginary-time formalism, which I will adopt here, and the real-time formalism, see, *e.g.*, [27] for details about these different approaches. In the imaginary-time formalism (sometimes referred to as the Matsubara formalism), expectation values of operators are essentially expressed as a sum of "probability amplitudes" in imaginary time, $t = 0 \to i\beta$, by analytic continuation. Here, $\beta = (k_B T)^{-1}$, k_B is Boltzmann's constant, and T is the temperature. An advantage of this approach is that calculations can be carried out with the same tools as in QFT, *e.g.*, functional integrals and Feynman diagrams, with the difference that the time coordinate is defined on a compact interval. In momentum space, this corresponds to a replacement of continuous frequencies with discrete, so-called Matsubara frequencies. I will return to the details of this method in the subsequent sections. The units used in this chapter are such that $\hbar = c = k_B = 1$, see Appendix A.1 for details.

3.1 Second quantisation

One approach to nonrelativistic many-body theory is the method of second quantisation. Before continuing with an alternative approach, which provides the theoretical framework for the quark matter models developed in this thesis, it is instructive to consider an example of second quantisation. To this end, consider a system with one fermionic degree of freedom. This system has two possible states, the vacuum state, $|0\rangle$, and the occupied state, $|1\rangle$. This is due to the Pauli exclusion principle, which forbids the occupation of a particle state by more than one fermion. By introducing particle creation and annihilation operators, $\alpha^\dagger$ and α, these states transform as

$$\alpha^\dagger|0\rangle = |1\rangle, \quad \alpha^\dagger|1\rangle = 0, \quad \alpha|1\rangle = |0\rangle, \quad \alpha|0\rangle = 0. \tag{3.1}$$

The particle number operator is $\hat{N} = \alpha^\dagger\alpha$, because

$$\hat{N}|0\rangle = \alpha^\dagger\alpha|0\rangle = 0, \quad \hat{N}|1\rangle = \alpha^\dagger\alpha|1\rangle = |1\rangle. \tag{3.2}$$

It follows that the creation and annihilation operators satisfy the anticommutation relation $\{\alpha, \alpha^\dagger\} = 1$. Neglecting the zero-point energy of the vacuum, which can be done without loss of generality as long as the vacuum is not affected by a background field, *e.g.*, as in the Casimir effect, the hamiltonian is

$$H = \omega\hat{N}. \tag{3.3}$$

Here $\omega = \omega(p)$ is the dispersion relation, *e.g.*, for a free relativistic particle $\omega = (p^2 + m^2)^{\frac{1}{2}}$, where p and m are the momentum and mass of the particle. The grand canonical partition function is

$$\begin{aligned} Z &= \operatorname{Tr} e^{-\beta(H-\mu\hat{N})} = \sum_{n=0}^{1}\langle n|e^{-\beta(H-\mu\hat{N})}|n\rangle = \sum_{n=0}^{1}\langle n|e^{-\beta(\omega-\mu)\hat{N}}|n\rangle \\ &= \sum_{n=0}^{1} e^{-\beta(\omega-\mu)n} = 1 + e^{-\beta(\omega-\mu)}, \end{aligned} \tag{3.4}$$

where μ is the fermion number chemical potential. The partition function is the single most important function in thermodynamics. From it, all other standard thermodynamic properties can be determined. For example, in the infinite-volume limit, the pressure, particle number, entropy, and energy of the system are

$$\begin{aligned} P &= T\frac{\partial \ln Z}{\partial V}, \qquad N_i = T\frac{\partial \ln Z}{\partial \mu_i}, \\ S &= \frac{\partial(T \ln Z)}{\partial T}, \qquad E = -PV + TS + \mu_i N_i. \end{aligned} \tag{3.5}$$

It follows from (3.4) that the mean number of fermions in the system is

$$N = T\frac{\partial}{\partial\mu}\ln Z = \frac{1}{e^{\beta(\omega-\mu)}+1}. \tag{3.6}$$

This is the Fermi-Dirac distribution function.

While second quantisation can be used also to solve complex problems, the method of choice for most theorists nowadays is a functional integral representation of the partition function, as many useful concepts and theoretical tools developed in QFT can be carried over to this formulation. In the following, I will briefly introduce the imaginary-time formalism and some techniques used in the appended papers.

3.2 Transition amplitude for bosons

As briefly mentioned at the beginning of this chapter, the partition function can be obtained from a transition amplitude by a transformation of the time coordinate. In this section, I will derive an expression for the transition amplitude for bosons. This result can then be used to formulate a functional integral representation of the partition function. To this end, consider a boson field operator $\hat{\phi}(0,\mathbf{x})$ at time $t=0$. The eigenstates, $|\phi\rangle$, and eigenvalues, $\phi(\mathbf{x})$, of the operator satisfy

$$\hat{\phi}(0,\mathbf{x})|\phi\rangle = \phi(\mathbf{x})|\phi\rangle. \tag{3.7}$$

The eigenstates constitute an orthonormal basis for the space, *i.e.*, the set of eigenstates is both orthonormal and complete,

$$\int d\phi(\mathbf{x})\,|\phi\rangle\langle\phi| = 1, \tag{3.8}$$

$$\langle\phi_a|\phi_b\rangle = \delta\left(\phi_a(\mathbf{x}) - \phi_b(\mathbf{x})\right). \tag{3.9}$$

In quantum mechanics, eigenstates of the position operator are related to eigenstates of the momentum operator by

$$\langle x|p\rangle = e^{ipx}. \tag{3.10}$$

Consequently, one can choose to work either in position space or in momentum space. Analogously, in quantum field theory there is a conjugate momentum field operator $\hat{\pi}(0,\mathbf{x})$, with eigenstates $|\pi\rangle$, and eigenvalues $\pi(\mathbf{x})$. The completeness and orthogonality conditions are

$$\int \frac{d\pi(\mathbf{x})}{2\pi}\,|\pi\rangle\langle\pi| = 1, \tag{3.11}$$

$$\langle\pi_a|\pi_b\rangle = \delta\left(\pi_a(\mathbf{x}) - \pi_b(\mathbf{x})\right), \tag{3.12}$$

and the overlap is

$$\langle\phi|\pi\rangle = \exp\left[i\int d^3x\,\pi(\mathbf{x})\phi(\mathbf{x})\right]. \tag{3.13}$$

Now, consider a system described by a hamiltonian $H = H(\pi, \phi)$, which is in a state $|\phi_a\rangle$ at time $t = 0$. After a time $t = t_f > 0$, the system has evolved into a new state $|\phi_b\rangle = e^{-iHt_f}|\phi_a\rangle$. In general, the probability amplitude for the system to evolve from a state $|\phi_a\rangle$ to a state $|\phi_b\rangle$ in a time t_f is $\langle\phi_b|e^{-iHt_f}|\phi_a\rangle$. As I will show later, the transition amplitude of interest for the derivation of the partition function is $\langle\phi_a|e^{-iHt_f}|\phi_a\rangle$, *i.e.*, the probability for the system to return to its initial state after a time t_f. One can calculate this amplitude by dividing the time interval $(0, t_f)$ into N intervals of equal duration $\Delta t = t_f/N$, and inserting the identities (3.8) and (3.11) in the following way

$$\begin{aligned}\langle\phi_a|e^{-iHt_f}|\phi_a\rangle &= \lim_{N\to\infty}\int\left(\prod_{i=1}^{N}\frac{d\pi_i d\phi_i}{2\pi}\right)\\ &\times\langle\phi_a|\pi_N\rangle\langle\pi_N|e^{-iH\Delta t}|\phi_N\rangle\\ &\times\langle\phi_N|\pi_{N-1}\rangle\langle\pi_{N-1}|e^{-iH\Delta t}|\phi_{N-1}\rangle\\ &\times\langle\phi_{N-1}|\pi_{N-2}\rangle\langle\pi_{N-2}|e^{-iH\Delta t}|\phi_{N-2}\rangle\\ &\times\ldots\\ &\times\langle\phi_2|\pi_1\rangle\langle\pi_1|e^{-iH\Delta t}|\phi_1\rangle\langle\phi_1|\phi_a\rangle. \qquad (3.14)\end{aligned}$$

Note that the expression on the right-hand side simplifies to a product of N exponential functions of the form $\exp(-iH\Delta t)$. After summing the exponents one obtains the expression on the left-hand side. According to the orthogonality condition (3.9), the last factor is

$$\langle\phi_1|\phi_a\rangle = \delta(\phi_1 - \phi_a), \qquad (3.15)$$

and the factors on the form $\langle\phi_i|\pi_{i-1}\rangle$ can be expressed using the overlap (3.13),

$$\langle\phi_i|\pi_{i-1}\rangle = \exp\left[i\int d^3x\,\pi_{i-1}(\mathbf{x})\phi_i(\mathbf{x})\right]. \qquad (3.16)$$

As usual, the hamiltonian can be expressed as an integral of the hamiltonian density,

$$H = \int d^3x\,\mathcal{H}(\pi, \phi). \qquad (3.17)$$

Because $N \to \infty$, and, consequently, $\Delta t \to 0$, the other factors of (3.14) can be expanded in the following way,

$$\begin{aligned}\langle\pi_i|e^{-iH\Delta t}|\phi_i\rangle &= \langle\pi_i|1 - iH\Delta t + \ldots|\phi_i\rangle\\ &= \langle\pi_i|\phi_i\rangle\left[1 - i\Delta t H_i + \ldots\right], \qquad (3.18)\end{aligned}$$

where

$$\begin{aligned}\langle\pi_i|\phi_i\rangle &= \exp\left[-i\int d^3x\,\pi_i(\mathbf{x})\phi_i(\mathbf{x})\right], \qquad (3.19)\\ H_i &= \int d^3x\,\mathcal{H}(\pi_i(\mathbf{x}), \phi_i(\mathbf{x})). \qquad (3.20)\end{aligned}$$

Using (3.15)-(3.16), and (3.18), the amplitude (3.14) becomes

$$\begin{aligned}\langle\phi_a|e^{-iHt_f}|\phi_a\rangle &= \lim_{N\to\infty}\int\left(\prod_{i=1}^{N}\frac{d\pi_i d\phi_i}{2\pi}\right)\delta\left(\phi_1-\phi_a\right)\\ &\times\exp\left(i\int d^3x\,\pi_1\phi_2+\pi_2\phi_3+\ldots+\pi_{N-1}\phi_N+\pi_N\phi_a\right)\\ &\times\exp\left(-i\int d^3x\sum_{j=1}^{N}\pi_j\phi_j\right)\\ &\times\exp\left[-i\Delta t\int d^3x\sum_{k=1}^{N}\mathcal{H}(\pi_k,\phi_k)\right]. \end{aligned}\tag{3.21}$$

This expression simplifies to

$$\begin{aligned}\langle\phi_a|e^{-iHt_f}|\phi_a\rangle &= \lim_{N\to\infty}\int\left(\prod_{i=1}^{N}\frac{d\pi_i d\phi_i}{2\pi}\right)\delta\left(\phi_1-\phi_a\right)\\ &\times\exp\left\{i\Delta t\sum_{j=1}^{N}\int d^3x\,\left[\pi_j\frac{(\phi_{j+1}-\phi_j)}{\Delta t}-\mathcal{H}(\pi_j,\phi_j)\right]\right\}, \end{aligned}\tag{3.22}$$

where it follows from (3.21) that $\phi_{N+1}\equiv\phi_a$. This means that the field should return to its initial state after a time t_f, as requested, and the delta function assures that $\phi_1=\phi_a$. In the continuum limit, $N\to\infty$, the integrals in (3.22) turn into functional integrals, because at each instant of time, the function values are integrated from $-\infty$ to $+\infty$. Consequently, the amplitude is

$$\begin{aligned}\langle\phi_a|e^{-iHt_f}|\phi_a\rangle &= \int\mathcal{D}\pi\int_{\phi(0,\mathbf{x})=\phi_a(\mathbf{x})}^{\phi(t_f,\mathbf{x})=\phi_a(\mathbf{x})}\mathcal{D}\phi\\ &\times\exp\left\{i\int_0^{t_f}dt\int d^3x\,\left[\pi(t,\mathbf{x})\frac{\partial\phi(t,\mathbf{x})}{\partial t}-\mathcal{H}(\pi(t,\mathbf{x}),\phi(t,\mathbf{x}))\right]\right\}, \end{aligned}\tag{3.23}$$

where $\mathcal{D}\pi$ and $\mathcal{D}\phi$ are functional integral measures. The integration over $\phi(t,\mathbf{x})$ is constrained such that the field returns to its initial value after a time t_f, while the integration over $\pi(t,\mathbf{x})$ is unrestricted. Note that π and ϕ in (3.23) are scalar fields, so there are no operators left in this expression. Next, I will show how the partition function for bosons can be obtained from this result.

3.3 Partition function for bosons

The general form of the grand canonical partition function is

$$Z = \mathrm{Tr}\,e^{-\beta(H-\mu_i\hat{N}_i)}=\int d\phi_a\,\langle\phi_a|e^{-\beta(H-\mu_i\hat{N}_i)}|\phi_a\rangle,\tag{3.24}$$

where $\hat{N}_i$ are the number operators of the conserved charges, and μ_i are the corresponding chemical potentials. This is the generalisation of (3.4), introduced in Section 3.1, to a system with a continuously infinite number of degrees of freedom. The partition function can be expressed in the probability amplitude (3.23) by the following substitutions: the time coordinate in (3.23) is replaced by an imaginary "time" coordinate $\tau = it$ (a so-called Wick rotation[1]), which is integrated from 0 to β, and the hamiltonian density is replaced with

$$\mathcal{H}(\pi(t,\mathbf{x}),\phi(t,\mathbf{x})) \longrightarrow \mathcal{H}(\pi(t,\mathbf{x}),\phi(t,\mathbf{x})) - \mu_i \mathcal{N}_i(\pi(t,\mathbf{x}),\phi(t,\mathbf{x})), \tag{3.25}$$

were $\mathcal{N}_i(\pi(t,\mathbf{x}),\phi(t,\mathbf{x}))$ are the conserved charge densities. The partition function is then obtained by integration of the transformed amplitude over all initial states, $\phi_a(\mathbf{x})$. The result is

$$Z = \int \mathcal{D}\pi \int_{\text{periodic}} \mathcal{D}\phi \exp\left\{ \int_0^\beta d\tau \int d^3x \left[i\pi \frac{\partial \phi}{\partial \tau} - \mathcal{H}(\pi,\phi) + \mu_i \mathcal{N}_i(\pi,\phi) \right] \right\}. \tag{3.26}$$

Here, periodic means that the functions, ϕ, should satisfy the condition $\phi(0,\mathbf{x}) = \phi(\beta,\mathbf{x})$. There are no constraints on the integration over π functions.

3.4 Neutral scalar field

In order to see how the partition function (3.26) can be evaluated in practise, consider the lagrangian density for a non-interacting neutral scalar field

$$\mathcal{L} = \frac{1}{2}\partial_\mu \phi \partial^\mu \phi - \frac{1}{2} m^2 \phi^2. \tag{3.27}$$

The conjugate momentum is

$$\pi = \frac{\partial \mathcal{L}}{\partial(\partial_0 \phi)} = \frac{\partial \phi}{\partial t}, \tag{3.28}$$

and the standard relation between the lagrangian and hamiltonian densities is

$$\mathcal{H} = \pi \frac{\partial \phi}{\partial t} - \mathcal{L} = \frac{1}{2}\left[\pi^2 + (\nabla\phi)^2 + m^2\phi^2 \right]. \tag{3.29}$$

There is no conserved charge, because the mass term breaks translational invariance. In order to evaluate the partition function, it is convenient to start with the

[1] Under a rotation of the time coordinate in the complex plane by an angle of $\pi/2$, the Minkowski metric is transformed to the Euclidean metric, and vice versa, because the invariant line element differs only in the sign of the dt^2 term.

discretised version of (3.26), *i.e.*, (3.22) with a modified ϕ integral. With (3.29) the partition function then is

$$Z = \lim_{N\to\infty}\left(\prod_{i=1}^{N}\int_{-\infty}^{\infty}\frac{d\pi_i}{2\pi}\int_{\text{periodic}}d\phi_i\right)\exp\Bigg\{\Delta\tau\sum_{j=1}^{N}\int d^3x\Big[\frac{i\pi_j(\phi_{j+1}-\phi_j)}{\Delta\tau} - \frac{1}{2}\left(\pi_j^2+(\nabla\phi_j)^2+m^2\phi_j^2\right)\Big]\Bigg\}. \tag{3.30}$$

By expanding the integral over spatial coordinates in the exponential, *e.g.*, as (the limit of) a Riemann sum, and changing the order of integration, the integrals over conjugate momenta are gaussian and can be evaluated using the standard result

$$\int_{-\infty}^{\infty}dx\,e^{-ax^2+bx} = \sqrt{\frac{\pi}{a}}e^{b^2/(4a)}. \tag{3.31}$$

The gaussian integrals are on the form

$$\frac{1}{2\pi}\int_{-\infty}^{\infty}d\pi_j\exp\left[-\frac{1}{2}\pi_j^2+\frac{i(\phi_{j+1}-\phi_j)}{\Delta\tau}\pi_j\right], \tag{3.32}$$

so it follows from (3.31) that each integral gives rise to a factor

$$(2\pi)^{-\frac{1}{2}}\exp\left[-\frac{1}{2}\left(\frac{\phi_{j+1}-\phi_j}{\Delta\tau}\right)^2\right]. \tag{3.33}$$

The partition function (3.30) can therefore be written

$$Z = N'\lim_{N\to\infty}\left(\prod_{i=1}^{N}\int_{\text{periodic}}d\phi_i\right)\exp\Bigg\{\Delta\tau\sum_{j=1}^{N}\int d^3x\Big[-\frac{1}{2}\left(\frac{\phi_{j+1}-\phi_j}{\Delta\tau}\right)^2 - \frac{1}{2}(\nabla\phi_j)^2-\frac{1}{2}m^2\phi_j^2\Big]\Bigg\}, \tag{3.34}$$

where N' denotes the product of the constant factor in (3.33). This factor is irrelevant, because the multiplication of Z by any constant does not change the thermodynamics. In the continuum limit, $N\to\infty$, this expression becomes

$$Z = N'\int_{\text{periodic}}\mathcal{D}\phi\exp\left(\int_0^\beta d\tau\int d^3x\;\mathcal{L}\right). \tag{3.35}$$

This result holds also if interaction terms are present in the lagrangian, because such terms depend on ϕ only and do not alter the derivation.

The functional integral in (3.35) can be evaluated in the following way. Define

$$S = \int_0^\beta d\tau \int d^3x \; \mathcal{L} = -\frac{1}{2}\int_0^\beta d\tau \int d^3x \; \left[\left(\frac{\partial\phi}{\partial\tau}\right)^2 + (\nabla\phi)^2 + m^2\phi^2\right]. \tag{3.36}$$

Using the periodicity constraint on ϕ, this expression can be integrated by parts and becomes

$$S = \frac{1}{2}\int_0^\beta d\tau \int d^3x \; \phi\left(\frac{\partial^2}{\partial\tau^2} + \nabla^2 - m^2\right)\phi. \tag{3.37}$$

Now, expand the field in a Fourier series

$$\phi(\tau, \mathbf{x}) = \left(\frac{\beta}{V}\right)^{\frac{1}{2}} \sum_{n=-\infty}^{\infty} \sum_{\mathbf{p}} e^{i(\mathbf{p}\cdot\mathbf{x}+\omega_n\tau)}\phi_n(\mathbf{p}), \tag{3.38}$$

where the normalisation constant is chosen such that the Fourier amplitudes are dimensionless. The periodicity constraint, $\phi(0, \mathbf{x}) = \phi(\beta, \mathbf{x})$, requires that the Fourier frequencies are chosen as

$$\omega_n = \frac{2\pi}{\beta}n = 2\pi nT. \qquad \text{(Bosons)} \tag{3.39}$$

Since ϕ is a scalar (real-valued) field, the basis functions satisfy $\phi_{-n}(-\mathbf{p}) = \phi_n^*(\mathbf{p})$. With (3.38), the expression (3.37) then becomes

$$S = -\frac{\beta^2}{2}\sum_n \sum_{\mathbf{p}} \left(\omega_n^2 + \mathbf{p}^2 + m^2\right)|\phi_n(\mathbf{p})|^2, \tag{3.40}$$

where the volume in (3.38) is cancelled by the integration over spatial coordinates, and there is an extra factor β coming from the integral over τ. The choice of normalisation in (3.38) now makes sense. As usual the dispersion relation is

$$\omega = \left(\mathbf{p}^2 + m^2\right)^{1/2}. \tag{3.41}$$

The partition function (3.35) can be expressed in S, and the functional integral over ϕ translates into an integral over the Fourier amplitudes[2],

$$Z = N' \prod_n \prod_{\mathbf{p}} \int_{-\infty}^{\infty} d|\phi_n(\mathbf{p})| \exp\left[-\frac{\beta^2}{2}\left(\omega_n^2 + \omega^2\right)|\phi_n(\mathbf{p})|^2\right]. \tag{3.42}$$

[2]This is a standard method to evaluate functional integrals over periodic functions. For a particular function ϕ, the Fourier amplitudes have fixed values, which are given by the inner products of ϕ and the orthonormal basis functions. All functions on the compact interval can be accounted for by integrating over all values and combinations of Fourier amplitudes.

This is a gaussian integral, which can be evaluated using (3.31). The result is

$$Z = N' \prod_n \prod_{\mathbf{p}} \left[\frac{2\pi}{\beta^2 \left(\omega_n^2 + \omega^2\right)} \right]^{\frac{1}{2}}. \tag{3.43}$$

Neglecting an overall constant factor, which does not affect the thermodynamics, the logarithm of the partition function is

$$\ln Z = -\frac{1}{2} \sum_n \sum_{\mathbf{p}} \ln \left[\beta^2 \left(\omega_n^2 + \omega^2\right) \right]. \tag{3.44}$$

This expression can be evaluated using a method analogous to that described in Section 3.6, except that the boson Matsubara frequencies (3.39) should be used in place of the fermion Matsubara frequencies. Omitting irrelevant constant terms, the result is

$$\ln Z = V \int \frac{d^3p}{(2\pi)^3} \left[-\frac{1}{2}\beta\omega - \ln\left(1 - e^{-\beta\omega}\right) \right], \tag{3.45}$$

where the sum over momenta is approximated with an integral in the standard way. The pressure, entropy and energy of the system is

$$P = T\frac{\partial \ln Z}{\partial V} - P_0, \tag{3.46}$$

$$S = \frac{\partial (T \ln Z)}{\partial T}, \tag{3.47}$$

$$E = -PV + TS. \tag{3.48}$$

The expression (3.45) includes the zero-point energy. In order to get zero pressure in vacuum, the corresponding pressure should be subtracted,

$$P_0 = \lim_{T \to 0} T\frac{\partial \ln Z}{\partial V} = \int \frac{d^3p}{(2\pi)^3}\, \omega. \tag{3.49}$$

There is no conserved charge. While this result is of little practical use itself, the derivation leading from the lagrangian density of a scalar field (3.27) to the corresponding partition function (3.45) illustrates a procedure that can be carried over to more realistic models. For example, a complex boson field can be treated in a similar way, and the physical consequences of that model is already interesting, as it comprises a conserved charge that forms a Bose-Einstein condensate. More information and further examples can be found in, *e.g.*, [26]. This procedure can to some extent be generalised also to fermions, but obviously the Pauli principle needs to be accounted for. I will return to this issue in the next section.

3.5 Partition function for fermions

Fermions are essential building blocks of compact stars. The Pauli principle forbids two fermions to occupy the same state. Consequently, at high densities particles are forced to occupy high-momentum states, and therefore generate a high pressure, which counterbalances gravity. The lagrangian density for a system of non-interacting fermions is essentially given by the Dirac equation

$$\mathcal{L} = \bar{\psi}\left(i\partial\!\!\!/ - m\right)\psi, \tag{3.50}$$

where $\bar{\psi} \equiv \psi^\dagger\gamma^0$, and $\partial\!\!\!/ \equiv \gamma^\mu\partial_\mu = \gamma^\mu\partial/\partial x^\mu$. The Dirac matrices, γ^μ, are defined in Appendix B.2. After expanding the derivative operator, the lagrangian reads

$$\mathcal{L} = \psi^\dagger\gamma^0\left(i\gamma^0\frac{\partial}{\partial t} + i\gamma\cdot\nabla - m\right)\psi. \tag{3.51}$$

This expression has a global U(1) symmetry, as it is invariant with respect to a phase shift $\psi \to e^{-i\alpha}\psi$. Consequently, according to Noether's theorem[3] there is a conserved current. One can determine this current by letting α be an independent field, and then solve the Euler-Lagrange equation for this field. Under the transformation $\psi \to e^{-i\alpha(t,\mathbf{x})}\psi$, the lagrangian becomes

$$\mathcal{L} \longrightarrow \mathcal{L} + \bar{\psi}\left[\gamma^\mu\partial_\mu\alpha(t,\mathbf{x})\right]\psi. \tag{3.52}$$

The equation of motion for α is the Euler-Lagrange equation,

$$\partial_\mu\frac{\partial\mathcal{L}}{\partial[\partial_\mu\alpha(t,\mathbf{x})]} - \frac{\partial\mathcal{L}}{\partial\alpha(t,\mathbf{x})} = 0, \tag{3.53}$$

which yields

$$\partial_\mu\bar{\psi}\gamma^\mu\psi = 0. \tag{3.54}$$

The conservation law therefore is

$$\partial_\mu j^\mu = 0, \tag{3.55}$$

$$j^\mu = \bar{\psi}\gamma^\mu\psi, \tag{3.56}$$

where j^μ is the conserved current. The total conserved charge is

$$Q = \int d^3x\, j^0 = \int d^3x\, \psi^\dagger\gamma^0\gamma^0\psi = \int d^3x\, \psi^\dagger\psi. \tag{3.57}$$

[3] Briefly, Noether's theorem states that there is a conserved current for each continuous symmetry of the local actions. The theorem was published by Noether in the early 20th century, and is a central result in theoretical physics.

Now the conserved charge of the system is known, and the derivation of the partition function can be carried out in a similar way as for the scalar boson field. The conjugate momentum of the field ψ is

$$\Pi = \frac{\partial \mathcal{L}}{\partial(\partial\psi/\partial t)} = \psi^\dagger \gamma^0 i\gamma^0 = i\psi^\dagger. \tag{3.58}$$

Consequently, ψ and $\psi^\dagger$ are independent quantities that should be integrated separately. The hamiltonian density is

$$\mathcal{H} = \Pi \frac{\partial \psi}{\partial t} - \mathcal{L} = \psi^\dagger \left(i \frac{\partial}{\partial t} \right) \psi - \mathcal{L} = \psi^\dagger \gamma^0 \left(-i\gamma \cdot \nabla + m \right) \psi. \tag{3.59}$$

The partition function is obtained from the fundamental relation

$$Z = \operatorname{Tr} e^{-\beta(H - \mu \hat{N})}, \tag{3.60}$$

where the trace is evaluated by a procedure analogous to that leading up to (3.26). The result is

$$Z = \int \mathcal{D}i\psi^\dagger \, \mathcal{D}\psi \exp\left[\int_0^\beta d\tau \int d^3x \; \psi^\dagger \gamma^0 \left(-\gamma^0 \frac{\partial}{\partial \tau} + i\gamma \cdot \nabla - m + \mu\gamma^0 \right) \psi \right], \tag{3.61}$$

where μ is the chemical potential of the conserved charge. Next, expand the field in a Fourier series

$$\psi_\alpha(\tau, \mathbf{x}) = V^{-\frac{1}{2}} \sum_n \sum_{\mathbf{p}} e^{i(\mathbf{p}\cdot\mathbf{x} + \omega_n \tau)} \tilde{\psi}_{\alpha;\, n}(\mathbf{p}), \tag{3.62}$$

where the normalisation constant is chosen such that the Fourier amplitudes are dimensionless. In general, the frequencies, ω_n, have values $n\pi T$ for functions defined on the compact interval $0 \leq \tau \leq \beta$. The functional integral over ϕ in the partition function for bosons (3.26) is restricted to periodic functions, $\phi(0, \mathbf{x}) = \phi(\beta, \mathbf{x})$. This is a consequence of the equivalence between the partition function and an analytic continuation of the probability amplitude for the system to return to its initial state after a "time" β. A consequence of this periodicity is that only even frequencies are accounted for in the Fourier expansion of a boson field. For fermions the situation is somewhat different. As shown in Section 3.1, the Pauli principle implies that the fermion operators are anticommuting objects. A consequence of this property (see, *e.g.*, [26] for details) is that the fermion field is antiperiodic,

$$\psi(0, \mathbf{x}) = -\psi(\beta, \mathbf{x}). \tag{3.63}$$

It then follows from (3.62) that only odd frequencies should be summed over

$$\omega_n = (2n+1)\pi T. \qquad \text{(Fermions)} \tag{3.64}$$

These are the Matsubara frequencies for fermions. The antiperiodicity of fermion fields is not in contradiction with the derivation of the partition function, because the sign of ψ is related only to an irrelevant constant factor of the partition function. With (3.62), the partition function (3.61) can be written

$$\begin{aligned} Z &= \left[\prod_n \prod_{\mathbf{p}} \prod_{\alpha} \int i d\tilde{\psi}^{\dagger}_{\alpha;\,n}(\mathbf{p}) d\tilde{\psi}_{\alpha;\,n}(\mathbf{p})\right] e^{S}, && (3.65)\\ S &= \sum_n \sum_{\mathbf{p}} i\tilde{\psi}^{\dagger}_{\alpha;\,n}(\mathbf{p}) D_{\alpha\nu} \tilde{\psi}_{\nu;\,n}(\mathbf{p}), && (3.66)\\ D_{\alpha\nu} &= -i\beta\left[(-i\omega_n + \mu) - \gamma^0\gamma\cdot\mathbf{p} - \gamma^0 m\right]. && (3.67) \end{aligned}$$

In order to evaluate these integrals it is essential to account for the anticommuting character of the fermion fields. The integrals are therefore Berezin integrals [28] over Grassman variables, and the standard result needed here is

$$\int i d\psi^{\dagger}_1 d\psi_1 \ \ldots i d\psi^{\dagger}_N d\psi_N \, e^{i\psi^{\dagger}_{\alpha} D_{\alpha\nu} \psi_{\nu}} = \det D. \tag{3.68}$$

Consequently,

$$Z = \det D, \tag{3.69}$$

where D is given by (3.67). With the mathematical identity $\ln\det D = \mathrm{Tr}\,\ln D$, the logarithm of the partition function (3.69) can be written

$$\begin{aligned} \ln Z &= 2\sum_n \sum_{\mathbf{p}} \ln\left\{\beta^2\left[(\omega_n + i\mu)^2 + \omega^2\right]\right\} \\ &= \sum_n \sum_{\mathbf{p}} \left\{\ln\left[\beta^2\left(\omega_n^2 + (\omega-\mu)^2\right)\right] + \ln\left[\beta^2\left(\omega_n^2 + (\omega+\mu)^2\right)\right]\right\}. \end{aligned} \tag{3.70}$$

The sum over Matsubara frequencies, ω_n, is calculated in Section 3.6. By using that result and approximating the sum over momenta with an integral in the standard way, the partition function simplifies to

$$\ln Z = 2V \int \frac{d^3p}{(2\pi)^3} \left\{\beta\omega + \ln\left[1 + e^{-\beta(\omega-\mu)}\right] + \ln\left[1 + e^{-\beta(\omega+\mu)}\right]\right\}. \tag{3.71}$$

This result agrees with the result obtained by the method of second quantisation in Section 3.1, but it includes also the zero-point energy and the contribution from antifermions. The prefactor of 2 represents spin degeneracy. The pressure, fermion number, entropy, and energy of the system can be calculated with

$$\begin{aligned} P &= T\frac{\partial \ln Z}{\partial V}, \qquad N_i = T\frac{\partial \ln Z}{\partial \mu_i}, \\ S &= \frac{\partial (T\ln Z)}{\partial T}, \quad E = -PV + TS + \mu_i N_i, \end{aligned} \tag{3.72}$$

presuming that the zero-point contribution to the pressure of vacuum is subtracted in the proper way, see (3.49).

3.6 Matsubara sums

The sum over fermion Matsubara frequencies in (3.70) is frequently encountered in TFT, see, *e.g.*, Paper III. It is on the form

$$\sum_n \ln\left(\frac{\omega_n^2+\omega^2}{T^2}\right), \tag{3.73}$$

where $\omega_n = (2n+1)\pi T$ are the Matsubara frequencies for fermions. In order to evaluate this sum, first rewrite the logarithm as an integral and change the order of summation and integration,

$$\begin{aligned}\sum_{n=-\infty}^{\infty} \ln\left(\frac{\omega_n^2+\omega^2}{T^2}\right) &= \sum_{n=-\infty}^{\infty} \int_1^{\omega^2/T^2} \frac{d(\theta^2)}{\theta^2+(2n+1)^2\pi^2} + \ln\left[1+(2n+1)^2\pi^2\right] \\ &= \int_1^{\omega^2/T^2} \sum_{n=-\infty}^{\infty} \frac{d(\theta^2)}{\theta^2+(2n+1)^2\pi^2} + \sum_{n=-\infty}^{\infty} \ln\left[1+(2n+1)^2\pi^2\right]. \end{aligned} \tag{3.74}$$

The first sum in this expression can be evaluated with the standard residue summation formula

$$\sum_{n=-\infty}^{\infty} \frac{1}{(n-x)(n-y)} = \frac{\pi\left[\cot(\pi x)-\cot(\pi y)\right]}{y-x}. \tag{3.75}$$

The result is

$$\begin{aligned}\sum_{n=-\infty}^{\infty} \frac{1}{\theta^2+(2n+1)^2\pi^2} &= \frac{1}{4\pi^2} \sum_{n=-\infty}^{\infty} \frac{1}{(n-\frac{\pi-i\theta}{2\pi})(n-\frac{\pi+i\theta}{2\pi})} \\ &= \frac{1}{4\pi^2} \frac{\pi\left[\cot\left(\frac{\pi-i\theta}{2}\right)-\cot\left(\frac{\pi+i\theta}{2}\right)\right]}{4i\theta/\pi} = \frac{1}{2\theta}\tanh\left(\frac{\theta}{2}\right) = \frac{1}{\theta}\left(\frac{1}{2}-\frac{1}{e^\theta+1}\right). \end{aligned} \tag{3.76}$$

Equations (3.74) and (3.76) yield

$$\begin{aligned}\sum_{n=-\infty}^{\infty} \ln\left(\frac{\omega_n^2+\omega^2}{T^2}\right) &= \int_1^{\omega^2/T^2} d(\theta^2)\frac{1}{\theta}\left(\frac{1}{2}-\frac{1}{e^\theta+1}\right) + \sum_{n=-\infty}^{\infty} \ln\left[1+(2n+1)^2\pi^2\right] \\ &= -\frac{|\omega|}{T} + 2\ln(1+e^{|\omega|/T}) + 1 - 2\ln(1+e^1) + \sum_{n=-\infty}^{\infty} \ln\left[1+(2n+1)^2\pi^2\right] \\ &= -\frac{|\omega|}{T} + 2\ln\left[e^{|\omega|/T}(1+e^{-|\omega|/T})\right] + 1 - 2\ln(1+e^1) + \sum_{n=-\infty}^{\infty} \ln\left[1+(2n+1)^2\pi^2\right] \\ &= \frac{|\omega|}{T} + 2\ln(1+e^{-|\omega|/T}) + \left\{1 - 2\ln(1+e^1) + \sum_{n=-\infty}^{\infty} \ln\left[1+(2n+1)^2\pi^2\right]\right\}. \end{aligned} \tag{3.77}$$

Terms independent of T and ω do not contribute to the thermodynamics and are therefore omitted. The expression simplifies to

$$\sum_{n=-\infty}^{\infty} \ln\left(\frac{\omega_n^2+\omega^2}{T^2}\right) = \frac{\omega}{T} + 2\ln\left(1+e^{-\omega/T}\right), \tag{3.78}$$

where I have used the fact that the expression on the left-hand side of (3.77) is an even function of ω. In order to see that this holds also for the right-hand side of (3.78), consider the following difference

$$\begin{aligned} f(T,\omega) - f(T,-\omega) &= \frac{2\omega}{T} + 2\ln\left(1+e^{-\omega/T}\right) - 2\ln\left(1+e^{\omega/T}\right) \\ &= \frac{2\omega}{T} + 2\ln\left(\frac{1+e^{-\omega/T}}{1+e^{\omega/T}}\right) = \frac{2\omega}{T} + 2\ln\left(\frac{1+e^{-\omega/T}}{1+e^{\omega/T}} \times \frac{1-e^{-\omega/T}}{1-e^{-\omega/T}}\right) \\ &= \frac{2\omega}{T} + 2\ln\left(\frac{1-e^{-2\omega/T}}{e^{\omega/T}-e^{-\omega/T}}\right) = \frac{2\omega}{T} + 2\ln\left(\frac{1-e^{-2\omega/T}}{e^{\omega/T}(1-e^{-2\omega/T})}\right) \\ &= \frac{2\omega}{T} + 2\ln\left(e^{-\omega/T}\right) = \frac{2\omega}{T} - \frac{2\omega}{T} = 0. \end{aligned} \tag{3.79}$$

The lesson to learn here is that the Matsubara sum (3.78) is independent of the sign of the dispersion relations, $\omega(\mathbf{p},\ldots)$. In general, Matsubara sums can be more complicated than (3.73) when particle interactions are taken into account. If an analytical solution cannot be obtained, it is possible to evaluate the sum numerically if the divergent terms can be subtracted. It is not possible to evaluate (3.73) directly on a computer, due to the divergent sum on the right-hand side of (3.77). A solution to this problem is to subtract a Matsubara sum that can be evaluated analytically, such that the difference of the two sums is convergent. One can then recover the original Matsubara sum by adding the analytical solution of the subtracted sum, neglecting divergent terms. It is crucial to subtract a Matsubara sum that is "similar" to the sum that should be computed, in order to get (rapid) convergence. A nice heuristic example where this method has been used can be found in [29]. There is, however, an alternative strategy that is more straightforward. I will return to this issue in Chapter 5.

3.7 Hubbard-Stratonovich transformations

For interacting classical systems, it is customary to treat the interactions between particles as an interaction between each particle and a potential generated by the others. A well-known example is the mean-field approximation, where each particle interacts with the average potential of the others. A general method to replace two-body interactions with single bodies in an external field is the Hubbard-Stratonovich (HS) transformation [30, 31]. In field theory, HS transformations reduce quartic

(four-fermion) interaction terms to quadratic terms that are coupled to a collective boson field, a so-called auxiliary field. However, unlike mean-field approximations, HS transformations are mathematical identities that preserve the physics of the original model. In this section I will derive two HS transformation rules that will prove useful in Chapter 5, where interactions in quark matter are discussed.

To this end, consider the path integral over a charge-neutral boson field, ϕ,

$$\int \mathcal{D}\phi \exp\left[-\frac{1}{2}\int_0^\beta d\tau \int d^3x\ \phi D\phi\right] = (\det D)^{-\frac{1}{2}}, \tag{3.80}$$

where D is an operator in $(\tau,\, \mathbf{x})$ space. This formula follows from the product of gaussian integrals

$$\int_{-\infty}^{\infty} dx_1 \dots dx_n e^{-\frac{1}{2}x_\alpha D_{\alpha\nu} x_\nu} = (2\pi)^{n/2} (\det D)^{-\frac{1}{2}}\,. \tag{3.81}$$

The path integral is invariant with respect to a scalar shift of the field. The boson field can therefore be shifted with a scalar Dirac bilinear

$$\phi \longrightarrow \phi \pm 2g\bar{\psi}\mathcal{O}\psi, \tag{3.82}$$

where $\mathcal{O}$ is an operator and g is a coupling constant. The sign of the shift is arbitrary. With $D = \mathbb{1}/(2g)$, (3.80) and (3.82) yields

$$\begin{aligned}
&\int \mathcal{D}\phi \exp\left[-\frac{1}{2}\int_0^\beta d\tau \int d^3x\ (\phi \pm 2g\bar{\psi}\mathcal{O}\psi)\frac{\mathbb{1}}{2g}(\phi \pm 2g\bar{\psi}\mathcal{O}\psi)\right] \\
&\quad = \exp\left[-\int_0^\beta d\tau \int d^3x\ g(\bar{\psi}\mathcal{O}\psi)^2\right] \int \mathcal{D}\phi \exp\left[\int_0^\beta d\tau \int d^3x\ \left(-\frac{\phi^2}{4g} \mp \phi\bar{\psi}\mathcal{O}\psi\right)\right] \\
&\quad = \det(\mathbb{1}/2g)^{-\frac{1}{2}}.
\end{aligned} \tag{3.83}$$

Consequently, up to a thermodynamically irrelevant prefactor, N', a four-fermion interaction, $g(\bar{\psi}\mathcal{O}\psi)^2$, can be transformed according to

$$\begin{aligned}
&\exp\left[\int_0^\beta d\tau \int d^3x\ g(\bar{\psi}\mathcal{O}\psi)^2\right] \\
&\qquad = N' \int \mathcal{D}\phi \exp\left[\int_0^\beta d\tau \int d^3x\ \left(-\frac{\phi^2}{4g} \pm \phi\bar{\psi}\mathcal{O}\psi\right)\right].
\end{aligned} \tag{3.84}$$

The auxiliary field, ϕ, represents collective modes generated by combinations of ψ and $\bar{\psi}$ in each space-time point. The four-fermion interaction is exactly transformed into a boson mass term, $-\frac{1}{2}m^2\phi^2$ where $m = 1/\sqrt{2g}$, and a local Yukawa coupling of the bosons to the fermions, $\phi\bar{\psi}\mathcal{O}\psi$. Since no information is lost in the transformation, the expression on the right-hand side of (3.84) in general needs to be simplified further before practical calculations can be carried out. One possibility is

to use a mean-field approximation for the collective field, which will be utilised in Chapter 5. In general, the Yukawa interaction can be expanded in a power series, and the corrections to the fermion propagator can be worked out term by term. The two lowest-order corrections are illustrated in Figure 3.1. The benefit of the

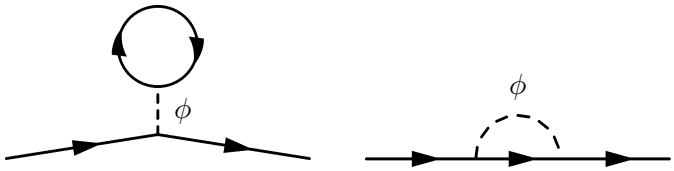

Figure 3.1: The two lowest-order corrections to the fermion propagator from the Yukawa interaction with an auxiliary field, ϕ.

transformed theory with auxiliary fields is that some important dynamical features can be revealed more readily than with the original fields. The four-fermion terms are reduced to quadratic terms, which can be integrated out analytically. This procedure is called bosonisation. Because the fermion fields are integrated out exactly, an infinite number of diagrams are summed even when the functional integrals over auxiliary fields are approximated with a truncated power series. Consequently, the transformed theory can be used to study certain non-perturbative phenomena, which would require a summation of infinitely many terms in the original theory.

The transformation rule (3.84) is limited to scalar Dirac bilinears. Next, consider a four-fermion interaction on the form

$$g(\psi^T \mathcal{O} \psi)^\dagger (\psi^T \mathcal{O} \psi). \tag{3.85}$$

In this case a complex shift is needed to obtain the transformation rule. The starting point is therefore a path integral over a complex (charged) boson field, Φ,

$$\int \mathcal{D}\Phi^* \, \mathcal{D}\Phi \exp\left[- \int_0^\beta d\tau \int d^3x \; \Phi^* D \Phi \right] = (\det D)^{-1}. \tag{3.86}$$

The fields are shifted according to,

$$\Phi \longrightarrow \Phi \pm 2g\psi^T \mathcal{O} \psi, \tag{3.87}$$

$$\Phi^* \longrightarrow \Phi^* \pm 2g(\psi^T \mathcal{O} \psi)^\dagger. \tag{3.88}$$

It follows that

$$\begin{aligned}
&\int \mathcal{D}\Phi^* \, \mathcal{D}\Phi \exp\left\{ - \int_0^\beta d\tau \int d^3x \; \left[\Phi^* \pm 2g(\psi^T \mathcal{O} \psi)^\dagger \right] \frac{\mathbb{1}}{4g} (\Phi \pm 2g \psi^T \mathcal{O} \psi) \right\} \\
&\quad = \exp\left[- \int_0^\beta d\tau \int d^3x \; g(\psi^T \mathcal{O} \psi)^\dagger (\psi^T \mathcal{O} \psi) \right] \\
&\quad \times \int \mathcal{D}\Phi^* \, \mathcal{D}\Phi \exp\left\{ \int_0^\beta d\tau \int d^3x \; \left[- \frac{|\Phi|^2}{4g} \mp (\psi^T \mathcal{O} \psi)^\dagger \frac{\Phi}{2} \mp \frac{\Phi^*}{2} (\psi^T \mathcal{O} \psi) \right] \right\} \\
&\quad = [\det(\mathbb{1}/4g)^{-1}]^{-1}.
\end{aligned} \tag{3.89}$$

Consequently, up to an irrelevant prefactor, N', the interaction term (3.85) can be transformed according to

$$\exp\left[\int_0^\beta d\tau \int d^3x \; g(\psi^T\mathcal{O}\psi)^\dagger(\psi^T\mathcal{O}\psi)\right]$$
$$= N'\int \mathcal{D}\Phi^*\,\mathcal{D}\Phi \exp\left\{\int_0^\beta d\tau\int d^3x \;\left[-\frac{|\Phi|^2}{4g} \pm (\psi^T\mathcal{O}\psi)^\dagger\frac{\Phi}{2} \pm \frac{\Phi^*}{2}(\psi^T\mathcal{O}\psi)\right]\right\}. \quad (3.90)$$

These transformation rules are applied in the derivation of the model of colour superconducting quark matter in Chapter 5.

Chapter 4

Quark Matter

It was suggested already in the 1960s that matter could be in the form of deconfined quarks in the core of neutron stars [32, 33], see also [34, 35]. In the 1970s, rather soon after it became clear that hadrons consist of quarks and gluons, and the asymptotic behaviour of the strong interaction had been understood [36, 37], it was suggested that quarks should be deconfined at high densities and temperatures, *e.g.*, in neutron stars and in the early universe [38, 39]. A heuristic argument for the deconfinement of quarks at high density or temperature follows from the asymptotic behaviour of the strong interaction. Since the strong force becomes arbitrarily weak as quarks are squeezed closer together, matter should behave as an ideal Fermi gas of quarks at asymptotically high densities and/or temperatures. A phase transition from the confined hadronic phase to a deconfined phase, a so-called quark-gluon plasma (QGP), is therefore expected at sufficiently high temperatures, T, or baryon number chemical potentials, μ_B. This is illustrated by the phase diagram in Figure 4.1.

The exploration of the phase structure of high density matter is one of the most active fields of strong-interaction physics. In particular, the main motivation for the study of dense matter in relativistic heavy-ion collisions is the prospect of observing the QGP. Experiments at the CERN Super Proton Synchrotron (SPS) and the Relativistic Heavy Ion Collider (RHIC) at Brookhaven National Laboratory (BNL) have already provided important clues about this novel state of matter. It was recently announced that a plasma-like state of nuclear matter with an extremely low ratio of shear viscosity to entropy has been created and detected in experiments at RHIC. With the approaching commission of the Large Hadron Collider (LHC) at CERN, the definite answer whether QGP exists should be within reach in the near-future. Observations of neutron stars with, *e.g.*, the Chandra X-ray Observatory, the International Gamma-Ray Astrophysics Laboratory (INTEGRAL), the Rossi X-ray Timing Explorer, and the X-ray Multi-Mirror Mission (XMM-Newton) also produce new information that are used to improve the models of high-density matter. For example, during the last few years such observations have provided information

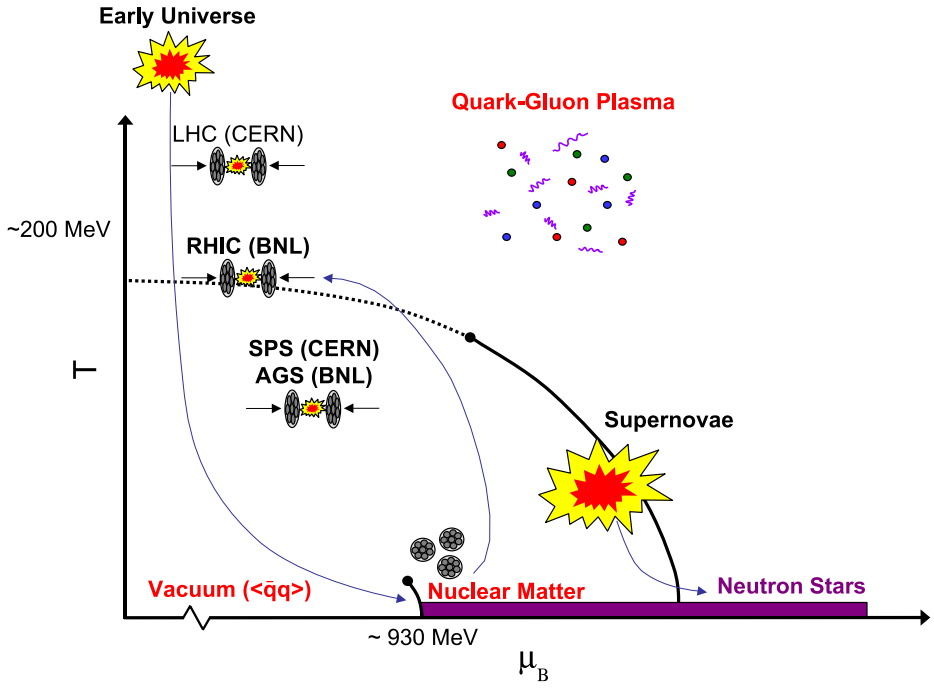

Figure 4.1: Conjectured phase diagram of strongly interacting matter. Since quarks are asymptotically free, a phase transition from the hadronic phase, where quarks are confined, to a deconfined quark-gluon plasma (QGP) is expected at high values of the baryon number chemical potential, μ_B, and temperature, T. The critical temperature of the phase transition has been estimated to $\sim 170 - 200$ MeV with lattice QCD-calculations, see [40, 41] and references therein. The energy per nucleon in ordinary nuclear matter, *e.g.*, in ^{56}Fe, is ~ 930 MeV. High-density colour superconducting phases are omitted in this figure, see Chapter 5 for further information. This diagram resembles early quark-matter phase diagrams, *e.g.*, as in [42].

about the mass spectrum of neutron stars, which put constraints on the compact-star sequence and, consequently, on the equation of state of high-density matter. In particular, the observations[1] of neutron stars with masses around 2 $M_\odot$ are difficult to explain with some exotic models, such as bare quark stars. For more information,

[1]The masses of neutron stars are deduced, *e.g.*, from timing observations of radio binary pulsars and observations of binaries containing an accreting neutron star, which emits x-rays. Observations of pulsar Doppler phenomenon in binaries yield information about orbital sizes and periods, from which the total mass of the binaries can be deduced. In some compact binaries, relativistic effects, *e.g.*, Shapiro delay and orbit shrinkage due to the gravitational radiation reaction can be used to constrain each mass in the binary.

see Paper V and references therein. In the following, I will introduce some basic concepts of quarks and the quark matter state. The interested reader is referred to the literature for further information, see, *e.g.*, [12, 43–48] and references therein.

4.1 Quarks and gluons

Hadrons are composite particles, composed of quarks. Two important subclasses of hadrons are the mesons and the baryons, which are composed of, respectively, a quark-antiquark pair and three quarks, plus a "sea" of virtual quark-antiquark pairs and gluons. Quarks are strongly interacting particles, which means that they interact by mediating gluons. Quarks also interact by the electromagnetic, the weak nuclear and the gravitational force, but these three forces are several orders of magnitude weaker than the strong interaction at microscopic scales. Analogous to the electric charge, which is associated with the electromagnetic force, there are charges associated with the strong interaction, so-called colour charges. Like colour, which can be decomposed into three distinct components, *e.g.*, red, green and blue, the charge of quarks can be described with three independent components. It is customary to denote these charges with red (r), green (g) and blue (b). Colour was originally introduced in order to reconcile early quark models of baryons with the Pauli exclusion principle. An additional quantum number was needed in order to explain how quarks can coexist inside the proton, in otherwise identical states. Unlike the charge-neutral photons, gluons carry colour charge. In fact, a gluon has both colour and anticolour ($\bar{r}$, $\bar{g}$, $\bar{b}$) charge. Naively, there would hence be nine different possibilities ($r\bar{r}$, $r\bar{g}$, $r\bar{b}$, $g\bar{r}$, $g\bar{g}$, $g\bar{b}$, $b\bar{r}$, $b\bar{g}$ and $b\bar{b}$) for the charge of a gluon. The colour-neutral superposition, $r\bar{r}\, g\bar{g}\, b\bar{b}$, does not, however, correspond to a gluon. So there are only 8 independent gluons. Technically, Quantum Chromodynamics has an SU(3) gauge symmetry and the number of gluons is equal to the dimension of this group, which for SU(N) is N^2-1. Since gluons carry both colour and anticolour charges, a quark that interacts strongly changes colour. Gluons interact also with each other.

Free quarks and gluons have never been detected. It is believed that they are always confined in composite colour-neutral aggregates, such as mesons and baryons. So far, six different types ("flavours") of quarks have been identified in particle physics experiments. The flavours are: down (d), up (u), strange (s), charm (c), bottom (b) and top (t). The masses[2] and the electric charges of the six different quarks

[2] The notion of mass for quarks is complicated, as they are bound in hadrons. In the renormalisation of a quantum field theory, a subtraction scheme must be used to remove the divergences occurring in the calculations of physical quantities. The u, d and s quark masses are estimates of so-called "current" quark masses in a mass-independent subtraction scheme, such as the minimal subtraction [49], or the modified minimal subtraction scheme [50, 51]. The c and b quark masses are the "running" masses obtained with the latter subtraction scheme, and the t quark mass is from measurements at the Tevatron at Fermi National Accelerator Laboratory (Fermilab). The current

Table 4-1: Electric charge and approximate masses of quarks [52].

Quark flavour	u	d	s	c	b	t
Mass [MeV]	1.5-3	3-7	70-120	1160-1340	~ 4500	~ 175000
Electric charge [e]	$+\frac{2}{3}$	$-\frac{1}{3}$	$-\frac{1}{3}$	$+\frac{2}{3}$	$-\frac{1}{3}$	$+\frac{2}{3}$

are presented in Table 4-1. The strength of the force mediated by gluons diminishes with increasing "interaction energy", *i.e.*, for large exchanges of momentum. This phenomenon is called asymptotic freedom and was theoretically discovered already in the early 1970s [36, 37]. Since quarks are asymptotically free, perturbation theory and effective models of the strong interaction can be applied at high densities. This discovery was a key development toward the emergence of a standard model of particle physics based on quantum field theory.

4.2 The strange quark matter hypothesis

The idea that strange quark matter (SQM) may be the ground state of strongly interacting dense matter, rather than normal atomic nuclei (^{56}Fe), was proposed already in the early 1970s [39], and later on in [53]. The essence of the SQM hypothesis is that the energy per baryon, *i.e.*, three quarks, in three-flavour quark matter may be smaller than the $\sim$ 930 MeV per baryon in nuclear matter. This could render the SQM phase more stable than nuclear matter and atomic nuclei. If correct, the SQM hypothesis would have implications of fundamental importance for our understanding of the early universe and its evolution. When RHIC was commissioned, one of the potential "disaster scenarios" was that the heavy-ion collisions would create a small droplet of SQM, which would devour the Earth [54]. The main argument against that is the empirical fact that the Moon still exists, even though it is constantly exposed to cosmic rays with extremely high energies. This conclusion is not foolproof, however, because in contrast to cosmic-ray events the centre of mass is fixed in space in a heavy-ion collision.

In contrast to nuclei, where quarks are confined to individual colour-neutral nucleons, SQM presumably is an extended or even macroscopic piece of matter, which is composed of deconfined u, d and s quarks. An essential point is that a large fraction of s quarks ($n_s \sim n_u \sim n_d$) might be necessary for a stable droplet

mass is lower than the "constituent" mass of the quarks. As an example, the mass of a neutron is $\sim$ 940 MeV, while the total current mass of the quarks is $m_u + 2\,m_d \lesssim 20$ MeV. The additional mass of the neutron is mainly due to the energy of the motion of quarks and of the strong force field.

of SQM to form, because hypernuclei, *i.e.*, nuclei that contain baryons with non-zero strangeness (hyperons), have higher masses than ordinary nuclei of the same mass number. This might explain why quarks are confined into hadrons in ordinary matter, as subsequent weak decay processes cannot create sufficient amounts of long-lived s quarks for stable SQM to form. It is also possible that SQM is stable only for a sufficiently large number of quarks, as surface effects could make hadronic states energetically favourable for smaller systems. In any case, three-flavour quark matter inevitably has lower energy than two-flavour quark matter at sufficiently high densities, due to the additional Fermi sea of the s quarks.

Neglecting the influence of leptons, for simplicity, electric neutrality requires that two-flavour quark matter is composed of twice as many d quarks as u quarks, see Table 4-1. For a relativistic, degenerate Fermi system, the number densities, n_i, are related to the chemical potentials, μ_i, by

$$n_i \propto g_i \mu_i^3, \tag{4.1}$$

where g_i is the degeneracy factor. For quarks, two spin states and three colour states for each flavour yield $g_i = 6$. Hence, if $n_d = 2n_u$, the chemical potentials are related by

$$\mu_d = 2^{1/3} \mu_u. \tag{4.2}$$

If the chemical potential of the d quarks is higher than the mass of the s quark, the system can lower its energy by transforming some of the d quarks into s quarks by weak interactions,

$$s + u \leftrightarrow d + u. \tag{4.3}$$

This process continues until all three flavours are in equilibrium with respect to weak interactions. At asymptotically high densities, the number densities and Fermi energies of all three flavours should hence be equal. Actually, at sufficiently high densities, all six flavours of quarks should be present in quark matter due to weak interactions. Neutron stars, however, become unstable before the chemical potential reaches the c quark mass. Quarks more massive than the s quark are therefore absent in compact stars. The massive flavours, c, b and t are relevant only for the hot and dense plasma in the early universe, and in particle physics experiments. See, *e.g.*, [12, 55] for a discussion about the non-appearance of charm quarks in compact stars.

4.3 Quantum chromodynamics

The properties of the strong interaction are, in principle, described by Quantum Chromodynamics (QCD). The QCD lagrangian density is

$$\mathcal{L} = \bar{q}_i^{\alpha} \left(i\gamma_\mu D^\mu_{\alpha\beta} - m_i \right) q_i^{\beta} - \frac{1}{4} F^a_{\mu\nu} F_a^{\mu\nu}, \tag{4.4}$$

where m_i are the current masses of the quark fields, q_i^α, which have six flavour (u, d, s, c, b, t) and three colour (r, g, b) degrees of freedom, see Section 4.1. Here, $\{i, j, k\}$ are flavour indices, $\{\alpha, \beta, \gamma\}$ are colour indices, and $\{a, b, c, d, e\}$ are free indices or dummy indices to be summed over. The colour gauge-invariant derivative, D^μ, is

$$D^\mu_{\alpha\beta} = \delta_{\alpha\beta}\partial^\mu - ig\frac{[\lambda_a]_{\alpha\beta}}{2}G_a^\mu, \tag{4.5}$$

where G_a^μ are the eight gluon fields, $a = 1, ..., 8$, and λ_a are the Gell-Mann matrices, see Appendix B.3. The gluon field-strength tensor, $F_a^{\mu\nu}$, is defined as

$$F_a^{\mu\nu} = \partial^\mu G_a^\nu - \partial^\nu G_a^\mu - g f_{abc} G_b^\mu G_c^\nu, \tag{4.6}$$

where g is the strong interaction coupling constant and f_{abc} are the $\mathrm{SU}(3)_c$ group structure constants, see Appendix B.3. The QCD Lagrangian is invariant under SU(3) transformations in colour space. The strong interactions conserve baryon number, electric charge and quark flavour. Only the weak interactions allow for flavour change. The colour current density, j_a^μ, and the colour charge generators, Q_a, are

$$j_a^\mu = \partial_\nu F_a^{\mu\nu}, \tag{4.7}$$

$$Q_a = \int \mathrm{d}^3x\, j_a^\mu. \tag{4.8}$$

Since isolated quarks and gluons have never been observed, only aggregates of quarks and gluons with zero net colour charge (colour singlets) should have finite energy. A consequence of this is discussed in Section 5.6.

Due to the presence of the last term in (4.6), QCD is a non-Abelian gauge theory, *i.e.*, the gluon fields do not commute. The non-Abelian character of QCD has a number of implications that make it difficult to obtain quantitative predictions from the theory, *e.g.*, the gluons have colour charge and interact with other gluons, as with themselves (self-coupling). This can readily bee seen by expanding the last term in (4.4). There is one term that is linear in the coupling constant, g, (a three-point interaction) and one term that is quadratic in g (a four-point interaction). Due to the complexity of the theory, one has to rely on either Monte Carlo calculations on a lattice of spacetime coordinates [56, 57] or on effective models. Until recently, the Monte Carlo approach has been restricted to zero chemical potential and was therefore not suitable for studying the properties of dense matter. It has also been necessary to extrapolate the results for large values of the u and d current quark masses. Recently, progress has been made both in the case of finite chemical potentials and realistic current-quark masses, see, *e.g.*, [41] and references therein. It is still necessary, however, to rely on non-perturbative effective models of QCD to investigate the properties of bulk matter at intermediate densities. Some examples are the MIT bag model, which is introduced in the next section, Nambu–Jona-Lasinio type models, which are discussed in the next chapter, the instanton liquid model [58], and random matrix models, see, *e.g.*, [59].

4.4 The MIT bag model

The most widely used description of quark matter is the MIT bag model [60], which originally was developed as an effective model of hadrons [61–63]. In this model, hadrons consist of free, or weakly interacting quarks confined to a small region of space, the "bag", by an artificial vacuum pressure. Formally, the bag is stabilised by a term $B\eta^{\mu\nu}$ in the energy-momentum tensor inside the bag, where B is the so-called bag constant. It follows that the bag constant gives a positive contribution to the energy density inside the bag, and a negative contribution to its pressure. This is analogous to a non-trivial vacuum with a positive pressure B and a negative energy density $-B$. The pressure of the vacuum is balanced by the pressure of the quarks inside the bag, which are therefore confined. The bag constant is treated as a free parameter of the model, which can be fitted, *e.g.*, to the hadron spectrum. Such estimates typically yield $B^{\frac{1}{4}} \simeq 100 - 200$ MeV, while a somewhat higher value is obtained by a fit to QCD sum-rule results, or to the critical temperature obtained with lattice calculations, $T_c \simeq 170 - 200$ MeV. For three quark flavours and a strange quark mass chosen as $m_s = 150$ MeV, a bag constant of $B^{\frac{1}{4}} \simeq 155$ MeV yields an energy per baryon that is less than that in the ^{56}Fe nucleus, see Figure 1 in [60].

For macroscopic systems, such as a quark core in a neutron star, the exact solutions of the Dirac equation within the bag can be replaced with plane-wave solutions. The partition function for each fermion degree of freedom is then given by (3.71)

$$\ln Z = 2V \int \frac{p^2 dp}{2\pi^2} \left\{ \ln\left[1 + e^{-\beta(\omega-\mu)}\right] + \ln\left[1 + e^{-\beta(\omega+\mu)}\right] \right\}, \tag{4.9}$$

where the zero-point energy is omitted, and $d^3p \to 4\pi p^2 dp$. According to (3.72) the pressure, P, number densities, n_f, and energy density, ϵ, are

$$P = -B + T \sum_f \sum_c \frac{\partial \ln Z}{\partial V}, \tag{4.10}$$

$$n_f = \frac{T}{V} \sum_c \frac{\partial \ln Z}{\partial \mu_f}, \tag{4.11}$$

$$\epsilon = B + \sum_f \sum_c \left(-T \frac{\partial \ln Z}{\partial V} + \frac{T}{V} \frac{\partial T \ln Z}{\partial T} + \mu_f n_f \right). \tag{4.12}$$

where the sums account for the colour, c, and flavour, f, degrees of freedom, and the contributions from the bag constant have been added. With (4.9), these quantities

can be written

$$P = -B + 6T\sum_f \int \frac{p^2 dp}{2\pi^2}\left\{\ln\left[1+e^{-\beta(\omega_f-\mu_f)}\right]+\ln\left[1+e^{-\beta(\omega_f+\mu_f)}\right]\right\}, \quad (4.13)$$

$$\epsilon = B + 6\sum_f \int \frac{p^2 dp}{2\pi^2}\left[\frac{\omega_f}{e^{\beta(\omega_f-\mu_f)}+1}+\frac{\omega_f}{e^{\beta(\omega_f+\mu_f)}+1}\right], \quad (4.14)$$

$$n_f = 6\int \frac{p^2 dp}{2\pi^2}\left[\frac{1}{e^{\beta(\omega_f-\mu_f)}+1}-\frac{1}{e^{\beta(\omega_f+\mu_f)}+1}\right], \quad (4.15)$$

where the dispersion relations are $\omega_f = (p^2 + m_f^2)^{\frac{1}{2}}$. The factor 6 corresponds to $2_{\rm spin} \times 3_{\rm colour}$ degrees of freedom. The number density is the integral of the Fermi-Dirac distribution function for particles, minus the distribution function for antiparticles.

Zero temperature

In the zero-temperature limit, the Fermi-Dirac distribution becomes a step function at energy μ_f. In this limit the momentum integrals can be evaluated,

$$P = -B + 6\sum_f \frac{1}{24\pi^2}\left[\mu_f p_f\left(\mu_f^2 - \frac{5m_f^2}{2}\right)+\frac{3m_f^4}{2}\ln\left(\frac{\mu_f+p_f}{m_f}\right)\right], \quad (4.16)$$

$$\epsilon = B + 6\sum_f \frac{1}{8\pi^2}\left[\mu_f p_f\left(\mu_f^2 - \frac{m_f^2}{2}\right)-\frac{m_f^4}{2}\ln\left(\frac{\mu_f+p_f}{m_f}\right)\right], \quad (4.17)$$

$$n_f = \sum_f \frac{p_f^3}{\pi^2}. \quad (4.18)$$

The Fermi momentum, p_f, is related to the chemical potential by $\mu_f = (m_f^2 + p_f^2)^{\frac{1}{2}}$.

Massless quark approximation

Analytic solutions can be obtained also in the limit of zero quark masses,

$$P = -B + 6\sum_f \left(\frac{7}{360}\pi^2 T^4 + \frac{1}{12}T^2\mu_f^2 + \frac{1}{24\pi^2}\mu_f^4\right), \quad (4.19)$$

$$\epsilon = 3P + 4B, \quad (4.20)$$

$$n_f = T^2\mu_f + \frac{\mu_f^3}{\pi^2}. \quad (4.21)$$

The expression (4.19) is valid for any massless fermion if the bag constant is omitted and the degeneracy factor is adjusted accordingly. In particular, it is useful in the description of neutrinos, see Paper VII.

Gluons

The contribution to the pressure and energy density from a massless Bose gas of gluons can be obtained from (3.45) with a degeneracy factor of $2_{\rm spin} \times 8_{\rm SU(3)}$,

$$P = \frac{8\pi^2}{45} T^4, \tag{4.22}$$

$$\epsilon = 3P. \tag{4.23}$$

While the gluon (like the photon) is a vector boson with spin 1, massless gauge bosons have two spin states only, because gauge invariance requires that the polarisation is transverse. The number of gluons is given by the dimension of the SU(3) group, which for SU(N) is $N^2 - 1$. Consequently, the degeneracy factor of gluons is 16, as taken into account above.

Chapter 5

Colour Superconductivity

The idea that quarks could form Cooper pairs in dense QGP originates from the mid-1970s [38]. However, except for a few investigations [64–66], this possibility did not get much attention at that time. Nearly two decades later, non-perturbative low-energy models of QCD were used to show that the diquark pairing gaps could be of the order of 100 MeV [67–69]. This is much larger than predicted by the earlier models. The investigation of the QCD phase diagram at high densities has since gained momentum, and a rich phase structure has been identified [44–47, 70–79]. The main reason for studying strongly interacting matter at low temperature and high density is that these conditions exist naturally in neutron stars. For a discussion of potential observable consequences of superconducting quark matter, see, *e.g.*, Paper III, Paper V, Paper VII, and references therein.

A qualitative argument for the formation of superconducting condensates in dense quark matter follows directly from the asymptotic freedom of the strong force [36, 37], and the pairing instability of weakly interacting Fermi systems [80]: For a macroscopic system of non-interacting fermions at low temperature, $T \sim 0$, all states are occupied up to the Fermi momentum, p_F, and nearly all other states are empty, *i.e.*, the occupied states form a Fermi sphere. The free energy cost, $|E(\vec{p}_F) - \mu|$, for creating a quark at the Fermi surface is zero. Consequently, the presence of a weak attraction between the quarks will lower the free energy and render the Fermi sphere unstable. According to the Bardeen-Cooper-Schrieffer (BCS) theory [81, 82], a condensate of Cooper pairs will therefore form, which creates a gap in the energy spectrum that forbids excitations with vanishing free energy. This is analogous to ordinary superconductors, except that quarks come in different flavours, and have both colour and electric charge (thereby the name 'colour superconductivity'). The existence of a pairing gap in the excitation spectrum of cold interacting Fermi systems has recently been verified in experiments [83]. An illustration of the conjectured phase diagram of strongly interacting matter is presented in Figure 5.1. Some relevant astrophysical phenomena, and (existing and planned) particle physics experiments are depicted also.

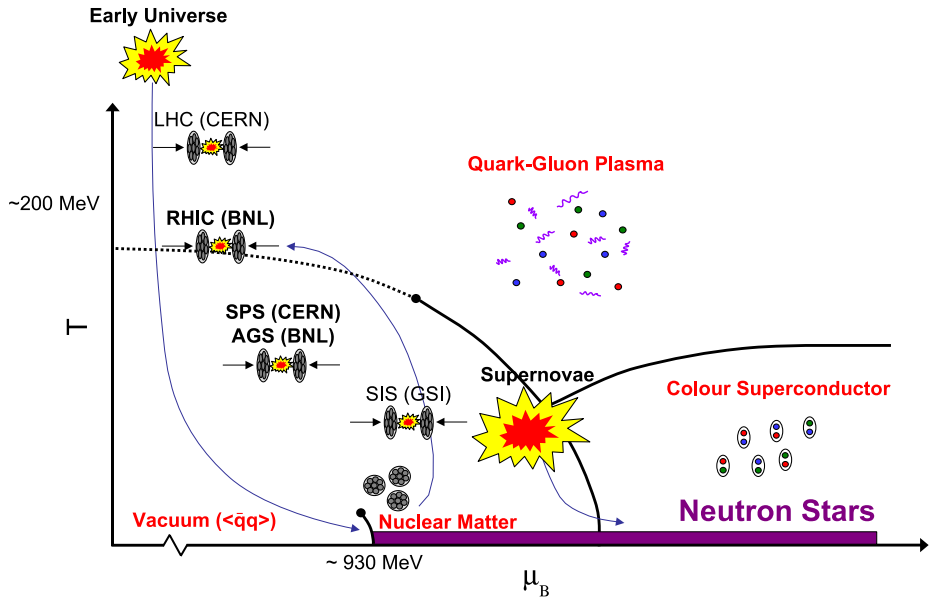

Figure 5.1: Conjectured phase diagram of strongly interacting matter. Since quarks are asymptotically free [36, 37], a phase transition from the hadronic phase, where quarks are confined, to a deconfined quark-gluon plasma (QGP) is expected at high baryon number chemical potentials, μ_B, and temperatures, T. The critical temperature of the phase transition has been estimated to $\sim 170 - 200$ MeV with lattice QCD calculations, see [40, 41] and references therein. The energy per nucleon in ordinary nuclear matter, *e.g.*, in ^{56}Fe, is ~ 930 MeV. Asymptotic freedom suggests that a Fermi surface of nearly free quarks should form at high density. Since a Fermi surface is unstable with respect to formation of Cooper pairs in the presence of a weak attractive force [80], QGP is expected to be a superconductor at low temperature and high density. See the text for further information.

In the following, after a brief review of the theory of classical superconductivity, I introduce the model of colour superconducting quark matter presented in Paper III. The further developments in Paper IV, Paper V and Paper VII are rather self-contained and are therefore not repeated here. For an introduction to superconducting quark matter, see also [84].

5.1 Introduction to classical superconductivity

At the beginning of the 20th century the Dutch physicist Onnes created liquid helium, thereby reaching the nearest approach to zero temperature then achieved. A

few years later, in 1911, he discovered that the electric resistance goes to zero when mercury is cooled at about 4.2 K. Other metals, such as tin and lead showed a similar behaviour. He found that the transition temperature of this new "superconducting" state was of the order of $1 - 10$ K and that the width of the transition was narrow, $\sim 10^{-5}$ K. By the early 1950s, experimentalists had shown that the transition temperature is inversely proportional to the square root of the atomic mass, the so-called isotope effect. Consequently, it was realised that the ions must be dynamically involved in the transition. This led Fröhlich [85] and, independently, Bardeen [86] to deduce that superconductivity was caused by a phonon-mediated electron-electron interaction in the metal, *i.e.*, interactions between the electrons and the thermal vibrations of the crystal. A few years later, Cooper showed that this interaction should lead to the formation of bound states (Cooper pairs) at the Fermi surface [80] and in 1957 the first microscopic theory (later rewarded with the physics Nobel Prize) of superconductivity was published by Bardeen, Cooper and Schrieffer [81], the so-called BCS theory.

In this section, some basic microscopic aspects of superconductivity are discussed. Readers interested in the applications and the physical properties of superconductors are referred to one of the classical books on the subject, *e.g.*, [87]. For a detailed discussion on superconductivity in relativistic systems, see [66]. The purpose of this section is merely to provide some theoretical background for the discussion of colour superconductivity in subsequent sections.

Electron-phonon interactions

In order to understand the basic properties of the superconducting state, it is instructive to study the phonon-mediated interaction in some detail. The second-order scattering process is illustrated by Figure 5.2. Using renormalisation group methods, it has been shown that the one-loop correction to this process is marginal and higher-order processes are irrelevant [88]. Unlike electromagnetic radiation, there

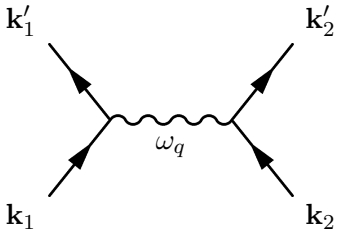

Figure 5.2: Diagram of the second-order phonon-mediated electron-electron interaction in classical superconductors.

is a maximum frequency of phonons. The minimum wavelength of a phonon is effectively twice the distance, a, between ions in the crystal and the corresponding

maximum frequency is the Debye frequency,

$$\omega_D = \frac{v_s}{a}(6\pi^2)^{1/3}. \tag{5.1}$$

Here, v_s is the speed of sound, which can be estimated with the Bohm-Staver relation

$$v_s^2 = \frac{Zm}{3M}v_f^2, \tag{5.2}$$

where Z (M) is the charge number (mass) of the ions, m the electron mass, and v_f the Fermi velocity. In the ground state the electron density, n_e, is related to the Fermi momentum, p_f, by

$$n_e = \frac{(p_f/\hbar)^3}{3\pi^2}. \tag{5.3}$$

The electron density depends on the charge of the ions and the lattice constant, $n_e = Z/a^3$. The Fermi energy is

$$\varepsilon_f = \frac{p_f^2}{2m}. \tag{5.4}$$

It follows that the maximum phonon energy, $\hbar\omega_D$, is related to the Fermi energy by

$$\frac{\hbar\omega_D}{\varepsilon_f} = \left(\frac{2^{8/3}}{3}\frac{Z^{1/3}m}{M}\right)^{1/2}. \tag{5.5}$$

Because $m \ll M$, the maximum phonon energy is several orders of magnitude smaller than the Fermi energy. Phonon-mediated interactions therefore affect electrons only in a thin shell in the vicinity of the Fermi surface. The momentum of the electron pair is conserved in the scattering process, so the wave vectors satisfy $\mathbf{k}_1 + \mathbf{k}_2 = \mathbf{k}_1' + \mathbf{k}_2' = \mathbf{k}_{CM}$. If the pair has a finite centre-of-mass momentum, $\hbar\mathbf{k}_{CM} \neq 0$, the overlap in phase space is significantly reduced, see Figure 5.3. Consequently, the interaction is most likely for electrons with opposite momenta and spin.

So far there is no information about the effect of the interaction. Is it repulsive or attractive? In order to answer this question qualitatively, one can consider the change in energy of a metal when the electrons interact with the phonons. If the interaction is described by a term in the hamiltonian, $\mathcal{V}$, the change in the energy of the system can be estimated with second-order perturbation theory,

$$\Delta E = \sum_i \frac{|\langle 0|\mathcal{V}|i\rangle|^2}{E_0 - E_i}. \tag{5.6}$$

Neglecting higher-order processes, the energy of an intermediate state, E_i, created by emission of a phonon differs from that of the ground state, E_0, by

$$E_i - E_0 = \varepsilon_{\mathbf{k}'} + \hbar\omega_q - \varepsilon_{\mathbf{k}}. \tag{5.7}$$

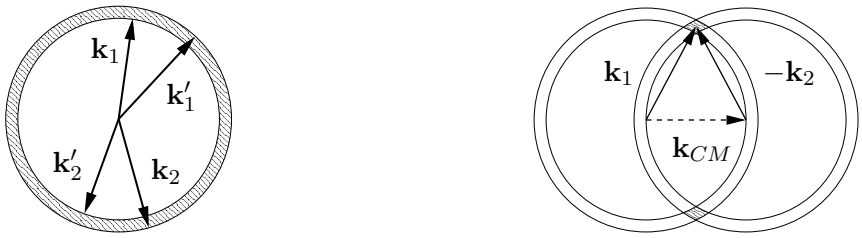

Figure 5.3: Overlap in phase space for electrons scattered by the exchange of phonons. a) The phonon-mediated interaction is restricted to a thin shell of energy width $\hbar\omega_D$ in the vicinity of the Fermi surface. b) Electrons with a finite centre-of-mass momentum, $\hbar\mathbf{k}_{CM}$, have a significantly reduced overlap in phase space. Consequently, the interaction is effective only if $\mathbf{k}_1 \simeq -\mathbf{k}_2$.

There is one such intermediate state for every pair of occupied and unoccupied one-electron levels in the unperturbed ground state. Denoting the matrix elements in (5.6) $g_{\mathbf{k},\mathbf{k}'}$, and accounting for both emission and absorption of phonons, the energy difference is a sum over all pairs of occupied and unoccupied levels

$$\begin{aligned}\Delta E &= \sum_{\mathbf{k},\mathbf{k}'} n_{\mathbf{k}}(1-n_{\mathbf{k}'})\left(\frac{|g_{\mathbf{k},\mathbf{k}'}|^2}{\varepsilon_{\mathbf{k}}-\varepsilon_{\mathbf{k}'}-\hbar\omega_q}+\frac{|g_{\mathbf{k},\mathbf{k}'}|^2}{\varepsilon_{\mathbf{k}'}-\varepsilon_{\mathbf{k}}-\hbar\omega_q}\right)\\ &= \sum_{\mathbf{k},\mathbf{k}'} n_{\mathbf{k}}(1-n_{\mathbf{k}'})|g_{\mathbf{k},\mathbf{k}'}|^2\frac{-2\hbar\omega_q}{(\hbar\omega_q)^2-(\varepsilon_{\mathbf{k}}-\varepsilon_{\mathbf{k}'})^2},\end{aligned} \tag{5.8}$$

where $n_{\mathbf{k}}$ and $n_{\mathbf{k}'}$ are occupation numbers. For a more rigorous discussion of the electron-phonon interaction, see [88, 89], or the original paper by Fröhlich [85].

It follows from (5.8) that the phonon-mediated interaction is attractive when $|\varepsilon_{\mathbf{k}}-\varepsilon_{\mathbf{k}'}|<\hbar\omega_q$. The major contribution to ΔE comes from phonons of maximum energy, because the density of states increases with momentum. Consequently, the phonon interaction is attractive within a thin shell, $|\varepsilon_{\mathbf{k}}-\varepsilon_{\mathbf{k}'}|\lesssim\hbar\omega_D$, in the vicinity of the Fermi surface. The spread in momentum space is $\Delta p\sim\hbar\omega_D/v_f$, and the corresponding spatial spread can be estimated with (5.1), (5.2), and the quantum uncertainty relation

$$\Delta x\sim\frac{\hbar}{\Delta p}\sim\frac{v_f}{\omega_D}\sim a(6\pi^2)^{-1/3}\left(\frac{3M}{Zm}\right)^{1/2}\sim a\sqrt{\frac{M}{m}}. \tag{5.9}$$

Thus, this is a long-range interaction. For $|\varepsilon_{\mathbf{k}}-\varepsilon_{\mathbf{k}'}|\ll\hbar\omega_q$, the interaction is independent of the $\mathbf{k}$ direction. The wave function should therefore be symmetric. Since the individual electrons have antisymmetric wave functions, the spin wavefunctions should also be antisymmetric. Thus, the phonon-mediated attraction mainly affects electrons with opposite momenta and spin, located in a thin shell in the vicinity of

the Fermi surface. In addition, there is a repulsive Coulomb interaction, but it is short-ranged due to screening and is therefore neglected here.

Cooper pairs

The existence of a phonon-mediated net attraction between electrons near the Fermi surface does not imply that bound states should form, because in three dimensions, two particles must interact with a certain minimum strength to form a bound state. Since the interaction is rather weak, one could expect that this should not occur. However, Cooper was the first to realise that due to the influence of the remaining electrons on the interacting pair, a bound state will form [80]. Coopers calculation showed that in the presence of a Fermi sphere, bound states (Cooper pairs) form at the Fermi surface for any strength of the attractive interaction.

In order to understand why this is the case, consider two interacting electrons that propagate above the Fermi sea. The electrons satisfy the Schrödinger equation

$$\left[\mathcal{H}_0(\mathbf{x}_1) + \mathcal{H}_0(\mathbf{x}_2) + \mathcal{V}(\mathbf{x}_1, \mathbf{x}_2)\right] \psi(\mathbf{x}_1, \mathbf{x}_2) = E\psi(\mathbf{x}_1, \mathbf{x}_2). \tag{5.10}$$

In absence of interactions, the spatial part of the wavefunction is a combination of two plane waves, $\psi_{\mathcal{V}=0} \propto \exp(i\mathbf{k}_1 \cdot \mathbf{x}_1) \exp(i\mathbf{k}_2 \cdot \mathbf{x}_2)$. The interactions mainly affect pairs of electrons with opposite spin and momenta, $\mathbf{k}_2 = -\mathbf{k}_1$, so if the coupling is weak, the wavefunction can be approximated with a spin-singlet variational state on the form

$$\psi(\mathbf{x}_1, \mathbf{x}_2) = \frac{1}{\sqrt{2}} \left(|\uparrow_1\rangle \otimes |\downarrow_2\rangle - |\uparrow_2\rangle \otimes |\downarrow_1\rangle \right) \sum_{|\mathbf{k}| \geq k_f} g_{\mathbf{k}} e^{i\mathbf{k}\cdot(\mathbf{x}_1 - \mathbf{x}_2)}. \tag{5.11}$$

The Schrödinger equation then yields

$$\sum_{|\mathbf{k}| \geq k_f} g_{\mathbf{k}} \left[2\varepsilon_{\mathbf{k}} + \mathcal{V}(\mathbf{x}_1 - \mathbf{x}_2)\right] e^{i\mathbf{k}\cdot(\mathbf{x}_1 - \mathbf{x}_2)} = E \sum_{|\mathbf{k}| \geq k_f} g_{\mathbf{k}} e^{i\mathbf{k}\cdot(\mathbf{x}_1 - \mathbf{x}_2)}. \tag{5.12}$$

The corresponding (Fourier-transformed) expression in k-space is

$$\begin{aligned} \sum_{\mathbf{k}'} g_{\mathbf{k}'} \tilde{\mathcal{V}}_{\mathbf{k}\mathbf{k}'} &= (E - 2\varepsilon_{\mathbf{k}}) g_{\mathbf{k}}, \\ \tilde{\mathcal{V}}_{\mathbf{k}\mathbf{k}'} &= \frac{1}{V} \int d^3x \, \mathcal{V}(\mathbf{x}) e^{i(\mathbf{k}-\mathbf{k}')\cdot\mathbf{x}}, \end{aligned} \tag{5.13}$$

where V is the normalisation volume. The phonon-mediated interaction is attractive only within a thin shell in the vicinity of the Fermi surface. The interaction can therefore be modelled as constant within the shell

$$\tilde{\mathcal{V}}_{\mathbf{k}\mathbf{k}'} \equiv \begin{cases} -\lambda, & |\varepsilon_{\mathbf{k}} - \varepsilon_f| \leq \hbar\omega_D, \, |\varepsilon_{\mathbf{k}'} - \varepsilon_f| \leq \hbar\omega_D, \\ 0 & \text{otherwise.} \end{cases} \tag{5.14}$$

The Schrödinger equation (5.13) then simplifies to

$$\begin{aligned} -\lambda \sum_{\mathbf{k}'} g_{\mathbf{k}'} &= (E - 2\varepsilon_{\mathbf{k}}) g_{\mathbf{k}} \implies \\ -\lambda \sum_{\mathbf{k}} \frac{1}{E - 2\varepsilon_{\mathbf{k}}} \sum_{\mathbf{k}'} g_{\mathbf{k}'} &= \sum_{\mathbf{k}} g_{\mathbf{k}} \implies \\ -\lambda \sum_{\mathbf{k}} \frac{1}{E - 2\varepsilon_{\mathbf{k}}} &= 1. \end{aligned} \tag{5.15}$$

As is customary, the sum over $\mathbf{k}$ is approximated by an integral. If this integral is independent of the direction of $\mathbf{k}$, *i.e.*, if the material is homogenous and there are no external fields, it can be reformulated as a one-dimensional integral over the density of states

$$\sum_{\mathbf{k}} \simeq \int \frac{d^3k}{(2\pi)^3} \simeq \int_{\varepsilon_f}^{\varepsilon_f + \hbar\omega_D} d\varepsilon \, \nu(\varepsilon). \tag{5.16}$$

The density of states is approximately constant over the integration interval, $\nu(\varepsilon) \simeq \nu(\varepsilon_f)$, because $\hbar\omega_D \ll \varepsilon_f$. Equation (5.15) can therefore be written

$$\begin{aligned} &\lambda\nu(\varepsilon_f) \int_{\varepsilon_f}^{\varepsilon_f + \hbar\omega_D} \frac{d\varepsilon}{2\varepsilon - E} \\ &= \frac{\lambda\nu(\varepsilon_f)}{2} \ln\left(\frac{E - 2\varepsilon_f - 2\hbar\omega_D}{E - 2\varepsilon_f} \right) = 1. \end{aligned} \tag{5.17}$$

Hence, the energy of the electron pair is

$$E = \frac{2\varepsilon_f \left[e^{\frac{2}{\lambda\nu(\varepsilon_f)}} - 1 \right] - 2\hbar\omega_D}{e^{\frac{2}{\lambda\nu(\varepsilon_f)}} - 1}. \tag{5.18}$$

In the weak-coupling limit, $\lambda\nu(\varepsilon_f) \ll 1$, this simplifies to

$$E \sim 2\varepsilon_f - 2\hbar\omega_D e^{-\frac{2}{\lambda\nu(\varepsilon_f)}}. \tag{5.19}$$

This means that the energy of a electron-pair with $k > k_f$ is below $2\varepsilon_f$, *i.e.*, the contribution to the energy from the attractive interaction outweighs the excess kinetic energy. The pair is therefore bound for any strength of the interaction. Observe that the binding energy in (5.18) is not analytic at $\lambda = 0$, *i.e.*, it cannot be expressed in a power series. Consequently, the energy of a Cooper pair is non-perturbative in λ.

The phonon-mediated interaction is effective at long range, and it mainly affects pairs of electrons with opposite momenta. Unlike ordinary bound states, such as

molecules, Cooper pairs are therefore not localised in the medium. Explicitly, the spread of the wavefunction is given by

$$\langle \mathbf{x}^2 \rangle = \frac{\int d^d x\, \mathbf{x}^2 |g(\mathbf{x})|^2}{\int d^d x\, |g(\mathbf{x})|^2} \simeq \frac{\sum_{\mathbf{k}} |\partial_{\mathbf{k}} g_{\vec{k}}|^2}{\sum_{\mathbf{k}} |g_{\mathbf{k}}|^2} \simeq \frac{\displaystyle\int_{\varepsilon_f}^{\varepsilon_f + \hbar\omega_D} \frac{4\hbar^2 v_f^2 d\varepsilon}{(E-2\varepsilon)^4}}{\displaystyle\int_{\varepsilon_f}^{\varepsilon_f + \hbar\omega_D} \frac{d\varepsilon}{(E-2\varepsilon)^2}}, \tag{5.20}$$

where $g(\mathbf{x}) \propto \sum_{\mathbf{k}} g_{\mathbf{k}} \exp(i\mathbf{k}\cdot\mathbf{x})$, $\partial_{\mathbf{k}} = (\partial\varepsilon_{\mathbf{k}}/\partial\mathbf{k})\partial_\varepsilon = \hbar v_f \partial_\varepsilon$, and from the first step in (5.15), $g_{\mathbf{k}} \propto (E - 2\varepsilon_{\mathbf{k}})^{-1}$. If the coupling is weak, $\lambda\nu(\varepsilon_f) \ll 1$, it follows that

$$\langle \mathbf{x}^2 \rangle^{1/2} \simeq \frac{e^{\frac{2}{\lambda\nu(\varepsilon_f)}}}{\sqrt{3}} \frac{v_f}{\omega_D}. \tag{5.21}$$

This expression is similar to the estimate for the range of the phonon interaction (5.9), with an extra coupling-dependent factor. Indeed, $v_f/\omega_D \sim a\sqrt{M/m} \sim 10^3$ Å, so Cooper pairs are not localised objects. In fact, the size of a Cooper pair exceeds the interparticle distance by several orders of magnitude. Consequently, the pairs overlap and a more rigorous theory of superconductivity should therefore take collective effects into account.

BCS theory

As illustrated above, two independent electrons in the Fermi sea have higher energy than a Cooper pair. The Fermi sea should therefore be unstable with respect to the formation of Cooper pairs. Consequently, equilibrium requires that the Fermi sea is modified such that the binding energy of an additional pair is zero. Indeed, in the derivation of the binding energy of a pair, the presence of a Fermi surface is inevitable. One could therefore suspect that if the Fermi surface is disturbed, the binding energy of additional Cooper pairs could vanish. One year after Cooper had published his paper on the pairing instability, Bardeen, Cooper and Schrieffer published the first theory of superconductivity [81], the BCS theory, which was formulated by the method of second quantisation, see Section 3.1 for an example. The BCS hamiltonian is

$$\mathcal{H}_{\rm BCS} = \sum_{\mathbf{k}} \varepsilon_{\mathbf{k}} \left(a^\dagger_{\mathbf{k}\uparrow} a_{\mathbf{k}\uparrow} + a^\dagger_{\mathbf{k}\downarrow} a_{\mathbf{k}\downarrow} \right) - \frac{\lambda}{V} \sum_{\mathbf{k}\mathbf{k}'} a^\dagger_{\mathbf{k}\uparrow} a^\dagger_{-\mathbf{k}\downarrow} a_{-\mathbf{k}'\downarrow} a_{\mathbf{k}'\uparrow}, \tag{5.22}$$

where the first sum accounts for the one-electron energies, and the second sum accounts for the attractive ($\lambda > 0$) pairing interaction due to exchange of virtual phonons. The interaction term corresponds to scattering of a pair of electrons ($\mathbf{k}\uparrow$, $-\mathbf{k}\downarrow$) to ($\mathbf{k}'\uparrow$, $-\mathbf{k}'\downarrow$). Here, it is assumed that the interaction strength is constant within a thin shell in the vicinity of the Fermi surface, as in (5.14). In the original

BCS theory, an approximate solution was obtained with the help of a variational ansatz for the wavefunction, and by minimising the energy with respect to the variational parameter. The solution obtained is the 'gap equation'

$$1 = \frac{\lambda}{2} \sum_{\mathbf{k}} \left\{ \frac{\tanh\left[\frac{\beta}{2}(\varepsilon_{\mathbf{k}}^2 + \Delta^2)^{\frac{1}{2}}\right]}{(\varepsilon_{\mathbf{k}}^2 + \Delta^2)^{\frac{1}{2}}} \right\}, \tag{5.23}$$

where $\varepsilon_{\mathbf{k}} = \hbar^2 k^2/(2m) - \varepsilon_f$ is the dispersion relation of non-interacting electrons, Δ is the energy gap and $\beta = 1/(k_B T)$. An alternative derivation of this result, with the functional integral and HS transformation methods introduced in Chapter 3 is provided in [90].

If the density of states, $\nu(\varepsilon)$, is approximated by its value at the Fermi energy, $\nu(\varepsilon_f)$, within a thin shell of width $\hbar\omega_D$ in the vicinity of the Fermi surface, the gap equation can be written

$$1 = \frac{\lambda\nu(\varepsilon_f)}{2} \int_0^{\hbar\omega_D} \frac{d\varepsilon}{E(\varepsilon)} \tanh\left[\frac{\beta E(\varepsilon)}{2}\right], \tag{5.24}$$

where $E(\varepsilon) = (\varepsilon^2 + \Delta^2)^{\frac{1}{2}}$ is the dispersion relation of Cooper pairs. Two interesting limits can be deduced from this expression. In the limit $T \to 0$, the hyperbolic tangent is unity, and (5.24) simplifies to

$$1 = \frac{\lambda\nu(\varepsilon_f)}{2} \ln\left[\frac{2\hbar\omega_D}{\Delta(T=0)}\right] \quad \Longrightarrow \quad \Delta(T=0) = 2\hbar\omega_D e^{-\frac{2}{\lambda\nu(\varepsilon_f)}}. \tag{5.25}$$

Observe that this result is consistent with the estimate of the Cooper pair energy (5.19). The critical temperature, T_c, where the superconducting state is destroyed by thermal excitations can be obtained from (5.24) in the limit $\Delta \to 0$. The result is

$$\begin{aligned} 1 \;&=\; \frac{\lambda\nu(\varepsilon_f)}{2} \int_0^{\hbar\omega_D} \frac{d\varepsilon}{\varepsilon} \tanh\left(\frac{\beta\varepsilon}{2}\right) = \frac{\lambda\nu(\varepsilon_f)}{2} \left[\ln\left(\frac{2\beta\hbar\omega_D}{\pi}\right) + \gamma\right] \\ &\Longrightarrow \quad T_c = \frac{e^\gamma}{\pi k_B} 2\hbar\omega_D e^{-\frac{2}{\lambda\nu(\varepsilon_f)}} = \frac{e^\gamma}{\pi k_B} \Delta(T=0), \end{aligned} \tag{5.26}$$

where $\gamma \simeq 0.577$ is the Euler–Mascheroni constant, and the last equality follows from (5.25). Consequently, in units where $k_B = 1$, the critical temperature is

$$T_c \simeq 0.57\Delta(T=0). \tag{5.27}$$

This result applies not only to ordinary superconductors, it is a good estimate also for the critical temperature of colour superconductors, see, *e.g.*, Figure 3 in Paper IV.

5.2 The Nambu–Jona-Lasinio model

The Nambu–Jona-Lasinio (NJL) model was originally developed by Nambu and Jona-Lasinio in 1961 [91, 92] in order to explain the mass gap in the spectrum of interacting nucleons (quarks were not invented at that time). Their idea was that the gap could be explained analogously to the energy gap in the BCS theory of superconductors, see the discussion in the previous section. In order to explain the large nucleon mass in terms of (nearly) massless fermions, Nambu and Jona-Lasinio introduced a Lagrangian for a nucleon field, ψ, with a point-like four-fermion interaction,

$$\mathcal{L} = \bar{\psi}(i\partial\!\!\!/ - m)\psi + g\left[(\bar{\psi}\psi)^2 + (\bar{\psi}i\gamma_5\tau\psi)^2\right]. \tag{5.28}$$

Here, m is the bare mass of the nucleon, g is a coupling constant and τ is a Pauli matrix acting in isospin space, see Appendix B.1. The self-energy induced by the four-point interaction generates an effective mass of the nucleon, which can be higher than the bare mass, even when $m = 0$. The NJL model has later been reinterpreted as as schematic model of deconfined quarks, which incorporates the effect of density and temperature dependent effective ("constituent") quark masses in a self-consistent way. For further information about NJL models of quark matter, see [72]. The relation between NJL models and QCD is discussed in, *e.g.*, [93, 94].

5.3 Lagrangian of three-flavour quark matter

The starting point in the derivation of the three-flavour model of colour superconducting[1] quark matter presented in Paper III is an NJL-type lagrangian with a quark-quark interaction term, $\mathcal{L}_{qq}$,

$$\mathcal{L}_{\mathit{eff}} = \bar{q}(i\partial\!\!\!/ - \hat{m} + \hat{\mu}\gamma^0)q + G_S\sum_{a=0}^{8}\left[(\bar{q}\tau_a q)^2 + (\bar{q}i\gamma_5\tau_a q)^2\right] + \mathcal{L}_{qq}. \tag{5.29}$$

Here, $\hat{m} = \mathrm{diag}(m_u, m_d, m_s)$ is the current-quark mass matrix in flavour space, and $\hat{\mu}$ is the chemical potential matrix in colour and flavour space. The dimensionful coupling constant, G_S, is determined by a fit to low-energy results. For $a = 1...8$, τ_a are the generators of SU(3), *i.e.*, the Gell-Mann matrices, and $\tau_0 = \sqrt{2/3} \times \mathbb{1}$. The quark fields, q, in flavour and colour space are

$$q = (\psi_{ur}, \psi_{ug}, \psi_{ub}, \psi_{dr}, \psi_{dg}, \psi_{db}, \psi_{sr}, \psi_{sg}, \psi_{sb}), \tag{5.30}$$

where each entry is a Dirac spinor, and $\bar{q} \equiv q^\dagger\gamma^0$. This lagrangian can be obtained from a generic local four-point interaction, $g(\bar{q}\mathcal{O}q)^2$, by Fierz transformations. For further information, see, *e.g.*, Appendix A in [72].

[1] Strictly speaking, NJL-type models describe colour superfluid quark matter, see [72], p. 80.

The pseudoscalar terms, $(\bar{q}i\gamma_5\tau_a q)^2$, are essential for the chiral symmetry of the lagrangian. However, calculations suggest that the pseudoscalar condensed phases are separated from the superconducting phases by a first-order phase transition [79]. Also, instanton interactions favour the scalar interactions at high density [67, 68]. The pseudoscalar condensates are therefore omitted in the following, as they should exist only at high temperature and do not affect the models of quark/hybrid stars considered in this work, see Figure 14 and 15 in Paper VII. Furthermore, the sum over a includes the following flavour-mixing terms,

$$
\begin{aligned}
(\bar{q}\tau_1 q)^2 &= (\bar{\psi}_u\psi_d)^2 + (\bar{\psi}_d\psi_u)^2 + \bar{\psi}_u\psi_d\bar{\psi}_d\psi_u + \bar{\psi}_d\psi_u\bar{\psi}_u\psi_d, && (5.31)\\
(\bar{q}\tau_2 q)^2 &= -(\bar{\psi}_u\psi_d)^2 - (\bar{\psi}_d\psi_u)^2 + \bar{\psi}_u\psi_d\bar{\psi}_d\psi_u + \bar{\psi}_d\psi_u\bar{\psi}_u\psi_d, && (5.32)\\
(\bar{q}\tau_4 q)^2 &= (\bar{\psi}_u\psi_s)^2 + (\bar{\psi}_s\psi_u)^2 + \bar{\psi}_u\psi_s\bar{\psi}_s\psi_u + \bar{\psi}_s\psi_u\bar{\psi}_u\psi_s, && (5.33)\\
(\bar{q}\tau_5 q)^2 &= -(\bar{\psi}_u\psi_s)^2 - (\bar{\psi}_s\psi_u)^2 + \bar{\psi}_u\psi_s\bar{\psi}_s\psi_u + \bar{\psi}_s\psi_u\bar{\psi}_u\psi_s, && (5.34)\\
(\bar{q}\tau_6 q)^2 &= (\bar{\psi}_d\psi_s)^2 + (\bar{\psi}_s\psi_d)^2 + \bar{\psi}_d\psi_s\bar{\psi}_s\psi_d + \bar{\psi}_s\psi_d\bar{\psi}_d\psi_s, && (5.35)\\
(\bar{q}\tau_7 q)^2 &= -(\bar{\psi}_d\psi_s)^2 - (\bar{\psi}_s\psi_d)^2 + \bar{\psi}_d\psi_s\bar{\psi}_s\psi_d + \bar{\psi}_s\psi_d\bar{\psi}_d\psi_s, && (5.36)
\end{aligned}
$$

which are omitted also, as they violate flavour conservation. Here, the colour indices of the quark fields have been omitted, because these terms are diagonal in colour space.

The quark-quark term, $\mathcal{L}_{qq}$, in (5.29) represents an effective interaction between quarks, which should account for the most important attractive features of QCD at high density. This attractive force gives rise to a Cooper pairing instability at the Fermi surface, analogously to the instability caused by the attractive phonon mediated interaction in ordinary superconductors, see Section 5.1. It is customary to refer to the quark Cooper pairs as "diquarks", even though it is clear that these objects are not localised bound states. Originally, the concept of a diquark (a two-quark system) comes from descriptions of hadron structure and hadron interactions, see [95] and references therein, and the interpretation in that context is different. Here, a diquark condensate is defined as an ensemble expectation value,

$$\langle q^T\mathcal{O}q\rangle, \tag{5.37}$$

where $\mathcal{O}$ is a local operator acting in the Dirac, flavour and colour spaces. Since quarks are fermions and obey the Pauli principle, $\{\psi_a, \psi_b\} = 0$, the operator $\mathcal{O}$ must be antisymmetric

$$q^T\mathcal{O}q = \mathcal{O}_{ab}q_a g_b = -\mathcal{O}_{ab}q_b g_a = -q^T\mathcal{O}^T q. \tag{5.38}$$

There are many possible operators that satisfy this condition, see [72]. However, the most important diquark condensates are on the form

$$s_{ab} = \langle q^T C\gamma_5\tau_a\lambda_b q\rangle, \tag{5.39}$$

where C is the charge conjugation operator, see Appendix B, and λ_b (τ_a) are the antisymmetric Gell-Mann matrices, λ_2, λ_5 and λ_7, in colour (flavour) space. The corresponding contribution to the lagrangian density is

$$\mathcal{L}_{qq} = G_D \sum_{a=2,5,7} \sum_{b=2,5,7} (\bar{q} i\gamma_5 \tau_a \lambda_b C \bar{q}^T)(q^T C i\gamma_5 \tau_a \lambda_b \, q), \tag{5.40}$$

where G_D is the coupling constant. This is the scalar colour-antitriplet channel, which is the most attractive channel in one-gluon exchange and instanton-mediated interactions. The symmetric Gell-Mann matrices correspond to a repulsive sextet channel, and the corresponding condensates are known to be "weak", *i.e.*, the sextet energy gap at the Fermi surface is relatively small as compared to the colour-antitriplet gap [96–99]. These two interactions are depicted in Figure 5.4. While

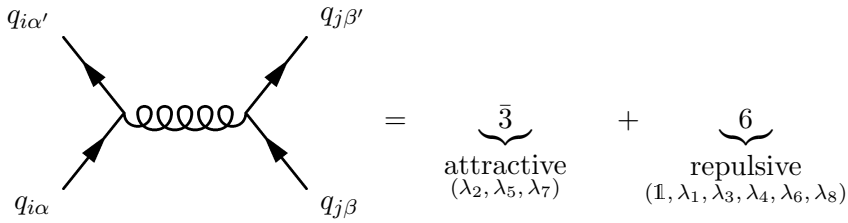

Figure 5.4: A diagrammatic representation of a perturbative QCD one-gluon exchange between two quarks with flavours (colours) i (α) and j (β). The antisymmetric combinations correspond to attractive colour-antitriplet channels, while the symmetric combinations are repulsive sextet channels.

small gaps affect the transport properties of quark matter and are essential in models of, *e.g.*, hybrid-star cooling [19, 100, 101], to lowest order, the EoS depends on the square of the gap and is therefore affected mainly by the antitriplet channel. As the results presented in this thesis would be practically unaffected by the presence of small gaps that do not significantly modify the EoS of high-density matter, only the colour-antitriplet quark-quark channel is considered here.

In general, (5.39) is a 3×3 matrix with orthogonal rows and columns in colour and flavour space. This matrix can be brought to triangular form by SU(3) rotations in colour space and U(3) transformations in flavour space, so (5.39) has six non-zero elements, out of which five can be chosen[2] to be real [72]. Two phases can be rotated away by diagonal SU(3) transformations in colour space, and the remaining three phases are removed by U(3) transformations in flavour space. Observe that SU(3)-flavour is explicitely broken by the unequal current quark masses, in particular

[2]In principle, one should average over the phases of the condensates when calculating the expectation values, which then would vanish. A condensate will arise due to some initial asymmetry, which causes the system to condense in a particular "direction". This is analogous to the magnetisation of the Ising model. Here, the direction can be chosen such that the diagonal condensates are real.

by the relatively large strange quark mass. Numerically it is found that the off-diagonal elements vanish, so only the diagonal elements are considered here. Indeed, a Ginzburg-Landau analysis shows that there are two ground states [72],

$$s_{22} \neq 0 \ \text{ and } \ s_{ab} = 0 \ \text{ if } \ (a,b) \neq (2,2), \tag{5.41}$$

$$s_{22} = s_{55} = s_{77} \neq 0 \ \text{ and } \ s_{ab} = 0 \ \text{ if } \ a \neq b. \tag{5.42}$$

These are the two-flavour colour superconducting (2SC) phase and the colour-flavour locked (CFL) phase. It has been shown that for three flavours, the ground state of QCD at asymptotic densities is the CFL phase [98, 102]. For three degenerate flavours, the same is true for NJL-type models. In the following sections, I will show briefly how to derive a mean-field thermodynamic potential from the NJL lagrangian. The additional interaction terms and details considered in the appended papers can be treated in a similar way and are therefore omitted here.

5.4 Partition function and bosonisation

The NJL lagrangian described in the previous section is the starting point in the derivation of the partition function and the effective potential of three-flavour colour superconducting quark matter. The partition function can be formulated using the results in Chapter 3. It follows from (3.61) that

$$\begin{aligned} Z(T,\hat{\mu}) \ &= \ \int \mathcal{D}iq^\dagger \, \mathcal{D}q \, \exp\Bigg\{ \int_0^\beta d\tau \int d^3x \, \Bigg[\bar{q} \left(-\gamma^0 \partial_\tau + i\gamma \cdot \nabla - \hat{m} + \hat{\mu}\gamma^0 \right) q \\ &\quad + G_S \sum_{a=0,3,8} (\bar{q}\tau_a q)^2 + G_D \sum_{A=2,5,7} (\bar{q} i\gamma_5 \tau_A \lambda_A C \bar{q}^T)(q^T i C \gamma_5 \tau_A \lambda_A q) \Bigg] \Bigg\}. \end{aligned} \tag{5.43}$$

The sum over a is

$$\begin{aligned} \sum_{a=0,3,8} (\bar{q}\tau_a q)^2 \ &= \ \frac{2}{3}\Big[(\bar{\psi_u}\psi_u)^2 + (\bar{\psi_d}\psi_d)^2 + (\bar{\psi_s}\psi_s)^2 \\ &\quad + 2\bar{\psi_u}\psi_u\bar{\psi_d}\psi_d + 2\bar{\psi_u}\psi_u\bar{\psi_s}\psi_s + 2\bar{\psi_d}\psi_d\bar{\psi_s}\psi_s \Big] \\ &\quad + (\bar{\psi_u}\psi_u)^2 + (\bar{\psi_d}\psi_d)^2 - 2\bar{\psi_u}\psi_u\bar{\psi_d}\psi_d \\ &\quad + \frac{1}{3}\Big[(\bar{\psi_u}\psi_u)^2 + (\bar{\psi_d}\psi_d)^2 + 4(\bar{\psi_s}\psi_s)^2 \\ &\quad + 2\bar{\psi_u}\psi_u\bar{\psi_d}\psi_d - 4\bar{\psi_u}\psi_u\bar{\psi_s}\psi_s - 4\bar{\psi_d}\psi_d\bar{\psi_s}\psi_s \Big] \\ &= \ 2\left[(\bar{\psi_u}\psi_u)^2 + (\bar{\psi_d}\psi_d)^2 + (\bar{\psi_s}\psi_s)^2 \right], \end{aligned} \tag{5.44}$$

where the colour indices of the quark spinors are omitted, because these interaction terms are diagonal in colour space. The four-fermion interactions in (5.43) can be

transformed to quadratic terms with the help of

$$\begin{aligned}\left(q^T iC\gamma_5\tau_a\lambda_b q\right)^\dagger &= q^\dagger\lambda_b^\dagger\tau_a^\dagger\gamma_5^\dagger C^\dagger(-i)q^* \\ &= q^\dagger\lambda_b\tau_a\gamma_5(-C)(-i)q^* \\ &= q^\dagger\lambda_b\tau_a\gamma_5\gamma^0\gamma^0 Ciq^* \\ &= q^\dagger\lambda_b\tau_a(-\gamma^0\gamma_5)\left[-C(\gamma^0)^T\right]iq^* \\ &= q^\dagger\gamma^0 i\gamma_5\tau_a\lambda_b C(\gamma^0)^T q^* \\ &= \bar{q}i\gamma_5\tau_a\lambda_b C\bar{q}^T, \end{aligned} \tag{5.45}$$

and the HS transformation rules (3.84) and (3.90),

$$\begin{aligned} Z(T,\hat{\mu}) &= \int \mathcal{D}iq^\dagger\,\mathcal{D}q\,\mathcal{D}\phi_u\,\mathcal{D}\phi_d\,\mathcal{D}\phi_s\,\mathcal{D}\Delta_{22}\,\mathcal{D}\Delta_{55}\,\mathcal{D}\Delta_{77}\,\mathcal{D}\Delta_{22}^*\,\mathcal{D}\Delta_{55}^*\,\mathcal{D}\Delta_{77}^* \\ &\times\exp\Bigg\{\int_0^\beta d\tau\int d^3x\,\Bigg[\bar{q}\left(-\gamma^0\partial_\tau + i\gamma\cdot\nabla - \hat{m} + \hat{\mu}\gamma^0\right)q \\ &-\frac{\phi_u^2+\phi_d^2+\phi_s^2}{8G_S} - \phi_u\bar{\psi}_u\psi_u\mathbb{1}_c - \phi_d\bar{\psi}_d\psi_d\mathbb{1}_c - \phi_s\bar{\psi}_s\psi_s\mathbb{1}_c \\ &+\sum_{A=2,5,7}\frac{-|\Delta_{AA}|^2}{4G_D} + \frac{\Delta_{AA}}{2}(\bar{q}i\gamma_5\tau_A\lambda_A C\bar{q}^T) + \frac{\Delta_{AA}^*}{2}(q^T iC\gamma_5\tau_A\lambda_A\, q)\Bigg]\Bigg\}. \end{aligned} \tag{5.46}$$

Here, ϕ_a and Δ_{AA} are the auxiliary fields introduced by the HS transformations. This expression can be simplified further with the renormalised quark masses,

$$\hat{M} = \hat{m} + \mathrm{diag}_f(\phi_u,\,\phi_d,\,\phi_s) = \mathrm{diag}_f(m_u+\phi_u,\,m_d+\phi_d,\,m_s+\phi_s). \tag{5.47}$$

The partition function can then be written

$$\begin{aligned} Z(T,\hat{\mu}) &= \int \mathcal{D}iq^\dagger\,\mathcal{D}q\,\mathcal{D}\phi_u\,\mathcal{D}\phi_d\,\mathcal{D}\phi_s\,\mathcal{D}\Delta_{22}\,\mathcal{D}\Delta_{55}\,\mathcal{D}\Delta_{77}\,\mathcal{D}\Delta_{22}^*\,\mathcal{D}\Delta_{55}^*\,\mathcal{D}\Delta_{77}^* \\ &\times\exp\Bigg\{\int_0^\beta d\tau\int d^3x\,\Bigg[\bar{q}(-\gamma^0\partial_\tau + i\gamma\cdot\nabla - \hat{M} + \hat{\mu}\gamma^0)q - \sum_{a=u,\,d,\,s}\frac{\phi_a^2}{8G_S} - \sum_{A=2,\,5,\,7}\frac{|\Delta_{AA}|^2}{4G_D} \\ &+\frac{1}{2}\sum_{A=2,5,7}\Delta_{AA}(\bar{q}i\gamma_5\tau_A\lambda_A C\bar{q}^T) + \Delta_{AA}^*(q^T iC\gamma_5\tau_A\lambda_A\, q)\Bigg]\Bigg\}. \end{aligned} \tag{5.48}$$

In order to evaluate the functional integrals over quark fields, one introduces 8-component Nambu-Gorkov spinors,

$$\Psi = \frac{1}{\sqrt{2}}\begin{bmatrix} q \\ \bar{q}^T \end{bmatrix} \text{ and } \bar{\Psi} = \Psi^\dagger\gamma^0 = \frac{1}{\sqrt{2}}\begin{bmatrix} \bar{q} & q^T \end{bmatrix}. \tag{5.49}$$

The free-particle (Dirac) term then separates into two terms, one for $\bar{q}$ and q, and one for q^T and $\bar{q}^T$, each carrying a factor 1/2. The partition function becomes

$$Z(T,\hat{\mu}) = \int \mathcal{D}i\Psi^\dagger\,\mathcal{D}\Psi\,\mathcal{D}\phi_u\,\mathcal{D}\phi_d\,\mathcal{D}\phi_s\,\mathcal{D}\Delta_{22}\,\mathcal{D}\Delta_{55}\,\mathcal{D}\Delta_{77}\,\mathcal{D}\Delta_{22}^*\,\mathcal{D}\Delta_{55}^*\,\mathcal{D}\Delta_{77}^*$$
$$\times\exp\left[\int_0^\beta d\tau\int d^3x\,\left(-\sum_{a=u,\,d,\,s}\frac{\phi_a^2}{8G_S}-\sum_{A=2,\,5,\,7}\frac{|\Delta_{AA}|^2}{4G_D}+\bar{\Psi}S(\tau,\,\mathbf{x})\Psi\right)\right], \quad (5.50)$$

$$S(\tau,\,\mathbf{x}) = \begin{pmatrix} -\gamma^0\partial_\tau + i\gamma\cdot\nabla - \hat{M} + \hat{\mu}\gamma^0 & i\sum_A \Delta_{AA}\gamma_5\tau_A\lambda_A C \\ i\sum_A \Delta_{AA}^*C\gamma_5\tau_A\lambda_A & -\gamma^0\partial_\tau + i\gamma^T\cdot\nabla + \hat{M} - \hat{\mu}\gamma^0 \end{pmatrix}, \quad (5.51)$$

where $S(\tau,\,\mathbf{x})$ is the inverse propagator of the Nambu-Gorkov fields. From here on, the derivation is analogous to that in Chapter 3, except that the final result has to be divided by a factor 2 to compensate for the double counting in the functional integrals over the Nambu-Gorkov fields. First expand the Nambu-Gorkov spinors in Fourier series

$$\Psi_\alpha(\tau,\mathbf{x}) = V^{-\frac{1}{2}}\sum_n\sum_{\mathbf{p}} e^{i(\mathbf{p}\cdot\mathbf{x}+\omega_n\tau)}\tilde{\Psi}_{\alpha;\,n}(\mathbf{p}). \quad (5.52)$$

The functional integrals over Nambu-Gorkov fields then simplify to a product of integrals over the Fourier amplitudes, *i.e.*, an expression analogous to (3.65), and the inverse propagator in momentum space is

$$S(i\omega_n,\mathbf{p}) = \begin{pmatrix} -i\omega_n - \gamma^0\gamma\cdot\mathbf{p} - \hat{M}\gamma^0 + \hat{\mu} & i\sum_A \Delta_{AA}\gamma^0\gamma_5\tau_A\lambda_A C \\ i\sum_A \Delta_{AA}^*C\gamma^0\gamma_5\tau_A\lambda_A & -i\omega_n - \gamma^0\gamma^T\cdot\mathbf{p} + \hat{M}\gamma^0 - \hat{\mu} \end{pmatrix}, \quad (5.53)$$

where ω_n are the fermion Matsubara frequencies (3.64). In order to evaluate the fermion determinant (3.68), note that

$$S(i\omega_n,\mathbf{p}) = -i\omega_n\mathbb{1} + D(\mathbf{p}), \quad (5.54)$$

$$D(\mathbf{p}) = \begin{pmatrix} -\gamma^0\gamma\cdot\mathbf{p} - \hat{M}\gamma^0 + \hat{\mu} & i\sum_A \Delta_{AA}\gamma^0\gamma_5\tau_A\lambda_A C \\ i\sum_A \Delta_{AA}^*C\gamma^0\gamma_5\tau_A\lambda_A & -\gamma^0\gamma^T\cdot\mathbf{p} + \hat{M}\gamma^0 - \hat{\mu} \end{pmatrix}. \quad (5.55)$$

Then arrange the orthonormal eigenvectors of the hermitian matrix $D(\mathbf{p})$ in the columns of a matrix X. The identity (D.1) then gives

$$\begin{aligned}\det S(i\omega_n,\mathbf{p}) &= \det\left[-i\omega_n\mathbb{1} + D(\mathbf{p})\right] = \det\left[-i\omega_n\mathbb{1} + X^{-1}D(\mathbf{p})X\right] \\ &= \det\left[-i\omega_n\mathbb{1} + \mathrm{diag}(\lambda_1,\,\lambda_2,\,\lambda_3,\ldots,\,\lambda_N)\right] \\ &= (-i\omega_n+\lambda_1)(-i\omega_n+\lambda_2)(-i\omega_n+\lambda_3)\ldots(-i\omega_n+\lambda_N), \quad (5.56)\end{aligned}$$

where λ_a are the eigenvalues of the hermitian matrix $D(\mathbf{p})$. These eigenvalues appear in $\pm$ pairs, thanks to the Nambu-Gorkov basis, and the determinant can therefore be written

$$\det S(i\omega_n,\mathbf{p}) = \prod_{a=1}^{N/2}(\omega_n^2+\lambda_a^2), \quad (5.57)$$

where one eigenvalue from each $\pm$ pair is omitted, *i.e.*, there are $N/2$ products. Consequently, the partition function is

$$Z(T,\hat{\mu}) = \int \mathcal{D}\phi_u\,\mathcal{D}\phi_d\,\mathcal{D}\phi_s\,\mathcal{D}\Delta_{22}\,\mathcal{D}\Delta_{55}\,\mathcal{D}\Delta_{77}\,\mathcal{D}\Delta_{22}^*\,\mathcal{D}\Delta_{55}^*\,\mathcal{D}\Delta_{77}^* \times \prod_n \prod_{\mathbf{p}} \prod_{a=1}^{N/2} \beta^2\left(\omega_n^2+\lambda_a^2\right) \times \exp\left[-\beta V\left(\sum_{b=u,\,d,\,s}\frac{\phi_b^2}{8G_S}+\sum_{A=2,\,5,\,7}\frac{|\Delta_{AA}|^2}{4G_D}\right)\right], \quad (5.58)$$

where λ_a are the positive (or negative) eigenvalues of the matrix (5.55), which is identical to Eq. 13 in Paper III and the matrix in [103]. An explicit representation of this matrix in colour and flavour space is provided in the Appendix of Paper III. It is possible to derive other matrices $D(\mathbf{p})$ that have the same eigenspectrum as (5.55), *e.g.*, with the use of

$$(\bar{q}i\gamma_5\tau_A\lambda_A C\bar{q}^T)(q^T iC\gamma_5\tau_A\lambda_A q) = (q^T C\gamma_5\tau_A\lambda_A q)^\dagger(q^T C\gamma_5\tau_A\lambda_A q), \quad (5.59)$$

a matrix without the imaginary factor i in the off-diagonal elements is obtained. If the Nambu-Gorkov spinors are defined in a different way, a matrix where the charge conjugation operators are absent in the off-diagonal elements can be obtained, see, *e.g.*, [72]. Observe that the quark fields are no longer present in the partition function (5.58), only the sum over fermion Matsubara frequencies remains. This is a so-called bosonised formulation of the partition function. In order to evaluate the functional integrals over the auxiliary fields, it is necessary[3] to make further approximations, *e.g.*, as in [104]. In the following, I will illustrate how to obtain the mean-field approximation of the model, which is the method used in the appended papers.

5.5 Mean-field thermodynamic potential

The grand canonical thermodynamic potential is related to the partition function obtained in the previous section by

$$\Omega_q(T,\hat{\mu}) = -\frac{T\ln Z}{V}. \quad (5.60)$$

Here, the index q denotes that this is the contribution from quarks only, as leptons have not yet been considered. In the mean-field (MF) approximation, the auxiliary fields are fixed at the extremum of the potential. Consequently, for each auxiliary field, ϕ, there is a gap equation on the form

$$\frac{\partial}{\partial\phi}\frac{T\ln Z}{V}\bigg|_{\phi\equiv\phi_{\rm MF}} = 0. \quad (5.61)$$

[3]Observe that the eigenvalues λ_a are functions of the auxiliary fields, as ϕ_a enters the renormalised masses (5.47) and Δ_{AA} appears explicitly in the matrix (5.55).

Using the fact that all Δ_{AA} can be chosen to be real, see the discussion in Section 5.3, and noting that

$$\frac{\partial}{\partial\phi}\ln Z = \frac{1}{Z}\frac{\partial Z}{\partial\phi}, \tag{5.62}$$

one gets that that

$$-\frac{2\phi_a}{8G_S} - \langle\bar{\psi}_a\psi_a\rangle = 0, \tag{5.63}$$

$$-\frac{2\Delta_{AA}}{4G_D} + \langle\bar{q}i\gamma_5\tau_A\lambda_A C\bar{q}^T\rangle = 0. \tag{5.64}$$

The mean-field values of the fields therefore are

$$\phi_a = -4G_S\langle\bar{\psi}_a\psi_a\rangle, \tag{5.65}$$

$$\Delta_{AA} = 2G_D\langle\bar{q}i\gamma_5\tau_A\lambda_A C\bar{q}^T\rangle. \tag{5.66}$$

This result has little practical use, however, because the values of all ϕ_a and Δ_{AA} have to be determined numerically at the global minimum of the potential, $\Omega_q(T,\hat{\mu})$.

With the expressions for the partition function (5.58) and the thermodynamic potential (5.60), and the standard result for the Matsubara sum (3.78), the expression for the mean-field potential becomes

$$\begin{aligned}\Omega_q(T,\hat{\mu}) = &\sum_{a=u,\,d,\,s}\frac{\phi_a^2}{8G_S} + \sum_{A=2,\,5,\,7}\frac{|\Delta_{AA}|^2}{4G_D} \\ &-\frac{1}{2}\int\frac{d^3p}{(2\pi)^3}\sum_{b=1}^{N/2}\left[\lambda_b + 2T\ln\left(1+e^{-\lambda_b/T}\right)\right].\end{aligned} \tag{5.67}$$

Here, a factor of $1/2$ has been inserted to compensate for the double-counting in the functional integrals over Nambu-Gorkov fields. There are 72 eigenvalues, because $N = 3_{\text{flavour}}\times 3_{\text{colour}}\times 4_{\text{Dirac}}\times 2_{\text{Nambu-Gorkov}} = 72$. These eigenvalues, which represent the quasiparticle dispersion relations, are obtained numerically from (5.55). The thermodynamic potential should be minimised with respect to the gaps,

$$\frac{\partial\Omega_q}{\partial\phi_u} = \frac{\partial\Omega_q}{\partial\phi_d} = \frac{\partial\Omega_q}{\partial\phi_s} = 0, \tag{5.68}$$

$$\frac{\partial\Omega_q}{\partial\Delta_{22}} = \frac{\partial\Omega_q}{\partial\Delta_{55}} = \frac{\partial\Omega_q}{\partial\Delta_{77}} = 0. \tag{5.69}$$

Observe that it is not sufficient to find a solution to these gap equations, because unphysical local minima normally exist. Only the global minimum corresponds to a physical equilibrium state. A useful method to solve the gap equations is described in Appendix E and Appendix F. As τ_A in Δ_{AA} combines two flavours for each value of A, the diquark gaps can be denoted with flavour indices, *e.g.*, $\Delta_{AA} = \Delta_{ud}$. This

notation is used in some of the appended papers. It is essential that the vacuum contribution to the potential is subtracted,

$$\Omega_0 \equiv \Omega_q(0,0) = \frac{\phi_{0u}^2 + \phi_{0d}^2 + \phi_{0s}^2}{8G_S} - 6\sum_i \int \frac{d^3p}{(2\pi)^3}\sqrt{M_i^2 + p^2}, \tag{5.70}$$

where ϕ_{0a} are the self-consistent vacuum solutions for ϕ_a. In addition, the contribution from leptons should be added to the potential. This is straightforward, and the results are presented in Paper III and Paper VII.

5.6 Charge neutrality

Bulk matter in compact stars should be electric- and colour-charge neutral. Strictly speaking, matter should be in a colour-singlet state, but the free energy cost for projecting a colour-neutral system into the colour-singlet state is negligible in the thermodynamic limit [105]. Therefore, only local colour neutrality is considered in this work. There are in total four conserved charges, the electric charge and three colour charges. The electric charge density, n_Q, is

$$n_Q = \frac{2}{3}n_u - \frac{1}{3}n_d - \frac{1}{3}n_s - n_e, \tag{5.71}$$

where n_e is the number density of electrons. The contribution from muons could be included also, and the effect is significant for the existence of mixed phases, see Paper VII. For the colour charges it is practical to introduce the following linear combinations of charge densities [72]

$$n_3 = n_r - n_g, \tag{5.72}$$

$$n_8 = \frac{1}{\sqrt{3}}\left(n_r + n_g - 2n_b\right), \tag{5.73}$$

$$n = n_r + n_g + n_b, \tag{5.74}$$

where n is the total quark number density. The baryon number density is proportional to the quark number density, n, so baryon number is also a conserved quantity. The conserved charges in (5.71)-(5.74) have four associated chemical potentials, μ_Q, μ_3, μ_8 and μ. The number densities are related to the chemical potentials by the standard relation

$$n_a = -\frac{\partial \Omega_q}{\partial \mu_a}. \tag{5.75}$$

The chemical potential matrix in colour and flavour space is

$$\hat{\mu} = \mu + \left(\frac{\tau_3}{2} + \frac{\tau_8}{2\sqrt{3}}\right)\mu_Q + \lambda_3\mu_3 + \lambda_8\mu_8, \tag{5.76}$$

where λ_a (τ_a) are Gell-Mann generators in colour (flavour) space. The quark number chemical potential, μ, is related to the baryon number chemical potential by $\mu = \mu_B/3$. Matter is electric- and colour-charge neutral if

$$n_Q = n_3 = n_8 = 0. \tag{5.77}$$

Thus, according to (5.75), the charge neutrality conditions are

$$\frac{\partial \Omega_q}{\partial \mu_Q} = \frac{\partial \Omega_q}{\partial \mu_3} = \frac{\partial \Omega_q}{\partial \mu_8} = 0. \tag{5.78}$$

These equations should be solved in parallel with the gap equations (5.68)-(5.69). For further information about charge neutrality, see Paper VII. A useful method to solve the charge neutrality equations is described in Appendix E and Appendix F.

Bibliography

[1] W. Baade and F. Zwicky, *Phys. Rev.* **45**, 138 (1934).

[2] I. A. D'Souza and C. S. Kalman, *Preons: Models of leptons, quarks and gauge bosons as composite objects*. Singapore, Singapore: World Scientific (1992) 108 p.

[3] J.-J. Dugne, S. Fredriksson, and J. Hansson, *Europhys. Lett.* **57**, 188 (2002); `arXiv:hep-ph/0208135`.

[4] S. Fredriksson, `arXiv:hep-ph/0309213`. Proc. of the Fourth Tegernsee Int. Conf. on Particle Physics Beyond the Standard Model, ed. H.-V. Klapdor-Kleingrothaus. Heidelberg, Germany: Springer-Verlag (2004), 1117 p.

[5] N. K. Glendenning, *Compact Stars: Nuclear Physics, Particle Physics, and General Relativity*. New York, USA: Springer (2000) 467 p.

[6] S. L. Shapiro and S. A. Teukolsky, *Black holes, white dwarfs, and neutron stars: The physics of compact objects*. New York, USA: Wiley (1983) 645 p.

[7] S. Weinberg, *Gravitation and cosmology: Principles and applications of the general theory of relativity*. New York, USA: Wiley (1972) 657 p.

[8] C. W. Misner, K. S. Thorne, and J. A. Wheeler, *Gravitation*. San Francisco, USA: W. H. Freeman and Co. (1973) 1279 p.

[9] J. M. Lattimer and M. Prakash, `arXiv:astro-ph/0612440`.

[10] D. Page and S. Reddy, *Ann. Rev. Nucl. Part. Sci.* **56**, 327 (2006); `arXiv:astro-ph/0608360`.

[11] A. Sedrakian, *Prog. Part. Nucl. Phys.* **58**, 168 (2007); `arXiv:nucl-th/0601086`.

[12] F. Weber, *Prog. Part. Nucl. Phys.* **54**, 193 (2005); `arXiv:astro-ph/0407155`.

[13] J. A. Pons, S. Reddy, M. Prakash, J. M. Lattimer, and J. A. Miralles, *Astrophys. J.* **513**, 780 (1999); arXiv:astro-ph/9807040.

[14] M. Prakash *et al.*, *Phys. Rept.* **280**, 1 (1997); arXiv:nucl-th/9603042.

[15] T. M. Davis *et al.*, arXiv:astro-ph/0701510.

[16] R. C. Tolman, *Phys. Rev.* **55**, 364 (1939).

[17] J. R. Oppenheimer and G. M. Volkoff, *Phys. Rev.* **55**, 374 (1939).

[18] T. Kodama and M. Yamada, *Progr. Theor. Phys.* **47**, 444 (1972).

[19] H. Grigorian, D. Blaschke, and D. Voskresensky, *Phys. Rev.* **C71**, 045801 (2005); arXiv:astro-ph/0411619.

[20] D. Page, U. Geppert, and F. Weber, *Nucl. Phys.* **A777**, 497 (2006); arXiv:astro-ph/0508056.

[21] D. Gondek, P. Haensel, and J. L. Zdunik, *Astron. Astrophys.* **325**, 217 (1997); arXiv:astro-ph/9705157.

[22] U. H. Gerlach, *Phys. Rev.* **172**, 1325 (1968).

[23] U. H. Gerlach, Ph.D. thesis, Princeton University (1968).

[24] N. K. Glendenning and C. Kettner, *Astron. Astrophys.* **353**, L9 (2000); arXiv:astro-ph/9807155.

[25] K. Schertler, C. Greiner, J. Schaffner-Bielich, and M. H. Thoma, *Nucl. Phys.* **A677**, 463 (2000); arXiv:astro-ph/0001467.

[26] J. I. Kapusta, *Finite-Temperature Field Theory.* 1993. New York, USA: Cambridge University Press (1993) 232 p.

[27] N. P. Landsman and C. G. van Weert, *Phys. Rept.* **145**, 141 (1987).

[28] F. A. Berezin and M. S. Marinov, *Ann. Phys.* **104**, 336 (1977).

[29] M. Buballa and M. Oertel, *Nucl. Phys.* **A703**, 770 (2002); arXiv:hep-ph/0109095.

[30] R. L. Stratonovich, *Doklady Akad. Nauk S.S.S.R.* **115**, 1097 (1957). translation: Soviet Phys. Doklady **2**, p. 416 (1958).

[31] J. Hubbard, *Phys. Rev. Lett.* **3**, 77 (1959).

[32] D. Ivanenko and D. F. Kurdgelaidze, *Astrofiz.* **1**, 479 (1965).

[33] D. Ivanenko and D. F. Kurdgelaidze, *Lett. Nuovo Cim.* **2**, 13 (1969).

[34] N. Itoh, *Progr. Theoret. Phys.* **44**, 291 (1970).

[35] F. Iachello, W. D. Langer, and A. Lande, *Nucl. Phys.* **A219**, 612 (1974).

[36] D. J. Gross and F. Wilczek, *Phys. Rev. Lett.* **30**, 1343 (1973).

[37] H. D. Politzer, *Phys. Rev. Lett.* **30**, 1346 (1973).

[38] J. C. Collins and M. J. Perry, *Phys. Rev. Lett.* **34**, 1353 (1975).

[39] A. R. Bodmer, *Phys. Rev.* **D4**, 1601 (1971).

[40] U. M. Heller, *PoS* **LAT2006**, 011 (2006); `arXiv:hep-lat/0610114`.

[41] M. A. Stephanov, `arXiv:hep-lat/0701002`.

[42] J. Cleymans, R. V. Gavai, and E. Suhonen, *Phys. Rept.* **130**, 217 (1986).

[43] M. Gyulassy and L. McLerran, *Nucl. Phys.* **A750**, 30 (2005); `arXiv:nucl-th/0405013`.

[44] D. H. Rischke, *Prog. Part. Nucl. Phys.* **52**, 197 (2004); `arXiv:nucl-th/0305030`.

[45] T. Schäfer, `arXiv:hep-ph/0304281`.

[46] M. G. Alford, *Ann. Rev. Nucl. Part. Sci.* **51**, 131 (2001); `arXiv:hep-ph/0102047`.

[47] K. Rajagopal and F. Wilczek, `arXiv:hep-ph/0011333`.

[48] H. Heiselberg and M. Hjorth-Jensen, *Phys. Rept.* **328**, 237 (2000); `arXiv:nucl-th/9902033`.

[49] G. 't Hooft, *Nucl. Phys.* **B61**, 455 (1973).

[50] W. A. Bardeen, A. J. Buras, D. W. Duke, and T. Muta, *Phys. Rev.* **D18**, 3998 (1978).

[51] W. A. Bardeen and A. J. Buras, *Phys. Rev.* **D20**, 166 (1979).

[52] Particle Data Group Collaboration, W. M. Yao *et al.*, *J. Phys.* **G33**, 1 (2006).

[53] E. Witten, *Phys. Rev.* **D30**, 272 (1984).

[54] W. Busza, R. L. Jaffe, J. Sandweiss, and F. Wilczek, *Rev. Mod. Phys.* **72**, 1125 (2000); arXiv:hep-ph/9910333.

[55] C. Kettner, F. Weber, M. K. Weigel, and N. K. Glendenning, *Phys. Rev.* **D51**, 1440 (1995).

[56] E. Laermann and O. Philipsen, *Ann. Rev. Nucl. Part. Sci.* **53**, 163 (2003); arXiv:hep-ph/0303042.

[57] S. Muroya, A. Nakamura, C. Nonaka, and T. Takaishi, *Prog. Theor. Phys.* **110**, 615 (2003); arXiv:hep-lat/0306031.

[58] E. V. Shuryak, *Nucl. Phys.* **B203**, 93 (1982).

[59] J. J. M. Verbaarschot and T. Wettig, *Ann. Rev. Nucl. Part. Sci.* **50**, 343 (2000); arXiv:hep-ph/0003017.

[60] E. Farhi and R. L. Jaffe, *Phys. Rev.* **D30**, 2379 (1984).

[61] A. Chodos, R. L. Jaffe, K. Johnson, C. B. Thorn, and V. F. Weisskopf, *Phys. Rev.* **D9**, 3471 (1974).

[62] A. Chodos, R. L. Jaffe, K. Johnson, and C. B. Thorn, *Phys. Rev.* **D10**, 2599 (1974).

[63] T. A. DeGrand, R. L. Jaffe, K. Johnson, and J. E. Kiskis, *Phys. Rev.* **D12**, 2060 (1975).

[64] B. C. Barrois, *Nucl. Phys.* **B129**, 390 (1977).

[65] S. C. Frautschi. Presented at Workshop on Hadronic Matter at Extreme Energy Density, Erice, Italy, Oct 13-21, 1978.

[66] D. Bailin and A. Love, *Phys. Rept.* **107**, 325 (1984).

[67] M. G. Alford, K. Rajagopal, and F. Wilczek, *Phys. Lett.* **B422**, 247 (1998); arXiv:hep-ph/9711395.

[68] R. Rapp, T. Schäfer, E. V. Shuryak, and M. Velkovsky, *Phys. Rev. Lett.* **81**, 53 (1998); arXiv:hep-ph/9711396.

[69] D. Blaschke and C. D. Roberts, *Nucl. Phys.* **A642**, 197 (1998); arXiv:nucl-th/9807008.

[70] D. K. Hong, *Acta Phys. Polon.* **B32**, 1253 (2001); arXiv:hep-ph/0101025.

[71] R. Casalbuoni and G. Nardulli, *Rev. Mod. Phys.* **76**, 263 (2004); arXiv:hep-ph/0305069.

[72] M. Buballa, *Phys. Rept.* **407**, 205 (2005); arXiv:hep-ph/0402234.

[73] H.-C. Ren, arXiv:hep-ph/0404074.

[74] M. Huang, arXiv:hep-ph/0409167.

[75] A. Schmitt, *Phys. Rev.* **D71**, 054016 (2005); arXiv:nucl-th/0412033.

[76] S. B. Rüster, V. Werth, M. Buballa, I. A. Shovkovy, and D. H. Rischke, *Phys. Rev.* **D72**, 034004 (2005); arXiv:hep-ph/0503184.

[77] D. Blaschke, S. Fredriksson, H. Grigorian, A. M. Öztaş, and F. Sandin, *Phys. Rev.* **D72**, 065020 (2005); arXiv:hep-ph/0503194.

[78] H. Abuki and T. Kunihiro, *Nucl. Phys.* **A768**, 118 (2006); arXiv:hep-ph/0509172.

[79] H. J. Warringa, D. Boer, and J. O. Andersen, *Phys. Rev.* **D72**, 014015 (2005); arXiv:hep-ph/0504177.

[80] L. N. Cooper, *Phys. Rev.* **104**, 1189 (1956).

[81] J. Bardeen, L. N. Cooper, and J. R. Schrieffer, *Phys. Rev.* **106**, 162 (1957).

[82] J. Bardeen, L. N. Cooper, and J. R. Schrieffer, *Phys. Rev.* **108**, 1175 (1957).

[83] C. Chin, M. B. A. Altmeyer, S. Riedl, S. Jochim, J. H. Denschlag, and R. Grimm, *Science* **305**, 1128 (2004); arXiv:cond-mat/0405632.

[84] I. A. Shovkovy, *Found. Phys.* **35**, 1309 (2005); arXiv:nucl-th/0410091.

[85] H. Fröhlich, *Phys. Rev.* **79**, 845 (1950).

[86] J. Bardeen, *Rev. Mod. Phys.* **23**, 261 (1951).

[87] M. Tinkham, *Introduction to superconductivity – 2nd ed.* Singapore: McGraw-Hill Book Co. (1996) 454 p.

[88] J. Polchinski, arXiv:hep-th/9210046.

[89] R. van Leeuwenn, *Phys. Rev.* **B69**, 1151101 (2004). See erratum [106].

[90] G. Fletcher, *American Journal of Physics* **58**, 50 (1990).

[91] Y. Nambu and G. Jona-Lasinio, *Phys. Rev.* **122**, 345 (1961).

[92] Y. Nambu and G. Jona-Lasinio, *Phys. Rev.* **124**, 246 (1961).

[93] J. Bijnens, C. Bruno, and E. de Rafael, *Nucl. Phys.* **B390**, 501 (1993); arXiv:hep-ph/9206236.

[94] J. Bijnens, *Phys. Rept.* **265**, 369 (1996); arXiv:hep-ph/9502335.

[95] M. Anselmino, E. Predazzi, S. Ekelin, S. Fredriksson, and D. B. Lichtenberg, *Rev. Mod. Phys.* **65**, 1199 (1993).

[96] M. G. Alford, K. Rajagopal, and F. Wilczek, *Nucl. Phys.* **B537**, 443 (1999); arXiv:hep-ph/9804403.

[97] I. A. Shovkovy and L. C. R. Wijewardhana, *Phys. Lett.* **B470**, 189 (1999); arXiv:hep-ph/9910225.

[98] T. Schäfer, *Nucl. Phys.* **B575**, 269 (2000); arXiv:hep-ph/9909574.

[99] S. B. Rüster, I. A. Shovkovy, and D. H. Rischke, *Nucl. Phys.* **A743**, 127 (2004); arXiv:hep-ph/0405170.

[100] D. Blaschke, D. N. Voskresensky, and H. Grigorian, *Nucl. Phys.* **A774**, 815 (2006); arXiv:hep-ph/0510368.

[101] S. Popov, H. Grigorian, and D. Blaschke, *Phys. Rev.* **C74**, 025803 (2006); arXiv:nucl-th/0512098.

[102] N. J. Evans, J. Hormuzdiar, S. D. H. Hsu, and M. Schwetz, *Nucl. Phys.* **B581**, 391 (2000); arXiv:hep-ph/9910313.

[103] A. W. Steiner, S. Reddy, and M. Prakash, *Phys. Rev.* **D66**, 094007 (2002); arXiv:hep-ph/0205201.

[104] B. Hiller, A. A. Osipov, V. Bernard, and A. H. Blin, *SIGMA* **2**, 026 (2006); arXiv:hep-ph/0602165.

[105] P. Amore, M. C. Birse, J. A. McGovern, and N. R. Walet, *Phys. Rev.* **D65**, 074005 (2002); arXiv:hep-ph/0110267.

[106] R. van Leeuwenn, *Phys. Rev.* **B69**, 199901(E) (2004).

Appendix A

Units

A.1 Natural units

The speed of light in vacuum, c, and the reduced Planck constant, $\hbar$, are frequently encountered constants in high-energy physics. It is therefore convenient to choose units such that these two constants are set to unity. In these so-called natural units, length, time and mass are related by

$$c = 1 = 2.9979 \times 10^{8} \text{ m s}^{-1}, \tag{A.1}$$

$$\hbar = 1 = 1.0546 \times 10^{-34} \text{ kg m}^{2} \text{ s}^{-1}. \tag{A.2}$$

Energy and mass are related by $E = mc^2$, so these quantities have the same unit. If the unit of energy is electron volt, 1 eV $= 1.6022 \times 10^{-19}$ J, and the unit of length is femtometre, fm $= 10^{-15}$ m, it follows that

$$\hbar c = 197.33 \text{ MeV fm}, \tag{A.3}$$

$$\hbar = 6.5821 \times 10^{-22} \text{ MeV s}. \tag{A.4}$$

The following conversion factors are useful

$$1 \text{ GeV}^3 = 1.3015 \times 10^{2} \text{ fm}^{-3}, \tag{A.5}$$

$$1 \text{ GeV}^4 = 1.3015 \times 10^{5} \text{ MeV fm}^{-3}, \tag{A.6}$$

$$1 \text{ MeV fm}^{-3} = 1.7827 \times 10^{12} \text{ g cm}^{-3}. \tag{A.7}$$

It is convenient to choose the unit of temperature such that Boltzmann's constant is set to unity,

$$k_B = 1 = 8.6173 \times 10^{-5} \text{ eV K}^{-1}. \tag{A.8}$$

Temperatures can then be expressed in electron volt,

$$1 \text{ MeV} = 1.1605 \times 10^{10} \text{ K}. \tag{A.9}$$

A.2 Gravitational units

For compact star calculations, it is convenient to choose units such that $c = G = 1$. In these units, length, time and mass are related by

$$c = 1 = 2.9979 \times 10^{8}\ \mathrm{m\ s^{-1}}, \tag{A.10}$$
$$G = 1 = 6.6742 \times 10^{-11}\ \mathrm{m^{3}\,kg^{-1}\,s^{-2}}. \tag{A.11}$$

It is customary to express all quantities in kilometres, $\mathrm{km} = 10^{3}$ m. The following conversion factors are useful

$$1\ \mathrm{s} = 2.9979 \times 10^{5}\ \mathrm{km}, \tag{A.12}$$
$$1\ \mathrm{kg} = 7.4237 \times 10^{-31}\ \mathrm{km}, \tag{A.13}$$
$$1\ \mathrm{g\ cm^{-3}} = 7.4237 \times 10^{-19}\ \mathrm{km^{-2}}. \tag{A.14}$$

The total gravitational mass of a star is typically given in units of the solar mass,

$$1\ \mathrm{M_{\odot}} = 1.9891 \times 10^{30}\,\mathrm{kg} = 1.4766\ \mathrm{km}. \tag{A.15}$$

An amusing fact is that it is the product GM that is measured in celestial mechanics, not the mass itself. The gravitational constant, G, is determined by experiments, similar to that by Cavendish (who improved and conducted the experiment invented by Michell). As the value of the gravitational constant is known only with a few digits of precision, the mass of the sun is more accurately known in kilometres than in kilogrammes!

A.3 Conversion factors

The properties of compact stars depend on both the microscopic physics of high-density matter and the general relativistic hydrostatic (/dynamic) equations. As it is customary to use natural units in microscopic calculations, and gravitational units in calculations of the stellar structure, it is necessary to convert units in-between these systems. The following conversion factor is useful

$$1\ \mathrm{MeV\ fm^{-3}} = 1.3234 \times 10^{-6}\ \mathrm{km^{-2}}, \tag{A.16}$$

because it can be used to convert both pressures and energy densities. Obviously, great care has to be taken when converting units in-between these systems, as the number of conditions ($G = c = \hbar = 1$) is equal to the number of dimensions.

Appendix B

Matrices and Generators

B.1 Pauli matrices

The Pauli matrices, σ_a, are infinitesimal generators of SU(2), which typically are used to describe the spin of non-relativistic fermions. In the standard basis

$$\sigma_1 = \begin{bmatrix} 0 & 1 \\ 1 & 0 \end{bmatrix}, \quad \sigma_2 = \begin{bmatrix} 0 & -i \\ i & 0 \end{bmatrix}, \quad \sigma_3 = \begin{bmatrix} 1 & 0 \\ 0 & -1 \end{bmatrix}. \tag{B.1}$$

These matrices satisfy the commutation and anticommutation relations

$$[\sigma_a, \sigma_b] = 2i\,\epsilon_{abc}\,\sigma_c, \tag{B.2}$$

$$\{\sigma_a, \sigma_b\} = 2\delta_{ab}, \tag{B.3}$$

and are traceless and hermitian.

B.2 Dirac matrices

The Dirac matrices, $\gamma^\mu = (\gamma^0, \gamma^1, \gamma^2, \gamma^3)$, are defined by the anticommutation relations $\{\gamma^\mu, \gamma^\nu\} = 2\eta^{\mu\nu}$, where $\eta^{\mu\nu}$ is the Minkowski metric. In the Weyl (/chiral) basis, the Dirac matrices are

$$\gamma^0 = \begin{bmatrix} 0 & \mathbb{1} \\ \mathbb{1} & 0 \end{bmatrix}, \quad \gamma^a = \begin{bmatrix} 0 & \sigma_a \\ -\sigma_a & 0 \end{bmatrix}, \tag{B.4}$$

where $\mathbb{1}$ is the 2x2 identity matrix and σ_a are the Pauli matrices. In this representation, the chirality matrix is

$$\gamma^5 \equiv \gamma_5 \equiv i\gamma^0\gamma^1\gamma^2\gamma^3 = \begin{bmatrix} -1 & 0 & 0 & 0 \\ 0 & -1 & 0 & 0 \\ 0 & 0 & 1 & 0 \\ 0 & 0 & 0 & 1 \end{bmatrix}, \tag{B.5}$$

and the charge conjugation matrix is

$$C = i\gamma^2\gamma^0 = \begin{bmatrix} 0 & -1 & 0 & 0 \\ 1 & 0 & 0 & 0 \\ 0 & 0 & 0 & 1 \\ 0 & 0 & -1 & 0 \end{bmatrix}. \tag{B.6}$$

The following relations are useful

$$C^{-1} = C^\dagger = C^T = -C, \tag{B.7}$$

$$C^{-1}\gamma^\mu C = -(\gamma^\mu)^T. \tag{B.8}$$

B.3 Gell-Mann matrices

The Gell-Mann matrices, λ_a, are infinitesimal generators of SU(3),

$$\begin{aligned}
\lambda_1 &= \begin{bmatrix} 0 & 1 & 0 \\ 1 & 0 & 0 \\ 0 & 0 & 0 \end{bmatrix}, \quad \lambda_2 = \begin{bmatrix} 0 & -i & 0 \\ i & 0 & 0 \\ 0 & 0 & 0 \end{bmatrix}, \\
\lambda_3 &= \begin{bmatrix} 1 & 0 & 0 \\ 0 & -1 & 0 \\ 0 & 0 & 0 \end{bmatrix}, \quad \lambda_4 = \begin{bmatrix} 0 & 0 & 1 \\ 0 & 0 & 0 \\ 1 & 0 & 0 \end{bmatrix}, \\
\lambda_5 &= \begin{bmatrix} 0 & 0 & -i \\ 0 & 0 & 0 \\ i & 0 & 0 \end{bmatrix}, \quad \lambda_6 = \begin{bmatrix} 0 & 0 & 0 \\ 0 & 0 & 1 \\ 0 & 1 & 0 \end{bmatrix}, \\
\lambda_7 &= \begin{bmatrix} 0 & 0 & 0 \\ 0 & 0 & -i \\ 0 & i & 0 \end{bmatrix}, \quad \lambda_8 = \tfrac{1}{\sqrt{3}} \begin{bmatrix} 1 & 0 & 0 \\ 0 & 1 & 0 \\ 0 & 0 & -2 \end{bmatrix}.
\end{aligned} \tag{B.9}$$

These satisfy the commutation relations,

$$[\lambda_a, \lambda_b] = i f_{abc} \lambda_c, \tag{B.10}$$

where f_{abc} are the antisymmetric group structure constants. The Gell-Mann matrices are used, *e.g.*, to describe colour charge, in a similar way as the Pauli matrices are used to describe spin and isospin. Like the Pauli matrices, the Gell-Mann matrices are traceless and hermitian.

Appendix C

Thermodynamic Relations

The following is a list of useful relations frequently encountered in thermal field theory. For more information, see Chapter 3. If variational parameters are introduced, *e.g.*, condensates, the equalities defined below hold at the extremum with respect to variations of these parameters. For a system described by a hamiltonian, H, and a set of conserved number operators, $\hat{N}_i$, the grand canonical partition function is

$$Z(\mu, T, V) = \mathrm{Tr}\, e^{-\beta(H-\mu_i \hat{N}_i)}. \tag{C.1}$$

Here, μ_i are the chemical potentials conjugate to the conserved charges and $\beta = 1/T$ (in units where $k_B = 1$). The number operators are hermitian and commute with H, as well as with each other. In most modern applications, it is convenient to express the partition function as a functional integral of the fields

$$Z(\mu, T, V) = N \int [\phi]\, e^{S}, \tag{C.2}$$

where N is a normalisation factor and S is the action,

$$S = \int_0^\beta d\tau \int d^3x\, \mathcal{L}. \tag{C.3}$$

The grand canonical thermodynamic potential is

$$\Omega(\mu, T) = -\frac{T \ln Z}{V}. \tag{C.4}$$

The pressure, P, is related to the thermodynamic potential by

$$P(\mu, T) = -\Omega(\mu, T), \tag{C.5}$$

at the minimum of Ω with respect to any variational parameters. The entropy density, s, and number densities, n_i, are

$$s(\mu, T) = \frac{\partial P(\mu, T)}{\partial T}, \tag{C.6}$$

$$n_i(\mu, T) = \frac{\partial P(\mu, T)}{\partial \mu_i}. \tag{C.7}$$

As the pressure in vacuum is zero, the thermodynamic potential should be normalised such that $P_0 = -\Omega(0,0) = 0$. The energy density, ϵ, then is

$$\epsilon = Ts + \sum_i \mu_i \, n_i - P. \tag{C.8}$$

Appendix D

Determinants

Determinants occur naturally in thermal field theory, because the trace in the partition function (C.1) is typically evaluated from the identity Tr $\ln S = \ln \det S$. The following relations are useful

$$\begin{aligned} |a\mathbb{1} + A| &= \left|a\mathbb{1} + B^{-1}AB\right|, & \text{(D.1)} \\ \left|\begin{array}{cc} A & B \\ C & D \end{array}\right| &= \left|\begin{array}{c} \\ A \end{array}\right| \left|\begin{array}{c} \\ D - CA^{-1}B \end{array}\right|, & \text{(D.2)} \end{aligned}$$

where A, B, C, and D are NxN matrices, $|S| \equiv \det S$, a is a scalar, and $\mathbb{1}$ is the identity matrix. The first relation (D.1) follows from

$$\begin{aligned} |a\mathbb{1} + A| &= |B^{-1}B|\,|a\mathbb{1} + A| = |B^{-1}|\,|B|\,|a\mathbb{1} + A| = |B^{-1}|\,|a\mathbb{1} + A|\,|B| \\ &= |B^{-1}a\mathbb{1}B + B^{-1}AB| = |a\mathbb{1} + B^{-1}AB|, \end{aligned} \qquad \text{(D.3)}$$

for any invertible matrix B. The block matrices in the second relation (D.2) should be ordered wisely with the help of the identities

$$\left|\begin{array}{cc} A & B \\ C & D \end{array}\right| = \left|\begin{array}{cc} D & C \\ B & A \end{array}\right| = (-1)^N \left|\begin{array}{cc} B & A \\ D & C \end{array}\right| = (-1)^N \left|\begin{array}{cc} C & D \\ A & B \end{array}\right|. \qquad \text{(D.4)}$$

These relations can be used recursively to evaluate and simplify determinants. The dimension of the operator is reduced by a factor two for each recursion. The trade-off is that the inverse of one submatrix must be evaluated for each recursion (in numerical applications) or that the matrix elements become more involved (in analytical applications). The proof of (D.2) is straightforward. If A has an inverse, it follows that

$$\left[\begin{array}{cc} \mathbb{1} & 0 \\ -CA^{-1} & \mathbb{1} \end{array}\right] \left[\begin{array}{cc} A & B \\ C & D \end{array}\right] = \left[\begin{array}{cc} \mathbb{1} & B \\ 0 & -CA^{-1}B + D \end{array}\right] \left[\begin{array}{cc} A & 0 \\ 0 & \mathbb{1} \end{array}\right]. \qquad \text{(D.5)}$$

Cofactor expansion yields

$$\begin{vmatrix} A & 0 \\ 0 & \mathbb{1} \end{vmatrix} = \mid A \mid, \tag{D.6}$$

$$\begin{vmatrix} \mathbb{1} & 0 \\ -CA^{-1} & \mathbb{1} \end{vmatrix} = 1, \tag{D.7}$$

$$\begin{vmatrix} \mathbb{1} & B \\ 0 & -CA^{-1}B + D \end{vmatrix} = \mid D - CA^{-1}B \mid. \tag{D.8}$$

Since $\det(AB) = \det(A)\det(B)$ it follows that

$$\begin{vmatrix} A & B \\ C & D \end{vmatrix} = \mid A \mid \mid D - CA^{-1}B \mid. \tag{D.9}$$

Appendix E

Derivatives of the Potential

The thermodynamic potential is on the form

$$\Omega(\mu,T)=\Omega_0-\frac{\gamma}{2}\int\frac{d^3p}{(2\pi)^3}\sum_{i=1}^{N}\left[\frac{\lambda_i(p,\mu)}{2}+T\ln\left(1+e^{-\lambda_i(p,\mu)/T}\right)\right], \tag{E.1}$$

where $\lambda_i(p,\mu)$ are the eigenvalues of a hermitian matrix and $\gamma=72/N$ is the eigenvalue degeneracy factor, *i.e.*, $\gamma=1$ if all 72 degrees of freedom in flavour, colour, Dirac, and Nambu-Gorkov space are summed over. Typically, some eigenvalues are equal, or differ only in the sign, and can therefore be omitted if γ is adjusted accordingly. The entropy density is

$$s=-\frac{\partial\Omega}{\partial T}=\frac{\gamma}{2}\int\frac{d^3p}{(2\pi)^3}\sum_{i=1}^{N}\left[\ln\left(1+e^{-\lambda_i(p,\mu)/T}\right)+\frac{\lambda_i(p,\mu)/T}{1+e^{\lambda_i(p,\mu)/T}}\right], \tag{E.2}$$

and any number density, n_a, can be obtained from the formula

$$n_a=-\frac{\partial\Omega}{\partial\mu_a}=\frac{\gamma}{2}\int\frac{d^3p}{(2\pi)^3}\sum_{i=1}^{N}\frac{\partial\lambda_i}{\partial\mu_a}\left[\frac{1}{2}-\frac{1}{1+e^{\lambda_i(p,\mu)/T}}\right]. \tag{E.3}$$

The entropy density and number densities are needed to calculate the energy density, $\epsilon=sT+\sum_a n_a\mu_a+\Omega$, and the conserved charges that should be neutralised. The gap equations are on a similar form,

$$0=\frac{\partial\Omega}{\partial\Delta_b}=\frac{\partial\Omega_0}{\partial\Delta_b}-\frac{\gamma}{2}\int\frac{d^3p}{(2\pi)^3}\sum_{i=1}^{N}\frac{\partial\lambda_i}{\partial\Delta_b}\left[\frac{1}{2}-\frac{1}{1+e^{\lambda_i(p,\mu)/T}}\right], \tag{E.4}$$

where Δ_b is a gap (or any other variational parameter). Consequently, all relevant quantities that can be derived from the thermodynamic potential can be calculated (integrated) in parallel. The derivatives of the eigenvalues are calculated with the method described in the following appendix, and can be obtained practically at the cost of computing the eigenvectors.

Appendix F

Derivatives of Eigenvalues

Let A be an NxN hermitian matrix with eigenvalues λ_i and eigenvectors v_i, where $i = 1...N$. Let the elements of A be functions of a variable x. The derivatives of the eigenvalues with respect to x are

$$\frac{\partial \lambda_i}{\partial x} = \frac{1}{v_i^\dagger v_i} \times v_i^\dagger \frac{\partial A}{\partial x} v_i. \tag{F.1}$$

Proof: The eigenvalue equation is

$$(A - \lambda I)\, v = 0. \tag{F.2}$$

Since A is hermitian, it follows that

$$v^\dagger (A - \lambda I) = 0. \tag{F.3}$$

The derivative of the eigenvalue equation with respect to x is

$$\frac{\partial}{\partial x}(Av - \lambda v) = \frac{\partial A}{\partial x} v + (A - \lambda I)\frac{\partial v}{\partial x} - \frac{\partial \lambda}{\partial x} v = 0. \tag{F.4}$$

Multiply with $v^\dagger$ from the left-hand side

$$v^\dagger \frac{\partial A}{\partial x} v + v^\dagger (A - \lambda I)\frac{\partial v}{\partial x} - v^\dagger \frac{\partial \lambda}{\partial x} v = 0. \tag{F.5}$$

The second term is zero, so the expression simplifies to

$$v^\dagger \frac{\partial A}{\partial x} v - v^\dagger \frac{\partial \lambda}{\partial x} v = 0, \tag{F.6}$$

which can be written

$$\frac{\partial \lambda}{\partial x} = \frac{1}{v^\dagger v} \times v^\dagger \frac{\partial A}{\partial x} v. \tag{F.7}$$

Paper I

Available online at www.sciencedirect.com
SCIENCE DIRECT®
Physics Letters B 616 (2005) 1–7
PHYSICS LETTERS B
www.elsevier.com/locate/physletb

Preon stars: a new class of cosmic compact objects

J. Hansson, F. Sandin

Department of Physics, Luleå University of Technology, SE-971 87 Luleå, Sweden

Received 8 June 2004; accepted 12 April 2005

Available online 26 April 2005

Editor: W. Haxton

Abstract

In the context of the standard model of particle physics, there is a definite upper limit to the density of stable compact stars. However, if a more fundamental level of elementary particles exists, in the form of preons, stability may be re-established beyond this limiting density. We show that a degenerate gas of interacting fermionic preons does allow for stable compact stars, with densities far beyond that in neutron stars and quark stars. In keeping with tradition, we call these objects "preon stars", even though they are small and light compared to white dwarfs and neutron stars. We briefly note the potential importance of preon stars in astrophysics, e.g., as a candidate for cold dark matter and sources of ultra-high energy cosmic rays, and a means for observing them.

PACS: 12.60.Rc; 04.40.Dg; 97.60.-s; 95.35.+d

Keywords: Preons; Preon stars; Compact objects; Dark matter; Cosmic rays

1. Introduction

The three different types of compact objects traditionally considered in astrophysics are white dwarfs, neutron stars (including quark and hybrid stars), and black holes. The first two classes are supported by Fermi pressure from their constituent particles. For white dwarfs, electrons provide the pressure counterbalancing gravity. In neutron stars, the neutrons play this role. For black holes, the degeneracy pressure is overcome by gravity and the object collapses indefinitely, or at least to the Planck density.

The distinct classes of degenerate compact stars originate directly from the properties of gravity, as was made clear by a theorem of Wheeler and collaborators in the mid 1960s [1]. The theorem states that for the solutions to the stellar structure equations, whether Newtonian or relativistic, there is a change in stability of one radial mode of normal vibration whenever the mass reaches a local maximum or minimum as a function of central density. The theorem assures that distinct classes of stars, such as white dwarfs and neu-

E-mail addresses: c.johan.hansson@ltu.se (J. Hansson), fredrik.sandin@ltu.se (F. Sandin).

0370-2693/$ – see front matter
doi:10.1016/j.physletb.2005.04.034

tron stars, are separated in central density by a region in which there are no stable configurations.

In the Standard Model of particle physics (SM), the theory of the strong interaction between quarks and gluons predicts that with increasing energy and density, the coupling between quarks asymptotically fades away [2,3]. As a consequence of this "asymptotic freedom", matter is expected to behave as a gas of free fermions at sufficiently high densities. This puts a definite upper limit to the density of stable compact stars, since the solutions to the stellar equations end up in a never-ending sequence of unstable configurations, with increasing central density. Thus, in the light of the standard model, the densest stars likely to exist are neutron stars, quark stars or the potentially more dense hybrid stars [4–6]. However, if there is a deeper layer of constituents, below that of quarks and leptons, asymptotic freedom will break down at sufficiently high densities, as the quark matter phase dissolves into the preon subconstituent phase.

There is a general consensus among the particle physics community, that something new should appear at an energy-scale of around one TeV. The possibilities are, e.g., supersymmetric particles, new dimensions and compositeness. In this Letter we consider "preon models" [7,8], i.e., models in which quarks and leptons, and sometimes some of the gauge bosons, are composite particles built out of more elementary preons. If fermionic preons exist, it seems reasonable that a new type of astrophysical compact object, a *preon star*, could exist. The density in preon stars should far exceed that inside neutron stars, since the density of preon matter must be much higher than the density of nuclear and deconfined quark matter. The sequence of compact objects, in order of increasing compactness, would thus be: white dwarfs, neutron stars, preon stars and black holes.

2. Mass–radius relations

Assuming that a compact star is composed of non-interacting fermions with mass m_f, the non-general relativistic (Chandrasekhar) expression for the maximum mass is [9,10]:

$$M \simeq \frac{1}{m_f^2}\left(\frac{\hbar c}{G}\right)^{3/2}. \tag{1}$$

This expression gives a correct order of magnitude estimate for the mass of a white dwarf and a neutron star. For quark stars, this estimate cannot be used literally, since the mass of quarks cannot be defined in a similar way as for electrons and neutrons. However, making the simplifying assumption that quarks are massless and subject to a 'bag constant', a maximum mass relation can be derived [11]. The bag constant is a phenomenological parameter. It represents the strong interactions that, in addition to the quark momenta, contribute mass–energy to deconfined quark matter, i.e., in the same way as the bag constant for ordinary hadrons [12]. The result in [11] is somewhat similar to the Chandrasekhar expression, but the role of the fermion mass is replaced by the bag constant B:

$$M = \frac{16\pi B R^3}{3c^2}, \tag{2}$$

$$R = \frac{3c^2}{16\sqrt{\pi G B}}. \tag{3}$$

For preon stars, one can naively insert a preon mass of $m_f \simeq 1\ \mathrm{TeV}/c^2$ in Eq. (1) to obtain a preon star mass of approximately one Earth mass ($M_\oplus \simeq 6\times 10^{24}$ kg). However, the energy scale of one TeV should rather be interpreted as a length scale, since it originates from the fact that in particle physics experiments, no substructure has been found down to a scale of a few hundred GeV ($\hbar c/\mathrm{GeV} \simeq 10^{-18}$ m). Since preons must be able to give light particles, e.g., neutrinos and electrons, the "bare" preon mass presumably is fairly small and a large fraction of the mass–energy should be due to interactions. This is the case for deconfined quark matter, where the bag constant contributes more than 10% of the energy density. Guided by this observation, and lacking a quantitative theory for preon interactions, we assume that the mass–energy contribution from preon interactions can be accounted for by a bag constant. We estimate the order of magnitude for the preon bag constant by fitting it to the minimum density of a composite electron, with mass $m_e = 511\ \mathrm{keV}/c^2$ and "radius" $R_e \lesssim \hbar c/\mathrm{TeV} \simeq 10^{-19}$ m. The bag-energy is roughly $4B\langle V\rangle$ [12], where $\langle V\rangle$ is the time-averaged volume of the bag (electron), so the bag constant is:

$$B \simeq \frac{E}{4\langle V\rangle} \gtrsim \frac{3\times 511\ \mathrm{keV}}{16\pi(10^{-19}\ \mathrm{m})^3} \simeq 10^4\ \mathrm{TeV/fm^3}$$
$$\Longrightarrow B^{1/4} \gtrsim 10\ \mathrm{GeV}. \tag{4}$$

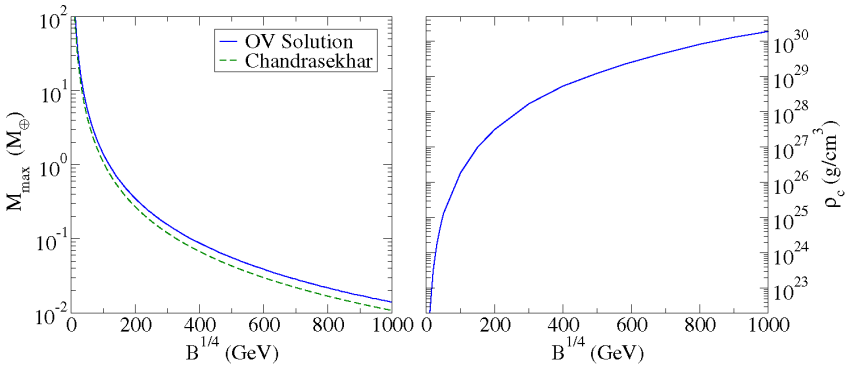

Fig. 1. The maximum mass and corresponding central density ρ_c of a preon star vs. the bag constant B. The solid lines represent the general relativistic OV solutions, while the dashed line represents the Newtonian (Chandrasekhar) estimate. Despite the high central density, the mass of these objects is below the Schwarzschild limit, as is always the case for static solutions to the stellar equations. $M_\oplus \simeq 6 \times 10^{24}$ kg is the Earth mass.

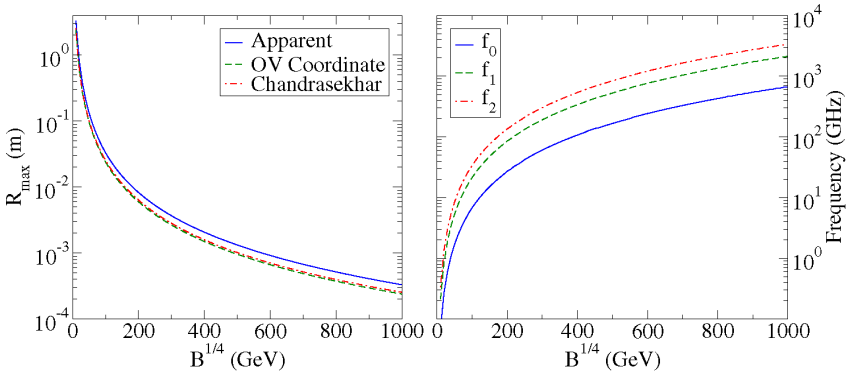

Fig. 2. The maximum radius and the corresponding first three eigenmode oscillation frequencies (f_0, f_1, f_2) vs. the bag constant. The solid line in the left-hand picture is the "apparent" radius, $R^\infty = R/\sqrt{1-2GM/Rc^2}$, as seen by a distant observer. The dashed line represents the general relativistic coordinate radius obtained from the OV solution, while the dotted line represents the Newtonian (Chandrasekhar) estimate. Since the fundamental mode f_0 is real ($\omega_0^2 > 0$), preon stars with mass below the maximum are stable, for each value of B.

Inserting this value of B in Eqs. (2), (3), we obtain an estimate for the maximum mass, $M_{\max} \simeq 10^2\ M_\oplus$, and radius, $R_{\max} \simeq 1$ m, of a preon star.

Since $B^{1/4} \simeq 10$ GeV only is an order of magnitude estimate for the minimum value of B, in the following, we consider the bag constant as a free parameter of the model, with a lower limit of $B^{1/4} = 10$ GeV and an upper limit chosen as $B^{1/4} = 1$ TeV. The latter value corresponds to an electron "radius" of $\hbar c/10^3$ TeV $\simeq 10^{-22}$ m. In Figs. 1 and 2 the (Chandrasekhar) maximum mass and radius of a preon star are plotted as a function of the bag constant.

Due to the extreme density of preon stars, a general relativistic treatment is necessary. This is especially important for the analysis of stability when a preon star is subject to small radial vibrations. In this introductory article we will neglect the effects of rotation on the composition. Thus, we can use the Oppenheimer–Volkoff (OV) equations [13] for hydrostatic, spherically symmetric equilibrium:

$$\frac{dp}{dr} = -\frac{G(p+\rho c^2)(mc^2 + 4\pi r^3 p)}{r(rc^4 - 2Gmc^2)}, \tag{5}$$

$$\frac{dm}{dr} = 4\pi r^2 \rho. \tag{6}$$

Here p is the pressure, ρ the total density and $m = m(r)$ the mass within the radial coordinate r. The total mass of a preon star is $M = m(R)$, where R is the coordinate radius of the star. Combined with an equation of state (EoS), $p = p(\rho)$, obtained from some microscopic theory, the OV solutions give the possible equilibrium states of preon stars.

Since no theory for the interaction between preons yet exists, we make a simple assumption for the EoS. The EoS for a gas of massless fermions is $\rho c^2 = 3p$ (see, e.g., [14]), independently of the degeneracy factor of the fermions. By adding a bag constant B, one obtains $\rho c^2 = 3p + 4B$. This is the EoS that we have used when solving the OV equations. The obtained (OV) maximum mass and radius configurations are also plotted in Figs. 1 and 2.

3. Stability analysis

A necessary, but not sufficient, condition for stability of a compact star is that the total mass is an increasing function of the central density $dM/d\rho_c > 0$ [14]. This condition implies that a slight compression or expansion of a star will result in a less favourable state, with higher total energy. Obviously, this is a necessary condition for a stable equilibrium configuration. Equally important, a star must be stable when subject to radial oscillations. Otherwise, any small perturbation would bring about a collapse of the star.

The equations for the analysis of such radial modes of oscillation are due to Chandrasekhar [15]. An overview of the theory, and some applications, can be found in [16]. For clarity, we reproduce some of the important points. Starting with the metric of a spherically symmetric equilibrium stellar model

$$ds^2 = -e^{2\nu(r)}\,dt^2 + e^{2\lambda(r)}\,dr^2 + r^2\bigl(d\theta^2 + \sin^2(\theta)\,d\phi^2\bigr), \tag{7}$$

and the energy–momentum tensor of a perfect fluid, $T_{\mu\nu} = (\rho + p)u_\mu u_\nu + p g_{\mu\nu}$, the equation governing radial adiabatic oscillations can be derived from Einstein's equation. By making an ansatz for the time dependence of the radial displacement of fluid elements of the form:

$$\delta r(r,t) = r^{-2} e^{\nu(r)} \zeta(r) e^{i\omega t}, \tag{8}$$

the equation simplifies to a Sturm–Liouville eigenvalue equation for the eigenmodes [15,16]:

$$\frac{d}{dr}\left(P\frac{d\zeta}{dr}\right) + \left(Q + \omega^2 W\right)\zeta = 0. \tag{9}$$

The coefficients P, Q and W are [16] (in geometric units where $G = c = 1$):

$$P = \Gamma r^{-2} p e^{\lambda(r)+3\nu(r)}, \tag{10}$$

$$Q = e^{\lambda(r)+3\nu(r)}\left[(p+\rho)^{-1} r^{-2}\left(\frac{dp}{dr}\right)^2 - 4r^{-3}\frac{dp}{dr} - 8\pi r^{-2} p(p+\rho)e^{2\lambda(r)}\right], \tag{11}$$

$$W = (p+\rho) r^{-2} e^{3\lambda(r)+\nu(r)}, \tag{12}$$

where the adiabatic index Γ is:

$$\Gamma = \frac{p+\rho}{p}\left(\frac{\partial p}{\partial \rho}\right)_S. \tag{13}$$

The boundary conditions for $\zeta(r)$ are that $\zeta(r)/r^3$ is finite or zero as $r \to 0$, and that the Lagrangian variation of the pressure,

$$\Delta p = -\frac{\Gamma p e^{\nu}}{r^2}\frac{d\zeta}{dr}, \tag{14}$$

vanishes at the surface of the star.

A catalogue of various numerical methods for the solution of Eq. (9) can be found in [17]. In principle, we first solve the OV equations, thereby obtaining the metric functions $\lambda(r)$ and $\nu(r)$, as well as $p(r)$, $\rho(r)$ and $m(r)$. Then, the metric functions $\lambda(r)$ and $\nu(r)$ must be corrected for, so that they match the Schwarzschild metric at the surface of the star (see, e.g., [14]). Once these quantities are known, Eq. (9) can be solved for $\zeta(r)$ and ω^2 by a method commonly known as the "shooting" method. One starts with an initial guess on ω^2, and integrates Eq. (9) from $r = 0$ to the surface of the star. At this point $\zeta(r)$ is known, and Δp can be calculated. The number of nodes of $\zeta(r)$ is a non-decreasing function of ω^2 (due to Sturm's oscillation theorem). Thus, one can continue making educated guesses for ω^2, until the correct boundary condition ($\Delta p = 0$) and number of nodes are obtained. This method is simple to use when only a few eigenmodes are needed.

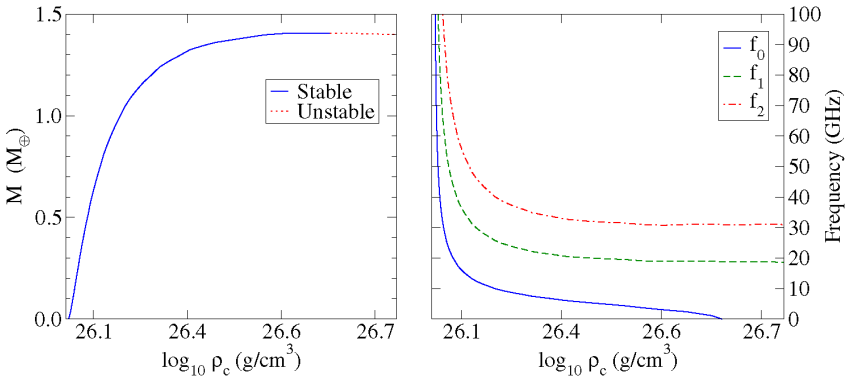

Fig. 3. The mass and the first three eigenmode oscillation frequencies (f_0, f_1, f_2) vs. the central density ρ_c of preon stars. Here, a fixed value of $B^{1/4} = 100$ GeV has been used. For the maximum mass configuration, the fundamental mode f_0 has zero frequency, indicating the onset of instability. Preon stars with mass and density below the maximum mass configuration of this sequence are stable.

Due to the time dependence in Eq. (8), a necessary (and sufficient) condition for stability is that all ω_i^2 are positive. Since ω_i^2 are eigenvalues of a Sturm–Liouville equation, and governed by Sturm's oscillation theorem, it is sufficient to prove that the fundamental mode, ω_0^2, is greater than zero for a star to be stable. In Fig. 3 the first three oscillation frequencies, $f_i = \omega_i/2\pi$, for various stellar configurations with $B^{1/4} = 100$ GeV are plotted. In agreement with the turning point theorem of Wheeler et al. [1], the onset of instability is the point of maximum mass, as ω_0^2 becomes negative for higher central densities. Thus, for this value of the bag constant, preon stars are stable up to the maximum mass configuration. In order to see if the same is true for other values of B, we plot the first three oscillation frequencies as a function of B, choosing the maximum radius configuration for each B. The result can be found in Fig. 2. Indeed, the previous result is confirmed; all configurations up to the maximum mass are stable.

The eigenmode frequencies for radial oscillations of preon stars are about six orders of magnitude higher than for neutron stars. This result can also be obtained by making a simple estimate for the frequency of the fundamental mode. The radius of a preon star is a factor of $\sim 10^5$ smaller than neutron stars. Hence, if the speed of sound is similar in preon stars and neutron stars, the frequency would increase by a factor of $\sim 10^5$, giving GHz frequencies. If the speed of sound is higher in preon stars, say approaching the speed of light, the maximum frequency is $\sim 10^8\ \mathrm{m\,s^{-1}}/0.1\ \mathrm{m} \simeq 1$ GHz. Thus, in either case, GHz oscillation frequencies are expected for preon stars.

4. Potential astrophysical consequences and detection

If preon stars do exist, and are as small as 10^{-1}–10^{-4} m, it is plausible that primordial preon stars (or "nuggets") formed from density fluctuations in the early universe. As this material did not take part in the ensuing nucleosynthesis, the abundance of preon nuggets is not constrained by the hot big bang model bounds on baryonic matter. Also, preon nuggets are immune to Hawking radiation [18] that rapidly evaporates small primordial black holes, making it possible for preon nuggets to survive to our epoch. They can therefore serve as the mysterious dark matter needed in many dynamical contexts in astrophysics and cosmology [19,20].

Preon stars born out of the collapse of massive ordinary stars [21] cannot contribute much to cosmological dark matter, as that material originally is baryonic and thus constrained by big bang nucleosynthesis. However, they could contribute to the dark matter in galaxies. Roughly 4% of the total mass of the universe is in baryonic form [22], but only 0.5% is observed as visible baryons [23]. Assuming, for simplicity, that all dark matter $\rho_{\mathrm{DM}} = 10^{-25}\ \mathrm{g/cm^3}$ in

spiral galaxies, e.g., our own Milky Way, is in the form of preon stars with mass 10^{24} kg, the number density of preon stars is of the order of 10^4 per cubic parsec (1 pc $\simeq 3.1 \times 10^{16}$ m). This translates into one preon star per 10^6 solar system volumes. However, even though it is not ruled out a priori, the possibility to form a very small and light preon star in the collapse of a large massive star remains to be more carefully investigated. In any case, preon nuggets formed in the primordial density fluctuations could account for the dark matter in galaxies. The existence of such objects can in principle be tested by gravitational microlensing experiments.

Today there is no known mechanism for the acceleration of cosmic rays with energies above $\sim 10^{17}$ eV. These so-called ultra-high energy cosmic rays [24] (UHE CR) are rare, but have been observed with energies approaching 10^{21} eV. The sources of UHE CR must, cosmologically speaking, be nearby ($\lesssim 50$ Mpc $\simeq 150$ million light years) due to the GZK-cutoff energy $\sim 10^{19}$ eV [25,26], since the cosmic microwave background is no longer transparent to cosmic rays at such high energies. This requirement is very puzzling, as there are no known sources capable of accelerating UHE CR within this distance. Preon stars open up a new possibility. It is known that neutron stars, in the form of pulsars, can be a dominant source of galactic cosmic rays [27], but cannot explain UHE CR. If for preon stars we assume, as in models of neutron stars, that the magnetic flux of the parent star is (more or less) frozen-in during collapse, induced electric fields more than sufficient for the acceleration of UHE CR become possible. As an example, assume that the collapse of a massive star is slightly too powerful for the core to stabilize as a 10 ms pulsar with radius 10 km, mass $1.4M_\odot$ ($M_\odot \simeq 2 \times 10^{30}$ kg is the mass of our sun) and magnetic field 10^8 T, and instead collapses to a preon star state with radius 1 m and mass $10^2 M_\oplus$. An upper limit estimate of the induced electric field of the remaining "preon star pulsar" yields $\sim 10^{34}$ V/m, which is more than enough for the acceleration of UHE CR. Also, such strong electric fields are beyond the limit where the quantum electrodynamic vacuum is expected to break down, $|\mathbf{E}| > 10^{18}$ V/m, and spontaneously start pair-producing particles [28]. This could provide an intrinsic source of charged particles that are accelerated by the electric field, giving UHE CR. With cosmic ray detectors, like the new Pierre Auger Observatory [29], this could provide means for locating and observing preon stars.

5. Conclusions

In this Letter we argue that if there is a deeper layer of fermionic constituents, so-called preons, below that of quarks and leptons, a new class of stable compact stars could exist. Since no detailed theory yet exists for the interaction between preons, we assume that the mass–energy contribution from preon interactions can be accounted for by a 'bag constant'. By fitting the bag constant to the energy density of a composite electron, the maximum mass for preon stars can be estimated to $\sim 10^2 M_\oplus$ ($M_\oplus \simeq 6 \times 10^{24}$ kg being the Earth mass), and their maximum radius to ~ 1 m. The central density is at least of the order of 10^{23} g/cm^3. Preon stars could have formed by primordial density fluctuations in the early universe, and in the collapse of massive stars. We have briefly noted their potential importance for dark matter and ultra-high energy cosmic rays, connections that also could be used to observe them. This might provide alternative means for constraining and testing different preon models, in addition to direct tests [8] performed at particle accelerators.

Acknowledgements

F. Sandin acknowledges support from the Swedish National Graduate School of Space Technology. We thank S. Fredriksson for several useful discussions and for reading the manuscript.

References

[1] B.K. Harrison, K.S. Thorne, M. Wakano, J.A. Wheeler, Gravitation Theory and Gravitational Collapse, University of Chicago Press, Chicago, 1965.
[2] D.J. Gross, F. Wilczek, Phys. Rev. Lett. 30 (1973) 1323.
[3] H.D. Politzer, Phys. Rev. Lett. 30 (1973) 1346.
[4] U.H. Gerlach, Phys. Rev. 172 (1968) 1325;
U.H. Gerlach, A third family of stable equilibria, Ph.D. thesis, Princeton University, 1968.
[5] N.K. Glendenning, C. Kettner, Astron. Astrophys. 353 (2000) L9.

[6] K. Schertler, et al., Nucl. Phys. A 677 (2000) 463.
[7] I.A. D'Souza, C.S. Kalman, Preons, World Scientific, Singapore, 1992.
[8] J.-J. Dugne, S. Fredriksson, J. Hansson, Europhys. Lett. 57 (2002) 188.
[9] S. Chandrasekhar, An Introduction to the Study of Stellar Structure, Dover, New York, 1958.
[10] L.D. Landau, Phys. Z. Sowjetunion 1 (1932) 285.
[11] S. Banerjee, S.K. Ghosh, S. Raha, J. Phys. G 26 (2000) L1.
[12] A. Chodos, et al., Phys. Rev. D 9 (1974) 3471.
[13] J.R. Oppenheimer, G. Volkoff, Phys. Rev. 55 (1939) 374.
[14] N.K. Glendenning, Compact Stars, Springer-Verlag, New York, 1997.
[15] S. Chandrasekhar, Phys. Rev. Lett. 12 (1964) 114.
[16] C.W. Misner, K.S. Thorne, J.A. Wheeler, Gravitation, Freeman, San Francisco, 1973.
[17] J.M. Bardeen, K.S. Thorne, D.W. Meltzer, Astrophys. J. 145 (1966) 505.
[18] S.W. Hawking, Commun. Math. Phys. 43 (1975) 199.
[19] M.S. Turner, Phys. Rep. 333 (2000) 619.
[20] L. Bergström, Rep. Prog. Phys. 63 (2000) 793.
[21] B. Paczyński, Astrophys. J. 494 (1998) L45.
[22] D.N. Spergel, et al., Astrophys. J. Suppl. 148 (2003) 175.
[23] K. Hagiwara, et al., Phys. Rev. D 66 (2002) 010001.
[24] M. Nagano, A.A. Watson, Rev. Mod. Phys. 72 (2000) 689.
[25] K. Greisen, Phys. Rev. Lett. 16 (1966) 748.
[26] G.T. Zatsepin, V.A. Kuzmin, JETP Lett. 41 (1966) 78.
[27] T. Gold, Nature 221 (1969) 25.
[28] J. Schwinger, Phys. Rev. 82 (1951) 664.
[29] M.T. Dova, et al., Nucl. Phys. B (Proc. Suppl.) 122 (2003) 170.

Paper II

Eur Phys J C (2005)
Digital Object Identifier (DOI) 10.1140/epjcd/s2005-03-003-y

EPJ C direct
electronic only

Young Scientist

Compact stars in the standard model – and beyond

F. Sandin

Department of Physics, Luleå University of Technology, 97187 Luleå, Sweden, e-mail: fredrik.sandin@ltu.se

Received: 24 January 2005 / Accepted: 10 February 2005 /
Published online: 23 February 2005 –

Abstract. In the context of the standard model of particle physics, there is a definite upper limit to the density of stable compact stars. However, if there is a deeper layer of constituents, below that of quarks and leptons, stability may be re-established far beyond this limiting density and a new class of compact stars could exist. These objects would cause gravitational lensing of gamma-ray bursts and white dwarfs, which might be observable as line features in the spectrum. Such observations could provide means for obtaining new clues about the fundamental particles and the nature of cold dark matter.

PACS. 12.60.Rc, 04.40.Dg, 95.35.+d

1 Introduction

The different types of compact objects traditionally considered in astrophysics are white dwarfs, neutron stars (including quark and hybrid stars), and black holes. The first two classes are supported by Fermi degeneracy pressure from their constituent particles. For white dwarfs, electrons provide the pressure counterbalancing gravity. In neutron stars, the neutrons play this role. For black holes, the degeneracy pressure is overcome by gravity and the object collapses to a singularity, or at least to the Planck scale ($\rho \sim 10^{93}$ g/cm^3). For a recent review of neutron stars, hybrid stars, and quark stars, see, e.g., [1] and references therein.

The distinct classes of degenerate compact stars originate directly from the properties of gravity, as was made clear by a theorem of Wheeler and collaborators in the mid 1960s [2]. This theorem states that for the solutions to the stellar structure equations, whether Newtonian or relativistic, there is a change in stability of one radial mode of vibration whenever the mass reaches a local maximum or minimum as a function of the central density. The theorem assures that distinct classes of stars, such as white dwarfs and neutron stars, are separated in central density by a region in which there are no stable configurations.

In the standard model of quarks and leptons (SM), the theory of the strong interaction between quarks and gluons predicts that with increasing energy and density, the coupling between quarks asymptotically fades away [3, 4]. As a consequence of this so-called asymptotic freedom, matter is expected to behave as a gas of free fermions at sufficiently high densities. This puts a definite upper limit to the density of stable compact stars, since the solutions to the stellar equations end up in a never-ending sequence of unstable configurations, with increasing central density. Thus, in the light of the standard model, the densest stars likely to exist are neutron stars, quark stars, or the slightly more dense hybrid stars [5–7]. However, if there is a deeper layer of constituents, below that of quarks and leptons, the possibility of a new class of compact stars opens up [8].

Though being a quantitatively successful theory, the SM consists of a large number of exogenous *ad hoc* rules and parameters, which were introduced solely to fit the experimental data. The SM provides no explanation for the deeper meaning of these rules. At a closer look, however, the SM seems to be full of hints to its deeper background. By considering these rules from a historical point of view, a "simple" and appealing explanation is *compositeness* [9], i.e., that the quarks, leptons, and gauge bosons are composite particles, built out of more elementary *preons* [10]. Preons provide natural explanations for the particle families of the SM and phenomena such as neutrino oscillations, mixing of the weak gauge bosons, and quarks of different flavour.

Over the last decades, many papers have been written about preons, but so far there are no direct evidence for (or against!) their existence. In the late 1970s, a number of consistency conditions were formulated by 't Hooft [11]. In the same work, a vector-like non-Abelian $SU(3)$ gauge group was considered, but no solution to the consistency conditions was found. Later, it was shown that with another choice for the gauge group and the flavour structure of preons, e.g., three different preon flavours, the consistency conditions are satisfied [12]. For a more detailed discussion of preon models, see [9, 10, 13] and references therein.

Not all clues favour preon models, but the existence of preons is still an open question and, as a consequence, so is the question whether a new class of compact stars exists or not. This paper is based on the ideas and results presented in [8]. Assuming that quarks and leptons are composite particles, built out of more elementary preons, I will:

I. Give an estimate for the mass and radius of stars composed of preons.
II. Show that for some particular equations of state, stable solutions to the general relativistic stellar equations do exist, with densities far beyond the maximum density in stars composed of quarks and leptons.
III. Briefly discuss some potential astrophysical consequences and how these objects could be observed. Herein lies the potential importance of this qualitative speculation, since these objects are candidates for cold dark matter and could be found as, e.g., gravitational "femtolenses".

2 The maximum density prophecy

In order to explain why there is a maximum density for stars composed of quarks and leptons, or any other composite particle composed of these two species, e.g., nucleons and ^{56}Fe, some basic knowledge about the theory of compact stars is needed. In the following, I give a short introduction and a summary of the main points.

Due to the high density and large mass of compact stars, a general relativistic treatment of the equilibrium configurations is necessary. This is especially important for the analysis of stability when a star is subject to radial oscillations. Such oscillations are inevitably excited to some extent, and for a star to be stable the amplitude of the oscillations must not grow spontaneously with time. The starting point for a general relativistic consideration of compact stars is the Oppenheimer-Volkoff (OV) equations [14] for hydrostatic, spherically symmetric equilibrium:

$$\frac{dp}{dr} = -\frac{G\left(p+\rho c^2\right)\left(mc^2+4\pi r^3 p\right)}{r\left(rc^4-2Gmc^2\right)}, \tag{1}$$

$$\frac{dm}{dr} = 4\pi r^2 \rho. \tag{2}$$

Here p is the pressure, ρ the density and $m = m(r)$ the mass within the radial coordinate r. The total mass of the star is:

$$M = 4\pi \int_0^R r^2 \rho \, dr, \tag{3}$$

where R is the coordinate radius of the star. Combined with an equation of state (EOS), $p = p(\rho)$, obtained from some microscopic (quantum field) theory, the OV solutions give the possible equilibrium states of spherically symmetric stars.

As an example, I show two sequences of compact star configurations. One is composed of nuclear matter (neutron stars) and the other of a deconfined quark matter core with a nuclear matter crust (hybrid stars), see Fig. 1. These configurations were obtained by solving the OV equations (1)–(2) numerically. The low-density part of the nuclear matter EOS was extracted from [15] and the high-density part comes from [16]. For the deconfined quark matter phase an unpaired massless quark approximation, $\rho c^2 = 3p + 4B$, was used. The "bag pressure", B, was fitted such that the transition from quark matter to nuclear matter occurs at 1% of the nuclear saturation density, $n_0 \sim 0.16$ fm^{-3}. The density where cold nuclear matter decompose into quark matter is unknown, so the transition density used here serves as an example only.

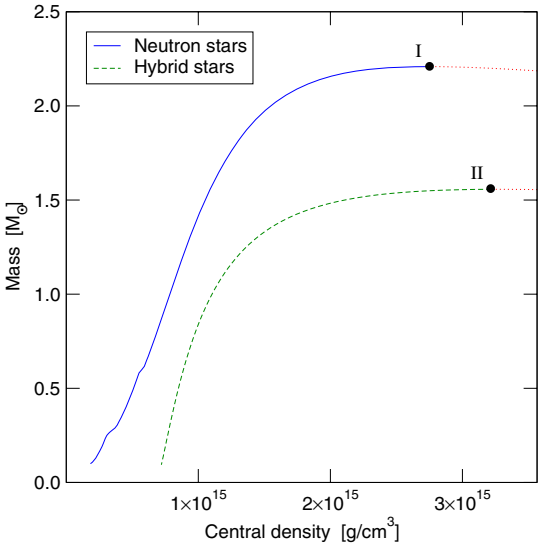

Fig. 1. Two sequences of compact stars obtained by solving the OV equations. The hybrid stars have a core of unpaired quarks and the nuclear matter crust extends down to 1% of the nuclear saturation density. The neutron star sequence is stable up to the maximum mass configuration (I). For this particular equation of state, this configuration has the highest possible (central) density, as stars more massive and dense than this are unstable and collapse into black holes. The stable hybrid star sequence terminates at II. $M_\odot \simeq 2 \times 10^{30}$ kg is the solar mass

The composition of matter at neutron star densities is an open question and many different models for the EOS exist, e.g., EOSs for nuclear matter, matter with hyperons, and superconducting quark matter. Regardless of the specific model, the maximum mass and corresponding radius are roughly a few solar masses, $M_\odot \simeq 2 \times 10^{30}$ kg, and 10 km. No substantially more dense configurations composed of quarks and leptons are possible. The motivation goes roughly like this: At white dwarf densities, the nucleons occupy nuclei that contribute little to the pressure, and electrons provide the pressure counterbalancing gravity. With increasing density, the pressure rises and the electrons become more energetic. Eventually, the elec-

trons are captured by protons and the pressure drops. As a consequence, the white dwarf sequence becomes unstable and terminates. At roughly six to seven orders of magnitude higher density than in the maximum-mass white dwarf, nuclei dissolve and the Fermi pressure of nucleons (in nuclear matter) and quarks (in quark matter) stabilize the next sequence of stable stars. The maximum mass of this sequence is a few solar masses, for all compositions (nuclear matter, quark matter, hyperons etc.). The reason why this is the limiting mass of stable compact stars, composed of quarks and leptons, is simply that there is no particle that may stabilize another sequence of stars. Each quark flavour is accompanied by an extra Fermi sea that relieves the growth of pressure and quark Fermi pressure is only won at the expense of pressure from other species. Also, the chemical potential is lower than the charm mass, so quarks heavier than the strange quark do not appear in stable stars [17, 18].

Hence, beyond the very rich and beautiful landscape of structures composed of quarks and leptons, at 10^{16} g/cm^3, there is again a desert of instability, just like there are no stable stellar configurations in-between white dwarfs and neutron stars. The question is now if the desert ends before the Planck scale.

3 Compact stars beyond the desert

A definite upper limit to the density of any spherically symmetric star can be obtained from the Schwarzschild radius,

$$R = 2GM/c^2, \tag{4}$$

since any object more dense than this would collapse into a black hole. By using the expression for the Schwarzschild radius and the relations:

$$M \sim mA, \tag{5}$$

$$R \sim d_0 A^{1/3}, \tag{6}$$

where A is the number of constituent particles, m their mass, and d_0 the distance between adjacent particles, an order of magnitude estimate for the maximum mass and radius of the corresponding class of compact stars can be calculated. For a neutron star composed of nucleons of mass $m_n \simeq 939$ MeV/c^2 and size $d_n \simeq 0.5 \times 10^{-15}$ m, (4)–(6) give $A \sim 3 \times 10^{57}$ baryons, $R \sim 7$ km, and $M \sim 5 \times 10^{30}$ kg~ 2.5 M$_\odot$. In reality, a somewhat larger radius and smaller mass are expected, since the density is non-uniform in the star, say $R \sim 10$ km and $M \sim 2$ M$_\odot$. In any case, the correct order of magnitude for the maximum mass and corresponding radius of a neutron star is obtained. The average density is $\bar{\rho} \simeq 10^{15}$ g/cm^3.

Since the Schwarzschild limit is almost reached already for the most massive neutron stars, it is reasonable to assume that this should be the case also for a more dense class of compact stars. Then, in order to provide similar estimates for the mass and radius of a star composed of preons, something must be known about the mass and "size" of preons. Before trying to achieve this, it should be emphasized that we know nothing about preons, not even if they exist. So whatever method used, the result is a speculative order of magnitude estimate. But as I will show, it is still possible to reach some qualitative results.

Guided by the observation that the density of nuclear matter is roughly of the same order of magnitude as for deconfined quark matter, I assume that the density of preon matter is roughly of the same order of magnitude as for a closely spaced lattice of some "fundamental" particle of the SM. In this case the problem is simplified to finding a fundamental SM particle, with known mass and maximum spatial extension. The simplest and least ambiguous choice seems to be the electron, since the mass of an electron is well known, and from scattering experiments it is known that electrons do not have any visible substructure down to a scale of $\sim \hbar c/\mathrm{TeV} \sim 10^{-19}$ m. Using the electron mass, $m_e \simeq 511$ keV/c^2, and an upper estimate for its radius, $r_e \sim 10^{-19}$ m, the maximum mass and radius of a star composed of preons is found to be of the order $M \sim 10^2$ M$_\oplus$ and $R \sim 1$ m. Here M$_\oplus \simeq 6 \times 10^{24}$ kg is the mass of the Earth. The average density is of the order $\sim 10^{23}$ g/cm^3.

This crude estimate gives metre-sized objects that are a hundred times more massive than the Earth. Now, I will try to be a bit more specific. Especially, it would be interesting to see whether such objects could be stable or not. In order to do this, I extrapolate an effective model for hadrons, the so-called MIT bag model [19]. In its simplest form the MIT bag is a gas of massless fermions (partons), enclosed in a region of space (the bag) subject to an external pressure B (the bag constant). The EOS for a gas of massless fermions is $\rho c^2 = 3p$ and by including B one obtains:

$$\rho c^2 = 3p + 4B. \tag{7}$$

This result does not depend on the degeneracy factor, i.e., the number of fermion species, spin, etc. For a single hadron the pressure is practically zero, so that $\rho c^2 = 4B$ and the total energy, E, of a hadron is [19]:

$$E = 4B\langle V \rangle, \tag{8}$$

where $\langle V \rangle$ is the time-averaged volume of the bag. Hence, the bag pressure, B, must be of the order of 1 GeV/fm^3 for hadrons. This is in agreement with experiments and other independent methods of calculating light-quark hadronic masses; most of the mass-energy is not due to the "bare mass" of the constituents, but the confining interactions.

The MIT bag model is frequently used for the description of deconfined quark matter and applications to compact stars. Its usefulness in this regime originates in asymptotic freedom, simplicity and the possibility to include pertubative corrections. The bag pressure, B, is introduced in order to confine partons, it is a phenomenological parametrization of the strong interactions that confine quarks into hadrons. These interactions are present also in deconfined quark matter, so the "bag model" should be applicable also in this regime. However, the value of the bag pressure is different, since the density is higher and the interactions weaker. Thus, the so-called bag constant, B,

is not really a constant, but a density dependent parameter. For strange quark matter, the bag constant is roughly $B^{1/4} \sim 150$ MeV$/(\hbar c)^{3/4}$ [20] and the corresponding contribution to the energy density is $4B \sim 260$ MeV/fm^3. This means that a considerable fraction of the density in quark matter, roughly 10^{15} g/cm^3, is due to the bag constant, i.e., interactions.

Now, the fundamental assumption here is that preons exist and are fermions. Since preons constitute light particles, such as neutrinos and electrons, the "bare" preon mass should be fairly small. Then a massless fermion approximation, $\rho c^2 = 3p$, can be used. This EOS does not allow for stable super-dense stars, however, so something more is needed. And that 'something' is dynamics, the preon interactions that give mass-energy to the particles of the SM. The question is how, since there is so far no quantitative model for preon interactions. Indeed, a fundamental problem in preon models is to find a suitable dynamics, capable of binding preons into fermions with masses essentially negligible with respect to their inverse radius. With this in mind, the principle of parsimony ("Occam's razor") seems to be the only guidance.

A simple solution is to include the dynamics in terms of a bag constant [8], which roughly reproduces the minimum energy density of an electron,

$$B = \frac{E}{4\langle V\rangle} \sim \frac{3\times 511\,\mathrm{keV}}{16\pi(10^{-19}\,\mathrm{m})^3} \sim 10^4\,\mathrm{TeV/fm^3}$$
$$\Longrightarrow B^{1/4} \sim 10\,\mathrm{GeV}/(\hbar c)^{3/4}. \quad (9)$$

The very high density contribution from the bag constant, $4B/c^2 \sim 10^5$ TeV $c^{-2} fm^{-3} \sim 10^{23}$ g/cm^3, might seem a bit peculiar. But then it should be kept in mind that the density contribution from the bag constant in deconfined quark matter is $\sim 10^{15}$ g/cm^3, which is a large fraction of the maximum density in any type of star composed of quark matter. So the high density is not that peculiar. On the contrary, if something is to be expected, it should be that B is much higher for preon matter than for quark matter, since a "preon bag" is smaller and more dense than a hadron. In the following, for simplicity, I put $\hbar c = 1$ for the bag constant and express $B^{1/4}$ in eV.

The density introduced by the bag constant is of the same order of magnitude as the density used in the mass-radius estimate above. The improvement here is the transition to a proper EOS for fermions; the possibility to apply the EOS in a general relativistic framework, for the analysis of mass-radius relations and stability. In addition to the general relativistic analysis, the mass and radius can be estimated from first principles as a function of the bag constant [21]. The result is somewhat similar to the original Chandrasekhar limit, but the role of the fermion mass is replaced by the bag constant, B,

$$M = \frac{16\pi}{3c^2} B R^3, \quad (10)$$

$$R = \frac{3c^2}{16\sqrt{\pi G B}}. \quad (11)$$

Inserting $B^{1/4} \sim 10$ GeV in (10)–(11) an estimate for the (maximum) mass $M \simeq 10^2$ M$_\oplus$ and radius $R \sim 1$ m of a preon star is obtained. This is consistent with the somewhat simpler mass-radius estimate given above.

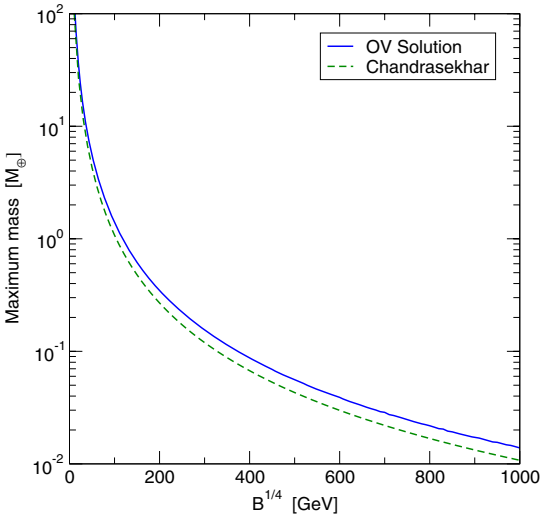

Fig. 2. The maximum mass of preon stars vs. the bag constant B. The solid line represents the general relativistic OV solutions, while the dashed line represents the Newtonian (Chandrasekhar) estimate. Despite the high central density, the mass of these objects is below the Schwarzschild limit, as is always the case for static solutions to the stellar equations. M$_\oplus \simeq 6\times 10^{24}$ kg is the Earth mass

Since $B^{1/4} \sim 10$ GeV is only an order of magnitude estimate for the lower limit, the bag constant is considered as a free parameter of the model, constrained by a lower limit of $B^{1/4} = 10$ GeV and an upper limit chosen as $B^{1/4} = 1$ TeV. The latter value corresponds to a spatial extension of the electron of the order $\sim \hbar c/10^3$ TeV $\sim 10^{-22}$ m. In Figs. 2 and 3 the maximum mass and radius of a preon star are plotted as a function of the bag constant.

A necessary (but not sufficient) condition for stability of a compact star is that the total mass is an increasing function of the central density, $dM/d\rho_c > 0$. This condition is a consequence of a generic microscopic relation known as Le Chatelier's principle. Roughly, this condition implies that a slight compression or expansion of a star will result in a less favourable state, with higher total energy. Obviously, this is a necessary condition for a stable equilibrium configuration. Equally important, a star must be stable when subject to (small) radial oscillations, in the sense that the amplitude of the oscillations must not grow spontaneously with time. Otherwise a small perturbation would bring about a collapse of the star.

The equation for the analysis of such radial modes of oscillation is due to Chandrasekhar [22]. An overview of the theory, and some applications, can be found in [23]. A catalogue of various numerical methods for solving the original set of equations can be found in [24]. However, a far more practical form of the oscillation equations has

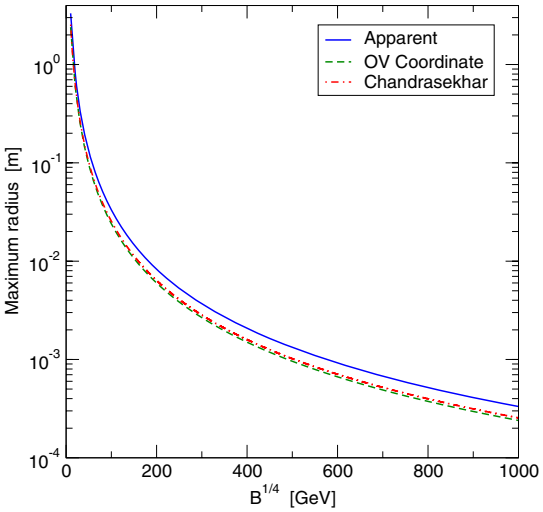

Fig. 3. The maximum radius of preon stars vs. the bag constant. The solid line is the "apparent" radius, $R^{\infty} = R/\sqrt{1-2GM/Rc^2}$, as seen by a distant observer. The dashed line represents the general relativistic coordinate radius obtained from the OV solution. The dotted line represents the Newtonian (Chandrasekhar) estimate

been derived by Gondek et al. [25]. The details of the stability analysis can be found in [8]. Here I summarise only the main points.

Assuming a time dependence of the radial displacement of fluid elements of the form $e^{i\omega t}$, the equation governing the radial oscillations is a Sturm-Liouville eigenvalue equation for ω^2. A necessary and sufficient condition for stability is that all ω_i^2 are positive, since imaginary frequencies give exponentially increasing amplitudes. Furthermore, since ω_i^2 are eigenvalues of a Sturm-Liouville equation, it turns out that it is sufficient to prove that the fundamental (nodeless) mode, ω_0^2, is positive for a star to be stable. In Fig. 4, the first three oscillation frequencies, $f_i = \omega_i/2\pi$, for various stellar configurations with $B^{1/4} = 100$ GeV are plotted. In agreement with the theorem of Wheeler et al. [2] the onset of instability is the point of maximum mass, as ω_0^2 becomes negative for higher central densities. Thus, for $B^{1/4} = 100$ GeV, preon stars are stable up to the maximum mass configuration. The same is true for other values of B [8].

Despite the large uncertainty regarding preon interactions, here manifested as a large uncertainty in the bag constant, preon stars should have central densities beyond $\sim 10^{23}$ g/cm^3. This makes preon stars fundamentally different from the traditional types of compact stars, since such high densities implies that the stars must be very small and light in order to be stable, see Fig. 5.

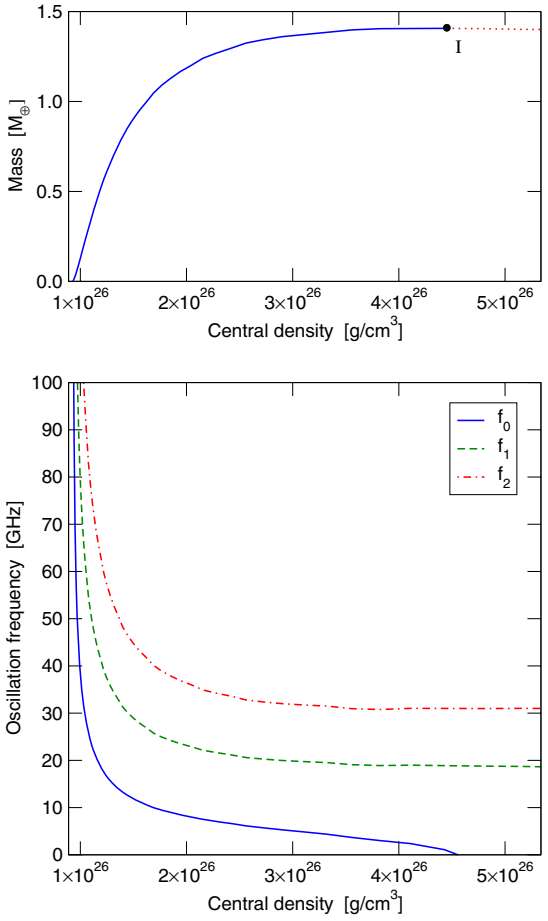

Fig. 4. The mass and the first three eigenmode oscillation frequencies (f_0, f_1, f_2) vs. the central density of preon stars. Here, a fixed value of $B^{1/4} = 100$ GeV has been used. For the maximum mass configuration (I) the fundamental (nodeless) mode, f_0, has zero frequency, indicating the onset of instability. Preon stars with densities below the density of the maximum mass configuration are stable

4 Formation and detection

The list of possible connections between the properties of the fundamental particles and the large scale structures in the universe is long. However, beyond a density of $\sim 10^{23}$ g/cm^3, not much has been proposed, since there are strong arguments against the existence of stable objects beyond $\rho \sim 10^{16}$ g/cm^3. That is, if quarks and leptons are fundamental entities.

If preons exist and objects composed of preon matter as small and light as suggested here are stable, density fluctuations in the early universe might have produced primordial preon stars (or "nuggets"). As this ma-

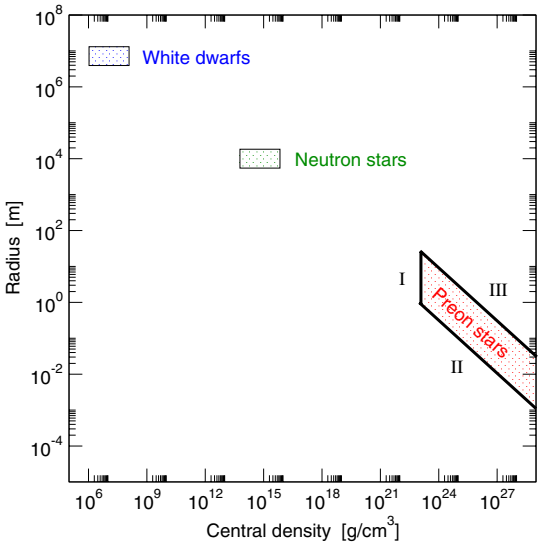

Fig. 5. The different types of compact stars traditionally considered in astrophysics are white dwarfs and neutron stars (including quark and hybrid stars). In white dwarfs, electrons provide the Fermi pressure counterbalancing gravity. In neutron stars, the neutrons (quarks, hyperons etc.) play this role. If quarks and leptons are composite particles, a new class of compact stars (preon stars) could exist. The minimum density (I) of preon stars is roughly given by the minimum density of leptons and quarks. The minimum size (II) for a given central density is due to the Schwarzschild radius (actually 4/3 of it) and a maximum size (III) exists due to instability

terial did not take part in the ensuing nucleosynthesis, the abundance of preon nuggets is not constrained by the hot big bang model bounds on baryonic matter. Also, preon nuggets are immune to Hawking radiation [26] that rapidly evaporates small primordial black holes, making it possible for them to survive to our epoch. They can therefore serve as the mysterious dark matter needed in many dynamical contexts in astrophysics and cosmology [27, 28]. The idea that preons could be connected to dark matter is already recognized in the literature [29, 30], but the picture presented here is rather different.

The Friedmann equation for the early universe is:

$$H^2(t) = \frac{8\pi G\rho}{3}, \tag{12}$$

where $\rho c^2 \sim T^4$ in the radiation-dominated era (Boltzmann's law). When including the number of internal degrees of freedom, $g_{\rm eff}$, an expression for the Hubble parameter, H, in units where $\hbar = c = k_B = 1$, is [31]:

$$H \simeq 1.66\sqrt{g_{\rm eff}}\frac{T^2}{m_{pl}}. \tag{13}$$

Here T is the temperature in eV, $g_{\rm eff}$ the effective number of degrees of freedom and $m_{pl} \simeq 1.2 \times 10^{19}$ GeV the Planck mass. For the SM, the fermions, and the gauge and Higgs bosons give $g_{\rm eff}(T = 1\,{\rm TeV}) = 106.75$. In the preon phase, this number should be smaller, say $g_{\rm eff} \sim 10$ for simplicity. Then the Hubble radius at a temperature of 1 TeV is $H^{-1} \sim 1$ mm and the mass within the Horizon (a causally connected region) is $\rho H^{-3} \sim 10^{-1}$ M$_\oplus$. This is the maximum mass of any structure that could have been formed in this early epoch. Hence, the maximum mass within causally connected regions, at the minimum temperature when deconfined preon matter might have formed preon nuggets (and the particles of the SM), is of the correct order of magnitude for stable configurations.

A potential problem is that the Jeans length, which defines the minimum length scale of regions that can contract gravitationally, was roughly of the same order of magnitude as the Hubble radius at that temperature. The Jeans length, λ_J, is [31]:

$$\lambda_J = v_s\sqrt{\frac{\pi}{G\rho_0}}, \tag{14}$$

where v_s is the speed of sound and ρ_0 the average background density. For a relativistic fluid with EOS $\rho c^2 = 3p + 4B$ the speed of sound is $v_s = c/\sqrt{3}$ and $\lambda_J \sim 1$ mm $\sim H^{-1}$. However, considering the high level of approximation used here, this is not yet a serious problem. It merely shows that the numbers are in the correct intervals.

But, perhaps it will be the other way around. After all, Popper's idea that we make progress by falsifying theories is not always true. By utilizing gamma-ray bursts (GRB) or white dwarfs in the large magellanic cloud as light sources, gravitational lenses with very small masses might be observable as diffraction line features in the spectrum [32–35]. For a lens of mass 10^{-16} M$_\odot \leq M \leq 10^{-11}$ M$_\odot$ the angular separation of images would be in the femto-arcsec range ("femtolensing"). For more massive lenses, $M \leq 10^{-7}$ M$_\odot$, the angular separation is in the pico-arcsec range ("picolensing"). The mass within the Hubble radius at $T = 1$ TeV is $\sim 10^{-1}$ M$_\oplus \sim 10^{-7}$ M$_\odot$. This roughly defines the maximum mass of preon nuggets that could be abundant enough to be observed as gravitational lenses. Hence, preon nuggets fall in the correct mass range for picolensing and femtolensing.

In Fig. 6, the magnification of a distant point light source due to gravitational lensing by an intermediate preon nugget is plotted as a function of the dimensionless frequency:

$$\nu = \frac{\tilde{\nu}(1+z_L)2GM}{c^3}, \tag{15}$$

where M (z_L) is the mass (redshift) of the lens and $\tilde{\nu}$ the frequency of light. This result was calculated with a physical-optics model, as described in [34]. In principle, the time dependent amplitude due to a single light pulse from the source was calculated and then the power spectrum was obtained by a Fourier transform of the amplitude. The magnification is normalized to a unit flux in the absence of a lens, i.e., the flux entering the detector is obtained by multiplying the magnification with the flux

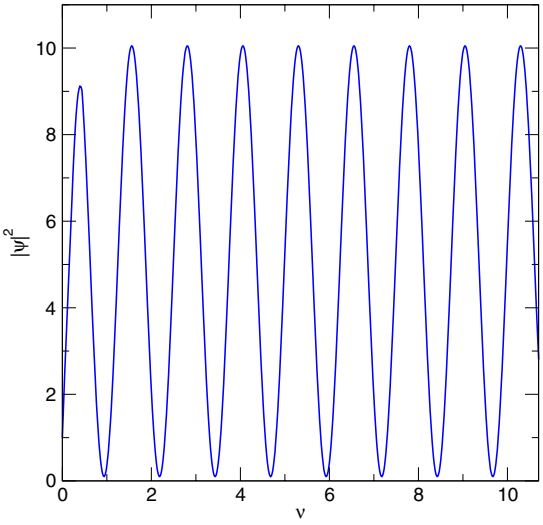

Fig. 6. $|\psi|^2$, the magnification of a distant point light source vs. the dimensionless frequency, $\nu = \tilde{\nu}(1 + z_L)2GM/c^3$, due to gravitational lensing by an intermediate preon star (or "nugget"). The flux entering the detector is obtained by multiplying the magnification, $|\psi|^2$, with the flux in the absence of a lens. For a 10^{-6} $M_\oplus$ preon star located in the halo of our galaxy, $\nu = 1$ corresponds to a photon energy of 0.14 keV. See the text for further details

in the absence of a lens. The shape of the magnification function depends on the relative position of the source and the lens. Here the source is slightly off-axis, corresponding to $\theta = 0.2$ in [34].

As mentioned in [8], preon stars might also form in the collapse of ordinary massive stars, if the collapse is slightly too powerful for the core to stabilize as a neutron star, but not sufficiently violent for the formation of a black hole. Due to the potentially very large magnetic field and rapid rotation of preon stars formed in this way, the astrophysical consequences could be important, e.g., for acceleration of ultra-high energy (UHE) cosmic rays. However, the possibility to expel such a large fraction of the mass of the progenitor star needs to be better understood. What should be noted here is merely a potential connection to UHE cosmic rays, which might provide a second means for locating and observing preon stars.

5 Conclusions

If there is a deeper layer of fermionic constituents (preons), below that of quarks and leptons, a new class of stable compact stars could exist. By fitting a simple equation of state for fermions to the minimum energy density of an electron, the maximum mass for stars composed of preons can be estimated to $\sim 10^2$ Earth masses and the maximum radius to ~ 1 m. The minimum central density is of the order of $\sim 10^{23}$ g/cm^3. Preon stars (or "nuggets") with a maximum mass of $\sim 10^{-1}$ Earth masses and radius $\sim 10^{-3}$ m could have been formed by the primordial density fluctuations in the early universe. By utilizing gamma-ray bursts, or white dwarfs in the large magellanic cloud as light sources, an intermediate preon star would produce diffraction lines in the spectrum, which might be observable. Due to the need for observational clues in the cold dark matter sector, this could prove compositeness plausible without much dedicated effort. This approach might complement direct tests of preon models at particle accelerators, especially at high energies, since preon stars might be observable even if the energy scale of preon interactions is far beyond reach of any existing or near future particle accelerator.

Acknowledgements. I acknowledge support from the Swedish National Graduate School of Space Technology. S. Fredriksson and J. Hansson deserve my gratitude for several useful discussions and for reading an early version of the manuscript. I thank M. Alford for providing me with the data tables of the high density nuclear matter equations of state, J. Goodman for useful discussions regarding the femtolensing signature, and J. Bourjaily, D. Casadei, A. Geiser, A. Giazotto, and J. Kamenik for interesting discussions about the astrophysical consequences of preon stars. Finally, I thank G. 't Hooft and A. Zichichi for organizing an excellent 42nd course of the international school of subnuclear physics, and for the award that was designated this work.

References

1. F. Weber, Prog. Part. Nucl. Phys. **54**, 193 (2005)
2. B.K. Harrison, K.S. Thorne, M. Wakano, J.A. Wheeler, *Gravitation Theory and Gravitational Collapse* (University of Chicago Press, Chicago, 1965)
3. D.J. Gross, F. Wilczek, Phys. Rev. Lett. **30**, 1323 (1973)
4. H.D. Politzer, Phys. Rev. Lett. **30**, 1346 (1973)
5. U.H. Gerlach, Phys. Rev. **172**, 1325 (1968); U.H. Gerlach, Ph.D. thesis, Princeton University, 1968
6. N.K. Glendenning, C. Kettner, Astron. Astrophys. **353**, L9 (2000)
7. K. Schertler et al., Nucl. Phys. A **677**, 463 (2000)
8. J. Hansson, F. Sandin, Preon stars: a new class of cosmic compact objects. astro-ph/0410417
9. S. Fredriksson, in: Proc. of the Fourth Tegernsee Int. Conf. on Particle Physics Beyond the Standard Model, 2004, ed. by H.-V. Klapdor-Kleingrothaus (Springer-Verlag, Heidelberg, 2004), p. 211, hep-ph/0309213
10. I.A. D'Souza, C.S. Kalman, Preons (World Scientific, Singapore, 1992)
11. G. 't Hooft, Cargèse Lecture Notes, 1979
12. R. Barbieri, L. Maiani, R. Petronzio, Phys. Lett. B **96**, 63 (1980)
13. J.-J. Dugne, S. Fredriksson, J. Hansson, Europhys. Lett. **57**, 188 (2002)
14. J.R. Oppenheimer, G. Volkoff, Phys. Rev. **55**, 374 (1939)
15. J.W. Negele, D. Vautherin, Nucl. Phys. A **207**, 298 (1973)
16. A. Akmal, V.R. Pandharipande, D.G. Ravenhall, Phys. Rev. C **58**, 1804 (1998)
17. C. Kettner et al., Phys. Rev. D **51**, 1440 (1995)

18. M. Prisznyak, B. Lukacs, P. Levai, Are There Top Quarks in Superdense Hybrid Stars? astro-ph/9412052
19. A. Chodos et al., Phys. Rev. D **9**, 3471 (1974)
20. N.K. Glendenning, Compact Stars (Springer-Verlag, New York, 1997)
21. S. Banerjee, S.K. Ghosh, S. Raha, J. Phys. G **26**, L1 (2000)
22. S. Chandrasekhar, Phys. Rev. Lett. **12**, 114 (1964)
23. C.W. Misner, K.S. Thorne, J.A. Wheeler, Gravitation (Freeman and Co., San Francisco, 1973)
24. J.M. Bardeen, K.S. Thorne, D.W. Meltzer, Astrophys. J. **145**, 505 (1966)
25. D. Gondek, P. Haensel, J.L. Zdunik, Astron. Astrophys. **325**, 217 (1997)
26. S.W. Hawking, Commun. Math. Phys. **43**, 199 (1975)
27. M.S. Turner, Phys. Rep. **333**, 619 (2000)
28. L. Bergström, Rep. Progr. Phys. **63**, 793 (2000)
29. V. Burdyuzha et al., in: Proc. of the Second Int. Workshop on Particle Physics and the Early Universe, 1999, ed. by D.O. Caldwell (Springer-Verlag, 1999), p. 392, astro-ph/9912555
30. O. Lalakulich, G. Vereshkov, in: Proc. of the Second Int. Conf. on Dark Matter in Astro and Particle Physics, 1999, ed. by H.-V. Klapdor-Kleingrothaus and L. Baudis (IOP Publishing, Great Yarmouth, 1999), p. 668
31. L. Bergström, A. Goobar, Cosmology and Particle Astrophysics, 2nd ed. (Springer-Verlag, Germany, 2004)
32. A. Gould, ApJ **386**, L5 (1992)
33. K.Z. Stanek, B. Paczyński, J. Goodman, ApJ **413**, L7 (1993)
34. A. Ulmer, J. Goodman, ApJ **442**, 67 (1995)
35. R.J. Nemiroff, A. Gould, Probing for MACHOs of Mass $10^{-15}M_{\odot}$–$10^{-7}M_{\odot}$ with Gamma-Ray Burst Parallax Spacecraft. astro-ph/9505019

Paper III

PHYSICAL REVIEW D **72,** 065020 (2005)

Phase diagram of three-flavor quark matter under compact star constraints

D. Blaschke,[1,*] S. Fredriksson,[2,†] H. Grigorian,[3,‡] A. M. Öztaş,[4,§] and F. Sandin[2,‖]

[1]*Gesellschaft für Schwerionenforschung mbH (GSI), D-64291 Darmstadt, Germany, and Bogoliubov Laboratory for Theoretical Physics, JINR Dubna, 141980 Dubna, Russia*

[2]*Department of Physics, Luleå University of Technology, SE-97187 Luleå, Sweden*

[3]*Institut für Physik, Universität Rostock, D-18051 Rostock, Germany, and Department of Physics, Yerevan State University, 375025 Yerevan, Armenia*

[4]*Department of Physics, Hacettepe University, TR-06532 Ankara, Turkey*

(Received 4 April 2005; revised manuscript received 29 August 2005; published 30 September 2005)

The phase diagram of three-flavor quark matter under compact star constraints is investigated within a Nambu–Jona-Lasinio model. Global color and electric charge neutrality is imposed for β-equilibrated superconducting quark matter. The constituent quark masses and the diquark condensates are determined self-consistently in the plane of temperature and quark chemical potential. Both strong and intermediate diquark coupling strengths are considered. We show that in both cases, gapless superconducting phases do not occur at temperatures relevant for compact star evolution, i.e., below $T \sim 50$ MeV. The stability and structure of isothermal quark star configurations are evaluated. For intermediate coupling, quark stars are composed of a mixed phase of normal (NQ) and two-flavor superconducting (2SC) quark matter up to a maximum mass of 1.21 $M_\odot$. At higher central densities, a phase transition to the three-flavor color flavor locked (CFL) phase occurs and the configurations become unstable. For the strong diquark coupling we find stable stars in the 2SC phase, with masses up to 1.33 $M_\odot$. A second family of more compact configurations (twins) with a CFL quark matter core and a 2SC shell is also found to be stable. The twins have masses in the range $1.30 \ldots 1.33$ $M_\odot$. We consider also hot isothermal configurations at temperature $T = 40$ MeV. When the hot maximum mass configuration cools down, due to emission of photons and neutrinos, a mass defect of 0.1 $M_\odot$ occurs and two final state configurations are possible.

DOI: 10.1103/PhysRevD.72.065020 PACS numbers: 12.38.Mh, 24.85.+p, 26.60.+c, 97.60.−s

I. INTRODUCTION

Theoretical investigations of the QCD phase diagram at high densities have recently gained momentum due to results of nonperturbative low-energy QCD models [1–3] of color superconductivity in quark matter [4,5]. These models predict that the diquark pairing condensates are of the order of 100 MeV and a remarkably rich phase structure has been identified [6–9]. The main motivation for studying the low-temperature domain of the QCD phase diagram is its possible relevance for the physics of compact stars [10–12]. Observable effects of color superconducting phases in compact stars are expected, e.g., in the cooling behavior [13–18], magnetic field evolution [19–22], and in burst-type phenomena [23–27].

The most prominent color superconducting phases with large diquark pairing gaps are the two-flavor scalar diquark condensate (2SC) and the color-flavor locking (CFL) condensate. The latter requires approximate SU(3) flavor symmetry and occurs therefore only at rather large quark chemical potentials, $\mu_q > 430$–500 MeV, of the order of the dynamically generated strange quark mass M_s, whereas the 2SC phase can appear already at the chiral restoration transition for $\mu_q > 330$–350 MeV [28–31]. Note that the quark chemical potential in the center of a typical compact star is expected to not exceed a value of $\sim$500 MeV, so that the volume fraction of a strange quark matter phase will be insufficient to entail observable consequences. However, when the strange quark mass is considered not dynamically, but as a free parameter independent of the thermodynamical conditions, it has been shown that for not too large M_s the CFL phase dominates over the 2SC phase [32,33]. Studies of the QCD phase diagram have recently been extended to the discussion of gapless CFL (gCFL) phases for fixed M_s in [34–36] and for dynamical M_s at zero temperature in [31]. The gapless phases occur when the asymmetry between Fermi levels of different flavors is large enough to allow for zero energy excitations while a nonvanishing diquark condensate exists. They have been found first for the 2SC phase (g2SC) within a dynamical chiral quark model [37,38].

Any scenario for compact star evolution that is based on the occurrence of quark matter relies on the assumptions about the properties of this phase. It is therefore of prior importance to obtain a phase diagram of three-flavor quark matter under compact star constraints with self-consistently determined dynamical quark masses. In the present paper we will employ the Nambu–Jona-Lasinio (NJL) model to delineate the different quark matter phases in the plane of temperature and chemical potential. We also address the question whether CFL quark matter and gap-

*Electronic address: Blaschke@theory.gsi.de
†Electronic address: Sverker.Fredriksson@ltu.se
‡Electronic address: Hovik.Grigorian@uni-rostock.de
§Electronic address: oztas@hacettepe.edu.tr
‖Electronic address: Fredrik.Sandin@ltu.se

less phases are likely to play a role in compact star interiors.

II. MODEL

In this paper, we consider an NJL model with quark-antiquark interactions in the color singlet scalar/pseudoscalar channel, and quark-quark interactions in the scalar color antitriplet channel. We neglect the less attractive interaction channels, e.g., the isospin-singlet channel, which could allow for weak spin-1 condensates. Such condensates allow for gapless excitations at low temperatures and could be important for the cooling behavior of compact stars. However, the coupling strengths in these channels are poorly known and we therefore neglect them here. The Lagrangian density is given by

$$\begin{aligned}\mathcal{L} &= \bar{q}_{i\alpha}(i\not{\partial}\delta_{ij}\delta_{\alpha\beta} - M^0_{ij}\delta_{\alpha\beta} + \mu_{ij,\alpha\beta}\gamma^0)q_{j\beta} \\ &+ G_S\sum_{a=0}^{8}[(\bar{q}\tau^a_f q)^2 + (\bar{q}i\gamma_5\tau^a_f q)^2] \\ &+ G_D\sum_{k,\gamma}[(\bar{q}_{i\alpha}\epsilon_{ijk}\epsilon_{\alpha\beta\gamma}q^C_{j\beta})(\bar{q}^C_{i'\alpha'}\epsilon_{i'j'k}\epsilon_{\alpha'\beta'\gamma}q_{j'\beta'}) \\ &+ (\bar{q}_{i\alpha}i\gamma_5\epsilon_{ijk}\epsilon_{\alpha\beta\gamma}q^C_{j\beta})(\bar{q}^C_{i'\alpha'}i\gamma_5\epsilon_{i'j'k}\epsilon_{\alpha'\beta'\gamma}q_{j'\beta'})],\end{aligned} \tag{1}$$

where $M^0_{ij} = \mathrm{diag}(m^0_u, m^0_d, m^0_s)$ is the current quark mass matrix in flavor space and $\mu_{ij,\alpha\beta}$ is the chemical potential matrix in color and flavor space. Due to strong and weak interactions, the various chemical potentials are not independent. In the superconducting phases a $U(1)$ gauge symmetry remains unbroken [39], and the associated charge is a linear combination of the electric charge, Q, and two orthogonal generators of the unbroken $SU(2)_c$ symmetry. Hence, there are in total four independent chemical potentials

$$\mu_{ij,\alpha\beta} = (\mu\delta_{ij} + Q\mu_Q)\delta_{\alpha\beta} + (T_3\mu_3 + T_8\mu_8)\delta_{ij}, \tag{2}$$

where $Q = \mathrm{diag}(2/3, -1/3, -1/3)$ is the electric charge in flavor space, and $T_3 = \mathrm{diag}(1, -1, 0)$ and $T_8 = \mathrm{diag}(1/\sqrt{3}, 1/\sqrt{3}, -2/\sqrt{3})$ are the generators in color space. The quark number chemical potential, μ, is related to the baryon chemical potential by $\mu = \mu_B/3$. The quark fields in color, flavor, and Dirac spaces are denoted by $q_{i\alpha}$ and $\bar{q}_{i\alpha} = q^\dagger_{i\alpha}\gamma^0$. τ^a_f are Gell-Mann matrices acting in flavor space. Charge conjugated quark fields are denoted by $q^C = C\bar{q}^T$ and $\bar{q}^C = q^T C$, where $C = i\gamma^2\gamma^0$ is the Dirac charge conjugation matrix. The indices α, β, and γ represent colors ($r = 1$, $g = 2$ and $b = 3$), while i, j, and k represent flavors ($u = 1$, $d = 2$, and $s = 3$). G_S and G_D are dimensionful coupling constants that must be determined by experiments.

Typically, three-flavor NJL models use a 't Hooft determinant interaction that induces a $\mathrm{U}_A(1)$ symmetry breaking in the pseudoscalar isoscalar meson sector, which can be adjusted such that the η–η' mass difference is described. This realization of the $\mathrm{U}_A(1)$ breaking leads to the important consequence that the quark condensates of different flavor sectors get coupled. The dynamically generated strange quark mass contains a contribution from the chiral condensates of the light flavors. There is, however, another possible realization of the $\mathrm{U}_A(1)$ symmetry breaking that does not arise on the mean-field level, but only for the mesonic fluctuations in the pseudoscalar isoscalar channel. This is due to the coupling to the nonperturbative gluon sector via the triangle anomaly, see, e.g., [40–42]. This realization of the η–η' mass difference gives no contribution to the quark thermodynamics at the mean-field level, which we will follow in this paper. Up to now it is not known, which of the two $\mathrm{U}_A(1)$ breaking mechanisms that is the dominant one in nature. In the present exploratory study of the mean-field thermodynamics of three-flavor quark matter, we will take the point of view that the 't Hooft term might be subdominant and can be disregarded. One possible way to disentangle both mechanisms is due to their different response to chiral symmetry restoration at finite temperatures and densities. While in heavy-ion collisions only the finite temperature aspect can be systematically studied [43], the state of matter in neutron star interiors may be suitable to probe the $\mathrm{U}_A(1)$ symmetry restoration and its possible implications for the quark matter phase diagram at high densities and low temperatures. A comparison of the results presented in this work with the alternative treatment of the phase diagram of three-flavor quark matter including the 't Hooft determinant term, see [44], may therefore be instructive.

The mean-field Lagrangian is

$$\begin{aligned}\mathcal{L}^{MF} &= \bar{q}_{i\alpha}[i\not{\partial}\delta_{ij}\delta_{\alpha\beta} - (M^0_{ij} - 4G_S\langle\bar{q}_{i\alpha}q_{j\beta}\rangle\delta_{ij})\delta_{\alpha\beta} \\ &+ \mu_{ij,\alpha\beta}\gamma^0]q_{j\beta} - 2G_S\sum_i\langle\bar{q}_i q_i\rangle^2 - \sum_{k,\gamma}\frac{|\Delta_{k\gamma}|^2}{4G_D} \\ &+ \frac{1}{2}\bar{q}_{i\alpha}\hat{\Delta}_{ij,\alpha\beta}q^C_{j\beta} + \frac{1}{2}\bar{q}^C_{i\alpha}\hat{\Delta}^\dagger_{ij,\alpha\beta}q_{j\beta},\end{aligned} \tag{3}$$

$$\begin{aligned}\hat{\Delta}_{ij,\alpha\beta} &= 2G_D i\gamma_5\epsilon_{\alpha\beta\gamma}\epsilon_{ijk}\langle\bar{q}_{i'\alpha'}i\gamma_5\epsilon_{\alpha'\beta'\gamma}\epsilon_{i'j'k}q^C_{j'\beta'}\rangle \\ &= i\gamma_5\epsilon_{\alpha\beta\gamma}\epsilon_{ijk}\Delta_{k\gamma}.\end{aligned} \tag{4}$$

We define the chiral gaps

$$\phi_i = -4G_S\langle\bar{q}_i q_i\rangle, \tag{5}$$

and the diquark gaps

$$\Delta_{k\gamma} = 2G_D\langle\bar{q}_{i\alpha}i\gamma_5\epsilon_{\alpha\beta\gamma}\epsilon_{ijk}q^C_{j\beta}\rangle. \tag{6}$$

The chiral condensates contribute to the dynamical masses of the quarks and the constituent quark mass matrix in flavor space is $M = \mathrm{diag}(m^0_u + \phi_u, m^0_d + \phi_d, m^0_s + \phi_s)$, where m^0_i are the current quark masses. For finite current quark masses the $U(3)_L \times U(3)_R$ symmetry of

the Lagrangian is spontaneously broken and only approximately restored at high densities.

The diquark gaps, $\Delta_{k\gamma}$, are antisymmetric in flavor and color, e.g., the condensate corresponding to Δ_{ur} is created by green down and blue strange quarks. Because of this property, the diquark gaps can be denoted with the flavor indices of the interacting quarks

$$\Delta_{ur} = \Delta_{ds}, \qquad \Delta_{dg} = \Delta_{us}, \qquad \Delta_{sb} = \Delta_{ud}. \tag{7}$$

After reformulating the mean-field lagrangian in 8-component Nambu-Gorkov spinors [45,46] and performing the functional integrals over Grassman variables [47] we obtain the thermodynamic potential

$$\begin{aligned}\Omega(T,\mu) = &\frac{\phi_u^2+\phi_d^2+\phi_s^2}{8G_S} + \frac{|\Delta_{ud}|^2+|\Delta_{us}|^2+|\Delta_{ds}|^2}{4G_D} \\ &- T\sum_n \int \frac{d^3p}{(2\pi)^3}\frac{1}{2}\,\mathrm{Tr}\,\ln\!\left(\frac{1}{T}S^{-1}(i\omega_n,\vec{p})\right) \\ &+ \Omega_e - \Omega_0.\end{aligned} \tag{8}$$

Here $S^{-1}(p)$ is the inverse propagator of the quark fields at four momentum $p = (i\omega_n, \vec{p})$,

$$S^{-1}(i\omega_n,\vec{p}) = \begin{bmatrix} \not{p} - M + \mu\gamma^0 & \hat{\Delta} \\ \hat{\Delta}^\dagger & \not{p} - M - \mu\gamma^0 \end{bmatrix}, \tag{9}$$

and $\omega_n = (2n+1)\pi T$ are the Matsubara frequencies for fermions. The thermodynamic potential of ultrarelativistic electrons,

$$\Omega_e = -\frac{1}{12\pi^2}\mu_Q^4 - \frac{1}{6}\mu_Q^2 T^2 - \frac{7}{180}\pi^2 T^4, \tag{10}$$

has been added to the potential, and the vacuum contribution,

$$\begin{aligned}\Omega_0 &= \Omega(0,0) \\ &= \frac{\phi_{0u}^2+\phi_{0d}^2+\phi_{0s}^2}{8G_S} - 2N_c\sum_i \int \frac{d^3p}{(2\pi)^3}\sqrt{M_i^2+p^2},\end{aligned} \tag{11}$$

has been subtracted in order to get zero pressure in vacuum. Using the identity $\mathrm{Trln}(D) = \mathrm{ln\,det}(D)$ and evaluating the determinant (see Appendix A), we obtain

$$\mathrm{ln\,det}\!\left(\frac{1}{T}S^{-1}(i\omega_n,\vec{p})\right) = 2\sum_{a=1}^{18}\ln\!\left(\frac{\omega_n^2+\lambda_a(\vec{p})^2}{T^2}\right). \tag{12}$$

The quasiparticle dispersion relations, $\lambda_a(\vec{p})$, are the eigenvalues of the Hermitian matrix,

$$\mathcal{M} = \begin{bmatrix} -\gamma^0\vec{\gamma}\cdot\vec{p} - \gamma^0 M + \mu & \gamma^0\hat{\Delta}C \\ \gamma^0 C\hat{\Delta}^\dagger & -\gamma^0\vec{\gamma}^T\cdot\vec{p} + \gamma^0 M - \mu \end{bmatrix}, \tag{13}$$

in color, flavor, and Nambu-Gorkov space. This result is in agreement with [33,44]. Finally, the Matsubara sum can be evaluated on closed form [47],

$$T\sum_n \ln\!\left(\frac{\omega_n^2+\lambda_a^2}{T^2}\right) = \lambda_a + 2T\ln(1+e^{-\lambda_a/T}), \tag{14}$$

leading to an expression for the thermodynamic potential on the form

$$\begin{aligned}\Omega(T,\mu) = &\frac{\phi_u^2+\phi_d^2+\phi_s^2}{8G_S} + \frac{|\Delta_{ud}|^2+|\Delta_{us}|^2+|\Delta_{ds}|^2}{4G_D} \\ &- \int \frac{d^3p}{(2\pi)^3}\sum_{a=1}^{18}(\lambda_a + 2T\ln(1+e^{-\lambda_a/T})) \\ &+ \Omega_e - \Omega_0.\end{aligned} \tag{15}$$

It should be noted that (14) is an even function of λ_a, so the signs of the quasiparticle dispersion relations are arbitrary. In this paper, we assume that there are no trapped neutrinos. This approximation is valid for quark matter in neutron stars, after the short period of deleptonization is over.

Equations (10), (11), (13), and (15) form a consistent thermodynamic model of superconducting quark matter. The independent variables are μ and T. The gaps, ϕ_i, and Δ_{ij}, are variational order parameters that should be determined by minimization of the grand canonical thermodynamical potential, Ω. Also, quark matter should be locally color and electric charge neutral, so at the physical minima of the thermodynamic potential the corresponding number densities should be zero

$$n_Q = -\frac{\partial\Omega}{\partial\mu_Q} = 0, \tag{16}$$

$$n_8 = -\frac{\partial\Omega}{\partial\mu_3} = 0, \tag{17}$$

$$n_3 = -\frac{\partial\Omega}{\partial\mu_8} = 0. \tag{18}$$

The pressure, P, is related to the thermodynamic potential by $P = -\Omega$ at the global minima of Ω. The quark density, entropy and energy density are then obtained as derivatives of the thermodynamical potential with respect to μ, T and $1/T$, respectively.

III. RESULTS

The numerical solutions to be reported in this Section are obtained with the following set of model parameters, taken from Table 5.2 of Ref. [8] for vanishing 't Hooft interaction,

$$m_{u,d}^0 = 5.5\ \mathrm{MeV}, \tag{19}$$

$$m_s^0 = 112.0 \text{ MeV}, \tag{20}$$

$$G_S\Lambda^2 = 2.319, \tag{21}$$

$$\Lambda = 602.3 \text{ MeV}. \tag{22}$$

With these parameters, the following low-energy QCD observables can be reproduced: $m_\pi = 135$ MeV, $m_K = 497.7$ MeV, $f_\pi = 92.4$ MeV. The value of the diquark coupling strength $G_D = \eta G_S$ is considered as a free parameter of the model. Here we present results for $\eta = 0.75$ (intermediate coupling) and $\eta = 1.0$ (strong coupling).

A. Quark masses and pairing gaps at zero temperature

The dynamically generated quark masses and the diquark pairing gaps are determined self-consistently at the absolute minima of the thermodynamic potential, in the plane of temperature and quark chemical potential. This is done for both the strong and the intermediate diquark coupling strengths. In Figs. 1 and 2 we show the dependence of masses and gaps on the quark chemical potential at $T = 0$ for $\eta = 0.75$ and $\eta = 1.0$, respectively. A characteristic feature of this dynamical quark model is that the critical quark chemical potentials where light and strange quark masses jump from their constituent mass values down to almost their current mass values do not coincide. With increasing chemical potential the system undergoes a sequence of two transitions: (1) vacuum $\rightarrow$ two-flavor quark matter, (2) two-flavor $\rightarrow$ three-flavor quark matter. The intermediate two-flavor quark matter phase occurs within an interval of chemical potentials typical for compact star interiors. While at intermediate coupling the asymmetry between the up and down quark chemical potentials leads to a mixed NQ-2SC phase below temperatures of 20–30 MeV, at strong coupling the pure 2SC phase extends down to $T = 0$. Simultaneously, the limiting chemical potentials of the two-flavor quark matter region are lowered by about 40 MeV. Three-flavor quark matter is always in the CFL phase where all quarks are paired. The robustness of the 2SC condensate under compact star constraints, with respect to changes of the coupling strength, as well as to a softening of the momentum cutoff by a form factor, has recently been investigated with a different parametrization [48]. The results at low temperatures are

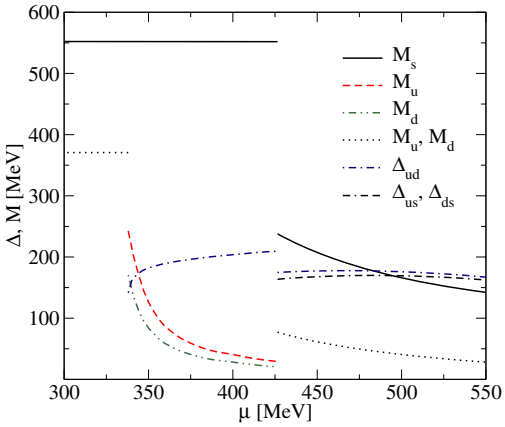

FIG. 2 (color online). Gaps and dynamical quark masses as functions of μ at $T = 0$ for strong diquark coupling, $\eta = 1$.

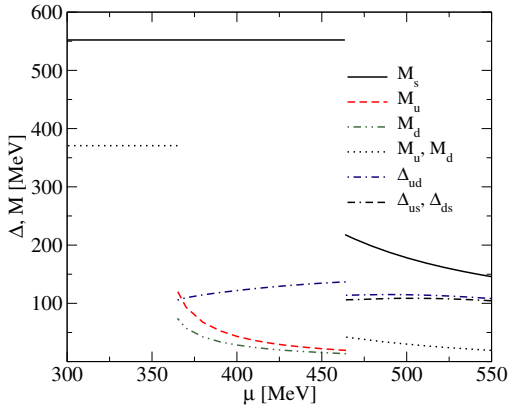

FIG. 1 (color online). Gaps and dynamical quark masses as functions of μ at $T = 0$ for intermediate diquark coupling, $\eta = 0.75$.

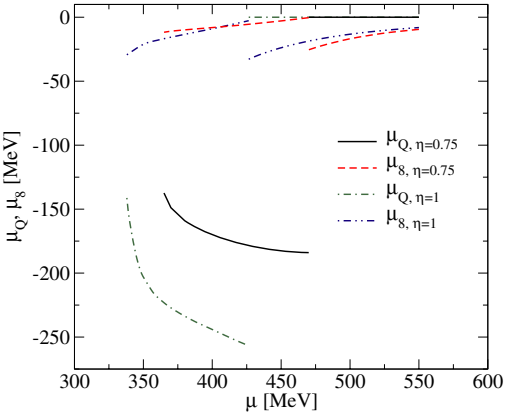

FIG. 3 (color online). Chemical potentials μ_Q and μ_8 at $T = 0$ for both values of the diquark coupling, $\eta = 0.75$ and $\eta = 1$. All phases considered in this work have zero n_3 color charge for $\mu_3 = 0$. Hence μ_3 is omitted in the plot.

similar: for $\eta = 0.75$ and the NJL form factor the 2SC condensate does not occur for moderate chemical potentials, while for $\eta = 1.0$ it occurs simultaneously with chiral symmetry restoration. Figure 3 shows the corresponding dependences of the chemical potentials conjugate to electric (μ_Q) and color (μ_8) charges.

B. Dispersion relations and gapless phases

In Fig. 4 we show the quasiparticle dispersion relations of different excitations at two points in the phase diagram: (I) the CFL phase (left panel), where there is a finite energy gap for all dispersion relations; (II) the gCFL phase (right panel), where the energy spectrum is shifted due to the assymetry in the chemical potentials, such that the CFL gap is zero and (gapless) excitations with zero energy are possible. A necessary condition for the occurrence of gapless superconducting phases is that the chemical potential difference of the quark species to be paired equals or exceeds the corresponding pairing gap. In the present model, this phenomenon occurs only at rather high temperatures, where the condensates are diminished by thermal fluctuations. A smaller diquark coupling constant, as in Ref. [44], would lead to a smaller pairing gap and could therefore entail the occurrence of gapless phases even at zero temperature.

C. Phase diagram

The thermodynamical state of the system is characterized by the values of the order parameters and their dependence on T and μ. Here we illustrate this dependency in a phase diagram. We identify the following phases:

(1) NQ: $\Delta_{ud} = \Delta_{us} = \Delta_{ds} = 0$;
(2) NQ-2SC: $\Delta_{ud} \neq 0$, $\Delta_{us} = \Delta_{ds} = 0$, $0 < \chi_{2SC} < 1$;
(3) 2SC: $\Delta_{ud} \neq 0$, $\Delta_{us} = \Delta_{ds} = 0$;
(4) uSC: $\Delta_{ud} \neq 0$, $\Delta_{us} \neq 0$, $\Delta_{ds} = 0$;
(5) CFL: $\Delta_{ud} \neq 0$, $\Delta_{ds} \neq 0$, $\Delta_{us} \neq 0$;

and their gapless versions. The resulting phase diagrams for intermediate and strong coupling are given in Figs. 5 and 6, respectively, and constitute the main result of this work, which is summarized in the following statements:

(a) Gapless phases occur only at high temperatures, above 50 MeV (intermediate coupling) or 80 MeV (strong coupling).
(b) CFL phases occur only at rather high chemical potential, well above the chiral restoration transition, i.e., above 462 MeV (intermediate coupling) or 419 MeV (strong coupling).
(c) Two-flavor quark matter for intermediate coupling is at low temperatures ($T < 20$–30 MeV) in a mixed NQ-2SC phase, at high temperatures in the pure 2SC phase.

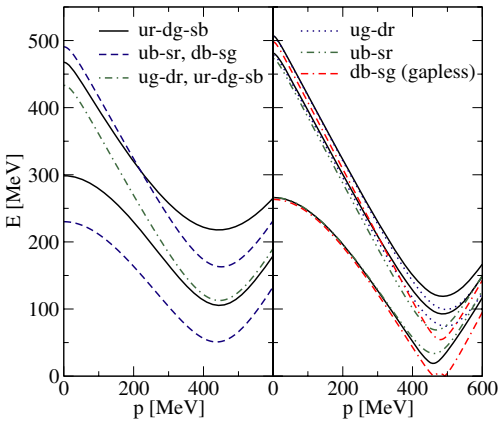

FIG. 4 (color online). Quark-quark quasiparticle dispersion relations. For $\eta = 0.75$, $T = 0$, and $\mu = 465$ MeV (left panel) there is a forbidden energy band above the Fermi surface. All dispersion relations are gapped at this point in the $\mu - T$ plane, see Fig. 5. There is no forbidden energy band for the $db - sg$ quasiparticles for $\eta = 0.75$, $T = 59$ MeV, and $\mu = 500$ MeV (right panel). This point in the $\mu - T$ plane constitutes a part of the gapless CFL phase of Fig. 5.

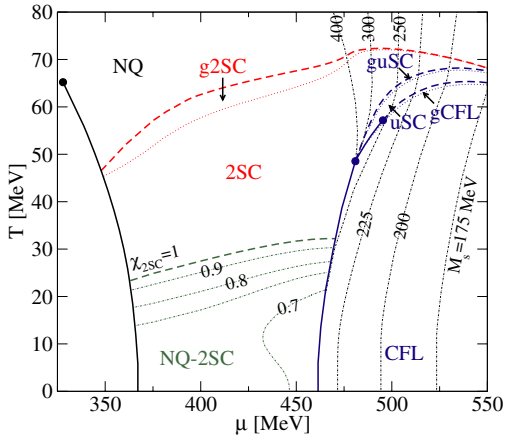

FIG. 5 (color online). Phase diagram of neutral three-flavor quark matter for intermediate diquark coupling, $\eta = 0.75$. First-order phase transition boundaries are indicated by bold solid lines, while bold dashed lines correspond to second-order phase boundaries. The dotted lines indicate gapless phase boundaries. The volume fraction, χ_{2SC}, of the 2SC component of the mixed NQ-2SC phase is denoted with thin dash-dotted lines, while the constituent strange quark mass is denoted with bold dotted lines.

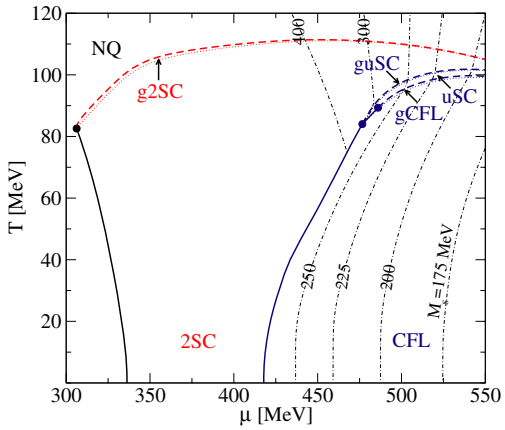

FIG. 6 (color online). Phase diagram of neutral three-flavor quark matter for strong diquark coupling, $\eta = 1$. Line styles as in Fig. 5.

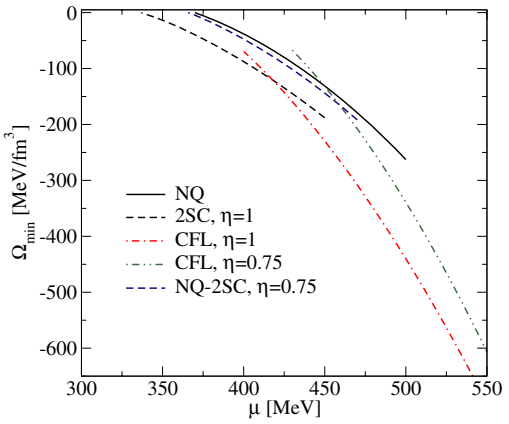

FIG. 7 (color online). Minima of the thermodynamical potential for neutral three-flavor quark matter at $T = 0$ as a function of the quark chemical potential. Note that at a given coupling η the state with the lowest $\Omega_{\rm min}$ is attained and the physical pressure is $P = -\Omega_{\rm min}$.

(d) Two-flavor quark matter for strong coupling is in the 2SC phase with rather high critical temperatures of $\sim$100 MeV.
(e) The critical endpoint of first-order chiral phase transitions is at$(T, \mu) = (65$ MeV, 328 MeV) for intermediate coupling and at (82 MeV, 307 MeV) for strong coupling.

D. Quark matter equation of state

The various phases of quark matter presented in the previous section have been identified by minimizing the thermodynamic potential, Ω, in the order parameters, Δ_{ij} and ϕ_i. For a homogenous system, the pressure is $P = -\Omega_{\rm min}$, see Fig. 7, where the μ-dependence of $\Omega_{\rm min}$ is shown at $T = 0$ for the different competing phases. The lowest value of $\Omega_{\rm min}$ corresponds to the negative value of the physical pressure. The intersection of two curves corresponds to a first-order phase transition. All other thermodynamic quantities can be obtained from the thermodynamic potential by derivatives. At intermediate coupling, we have a first-order transition from the NQ-2SC phase to the CFL phase, whereas at strong coupling the first-order transition is from the 2SC phase to the CFL phase, with a lower critical energy density. In Fig. 8 the equation of state for cold three-flavor quark matter is given in a form suitable for the investigation of the hydrodynamic stability of gravitating compact objects, so-called quark stars. This is the topic of the next Subsection.

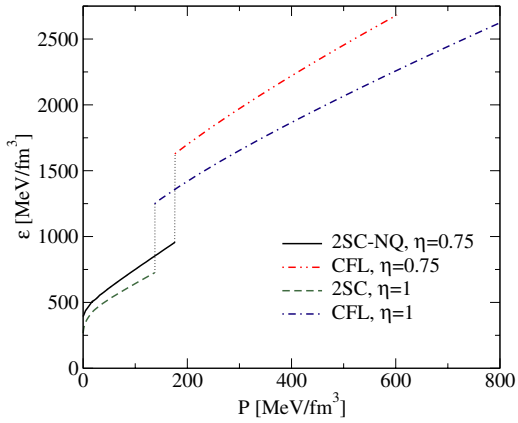

FIG. 8 (color online). Equation of state for three-flavor quark matter at $T = 0$ with first-order phase transitions. For intermediate diquark coupling ($\eta = 0.75$): from the mixed NQ-2SC phase to the CFL phase. For strong diquark coupling ($\eta = 1$): from the 2SC phase to the CFL phase.

E. Quark star configurations

The properties of spherically symmetric, static configurations of dense matter can be calculated with the well-known Tolman-Oppenheimer-Volkoff equations for hydrostatic equilibrium of self-gravitating matter, see also [49],

$$\frac{dP(r)}{dr} = -\frac{[\varepsilon(r) + P(r)][m(r) + 4\pi r^3 P(r)]}{r[r - 2m(r)]}. \qquad (23)$$

Here $\varepsilon(r)$ is the energy density and $P(r)$ the pressure at distance r from the center of the star. The mass enclosed in a sphere with radius r is defined by

$$m(r) = 4\pi \int_0^r \varepsilon(r') r'^2 dr'. \tag{24}$$

These equations are solved for given central baryon number densities, $n_B(r = 0)$, thereby defining a sequence of quark star configurations. For the generalization to finite temperature configurations, see [50]. Hot quark stars have been discussed, e.g., in [25,26,51–53]. In Fig. 9 we show the stable configurations of quark stars for the three-flavor quark matter equation of state described above. The obtained mass-radius relations allow for very compact self-bound objects, with a maximum radius that is less than 10 km. For intermediate diquark coupling, $\eta = 0.75$, stable stars consist of a NQ-2SC mixed phase with a maximum mass of 1.21 $M_\odot$. With increasing density, a phase transition to the CFL phase renders the sequence unstable.

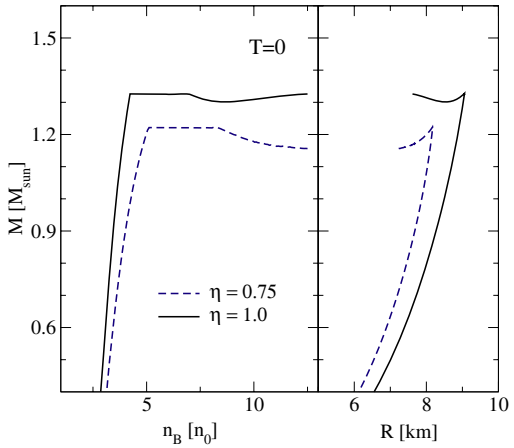

FIG. 9 (color online). Sequences of cold quark stars for the three-flavor quark matter equation of state described in the text. The rising branches in the mass-central density relation (left panel) indicate stable compact object configurations. The mass-radius relations (right panel) show that the three-flavor quark matter described in this paper leads to very compact self-bound objects. For intermediate diquark coupling, $\eta = 0.75$, stable stars consist of a mixed phase of NQ-2SC matter with a maximum mass of 1.21 $M_\odot$ (dashed line). At higher densities a phase transition to CFL quark matter occurs, which entails a collapse of the star. For strong coupling, $\eta = 1$, the low-density quark matter is in the 2SC phase and corresponding quark stars are stable up to a maximum mass of 1.33 $M_\odot$ (solid line). The phase transition to CFL quark matter entails an instability, which at $T = 0$ leads to a third family of stable stars for central densities above $9n_0$ and a mass twin window of 1.30–1.33 $M_\odot$.

For the strong diquark coupling, $\eta = 1$, quark matter is in the 2SC phase at low densities and the corresponding sequence of quark stars is stable up to a maximum mass of 1.33 $M_\odot$. The phase transition to CFL quark matter entails an instability that leads to a third family of stable stars, with masses in-between 1.30 and 1.33 $M_\odot$. For non-accreting compact stars the baryon number is an invariant during the cooling evolution. By comparing the masses of cold and hot isothermal configurations of quark stars of equal baryon number, the maximum mass defect (energy release due to cooling) can be calculated. The result for the strong diquark coupling, $\eta = 1$, is shown if Fig. 10. For an initial temperature of 40 MeV and a given baryon number of $N = 1.46\, N_\odot$, the initial mass is $M = 1.41\, M_\odot$. By cooling this object down to $T = 0$, a mass defect of $\Delta M = 0.1\, M_\odot$ occurs. For the chosen baryon number, $N = 1.46\, N_\odot$, there are two possible $T = 0$ configurations (twins). A hot star could thus evolve into the more compact mass-equivalent (twin) final state, if a fluctuation triggers the transition to a CFL phase in the core of the star. The structures of these two twin configurations are given in Fig. 11. The energy release of 0.1 $M_\odot$ is of the same order of magnitude as the energy release in supernova explosions and gamma-ray bursts. Disregarding the possible influence of a hadronic shell and the details regarding the heat transport, the cooling induced first-order phase transition to the CFL phase could serve as

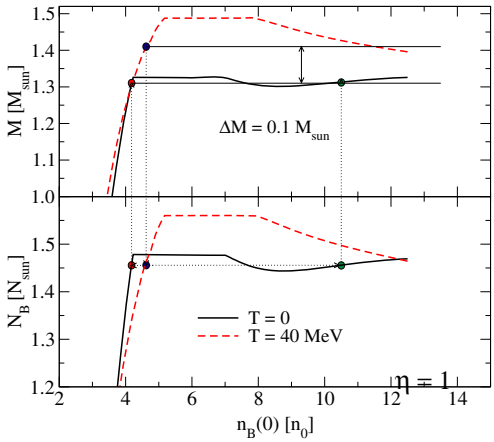

FIG. 10 (color online). Cooling an isothermal quark star configuration with initial mass $M = 1.41\, M_\odot$ at temperature $T = 40$ MeV under conservation of the given baryon number $N = 1.46\, N_\odot$ down to $T = 0$ leads to a mass defect $\Delta M = 0.1\, M_\odot$ for the strong coupling case ($\eta = 1.0$). Because of the twin structure at $T = 0$, two alternatives for the final state can be attained, a homogeneous 2SC quark star or a dense 2SC-CFL quark hybrid star.

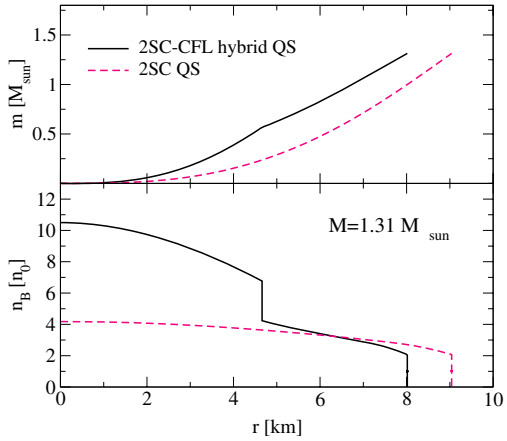

FIG. 11 (color online). Structure of two quark star (QS) configurations with $M = 1.31\ M_\odot$ (mass twins) for the three-flavor quark matter equation of state described in the text in the case of strong coupling ($\eta = 1$). The low-density twin has a radius of 9 km and is a homogeneous 2SC quark star, the high-density twin is more compact with a radius of 8 km and consists of a CFL quark matter core with 4.65 km radius and a 2SC quark matter shell.

a candidate process for the puzzling engine of these energetic phenomena [25,26,53].

IV. CONCLUSIONS

We have investigated the phase diagram of three-flavor quark matter within an NJL model under compact star constraints. Local color and electric charge neutrality is imposed for β-equilibrated superconducting quark matter. The constituent quark masses are self-consistently determined. The model refrains from adopting the 't Hooft determinant interaction in the mean-field Lagrangian as a realization of the $U_A(1)$ symmetry breaking. Instead, it is assumed that the $\eta - \eta'$ mass difference originates from an anomalous coupling of the pseudoscalar isosinglet fluctuation to the nonperturbative gluon sector, which gives no contribution to the quark thermodynamics at the mean-field level. The resulting parametrization of this $SU_f(3)$ NJL model results in a stronger coupling than NJL models with a 't Hooft term and thus in different phase diagrams, cf. Ref. [44]. The diquark condensates are determined self-consistently by minimization of the grand canonical thermodynamic potential. The various condensates are order parameters that characterize the different phases in the plane of temperature and quark chemical potential. These phases are in particular the NQ-2SC mixed phase, the 2SC, uSC, and CFL phases, as well as the corresponding gapless phases. We have investigated strong and intermediate diquark coupling strengths. It is shown that in both cases gapless superconducting phases do not occur at temperatures relevant for compact star evolution, i.e., below $\sim$50 MeV. Three-flavor quark matter phases, e.g., the CFL phase, occur only at rather large chemical potential, so the existence of such phases in stable compact stars is questionable. The stability and structure of isothermal quark star configurations are evaluated. For the strong diquark coupling, 2SC stars are stable up to a maximum mass of 1.33 $M_\odot$. A second family of more compact stars (twins) with a CFL quark matter core and masses in between 1.30 and 1.33 $M_\odot$ are found to be stable. For intermediate coupling, the quark stars are composed of a mixed NQ-2SC phase up to a maximum mass of 1.21 $M_\odot$, where a phase transition to the CFL phase occurs and the configurations become unstable. When the isothermal star configuration with an initial temperature of 40 MeV cools under conservation of baryon number, the mass defect is 0.1 $M_\odot$ for the strong diquark coupling. It is important to investigate the robustness of these statements, in particular, by including nonlocal form factors [30,54,55] and by going beyond the mean-field level by including the effects of a hadronic medium on the quark condensates. Finally, any statement concerning the occurrence and stability of quark matter in compact stars shall include an investigation of the influence of a hadronic shell [56–58] on the solutions of the equations of compact star structure.

ACKNOWLEDGMENTS

F. S. acknowledges support from the Swedish National Graduate School of Space Technology. A research visit of H. G. has been supported by Luleå University of Technology. S. F. visited Rostock thanks to EU support within the Erasmus program. A. M. Ö. received support from Hacettepe University Research Fund, Grant No. 02 02 602 001. D. B. thanks for partial support of the Department of Energy during the program INT-04-1 on *QCD and Dense Matter: From Lattices to Stars* at the University of Washington, where this project has been started. This work has been supported in part by the Virtual Institute of the Helmholtz Association under Grant No. VH-VI-041. We are grateful to our colleagues in Darmstadt and Frankfurt who made the results of their study in Ref. [44] available to us prior to submission.

APPENDIX: DISPERSION RELATIONS

The dispersion relations of the quasiparticles that appear in the expression for the thermodynamic potential (15) are the eigenvalues of the Nambu-Gorkov matrix (13). For each color and flavor combination of the eight component Nambu-Gorkov spinors, there is a corresponding 8×8 entry in this matrix. For three flavors and three colors (13) is a 72×72 matrix. The explicit form of this matrix can be represented by a table, where the rows and columns

denote the flavor and color degrees of freedom

$$
\begin{array}{c|cccccccccccccccccc}
 & q_{ur} & q_{ug} & q_{ub} & q_{dr} & q_{dg} & q_{db} & q_{sr} & q_{sg} & q_{sb} & q_{ur}^{\dagger} & q_{ug}^{\dagger} & q_{ub}^{\dagger} & q_{dr}^{\dagger} & q_{dg}^{\dagger} & q_{db}^{\dagger} & q_{sr}^{\dagger} & q_{sg}^{\dagger} & q_{sb}^{\dagger} \\
\hline
q_{ur}^{\dagger} & A_{ur} & 0 & 0 & 0 & 0 & 0 & 0 & 0 & 0 & 0 & 0 & 0 & 0 & D_{ud} & 0 & 0 & 0 & D_{us} \\
q_{ug}^{\dagger} & 0 & A_{ug} & 0 & 0 & 0 & 0 & 0 & 0 & 0 & 0 & 0 & 0 & -D_{ud} & 0 & 0 & 0 & 0 & 0 \\
q_{ub}^{\dagger} & 0 & 0 & A_{ub} & 0 & 0 & 0 & 0 & 0 & 0 & 0 & 0 & 0 & 0 & 0 & 0 & -D_{us} & 0 & 0 \\
q_{dr}^{\dagger} & 0 & 0 & 0 & A_{dr} & 0 & 0 & 0 & 0 & 0 & 0 & -D_{ud} & 0 & 0 & 0 & 0 & 0 & 0 & 0 \\
q_{dg}^{\dagger} & 0 & 0 & 0 & 0 & A_{dg} & 0 & 0 & 0 & 0 & D_{ud} & 0 & 0 & 0 & 0 & 0 & 0 & 0 & D_{ds} \\
q_{db}^{\dagger} & 0 & 0 & 0 & 0 & 0 & A_{db} & 0 & 0 & 0 & 0 & 0 & 0 & 0 & 0 & 0 & 0 & -D_{ds} & 0 \\
q_{sr}^{\dagger} & 0 & 0 & 0 & 0 & 0 & 0 & A_{sr} & 0 & 0 & 0 & 0 & -D_{us} & 0 & 0 & 0 & 0 & 0 & 0 \\
q_{sg}^{\dagger} & 0 & 0 & 0 & 0 & 0 & 0 & 0 & A_{sg} & 0 & 0 & 0 & 0 & 0 & 0 & -D_{ds} & 0 & 0 & 0 \\
q_{sb}^{\dagger} & 0 & 0 & 0 & 0 & 0 & 0 & 0 & 0 & A_{sb} & D_{us} & 0 & 0 & 0 & D_{ds} & 0 & 0 & 0 & 0 \\
q_{ur} & 0 & 0 & 0 & 0 & D_{ud}^{\dagger} & 0 & 0 & 0 & D_{us}^{\dagger} & B_{ur} & 0 & 0 & 0 & 0 & 0 & 0 & 0 & 0 \\
q_{ug} & 0 & 0 & 0 & -D_{ud}^{\dagger} & 0 & 0 & 0 & 0 & 0 & 0 & B_{ug} & 0 & 0 & 0 & 0 & 0 & 0 & 0 \\
q_{ub} & 0 & 0 & 0 & 0 & 0 & 0 & -D_{us}^{\dagger} & 0 & 0 & 0 & 0 & B_{ub} & 0 & 0 & 0 & 0 & 0 & 0 \\
q_{dr} & 0 & -D_{ud}^{\dagger} & 0 & 0 & 0 & 0 & 0 & 0 & 0 & 0 & 0 & 0 & B_{dr} & 0 & 0 & 0 & 0 & 0 \\
q_{dg} & D_{ud}^{\dagger} & 0 & 0 & 0 & 0 & 0 & 0 & 0 & D_{ds}^{\dagger} & 0 & 0 & 0 & 0 & B_{dg} & 0 & 0 & 0 & 0 \\
q_{db} & 0 & 0 & 0 & 0 & 0 & 0 & 0 & -D_{ds}^{\dagger} & 0 & 0 & 0 & 0 & 0 & 0 & B_{db} & 0 & 0 & 0 \\
q_{sr} & 0 & 0 & -D_{us}^{\dagger} & 0 & 0 & 0 & 0 & 0 & 0 & 0 & 0 & 0 & 0 & 0 & 0 & B_{sr} & 0 & 0 \\
q_{sg} & 0 & 0 & 0 & 0 & 0 & -D_{ds}^{\dagger} & 0 & 0 & 0 & 0 & 0 & 0 & 0 & 0 & 0 & 0 & B_{sg} & 0 \\
q_{sb} & D_{us}^{\dagger} & 0 & 0 & 0 & D_{ds}^{\dagger} & 0 & 0 & 0 & 0 & 0 & 0 & 0 & 0 & 0 & 0 & 0 & 0 & B_{sb}
\end{array}
. \tag{A1}
$$

Each entry is a 4×4 Hermitian matrix in Dirac space. The diagonal submatrices are

$$
A_{i\alpha} = \begin{bmatrix} p + \mu_{i\alpha} & 0 & -M_i & 0 \\ 0 & -p + \mu_{i\alpha} & 0 & -M_i \\ -M_i & 0 & -p + \mu_{i\alpha} & 0 \\ 0 & -M_i & 0 & p + \mu_{i\alpha} \end{bmatrix}, \tag{A2}
$$

$$
B_{j\beta} = \begin{bmatrix} -p - \mu_{j\beta} & 0 & M_j & 0 \\ 0 & p - \mu_{j\beta} & 0 & M_j \\ M_j & 0 & p - \mu_{j\beta} & 0 \\ 0 & M_j & 0 & -p - \mu_{j\beta} \end{bmatrix}, \tag{A3}
$$

whereas the off-diagonal blocks are given by

$$
D_{ij} = \begin{bmatrix} 0 & 0 & 0 & i\Delta_{ij} \\ 0 & 0 & -i\Delta_{ij} & 0 \\ 0 & i\Delta_{ij} & 0 & 0 \\ -i\Delta_{ij} & 0 & 0 & 0 \end{bmatrix}. \tag{A4}
$$

The eigenvalues of (A1) are the quasiparticle energies, λ_a, that enter the thermodynamic potential (15), i.e., the 72 dispersion relations of the various quark-quark and antiquark-antiquark excitations. These eigenvalues can be calculated using a standard numerical library. However, in order to reduce the computational cost, the matrix can be decomposed into a block-diagonal matrix by elementary row and column operations.

	q_{ur}	q_{dg}	q_{sb}	$q_{ur}^\dagger$	$q_{dg}^\dagger$	$q_{sb}^\dagger$	q_{ug}	$q_{dr}^\dagger$	q_{dr}	$q_{ug}^\dagger$	q_{ub}	$q_{sr}^\dagger$	q_{sr}	$q_{ub}^\dagger$	q_{db}	$q_{sg}^\dagger$	q_{sg}	$q_{db}^\dagger$
$q_{ur}^\dagger$	A_{ur}	0	0	0	D_{ud}	D_{us}	0	0	0	0	0	0	0	0	0	0	0	0
$q_{dg}^\dagger$	0	A_{dg}	0	D_{ud}	0	D_{ds}	0	0	0	0	0	0	0	0	0	0	0	0
$q_{sb}^\dagger$	0	0	A_{sb}	D_{us}	D_{ds}	0	0	0	0	0	0	0	0	0	0	0	0	0
q_{ur}	0	$D_{ud}^\dagger$	$D_{us}^\dagger$	B_{ur}	0	0	0	0	0	0	0	0	0	0	0	0	0	0
q_{dg}	$D_{ud}^\dagger$	0	$D_{ds}^\dagger$	0	B_{dg}	0	0	0	0	0	0	0	0	0	0	0	0	0
q_{sb}	$D_{us}^\dagger$	$D_{ds}^\dagger$	0	0	0	B_{sb}	0	0	0	0	0	0	0	0	0	0	0	0
$q_{ug}^\dagger$	0	0	0	0	0	0	A_{ug}	$-D_{ud}$	0	0	0	0	0	0	0	0	0	0
q_{dr}	0	0	0	0	0	0	$-D_{ud}^\dagger$	B_{dr}	0	0	0	0	0	0	0	0	0	0
$q_{dr}^\dagger$	0	0	0	0	0	0	0	0	A_{dr}	$-D_{ud}$	0	0	0	0	0	0	0	0
q_{ug}	0	0	0	0	0	0	0	0	$-D_{ud}^\dagger$	B_{ug}	0	0	0	0	0	0	0	0
$q_{ub}^\dagger$	0	0	0	0	0	0	0	0	0	0	A_{ub}	$-D_{us}$	0	0	0	0	0	0
q_{sr}	0	0	0	0	0	0	0	0	0	0	$-D_{us}^\dagger$	B_{sr}	0	0	0	0	0	0
$q_{sr}^\dagger$	0	0	0	0	0	0	0	0	0	0	0	0	A_{sr}	$-D_{us}$	0	0	0	0
q_{ub}	0	0	0	0	0	0	0	0	0	0	0	0	$-D_{us}^\dagger$	B_{ub}	0	0	0	0
$q_{db}^\dagger$	0	0	0	0	0	0	0	0	0	0	0	0	0	0	A_{db}	$-D_{ds}$	0	0
q_{sg}	0	0	0	0	0	0	0	0	0	0	0	0	0	0	$-D_{ds}^\dagger$	B_{sg}	0	0
$q_{sg}^\dagger$	0	0	0	0	0	0	0	0	0	0	0	0	0	0	0	0	A_{sg}	$-D_{ds}$
q_{db}	0	0	0	0	0	0	0	0	0	0	0	0	0	0	0	0	$-D_{ds}^\dagger$	B_{db}

(A5)

This matrix has one 24×24 and six 8×8 independent submatrices. Expressing these submatrices explicitly, using (A2)–(A4), the 24×24 matrix can be decomposed into two independent 12×12 submatrices by elementary row and column operations. Similarly, the six 8×8 matrices can be transformed into 12 independent 4×4 submatrices. There is a two-fold degeneracy due to the Nambu-Gorkov basis, each matrix appears both as $\mathcal{M}$ and $\mathcal{M}^\dagger$, so there are only one independent 12×12 matrix and six 4×4 matrices. The 12×12 matrix is

$$\mathcal{M}_{12} = \begin{bmatrix}
p+\mu_{ur} & 0 & 0 & -M_u & 0 & 0 & 0 & i\Delta_{ud} & i\Delta_{us} & 0 & 0 & 0 \\
0 & p+\mu_{dg} & 0 & 0 & -M_d & 0 & i\Delta_{ud} & 0 & i\Delta_{ds} & 0 & 0 & 0 \\
0 & 0 & p+\mu_{sb} & 0 & 0 & -M_s & i\Delta_{us} & i\Delta_{ds} & 0 & 0 & 0 & 0 \\
-M_u & 0 & 0 & -p+\mu_{ur} & 0 & 0 & 0 & 0 & 0 & i\Delta_{ud} & i\Delta_{us} & \\
0 & -M_d & 0 & 0 & -p+\mu_{dg} & 0 & 0 & 0 & 0 & i\Delta_{ud} & 0 & i\Delta_{ds} \\
0 & 0 & -M_s & 0 & 0 & -p+\mu_{sb} & 0 & 0 & 0 & i\Delta_{us} & i\Delta_{ds} & 0 \\
0 & -i\Delta_{ud} & -i\Delta_{us} & 0 & 0 & 0 & -p-\mu_{ur} & 0 & 0 & M_u & 0 & 0 \\
-i\Delta_{ud} & 0 & -i\Delta_{ds} & 0 & 0 & 0 & 0 & -p-\mu_{dg} & 0 & 0 & M_d & 0 \\
-i\Delta_{us} & -i\Delta_{ds} & 0 & 0 & 0 & 0 & 0 & 0 & -p-\mu_{sb} & 0 & 0 & M_s \\
0 & 0 & 0 & 0 & -i\Delta_{ud} & -i\Delta_{us} & M_u & 0 & 0 & p-\mu_{ur} & 0 & 0 \\
0 & 0 & 0 & -i\Delta_{ud} & 0 & -i\Delta_{ds} & 0 & M_d & 0 & 0 & p-\mu_{dg} & 0 \\
0 & 0 & 0 & -i\Delta_{us} & -i\Delta_{ds} & 0 & 0 & 0 & M_s & 0 & 0 & p-\mu_{sb}
\end{bmatrix}, \tag{A6}$$

and the 4×4 matrices are

$$\mathcal{M}_4 = \begin{bmatrix} p + \mu_{i\alpha} & -i\Delta_{ij} & -M_i & 0 \\ i\Delta_{ij} & -p - \mu_{j\beta} & 0 & M_j \\ -M_i & 0 & -p + \mu_{i\alpha} & -i\Delta_{ij} \\ 0 & M_j & i\Delta_{ij} & p - \mu_{j\beta} \end{bmatrix}, \tag{A7}$$

for spinor products $ug - dr$, $ub - sr$, $db - sg$, $dr - ug$, $sr - ub$, and $sg - db$, respectively.

The eigenvalues of the 12×12 matrix appear in $\pm$ pairs. For the 4×4 matrices, the dispersion relations of the $i\alpha - j\beta$ and $j\beta - i\alpha$ quasiparticles have the same magnitude but opposite signs. Thus, there are in general nine independent dispersion relations for quark-quark excitations and nine for antiquark-antiquark excitations. Each dispersion relation is two-fold degenerate due to the Nambu-Gorkov basis and two-fold "degenerate" due to the $\pm$ pairs. The eigenvalues of (A6) must be calculated numerically. The eigenvalues of (A7) can be obtained analytically by solving for the roots of the quartic characteristic polynomial,

$$\lambda^4 + a_3\lambda^3 + a_2\lambda^2 + a_1\lambda + a_0 = 0, \tag{A8}$$

where

$$\begin{aligned} a_0 &= P^4 + (M_i^2 + M_j^2 + 2\Delta_{ij}^2 - \mu_{i\alpha}^2 - \mu_{j\beta}^2)P^2 + (\mu_{i\alpha}\mu_{j\beta} + M_iM_j + \Delta_{ij}^2 + \mu_{i\alpha}M_j + \mu_{j\beta}M_i) \\ &\quad \times (\mu_{i\alpha}\mu_{j\beta} + M_iM_j + \Delta_{ij}^2 - \mu_{i\alpha}M_j - \mu_{j\beta}M_i), \\ a_1 &= 2(\mu_{i\alpha} - \mu_{j\beta})P^2 + 2\Delta_{ij}^2(\mu_{i\alpha} - \mu_{j\beta}) + 2(\mu_{i\alpha}M_j^2 - \mu_{j\beta}M_i^2 + \mu_{i\alpha}^2\mu_{j\beta} - \mu_{j\beta}^2\mu_{i\alpha}), \\ a_2 &= \mu_{i\alpha}^2 + \mu_{j\beta}^2 - 2P^2 - M_i^2 - M_j^2 - 2\Delta_{ij}^2 - 4\mu_{i\alpha}\mu_{j\beta}, \\ a_3 &= -2(\mu_{i\alpha} - \mu_{j\beta}). \end{aligned}$$

In the limit when $M_i = M_j = M$, which is approximately valid for the $ug - dr$ and $dr - ug$ quasiparticles, the four solutions are

$$\lambda = \frac{\mu_{i\alpha} - \mu_{j\beta}}{2} \pm \sqrt{\left(\frac{\mu_{i\alpha} + \mu_{j\beta}}{2} \pm E\right)^2 + \Delta_{ij}^2}, \tag{A9}$$

where $E = \sqrt{p^2 + M^2}$. This result is in agreement with [44]. More generally, the solutions of the quartic equation can be found in textbooks, see, e.g., [59]. In this work the eigenvalues of the 4×4 matrices were calculated with the exact solutions of the quartic equation and the eigenvalues of the 12×12 matrix were calculated with LAPACK. The momentum integral in (15) was calculated with a Gaussian quadrature. The minimization of the thermodynamic potential was performed with conjugate gradient methods, choosing the initial values of the variational parameters carefully, and then comparing the free energies of the various minima. The color and electric charges were neutralized with a globally convergent Newton-Raphson method in multidimensions.

Gapless quasiparticle excitations are characterized by a nonzero gap, Δ_{ij}, and a corresponding dispersion relation that is zero for at least one value of the quasiparticle momentum, i.e., the dispersion relation reaches the Fermi surface and there is no forbidden energy band.

[1] R. Rapp, T. Schäfer, E. V. Shuryak, and M. Velkovsky, Phys. Rev. Lett. **81**, 53 (1998).
[2] M. G. Alford, K. Rajagopal, and F. Wilczek, Phys. Lett. B **422**, 247 (1998).
[3] D. Blaschke and C. D. Roberts, Nucl. Phys. **A642**, c197 (1998).
[4] B. C. Barrois, Nucl. Phys. **B129**, 390 (1977).
[5] D. Bailin and A. Love, Phys. Rep. **107**, 325 (1984).
[6] K. Rajagopal and F. Wilczek, hep-ph/0011333.
[7] M. G. Alford, Annu. Rev. Nucl. Part. Sci. **51**, 131 (2001).
[8] M. Buballa, Phys. Rep. **407**, 205 (2005).
[9] A. Schmitt, Phys. Rev. D **71**, 054016 (2005).
[10] D. Blaschke, N. K. Glendenning, and A. Sedrakian, *Physics of Neutron Star Interiors* (Springer, Heidelberg, 2001).
[11] D. K. Hong *et al.*, *Compact Stars: The Quest for New States of Matter* (World Scientific, Singapore, 2004).
[12] D. Blaschke and D. Sedrakian, *Superdense QCD Matter in Compact Stars* (Springer, Heidelberg, 2005).
[13] J. E. Horvath, O. G. Benvenuto, and H. Vucetich, Phys. Rev. D **44**, 3797 (1991).
[14] D. Blaschke, T. Klähn, and D. N. Voskresensky, Astrophys. J. **533**, 406 (2000).
[15] D. Page, M. Prakash, J. M. Lattimer, and A. Steiner, Phys. Rev. Lett. **85**, 2048 (2000).
[16] D. Blaschke, H. Grigorian, and D. N. Voskresensky, Astron. Astrophys. **368**, 561 (2001).
[17] H. Grigorian, D. Blaschke, and D. Voskresensky, Phys. Rev. C **71**, 045801 (2005).
[18] D. N. Aguilera, D. Blaschke, M. Buballa, and V. L. Yudichev, Phys. Rev. D **72**, 034008 (2005).

[19] D. Blaschke, D. M. Sedrakian, and K. M. Shahabasian, Astron. Astrophys. **350**, L47 (1999).
[20] M. G. Alford, J. Berges, and K. Rajagopal, Nucl. Phys. **B571**, 269 (2000).
[21] K. Iida and G. Baym, Phys. Rev. D **66**, 014015 (2002).
[22] D. M. Sedrakian, D. Blaschke, K. M. Shahabasian, and D. N. Voskresensky, Phys. Part. Nuclei **33**, S100 (2002).
[23] D. K. Hong, S. D. H. Hsu, and F. Sannino, Phys. Lett. B **516**, 362 (2001).
[24] R. Ouyed and F. Sannino, Astron. Astrophys. **387**, 725 (2002).
[25] D. N. Aguilera, D. Blaschke, and H. Grigorian, Astron. Astrophys. **416**, 991 (2004).
[26] D. N. Aguilera, D. Blaschke, and H. Grigorian, astro-ph/0402073.
[27] R. Ouyed, R. Rapp, and C. Vogt, astro-ph/0503357.
[28] F. Neumann, M. Buballa, and M. Oertel, Nucl. Phys. **A714**, 481 (2003).
[29] M. Oertel and M. Buballa, hep-ph/0202098.
[30] C. Gocke, D. Blaschke, A. Khalatyan, and H. Grigorian, hep-ph/0104183.
[31] H. Abuki, M. Kitazawa, and T. Kunihiro, hep-ph/0412382.
[32] M. Alford and K. Rajagopal, J. High Energy Phys. 06 (2002) 031.
[33] A. W. Steiner, S. Reddy, and M. Prakash, Phys. Rev. D **66**, 094007 (2002).
[34] M. G. Alford, C. Kouvaris, and K. Rajagopal, Phys. Rev. Lett. **92**, 222001 (2004).
[35] M. Alford, C. Kouvaris, and K. Rajagopal, Phys. Rev. D **71**, 054009 (2005).
[36] S. B. Rüster, I. A. Shovkovy, and D. H. Rischke, Nucl. Phys. **A743**, 127 (2004).
[37] I. Shovkovy and M. Huang, Phys. Lett. B **564**, 205 (2003).
[38] M. Huang and I. Shovkovy, Nucl. Phys. **A729**, 835 (2003).
[39] M. G. Alford, K. Rajagopal, and F. Wilczek, Nucl. Phys. **B537**, 443 (1999).
[40] D. Blaschke, H. P. Pavel, V. N. Pervushin, G. Ropke, and M. K. Volkov, Phys. Lett. B **397**, 129 (1997).
[41] L. von Smekal, A. Mecke, and R. Alkofer, hep-ph/9707210.
[42] H. B. Nielsen, M. Rho, A. Wirzba, and I. Zahed, Phys. Lett. B **281**, 345 (1992).
[43] R. Alkofer, P. A. Amundsen, and H. Reinhardt, Phys. Lett. B **218**, 75 (1989).
[44] S. B. Ruster, V. Werth, M. Buballa, I. A. Shovkovy, and D. H. Rischke, Phys. Rev. D **72**, 034004 (2005).
[45] L. P. Gor'kov, Zh. Eksp. Teor. Fiz. **36**, 1918 (1959).
[46] Y. Nambu, Phys. Rev. **117**, 648 (1960).
[47] J. I. Kapusta, *Finite-temperature Field Theory* (University Press, Cambridge, 1989).
[48] D. N. Aguilera, D. Blaschke, and H. Grigorian, Nucl. Phys. **A757**, 527 (2005).
[49] N. K. Glendenning, *Compact Stars* (Springer, New York, 2000).
[50] S. L. Shapiro and S. A. Teukolsky, *Black Holes, White Dwarfs, and Neutron Stars* (Wiley, New York, 1983).
[51] C. Kettner, F. Weber, M. K. Weigel, and N. K. Glendenning, Phys. Rev. D **51**, 1440 (1995).
[52] D. Blaschke, H. Grigorian, G. S. Poghosyan, C. D. Roberts, and S. M. Schmidt, Phys. Lett. B **450**, 207 (1999).
[53] D. Blaschke, S. Fredriksson, H. Grigorian, and A. M. Oztas, Nucl. Phys. **A736**, 203 (2004).
[54] D. Blaschke, H. Grigorian, A. Khalatyan, and D. N. Voskresensky, Nucl. Phys. B Proc. Suppl. **141**, 137 (2005).
[55] R. S. Duhau, A. G. Grunfeld, and N. N. Scoccola, Phys. Rev. D **70**, 074026 (2004).
[56] M. Baldo, M. Buballa, F. Burgio, F. Neumann, M. Oertel, and H. J. Schulze, Phys. Lett. B **562**, 153 (2003).
[57] I. Shovkovy, M. Hanauske, and M. Huang, Phys. Rev. D **67**, 103004 (2003).
[58] H. Grigorian, D. Blaschke, and D. N. Aguilera, Phys. Rev. C **69**, 065802 (2004).
[59] M. Abramowitz and I. A. Stegun, *Handbook of Mathematical Functions with Formulas, Graphs, and Mathematical Tables* (Dover, New York, 1972), p. 17.

Paper IV

Condition for gapless color-antitriplet excitations in Nambu–Jona-Lasinio models

F. Sandin[1] and A. M. Öztaş[2]
[1]*Department of Physics, Luleå University of Technology, SE-97187 Luleå, Sweden*
[2]*Department of Physics, Hacettepe University, TR-06532 Ankara, Turkey*
(Received 8 December 2005; published 8 March 2006)

We present an exact condition for the existence of gapless quasiparticle excitations in Nambu–Jona-Lasinio models of color superconducting quark matter with a quark-quark interaction in the scalar color-antitriplet channel. The condition can be represented by a rotated ellipse in the plane of mass and chemical potential differences for the paired quark fields.

DOI: 10.1103/PhysRevC.73.035203 PACS number(s): 24.85.+p, 12.38.Mh, 25.75.Nq, 26.60.+c

I. INTRODUCTION

At high baryon density and low temperature, matter is believed to be in a color superconducting state, which is characterized by condensates of quark Cooper pairs [1–4]. A superconducting phase typically has an energy gap in the density of states, which corresponds to the lowest excitation energy of a quasiparticle pair. However, if the difference between the Fermi momenta of the paired quarks is sufficiently large, *gapless* quasiparticle excitations could exist [5–8]. The presence of gapless phases could have observable consequences, e.g., the high specific heat and neutrino emissivity could affect the cooling behavior of compact stars [9]. It has been found, however, that gapless phases might suffer from a chromomagnetic instability [10–15], and it is currently unclear whether gapless phases appear at temperatures relevant for compact star evolution [8,15–17]. It is therefore important to improve the understanding of gapless phases. In this paper we derive an exact condition for the existence of gapless excitations in the frequently used Nambu–Jona-Lasinio (NJL) model of color superconducting quark matter. A qualitatively useful graphical representation of the condition and some well-known approximations are also presented.

II. MODEL

The most dense environment where quark matter is expected to exist is in the core of neutron stars, which are subject to a gravitational instability that limits the maximum density to $\sim 10^{15}$ g/cm^3 [18]. This corresponds to a maximum quark-number chemical potential of $\mu \sim 500$ MeV and a maximum baryon number density of $n_B \sim 10\, n_0$, where $n_0 = 0.17$ fm^{-3} is the baryon number density in nuclear matter. Since the charm quark mass is higher than the maximum chemical potential, it is sufficient to consider up (u), down (d), and strange (s) quarks. The quark spinors are

$$q^T = (\psi_{ur}, \psi_{ug}, \psi_{ub}, \psi_{dr}, \psi_{dg}, \psi_{db}, \psi_{sr}, \psi_{sg}, \psi_{sb}), \quad (1)$$

where r, g, and b represent red, green, and blue colors. The NJL model of superconducting quark matter is based on effective pointlike four-fermion interactions and is described in, e.g., Refs. [15–17,19]. Here we repeat some of the essential points. The Lagrangian density is

$$\mathcal{L}_{\text{eff}} = \bar{q}(i\partial\!\!\!/ - \hat{m} + \hat{\mu}\gamma^0)q + \mathcal{L}_{\bar{q}q} + \mathcal{L}_{qq}, \quad (2)$$

where $\hat{m} = \text{diag}_f(m_u, m_d, m_s)$ is the current quark mass matrix in flavor space. $\mathcal{L}_{\bar{q}q}$ and $\mathcal{L}_{qq}$ are the effective interaction terms, which are used at mean-field level in the Hartree approximation. Explicitly,

$$\mathcal{L}_{\bar{q}q} = G_S \sum_{a=0}^{8} [(\bar{q}\tau_a q)^2 + (\bar{q} i\gamma_5 \tau_a q)^2] - K\{\det{}_f[\bar{q}(1+\gamma_5)q] + \det{}_f[\bar{q}(1-\gamma_5)q]\}, \quad (3)$$

$$\mathcal{L}_{qq} = G_D \sum_{a,b=2,5,7} (\bar{q} i\gamma_5 \tau_a \lambda_b C \bar{q}^T)(q^T C i\gamma_5 \tau_a \lambda_b q), \quad (4)$$

where τ_a and λ_b are the antisymmetric Gell-Mann matrices acting in, respectively, flavor and color space. G_S, K, and G_D are coupling constants that must be determined by experiments.

The quark-quark interaction term $\mathcal{L}_{qq}$ gives rise to superconducting condensates, $s_{ab} = \langle q^T C\gamma_5 \tau_a \lambda_b q\rangle$, which break SU(3)$_c$ and U(1) symmetry. The symmetries of $\mathcal{L}$ correspond to a conserved chromoelectromagnetic charge. The associated chemical potential is [19]

$$\hat{\mu} = \mu + \mu_Q \left(\frac{\tau_3}{2} + \frac{\tau_8}{2\sqrt{3}}\right) + \mu_3\lambda_3 + \mu_8\lambda_8. \quad (5)$$

Here, μ is the quark-number chemical potential, μ_Q is the positive electric-charge chemical potential, and μ_3 and μ_8 are color-charge chemical potentials. By linearizing Eq. (2) in the quark-quark (diquark) gaps, $\Delta_{ab} = 2G_D s_{ab}$, and the quark-antiquark (chiral) gaps, $\phi_i = -4G_S\langle\bar{q}_i q_i\rangle$, one can obtain a grand canonical thermodynamic potential by standard methods [15–17,19]:

$$\Omega(T,\mu) = \frac{\phi_u^2+\phi_d^2+\phi_s^2}{8G_S} + \frac{K\phi_u\phi_d\phi_s}{16G_S^3} + \frac{\Delta_{ud}^2+\Delta_{us}^2+\Delta_{ds}^2}{4G_D} - \int \frac{d^3p}{(2\pi)^3} \sum_{n=1}^{18} [E_n + 2T\ln(1+e^{-E_n/T})] + \Omega_{\text{lep}} - \Omega_0. \quad (6)$$

Here, $E_n(p, \mu; \mu_Q, \mu_3, \mu_8, \phi_u, \phi_d, \phi_s, \Delta_{ud}, \Delta_{us}, \Delta_{ds})$ are the quasiparticle dispersion relations, Ω_{lep} is the contribution from leptons (e.g., electrons, muons, and the corresponding

neutrino flavors), and Ω_0 is the vacuum, i.e., $\Omega(0,\ 0) = 0$. It should be noted that Eq. (6) is an even function of E_n, so the signs of the dispersion relations are arbitrary. We therefore follow the standard convention that all states below the Fermi surface ($E_n < 0$) are occupied, and only positive-energy states are considered. In Eq. (6) the diquark gaps are denoted with flavor indices. One can readily do this by considering the color and flavor structure of the Gell-Mann matrices

$$\Delta_{ud} \equiv \Delta_{22} \quad (u\text{-}d,\ r\text{-}g \text{ pairing}), \tag{7}$$
$$\Delta_{us} \equiv \Delta_{55} \quad (u\text{-}s,\ r\text{-}b \text{ pairing}), \tag{8}$$
$$\Delta_{ds} \equiv \Delta_{77} \quad (d\text{-}s,\ g\text{-}b \text{ pairing}), \tag{9}$$

and $\Delta_{ab} = 0$ if $a \neq b$ [19]. The chiral gaps and the diquark gaps are variational parameters that are determined by minimization of Eq. (6). The constituent quark masses are

$$M_i = m_i + \phi_i + \frac{K}{8G_S^2}\phi_j\phi_k, \tag{10}$$

where $(i,\ j,\ k)$ is any permutation of $(u,\ d,\ s)$.

In QCD, a color superconducting ground state is automatically color neutral because of the generation of gluon condensates in one or more of the eight components of the gluon field. In NJL models there are no gauge fields that neutralize the color charge dynamically, because the gluons have been replaced with effective pointlike quark-antiquark [Eq. (3)] and quark-quark [Eq. (4)] interactions. One must therefore enforce color neutrality by solving for the charge chemical potentials μ_Q, μ_3, and μ_8 such that the corresponding charge densities $n_a = \langle\psi^\dagger T_a \psi\rangle = -\partial\Omega/\partial\mu_a$ are zero [20].

The values of the gaps and the (charge) chemical potentials depend on the coupling constants (G_S, K, and G_D), the current quark masses (m_u, m_d, and m_s), and the regularization method. These input parameters are fitted to low-density hadronic results and are therefore only approximately known. In addition, approximations are frequently used to simplify the evaluation of Eq. (6). In this context it would be useful to have a mathematically exact condition for the appearance of gapless quasiparticle dispersion relations, without reference to specific input parameters and further assumptions. This condition is presented below.

III. GAPLESS CONDITIONS

The dispersion relations E_n are eigenvalues of six 4×4 matrices and one 12×12 matrix [15–17]. Disregarding the signs, three 4×4 matrices and 6 of the 12 eigenvalues of the 12×12 matrix remain ($3 \times 4 + 6 = 18$). The 12×12 matrix corresponds to *ur-dg-sb* pairing, and the three 4×4 matrices correspond to *ug-dr*, *ub-sr*, and *db-sg* pairing. There are strong indications that the *ur-dg-sb* modes are never gapless, because the Fermi momenta of these three species are approximately equal [8], and no such gapless modes have been found in numerical evaluations [15–17]. A proof has turned out to be difficult to obtain because of the complexity of the characteristic polynomial of the 12×12 matrix. We therefore leave this analysis to a future publication. Here the 4×4 matrices are considered. The characteristic polynomials of these matrices can be written as

$$E_n^4 + a_3 E_n^3 + a_2 E_n^2 + a_1 E_n + a_0. \tag{11}$$

The a_0 coefficient of the polynomial is [17]

$$\begin{aligned} a_0 = {} & p^4 + \left(M_i^2 + M_j^2 + 2\Delta_{ij}^2 - \mu_{i\alpha}^2 - \mu_{j\beta}^2\right) \\ & + p^2\left(\mu_{i\alpha}\mu_{j\beta} + M_i M_j + \Delta_{ij}^2 + \mu_{i\alpha}M_j + \mu_{j\beta}M_i\right) \\ & \times \left(\mu_{i\alpha}\mu_{j\beta} + M_i M_j + \Delta_{ij}^2 - \mu_{i\alpha}M_j - \mu_{j\beta}M_i\right), \end{aligned} \tag{12}$$

for quark flavors $(i,\ j)$ and colors $(\alpha,\ \beta)$. The chemical potential $\mu_{i\alpha}$ for a quark field with flavor i and color α can be extracted from Eq. (5) ($\hat{\mu}$ is diagonal in color and flavor space). A gapless dispersion relation is characterized by $E_n(p) = 0$ for some real value(s) of p when $\Delta_{ij} \neq 0$. This requires that $a_0(p) = 0$ have at least one real root. The solutions are

$$\begin{aligned} p^2 = {} & \bar{\mu}^2 + \delta\mu^2 - \bar{M}^2 - \delta M^2 - \Delta^2 \\ & \pm 2\sqrt{(\bar{\mu}\delta\mu - \bar{M}\delta M)^2 - \Delta^2(\bar{\mu}^2 - \delta M^2)}. \end{aligned} \tag{13}$$

Here we have introduced the quantities

$$\bar{M} = (M_i + M_j)/2, \quad \delta M = (M_i - M_j)/2, \tag{14}$$
$$\bar{\mu} = (\mu_{i\alpha} + \mu_{j\beta})/2, \quad \delta\mu = (\mu_{i\alpha} - \mu_{j\beta})/2, \tag{15}$$

and $\Delta = \Delta_{ij}$. The indices in Eq. (12) can be omitted without ambiguity, since we are dealing with two-species pairing. Observe that the masses and chemical potentials of the paired quark fields are $\bar{M} \pm \delta M$ and $\bar{\mu} \pm \delta\mu$. A real square root in Eq. (13) requires that

$$\Delta \leqslant \Delta^g \equiv \frac{|\bar{\mu}\delta\mu - \bar{M}\delta M|}{\sqrt{\bar{\mu}^2 - \delta M^2}}, \tag{16}$$

and a positive solution for p^2 requires that

$$\begin{aligned} & \bar{M}^2 + \delta M^2 + \Delta^2 - \bar{\mu}^2 - \delta\mu^2 \\ & \qquad \leqslant 2\sqrt{(\bar{\mu}\delta\mu - \bar{M}\delta M)^2 - \Delta^2(\bar{\mu}^2 - \delta M^2)}. \end{aligned} \tag{17}$$

Inequality (16) can be represented with a rotated ellipse in the δM-$\delta\mu$ plane, as in Fig. 1. The interior region of the ellipse violates inequality (16) and hence represents gapped modes. Outside the ellipse the square root in inequality (17) is real, and inequality (17) is obviously satisfied as long as the left-hand side is negative. A negative left-hand side of inequality (17) is represented by the region in between the two branches of the hyperbola, $\bar{\mu}^2 + \delta\mu^2 = \bar{M}^2 + \delta M^2 + \Delta^2$, in Fig. 1. For a positive left-hand side, which corresponds to the two regions on the left- and right-hand sides of the hyperbola, inequality (17) can be squared, and four coupled inequalities linear in δM and $\delta\mu$ are obtained. These correspond to tangent lines of the ellipse. The hatched areas enclosed by the tangent lines, the hyperbola and the ellipse violate inequality (17) and hence represent gapped modes. For each tangent line the intersection with the hyperbola coincides with the point on the ellipse. Inequality (17) is relevant if $\delta M/\bar{\mu} \sim 1 - \Delta^2(\bar{\mu} - \bar{M})^{-2}/2$, which is not the case for realistic values of the masses and chemical potentials. This is explicitely demonstrated by the examples in Fig. 2. Inequality (16) is therefore the relevant condition for gapless modes. In achieving this result, no further approximations other than those leading up to Eq. (6) were made.

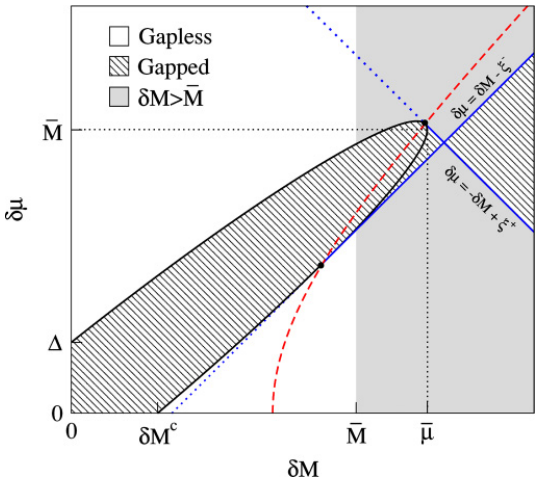

FIG. 1. (Color online) Graphical representation of gapless inequalities (16) and (17). For clarity only the first quadrant is shown. The third quadrant is a reflection of the first quadrant in the origin. In this figure an unreasonably large value of $\bar{M}$ has been used to emphasize the role of the tangent lines. Qualitatively, the gapped region can be represented by the rotated ellipse; see the text. The values of $\delta\mu$ and δM can be represented by a point in the δM-$\delta\mu$ plane. If this point is enclosed by the hatched area, the dispersion relations are gapped. Otherwise a gapless dispersion relation exists. Here $\delta M^c = \bar{\mu}/(1+\bar{M}^2/\Delta^2)^{1/2}$ and $\xi^{\pm} = [\Delta^2 + (\bar{\mu} \pm \bar{M})^2]^{1/2}$.

For the two-flavor color superconducting phase, which is characterised by $\Delta_{ud} \neq 0$ and $\Delta_{us} = \Delta_{ds} = \mu_3 = 0$, one can use the fact that $\delta M \ll \delta\mu$ and $M \ll \mu$, so the gapless

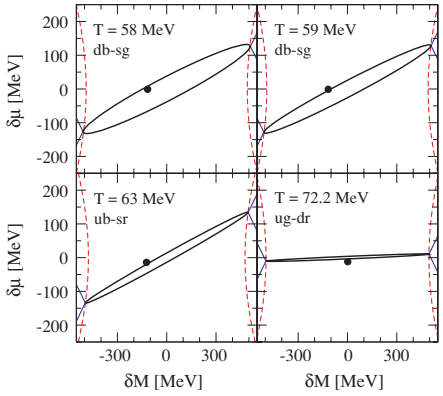

FIG. 2. (Color online) Graphical representation of gapless conditions (16) and (17) for some of the quasiparticle dispersion relations represented in Fig. 4. The values of δM and $\delta\mu$ are represented by bold points. If the center of a point is enclosed by an ellipse, the corresponding quasiparticle has gapped dispersion relations; otherwise a gapless dispersion relation exists.

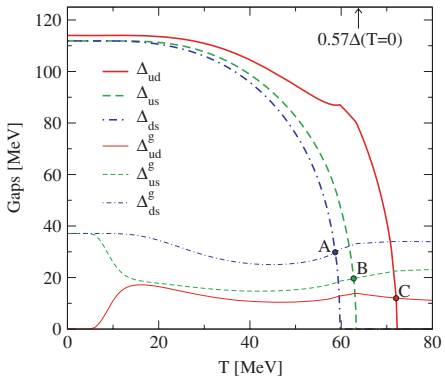

FIG. 3. (Color online) Diquark gaps vs. the temperature at $\mu = 500$ MeV and $\eta = 0.75$. Δ^g_{ij} is the threshold for gapless quasiparticle dispersion relations (16), i.e., gapless modes exist iff $\Delta_{ij} \leqslant \Delta^g_{ij}$. The critical points where gapless *db-sg*, *ub-sr*, and *ug-dr* quasiparticles appear are denoted by, respectively, A, B, and C. The BCS result for the critical temperature of a superconducting condensate, $T \sim 0.57\Delta$ ($T = 0$), is indicated in the plot. This figure represents a cross section of Fig. 5 in Ref. [17].

condition [Eq. (16)] is approximately

$$\Delta_{ud} \lesssim |\delta\mu| = -\mu_Q. \tag{18}$$

For the three-flavor color-flavor-locked phase, which is characterized by $\Delta_{ij} \neq 0$ and $\bar{M} \sim \delta M \sim M_s/2$, a series expansion of inequality (16) to first order in $M_s^2/\bar{\mu}$ yields

$$\Delta_{is} \lesssim |\delta\mu| + \left[\frac{\mathrm{sign}(\delta\mu)}{4} + \frac{|\delta\mu|}{8\bar{\mu}}\right]\frac{M_s^2}{\bar{\mu}}, \tag{19}$$

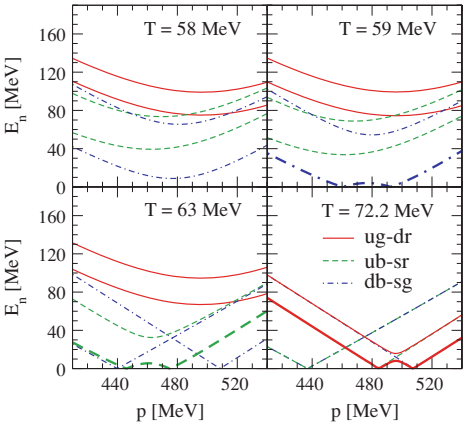

FIG. 4. (Color online) Dispersion relations at $\mu = 500$ MeV and $\eta = 0.75$ for four different temperatures. Gapless modes are denoted by the thick curves. Gapped modes and modes of unpaired quarks are denoted by the thin curves. Compare with Fig. 3.

where $\delta\mu = (\mu_{i\alpha} - \mu_{s\beta})/2$. These well-known approximate results are instructive at the qualitative level, but should not be used mechanically; see the discussion below.

IV. NUMERICAL EXAMPLE

Next we present a numerical example and therefore constrain the discussion to a specific parametrization of the model, as in Ref. [17]. The momentum integral is regularized with a cutoff, $\Lambda = 602.3$ MeV. The coupling constants are $G_S\Lambda^2 = 2.319$, $G_D/G_S \equiv \eta = 0.75$, and $K = 0$. The current quark masses are $m_u = m_d = 5.5$ MeV and $m_s = 112$ MeV. By the insertion of these parameters into the thermodynamic potential (6), the gaps ($\phi_u, \phi_d, \phi_s, \Delta_{ud}, \Delta_{us}, \Delta_{ds}$) can be determined by minimization of the free energy, while simultaneously neutralizing all charge densities with μ_Q, μ_3, and μ_8. In Fig. 3 the diquark gaps Δ_{ij} and the gapless thresholds [inequality (16)], Δ^g_{ij} are plotted versus the temperature for a fixed value of the quark-number chemical potential, $\mu = 500$ MeV. In Fig. 4 the quark-quark quasiparticle dispersion relations are plotted for four different temperatures represented in Fig. 3. Observe that gapless dispersion relations exist iff $\Delta_{ij} \leqslant \Delta^g_{ij}$. Figure 2 shows the graphical representation of the gapless condition for some quasiparticles represented in Fig. 4, see Fig. 1 for further information.

V. CONCLUSIONS

We find that the difference between approximate results (18) and (19) and exact gapless condition (16) is typically below 5% in the plane of temperature and quark-number chemical potential. However, even a small error in Δ^g_{ij} could lead to qualitatively incorrect conclusions if $\Delta_{ij}(T \sim 0) \sim \Delta^g_{ij}$, because $\Delta_{ij}(T)$ are roughly constant at the low temperatures relevant for compact star evolution. The exact condition for gapless quasiparticle excitations presented here [Eq. (16)], which is the main result of this paper, is a safe alternative to the approximative results. Moreover, Fig. 1 is an accurate qualitative picture of the prerequisites for gapless color-antitriplet excitations in NJL models.

ACKNOWLEDGMENTS

We thank D. Blaschke, M. Buballa, S. Fredriksson, and H. Grigorian for useful discussions and suggestions. A. M. Öztaş received support from Hacettepe University Research Fund, grant no. 02 02 602 001. F. Sandin acknowledges support from the Swedish National Graduate School of Space Technology and thanks D. Blaschke and the organizers of the Helmholtz International Summer School, Dubna, for partial support and their hospitality.

[1] B. C. Barrois, Nucl. Phys. **B129**, 390 (1977).
[2] D. Bailin and A. Love, Phys. Rep. **107**, 325 (1984).
[3] M. G. Alford, K. Rajagopal, and F. Wilczek, Phys. Lett. **B422**, 247 (1998).
[4] R. Rapp, T. Schäfer, E. V. Shuryak, and M. Velkovsky, Phys. Rev. Lett. **81**, 53 (1998).
[5] I. Shovkovy and M. Huang, Phys. Lett. **B564**, 205 (2003).
[6] M. Huang and I. Shovkovy, Nucl. Phys. **A729**, 835 (2003).
[7] M. Alford, C. Kouvaris, and K. Rajagopal, Phys. Rev. Lett. **92**, 222001 (2004).
[8] M. Alford, C. Kouvaris, and K. Rajagopal, Phys. Rev. D **71**, 054009 (2005).
[9] M. Alford, P. Jotwani, C. Kouvaris, J. Kundu, and K. Rajagopal, Phys. Rev. D **71**, 114011 (2005).
[10] M. Huang and I. A. Shovkovy, Phys. Rev. D **70**, 094030 (2004).
[11] M. Huang and I. A. Shovkovy, Phys. Rev. D **70**, 051501(R) (2004).
[12] R. Casalbuoni, R. Gatto, M. Mannarelli, G. Nardulli, and M. Ruggieri, Phys. Lett. **B605**, 362 (2005).
[13] I. Giannakis and H.-C. Ren, Phys. Lett. **B611**, 137 (2005).
[14] K. Fukushima, Phys. Rev. D **72**, 074002 (2005).
[15] H. Abuki and T. Kunihiro, Nucl. Phys. **A768** 118 (2006); hep-ph/0509172.
[16] S. B. Rüster, V. Werth, M. Buballa, I. A. Shovkovy, and D. H. Rischke, Phys. Rev. D **72**, 034004 (2005).
[17] D. Blaschke, S. Fredriksson, H. Grigorian, A. M. Öztaş, and F. Sandin, Phys. Rev. D **72**, 065020 (2005).
[18] C. Kettner, F. Weber, M. K. Weigel, and N. K. Glendenning, Phys. Rev. D **51**, 1440 (1995).
[19] M. Buballa and I. A. Shovkovy, Phys. Rev. D **72**, 097501 (2005); hep-ph/0508197.
[20] M. Buballa and I. A. Shovkovy, Phys. Rev. D **72**, 097501 (2005).

Paper V

Modern compact star observations and the quark matter equation of state

T. Klähn, [a,b] D. Blaschke, [a,c,d] F. Sandin, [e] Ch. Fuchs, [f]
A. Faessler, [f] H. Grigorian, [g,h] G. Röpke, [a] J. Trümper [i]

[a] *Institut für Physik, Universität Rostock, D-18051 Rostock, Germany*

[b] *Gesellschaft für Schwerionenforschung mbH (GSI), D-64291 Darmstadt, Germany*

[c] *Institute for Theoretical Physics, University of Wroclaw PL-50-204 Wroclaw, Poland*

[d] *Bogoliubov Laboratory of Theoretical Physics, Joint Institute for Nuclear Research, RU-141980 Dubna, Russia*

[e] *Department of Physics, Luleå University of Technology, SE-97187 Luleå, Sweden*

[f] *Institut für Theoretische Physik, Universität Tübingen, D-72076 Tübingen, Germany*

[g] *Laboratory for Information Technologies, Joint Institute for Nuclear Research, RU-141980 Dubna, Russia*

[h] *Department of Physics, Yerevan State University, 375049 Yerevan, Armenia*

[i] *Max-Planck-Institut für Extraterrestrische Physik, D-85741 Garching, Germany*

Abstract

We present a hybrid equation of state (EoS) for dense matter that satisfies phenomenological constraints from modern compact star (CS) observations which indicate high maximum masses ($M \sim 2M_\odot$) and large radii ($R > 12$ km). The corresponding isospin symmetric EoS is consistent with flow data analyses of heavy-ion collisions and a deconfinement transition at ~ 0.55 fm^{-3}. The quark matter phase is described by a 3-flavor Nambu–Jona-Lasinio model that accounts for scalar diquark condensation and vector meson interactions while the nuclear matter phase is obtained within the Dirac-Brueckner-Hartree-Fock (DBHF) approach using the Bonn-A potential. We demonstrate that both pure neutron stars and neutron stars with quark matter cores (QCSs) are consistent with modern CS observations. Hybrid star configurations with a CFL quark core are unstable.

PACS number(s): 04.40.Dg, 12.38.Mh, 26.60.+c, 97.60.Jd

1 Introduction

Recently, new observational limits for the mass and the mass-radius relationship of compact stars have been obtained which provide stringent constraints on the equation of state of strongly interacting matter at high densities, see [1] and references therein. In particular, the high mass of $M = 2.1 \pm 0.2\ M_\odot$ for the pulsar J0751+1807 in a neutron star - white dwarf binary system [2] and the large radius of $R > 12$ km for the isolated neutron star RX J1856.5-3754 (shorthand: RX J1856) [3] point to a stiff equation of state at high densities. Measurements of high masses are also reported for compact stars in low-mass X-ray binaries (LMXBs) as, e.g., $M = 2.0 \pm 0.1\ M_\odot$ for the compact object in 4U 1636-536 [4]. For another LMXB, EXO 0748-676, constraints for the mass $M \geq 2.10 \pm 0.28\ M_\odot$ *and* the radius $R \geq 13.8 \pm 0.18$ km have been reported [5]. The status of these data is, however, unclear since the observation of a gravitational redshift $z = 0.35$ in the X-ray burst spectra [6] could not be confirmed thereafter despite numerous attempts [7]. We exclude possible constraints from LMXBs from the discussion in the present paper as their status is not settled and they would not tighten the mass and mass-radius limits provided by J0751+1807 and RX J1856, respectively. It has been argued [3,5] that deconfined quark matter cannot exist in the centers of compact stars with masses and radii as reported for these objects. In view of recent works on the quark matter EoS, however, this claim appears to be premature [8].

In the present paper, we demonstrate that the present-day knowledge of hydrodynamical properties of dense matter allows to construct hybrid EsoS with a critical density of the deconfinement phase transition low enough to allow for extended quark matter cores and stiff enough to comply with the new mass measurements of compact stars. It has been shown recently by Alford et al. [9] that hybrid stars can masquerade as neutron stars once the parameters of a generic phenomenological quark matter EoS have been chosen appropriately. While in [9] the APR EoS [10] for the hadronic phase has been used, we base our investigation on a nuclear EoS obtained from the ab initio DBHF approach using the Bonn A potential [11,12] which results in star configurations with larger radii and masses. The DBHF EoS is soft at moderate densities (compressibility K=230 MeV) [11,13] but tends to become stiffer at high densities. At densities up to 2-3 times nuclear saturation density it is in agreement with constraints from heavy ion collisions based on collective flow [14,15] and kaon production [16]. However, at higher densities this EoS seems to be too repulsive concernig the flow constraint. As we will show in the present paper, the problems of this EoS with an early onset of the nuclear direct Urca (DU) process and a violation of the flow constraint for heavy-ion collisions at high densities can be solved by adopting a phase transition to quark matter.

We have no first principle information from QCD about the quark matter EoS

in the nonperturbative domain close to the chiral/ deconfinement transition at zero temperature and finite density which would be required for an ab-initio study of the problem whether deconfined quark matter can exist in neutron stars or not. Therefore it is desireable to develop microscopic approaches to the quark matter EoS on the basis of effective models implementing, as far as possible, QCD symmetries into the model Lagrangian. The Lagrangian of the Nambu–Jona-Lasinio (NJL) type models has chiral symmetry which is dynamically broken in the nonperturbative vacuum and restored at finite temperatures in accordance with lattice QCD simulations. Therefore, the application of the NJL model to finite densities where presently no reliable lattice QCD simulations exist, can be regarded as state-of-the-art for present dense quark matter studies, see [18] and references therein.

In contrast to Ref. [9] we base our investigation on a three-flavor chiral quark model with selfconsistently determined quark masses and pairing gaps [19] similar to the parallel developments in Refs. [20,21]. This approach has the advantage that it allows, e.g., to distinguish two- and three-flavor phases in quark matter (for a first discussion, see [22]) and to allow conclusions about the presence of gapless phases at zero temperature as a function of the coupling strengths in the current-current-type interaction of the model Lagrangian [23]. Moreover, we will investigate the question of the stability of neutron stars with a color superconducting quark matter core in the celebrated CFL phase, for which a number of phenomenological applications have been studied, in particular the cooling problem [24,25,26,27], gamma-ray bursts [28,29], and superbursts [30]. We will confirm in this work the earlier result by Buballa et al. [31] that a CFL quark matter core renders the hybrid star unstable.

Here we generalize the model [19] by including an isoscalar vector meson current which, similar to the Walecka model for nuclear matter, leads to a stiffening of the quark matter EoS. Increasing the scalar diquark coupling constant leads to a lowering of the phase transition density. It is the aim of the present work to determine the unknown coupling strengths in both these channels such that an optimal hybrid star EoS is obtained. It fulfills all recently developed constraints from modern compact star observations [1,5] while providing sufficient softness of the isospin-symmetric limit of this EoS as required from the analysis of heavy-ion collision transverse flow data [14,15] and K^+ production data [16].

2 Equation of state

The thermodynamics of the deconfined quark matter phase is described within a three-flavor quark model of Nambu–Jona-Lasinio (NJL) type. The path-integral representation of the partition function is given by

$$Z(T,\hat{\mu}) = \int \mathcal{D}\bar{q}\mathcal{D}q \exp\left\{\int_0^\beta d\tau \int d^3x \left[\bar{q}\left(i\partial\!\!\!/ - \hat{m} + \hat{\mu}\gamma^0\right) q + \mathcal{L}_{\rm int}\right]\right\}, \qquad (1)$$

$$\mathcal{L}_{\rm int} = G_S\Bigg[\sum_{a=0,3,8}(\bar{q}\tau_a q)^2 - \eta_V(\bar{q}\gamma^0 q)^2 + \eta_D\sum_{A=2,5,7}(\bar{q}i\gamma_5\tau_A\lambda_A C\bar{q}^T)(q^T iC\gamma_5\tau_A\lambda_A q),\Bigg], \qquad (2)$$

where $\hat{\mu}$ and $\hat{m} = \mathrm{diag}_f(m_u, m_d, m_s)$ are the diagonal chemical potential and current quark mass matrices. For $a = 0$, $\tau_0 = (2/3)^{1/2}\mathbf{1}_f$, otherwise τ_a and λ_a are Gell-Mann matrices acting in flavor and color spaces, respectively. $C = i\gamma^2\gamma^0$ is the charge conjugation operator and $\bar{q} = q^\dagger\gamma^0$. G_S, η_V, and η_D determine the coupling strengths of the interactions.

The interaction terms represent current-current interactions in the color singlet scalar and vector meson channels, and the scalar color antitriplet diquark channel. In the choice of the four-fermion interaction channels we have omitted the pseudoscalar quark-antiquark terms, which should be present in a chirally symmetric Lagrangian. These terms do not contribute to the thermodynamic properties of the deconfined quark matter phase at the mean-field (Hartree) level [32] to which we restrict the discussion in the present paper. The Lorentz three-current, $\nu \in \{1,2,3\} : (\bar{q}\gamma^\nu q)^2$, vanishes in the static ground state of matter and is therefore omitted. The model is similar to the models in [19,20,21], except that we include also the isoscalar vector meson channel. We follow the argument given in [19], that the $\mathrm{U}_A(1)$ symmetry breaking in the pseudoscalar isoscalar meson sector is dominated by quantum fluctuations and no 't Hooft determinant interaction needs to be adopted for its realization.

After bosonization using Hubbard-Stratonovich transformations, we obtain an exact transformation of the original partition function (1). The transformed expression constitutes the starting point for powerful approximations, defined as truncations of the Taylor expanded action functional to different orders in the collective boson fields. In the following, we use the mean-field (MF) approximation. This means that the bosonic functional integrals are omitted and the collective fields are fixed at the extremum of the action. The corresponding mean-field thermodynamic potential, from which all thermodynamic quantities can be derived, is given by

$$\Omega_{MF}(T,\mu) = -\frac{1}{\beta V}\ln Z_{MF}(T,\mu) = \frac{1}{8G_S}\left[\sum_{i=u,d,s}(m_i^* - m_i)^2 - \frac{2}{\eta_V}(2\omega_0^2 + \phi_0^2) + \frac{2}{\eta_D}\sum_{A=2,5,7}|\Delta_{AA}|^2\right]$$

$$-\int \frac{d^3p}{(2\pi)^3} \sum_{a=1}^{18} \left[E_a + 2T \ln\left(1 + e^{-E_a/T}\right)\right] + \Omega_l - \Omega_0 \ . \qquad (3)$$

Here, Ω_l is the thermodynamic potential for electrons and muons, and Ω_0 is a divergent term that is subtracted in order to get zero pressure and energy density in vacuum ($T = \mu = 0$). The quasiparticle dispersion relations, $E_a(p)$, are the eigenvalues of the Hermitian matrix

$$\mathcal{M} = \begin{bmatrix} -\vec{\gamma}\cdot\vec{p} - \hat{m}^* + \gamma^0\hat{\mu}^* & \gamma_5\tau_A\lambda_A\Delta_{AA} \\ -\gamma_5\tau_A\lambda_A\Delta^*_{AA} & -\vec{\gamma}^T\cdot\vec{p} + \hat{m}^* - \gamma^0\hat{\mu}^* \end{bmatrix}, \qquad (4)$$

in color, flavor, Dirac, and Nambu-Gorkov space. Here, Δ_{AA} are the diquark gaps. $\hat{m}^*$ is the diagonal renormalized mass matrix and $\hat{\mu}^*$ the renormalized chemical potential matrix, $\hat{\mu}^* = \mathrm{diag}_f(\mu_u - G_S\eta_V\omega_0, \mu_d - G_S\eta_V\omega_0, \mu_s - G_S\eta_V\phi_0)$. The gaps and the renormalized masses are determined by minimization of the mean-field thermodynamic potential (3), subject to charge neutrality constraints which depend on the application we consider. In the (approximately) isospin symmetric situation of a heavy-ion collision, the color charges are neutralized, while the electric charge in general is non-zero. For matter in β-equilibrium, also the electric charge is neutralized. For further details, see [19,20,21].

We consider η_D as a free parameter of the quark matter model, to be tuned with the present phenomenological constraints on the high-density EoS. Similarly, the relation between the coupling in the scalar and vector meson channels, η_V, is considered as a free parameter of the model. The remaining degrees of freedom are fixed according to the NJL model parameterization in Table I of [33], where a fit to low-energy phenomenological results has been made.

A consistent relativistic approach to the quark hadron phase transition where the hadrons appear as bound states of quarks is not yet developed. First steps in the direction of such a unified approach to quark-hadron matter have been accomplished within the NJL model in [34]. In this paper, however, the role of quark exchange interactions between hadrons (Pauli principle on the quark level) has yet been disregarded. As has been demonstrated within a nonrelativistic potential model approach, these contributions may be essential for a proper understanding of the short-range repulsion [35] as well as the asymmetry energy at high-densities [36]. In the present work we apply a so-called two-phase description where the nuclear matter phase is described within the relativistic Dirac-Brueckner-Hartree-Fock (DBHF) approach considered in [1] and the transition to the quark matter phase is obtained by a Maxwell construction. The critical chemical potential of the phase transition is obtained from the equality of hadronic and quark matter pressures. A discussion of the reliability of the Maxwell construction for the case of a set of conserved

charges is discussed in [37].

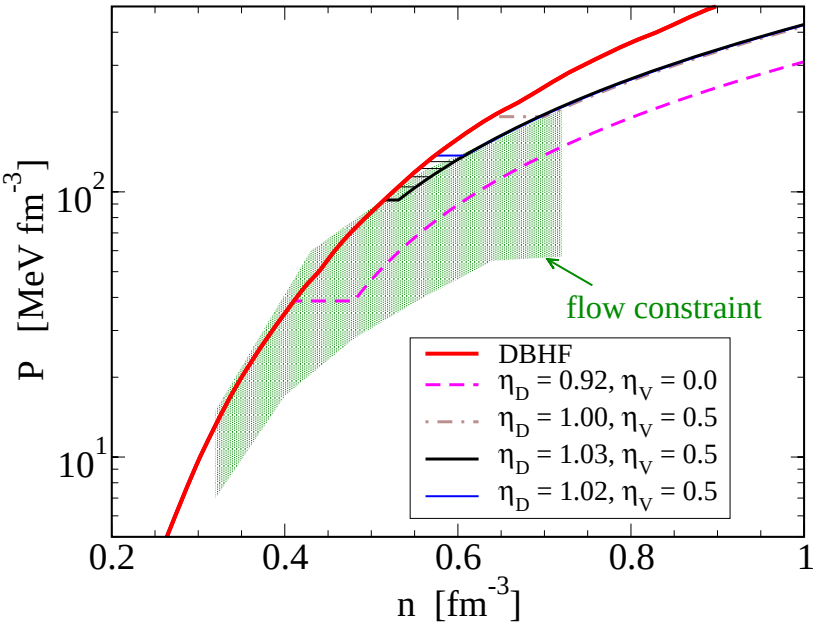

Fig. 1. Pressure vs. density of the isospin symmetric EoS for different values of the relative coupling strengths η_D and η_V. The behaviour of elliptic flow in heavy-ion collisions is related to the EoS of isospin symmetric matter. The upper and lower limits for the stiffness deduced from such analyses are indicated in the figure (shaded region). The quark matter EoS favored by the flow constraint has a vector coupling $\eta_V = 0.50$ and a diquark coupling between $\eta_D = 1.02$ (blue solid line) and $\eta_D = 1.03$ (black fat solid line); results for four intermediate values $\eta_D = 1.022 \ \ldots \ 1.028$ are also shown (thin solid lines).

The baryon density as derivative of the pressure with respect to the baryochemical potential exhibits a jump at the phase transition, as shown for isospin-symmetric matter in Fig. 1. As can be seen in that Figure, a slight variation of the quark matter model parameters η_D and η_V results in considerable changes of the critical density for the phase transition and the behaviour of the pressure (stiffness) at high densities. There appears the problem of a proper choice of these parameters which we suggest to solve by applying the flow constraint [14] to symmetric matter, shown as the hatched area in Fig.1. At first we fix the vector coupling by demanding that the high density behavior of the hybrid EoS should be as stiff as possible but still in accordance with the flow constraint. We obtain $\eta_V = 0.50$, independent of the choice of the scalar diquark coupling. The latter we want to determine such that the problem of the violation of the flow constraint for the DBHF EoS in symmetric nuclear matter at high densities is resolved by the phase transition to quark matter. The optimal choice for η_D is thus between 1.02 and 1.03. In the following we will investigate the compatibility of the now defined hybrid star equation of

state with CS constraints.

3 Astrophysical constraints on the high-density EoS

Recently, observations of compact objects have resulted in new limits for masses and radii which put stringent constraints on the high-density behaviour of the nuclear matter EoS, see [1].

Particularly demanding data come from the pulsar PSR J0751+1807 with a lower mass limit of $M \geq 1.9\ M_\odot$ [2], and the isolated compact star RX J1856 with a mass-radius relationship supporting a radius exceeding 13.5 km for typical masses below 1.4 $M_\odot$ or masses above 1.9 $M_\odot$ for stars with radii $R \leq 12$ km [3]. In Fig.2 we display these constraints together with lines of constant gravitational redshift.

The above constraints have to be explained by any reliable CS EoS, i.e. the mass radius relation resulting from a corresponding solution of the Tolman-Oppenheimer-Volkoff equations has to touch each of the regions shown in Fig. 2. This is well fulfilled for the purely hadronic DBHF EoS.

It is widely assumed that if quark matter would exist in CSs, the maximum mass would be significantly lower than for nuclear matter stars (NMS). This argumentation has been used to claim that quark matter in neutron stars is in contradiction with observations [5].

As we will show in this work, large hybrid star masses can be obtained for sufficiently stiff quark matter EsoS. In this case, the corresponding hybrid (NJL+DBHF) QCS sequence is not necessarily ruled out by phenomenology. The stiffness of the quark matter EoS can be significantly increased when the vector meson interaction of the NJL model introduced in Section 2 is active. The maximum value of the vector coupling which is still in accordance with the upper limit extrapolation of the flow constraint, $\eta_V = 0.50$, see Fig. 1, allows a maximum mass of 2.1 $M_\odot$. With this choice the constraints from PSR J0751+1807 and RX J1856 displayed in Fig. 2 can be fulfilled.

The maximum mass is rather inert to changes of the diquark coupling η_D whereas the critical mass for the occurrence of a quark matter core gets significantly lowered by increasing the value of η_D. For example, the choice of η_D in the range $1.02\ -1.03$ corresponds to critical star masses from 1.35 $M_\odot$ to 1.0 $M_\odot$, see Fig. 2.

Another robust statement from our studies of the hybrid EoS is that the occurrence of a CFL quark matter core renders the compact star unstable.

This confirms an earlier findings by Baldo et al. [17] and Buballa et al.[31] for slightly different hybrid EsoS.

An additional test to the mass-radius relation could be provided by a measurement of the gravitational redshift. We note that the redshift z=0.35 found for EXO 0748-676 [6], which could not be confirmed by further measurements [7], would be in accordance with both NMS and QCS interpretations. A measurement of $z \geq 0.5$ could not be accommodated with the QCS model suggested here, while the NMS would not be invalidated by redshift measurements up to $z = 0.6$.

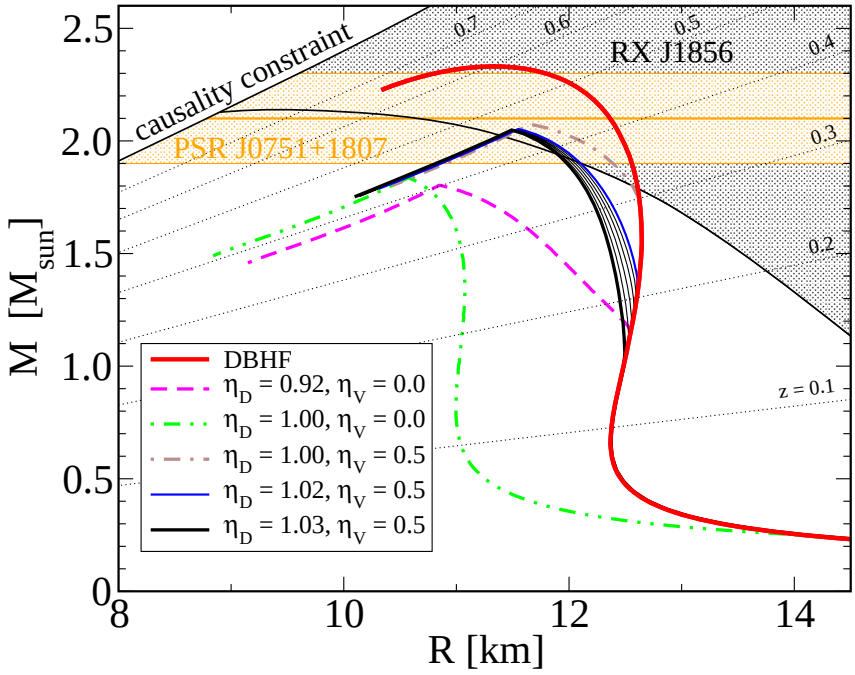

Fig. 2. Mass - radius relationship for CS sequences corresponding to a nuclear matter EoS (DBHF) and different hybrid star EsoS (DBHF+NJL), see text. Indicated are also the constraint on the mass from the pulsar J0751+1807 [2] and on the mass-radius relationship from the isolated neutron star RX J1856 [3] Present constraints on the mass-radius relation of CSs do not rule out hybrid stars. The dotted lines indicate the gravitational redshift, $z = (1 - 2GM/R)^{-1/2} - 1$, of photons emitted from the compact star surface.

Next we want to discuss the question whether measurements of the moment of inertia (MoI) I might serve as a tool to distinguish pure NMS from QCS models. Due to the discovery of the relativistic double pulsar PSR J0737+3039 a measurement of the MoI became a possibility and has been recently discussed as another constraint on the EoS of compact stars, assuming that future mea-

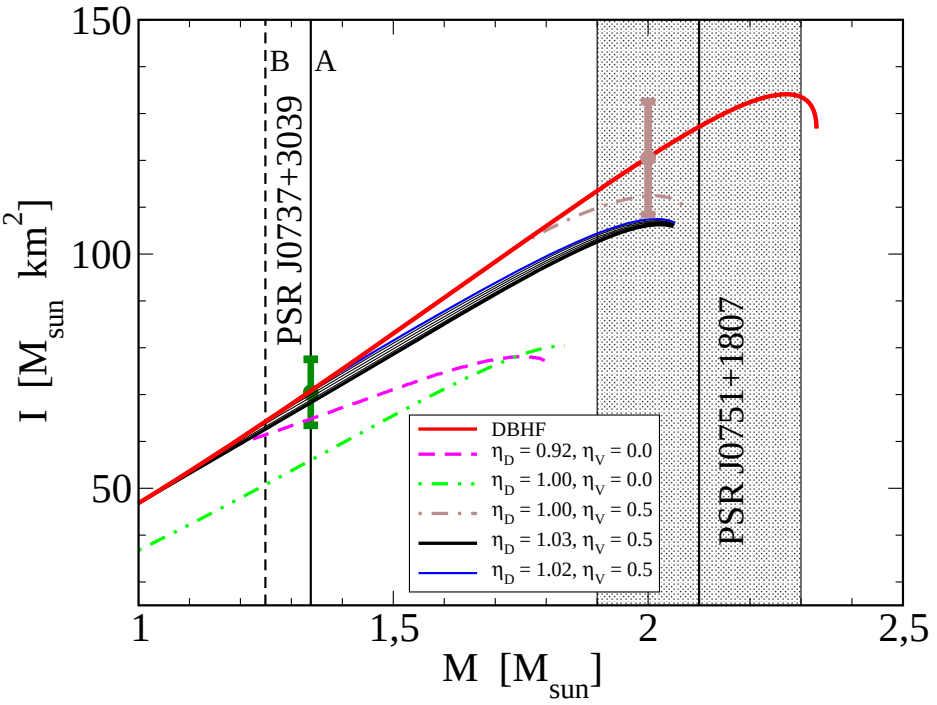

Fig. 3. Moment of inertia vs. the gravitational mass for the compact star EsoS discussed in the text. The highlighted mass regions correspond to the double pulsar J0737+3039 A+B and the pulsar J0751+1807. We also show anticipated data points with error bars corresponding to a measurement with a 1 σ level of 10%.

surements will exhibit an error of only about 10% [47,48]. In our calculations we follow the definition of the MoI given in Ref. [46] and show the results for the EsoS of the present paper in Fig. 3. Due to the fact that the mass 1.338 $M_\odot$ of PSR J0737+3039 A is in the vicinity of the suggested critical mass region, the quark matter core is small and the expected MoI of the hybrid star will be practically indistinguishable from that of a pure hadronic one. The situation would improve if the MoI could be measured for more massive objects because the difference in the MoI of both alternative models for masses as high as 2 $M_\odot$ could reach the 10% accuracy level.

Finally we would like to discuss the question whether there are observables suited to distinguish between pure neutron stars and those with a quark matter interior. As we have seen in the previous results, the hydrodynamic behavior of the hybrid star EoS has to be rather similar to that of pure hadronic matter in order to allow for sufficiently large masses. If so, the moment of inertia and other mechanical properties of the resulting stars will turn out to be indistinguishable to the level of a few percent. A different situation might occur for CS cooling where the transport properties and thus the excitation spectra of the dense matter play the essential role. As an example, pairing

gaps of the order of an MeV or below will not affect the thermodynamics but are sufficiently large to influence on neutrino cooling processes. Let us discuss the example of the direct Urca (DU) process.

If the DU process would occur in hadronic matter, it would give rise to a fast cooling and result in a strong sensitivity to slightest mass changes of the corresponding compact object. Therefore, it should not occur in CSs with masses below 1.5 $M_\odot$, as this would provide a cooling rate that is inconsistent with CS population syntheses [38,39]. If on the other hand the DU process does *not* occur in a hadronic star, one would require that young, fast coolers such as Vela and 3C58 should have a rather large mass, again in contradiction with the present population syntheses.

A possible resolution to this hadronic cooling problem could be a phase transition to quark matter with moderately enhanced cooling. This has been demonstrated for hybrid stars with a 2SC+X quark matter phase [40] which is in accordance with all presently known cooling constraints [39]. The physical nature of the hypothetical X-gap is, however, not yet clarified. A discussion of this issue can be found in Refs. [41,42].

For the DBHF EoS the DU threshold is at $n_{\rm DU} = 0.375$ fm^{-3} corresponding to a CS mass of $M_{\rm DU} = 1.26\ M_\odot$, see Fig. 4. The hybrid EoS presented in this work has a critical density for the quark matter phase transition which is below $n_{\rm DU}$ provided a value $\eta_D \geq 1.024$ is chosen.

Thus for the parameter values $\eta_V = 0.50$ and $\eta_D \gtrsim 1.024$ the present EoS for hybrid star matter fulfills all modern observational constraints discussed above.

4 Summary

We have investigated the compatibility of present constraints on the high density EoS with the concept of CSs possessing a QM core. The hadronic part of the EoS was taken from the DBHF approach, while the QM EoS is provided by a chiral NJL-type quark model with current-current interactions in the color singlet (isoscalar) scalar and vector meson channels as well as in the color antitriplet scalar diquark channels. The finite vector meson coupling enables us to describe large hybrid star masses by stiffening the QM EoS, whereas the chosen value for the diquark coupling ensures a sufficiently early phase transition to QM in order to avoid the activation of DU cooling within the hadronic shell of the hybrid star. Since the high density QM part of the EoS is softer than the corresponding pure hadronic EoS also the flow constraint is fulfilled in this scenario. We discussed the possibility to distinguish between

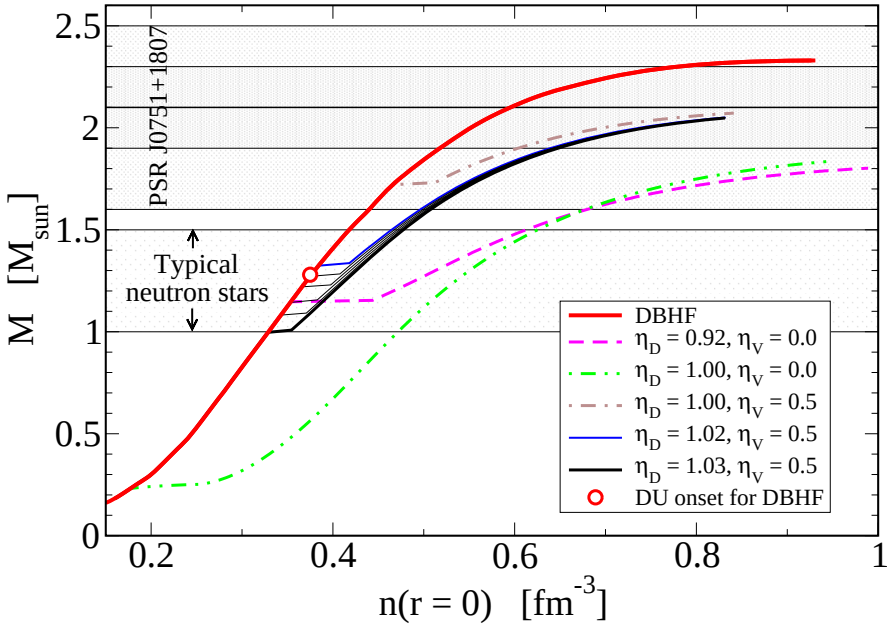

Fig. 4. Compact star masses vs. the central density for different values of the relative coupling strengths η_D and η_V, see Section 2. In a pure neutron (DBHF) star, DU processes occur for $M > M_{\rm DU} = 1.26\ M_\odot$ (circle). The maximum mass of hybrid star configurations depends mainly on the relative strength of the vector meson coupling, η_V, while the transition density depends on η_V and η_D.

pure NSs and hybrid stars by hypothetical data from successful measurements of the MoI for stars of a given mass. It turned out, that this would be possible for rather massive objects ($M \approx 2.0\ M_\odot$) provided the standard deviation of the measurements is less than 10%, as expected for PSR J0737+3039 A.

As our main result we conclude that *no present phenomenological finding bears a strong argument against the presence of a QM core inside NSs.* Moreover, we demonstrated that problems with cooling and flow which appear as weak points of a purely hadronic EoS at large densities can be resolved in a natural way when a transition to QM occurs at not too large densities.

The most common argument against the presence of QM in CSs, resulting from the *prejudice* of the softness of QM EsoS, is no longer valid if we account for a vector meson interaction channel which stiffens the EoS. The earlier finding that CFL quark matter cannot be found in stable hybrid stars has been reconfirmed and appears thus as a severe constraint for phenomenological scenarios of compact star evolution.

However, there is a discrepancy between the phenomenologically deduced values of the coupling constants $(\eta_D, \eta_V)_{\rm phen} = (1.024, 0.5)$ and those expected

from the Fierz rearrangement argument $(\eta_D, \eta_V)_{\rm Fierz} = (0.75, 0.5)$. It is necessary to repeat the present study for more realistic microscopic approaches to the QCD EoS taking into account, e.g., that QCD interactions are nonlocal and momentum-dependent. One possible strategy could consist in the application of nonlocal, separable models [49,50] which can be generalized to use covariant formfactors [51,52] to be adjusted such that Lattice QCD results on the momentum dependence of the quark selfenergies [53] could be reproduced. Moreover, one should go beyond the mean-field level of description and treat hadrons as bound states of quarks. This would allow to model the hadron-to-quark-matter phase transition in a more consistent way as the dissolution of hadronic bound states into correlations in the continuum of quark matter.

Acknowledgments

We are grateful for critical reading and comments by M. Alford, M. Buballa, A. Drago, G. Grunfeld and F. Weber. We acknowledge the support by the Virtual Institute of the Helmholtz Association under grant VH-VI-041. The work of H.G. was supported in part by DFG grant No. 436 ARM 17/4/05 and that of F.S. by the Swedish Graduate School of Space Technology and the Royal Swedish Academy of Sciences.

References

[1] T. Klähn *et al.*, Phys. Rev. C **74**, 035802 (2006).

[2] D.J. Nice, E.M. Splaver, I.H. Stairs, O. Löhmer, A. Jessner, M. Kramer, and J.M. Cordes, Astrophys. J. **634**, 1242 (2005).

[3] J. E. Trümper, V. Burwitz, F. Haberl and V. E. Zavlin, Nucl. Phys. Proc. Suppl. **132**, 560 (2004).

[4] D. Barret, J. F. Olive and M. C. Miller, Mon. Not. Roy. Astron. Soc. **361**, 855 (2005).

[5] F. Özel, Nature **441**, 1115 (2006)

[6] J. Cottam, F. Paerels and M. Mendez, Nature **420**, 51 (2002)

[7] M. Mendez, private communication (2006).

[8] M. Alford, D. Blaschke, A. Drago, T. Klähn, G. Pagliara and J. Schaffner-Bielich, arXiv:astro-ph/0606524.

[9] M. Alford, M. Braby, M. W. Paris and S. Reddy, Astrophys. J. **629**, 969 (2005)

[10] A. Akmal, V.R. Pandharipande and D.G. Ravenhall, Phys. Rev. C **58** (1998) 1804

[11] E.N.E. van Dalen, C. Fuchs, and A. Faessler, Nucl. Phys. A **744**, 227 (2004); Phys. Rev. C **72**, 065803 (2005).

[12] E.N.E. van Dalen, C. Fuchs, and A. Faessler, Phys. Rev. Lett. **95**, 022302 (2005).

[13] T. Gross-Boelting, C. Fuchs, A. Faessler, Nucl. Phys. A **648**, 105 (1999).

[14] P. Danielewicz, R. Lacey and W. G. Lynch, Science **298**, 1592 (2002).

[15] G. Stoicea *et al.* [FOPI Coll.], Phys. Rev. Lett. **92**, 072303 (2004).

[16] C. Fuchs, Prog. Part. Nucl. Phys. **56**, 1 (2006); C. Fuchs et al., Phys. Rev. Lett. **86**, 1974 (2001); Ch. Hartnack, H. Oeschler, J. Aichelin, Phys. Rev. Lett. **96**, 012302 (2006).

[17] M. Baldo, M. Buballa, F. Burgio, F. Neumann, M. Oertel and H. J. Schulze, Phys. Lett. B **562** (2003) 153

[18] M. Buballa, Phys. Rept. **407** (2005) 205

[19] D. Blaschke, S. Fredriksson, H. Grigorian, A. M. Öztas and F. Sandin, Phys. Rev. D **72** (2005) 065020

[20] S. B. Rüster, V. Werth, M. Buballa, I. A. Shovkovy and D. H. Rischke, Phys. Rev. D **72** (2005) 034004

[21] H. Abuki and T. Kunihiro, Nucl. Phys. A **768** (2006) 118

[22] C. Gocke, D. Blaschke, A. Khalatyan and H. Grigorian, [arxiv:hep-ph/0104183]

[23] F. Sandin and A. M. Öztas, Phys. Rev. C **73** (2006) 035203 [arXiv:hep-ph/0512087].

[24] D. Blaschke, T. Klähn and D. N. Voskresensky, Astrophys. J. **533** (2000) 406 [arXiv:astro-ph/9908334].

[25] D. Page, M. Prakash, J. M. Lattimer and A. Steiner, Phys. Rev. Lett. **85** (2000) 2048 [arXiv:hep-ph/0005094].

[26] D. Blaschke, H. Grigorian and D. N. Voskresensky, Astron. Astrophys. **368**, 561 (2001) [arXiv:astro-ph/0009120].

[27] M. Alford, P. Jotwani, C. Kouvaris, J. Kundu and K. Rajagopal, Phys. Rev. D **71** (2005) 114011 [arXiv:astro-ph/0411560].

[28] J. Berdermann, D. Blaschke, H. Grigorian and D. N. Voskresensky, Prog. Part. Nucl. Phys. **57** (2006) 334 [arXiv:astro-ph/0512655].

[29] A. Drago, A. Lavagno and G. Pagliara, Nucl. Phys. A **774** (2006) 823 [arXiv:astro-ph/0510018].

[30] D. Page and A. Cumming, Astrophys. J. **635** (2005) L157 [arXiv:astro-ph/0508444].

[31] M. Buballa, F. Neumann, M. Oertel and I. Shovkovy, Phys. Lett. B **595** (2004) 36 [arXiv:nucl-th/0312078].

[32] H. J. Warringa, D. Boer and J. O. Andersen, Phys. Rev. D **72**, 014015 (2005) [arXiv:hep-ph/0504177].

[33] H. Grigorian, arXiv:hep-ph/0602238.

[34] S. Lawley, W. Bentz and A. W. Thomas, J. Phys. G **32** (2006) 667 [arXiv:nucl-th/0602014].

[35] G. Röpke, D. Blaschke and H. Schulz, Phys. Rev. D **34** (1986) 3499.

[36] D. Blaschke, T. Tovmasian and B. Kämpfer, Sov. J. Nucl. Phys. **52** (1990) 675 [Yad. Fiz. **52** (1990) 1059].

[37] D. N. Voskresensky, M. Yasuhira and T. Tatsumi, Nucl. Phys. A **723** (2003) 291

[38] S. Popov, H. Grigorian, R. Turolla and D. Blaschke, A&A **448**, 327 (2006).

[39] S. Popov, H. Grigorian and D. Blaschke, Phys. Rev. C **74**, 025803 (2006) [arXiv:nucl-th/0512098].

[40] H. Grigorian, D. Blaschke and D. Voskresensky, Phys. Rev. C **71** (2005) 045801 [arXiv:astro-ph/0411619].

[41] D. Blaschke, D. N. Voskresensky and H. Grigorian, Nucl. Phys. A **774** (2006) 815 [arXiv:hep-ph/0510368].

[42] D. Blaschke, PoS **JHW2005** (2006) 003 [arXiv:nucl-th/0603063].

[43] J. M. Lattimer and M. Prakash, Astrophys. J. **550**, 426 (2001).

[44] S. M. Schmidt, D. Blaschke and Y. L. Kalinovsky, Phys. Rev. C **50** (1994) 435.

[45] M. Buballa and I. A. Shovkovy, Phys. Rev. D **72** (2005) 097501

[46] F. Weber, "Pulsars as astrophysical laboratories for nuclear and particle physics," Bristol, UK: IOP (1999)

[47] M. Bejger, T. Bulik and P. Haensel, Mon. Not. Roy. Astron. Soc. **364** (2005) 635

[48] J. M. Lattimer and B. F. Schutz, Astrophys. J. **629** (2005) 979

[49] D. Blaschke, S. Fredriksson, H. Grigorian and A. M. Oztas, Nucl. Phys. A **736** (2004) 203 [arXiv:nucl-th/0301002].

[50] H. Grigorian, D. Blaschke and D. N. Aguilera, Phys. Rev. C **69** (2004) 065802 [arXiv:astro-ph/0303518].

[51] D. Blaschke, H. Grigorian, A. Khalatyan and D. N. Voskresensky, Nucl. Phys. Proc. Suppl. **141** (2005) 137.

[52] D. Gomez Dumm, D. B. Blaschke, A. G. Grunfeld and N. N. Scoccola, Phys. Rev. D **73** (2006) 114019.

[53] M. B. Parappilly, P. O. Bowman, U. M. Heller, D. B. Leinweber, A. G. Williams and J. B. Zhang, Phys. Rev. D **73** (2006) 054504.

Paper VI

The observational legacy of preon stars – probing new physics beyond the LHC

F. Sandin and J. Hansson

*Department of Physics, Luleå University of Technology, SE-97187 Luleå, Sweden**

We discuss possible ways to observationally detect the superdense cosmic objects composed of hypothetical sub-constituent fermions beneath the quark/lepton level, recently proposed by us. The characteristic mass and size of such objects depend on the compositeness scale, and their huge density cannot arise within a context of quarks and leptons alone. Their eventual observation would therefore be a direct vindication of physics beyond the standard model of particle physics, possibly far beyond the reach of the Large Hadron Collider (LHC), in a relatively simple and inexpensive manner. If relic objects of this type exist, they can possibly be detected by present and future x-ray observatories, high-frequency gravitational wave detectors, and seismological detectors. To have a realistic detection rate, *i.e.*, to be observable, they must necessarily constitute a significant fraction of cold dark matter.

PACS numbers: 12.60.Rc, 04.40.Dg, 95.35.+d

I. INTRODUCTION

It is often assumed that cold dark matter (CDM) is some "exotic" type of weakly interacting elementary particles, primordial relics created in the early universe, not yet detected in particle accelerator experiments. This hypothesis works well in cosmology, but both astrophysical observations, and discrepancies between simulations and observations of galaxies suggest that such a picture may be oversimplified. For example, simulated density profiles of CDM halos are too cuspy, more dwarf galaxies should have been observed because the number of halos is expected to be inversely proportional to the mass, and hydrodynamic simulations produce galaxy disks that are too small, with too low angular momenta [1]. Moreover, there is a close relation between the rotation curve shape and luminosity distribution in spiral galaxies, indicating that CDM couples to luminous matter [2], and the core density in spiral galaxies is roughly constant, scaling with the size of the core [3], in conflict with predictions from such models. Further information and more examples can be found in [4] and references therein.

Considering the complexity of galaxies and the overall success of the traditional view [5], *i.e.*,

*Electronic address: Fredrik.Sandin@ltu.se

that CDM is composed of stable weakly interacting (massive) particles (WIMPs), there are no truly compelling reasons to abandon it. It is sensible, however, to also explore alternative possibilities. In particular, since there are indications that CDM couples to baryons, parsimony ("Occam's razor") suggests that it could be a novel state of "ordinary" matter, which decoupled from the radiation in the early universe before the onset of primordial nucleosynthesis. Any structure created at such an early epoch would necessarily have a low characteristic mass and could therefore have remained unnoticed.

The spirit of this idea is not new. Already in the 1980s it was suggested that lumps of stable quark matter, so-called quark nuggets, could have formed in the early universe [6]. Should they exist, such objects contribute to CDM and if they were produced in abundance they could explain some observations that are inconsistent with the traditional view [4]. No observation precludes the possibility that such objects compose the bulk of CDM, provided that the mass of the objects does not exceed $\sim 10^{23}$ kg [4, 7]. This idea has a natural extension to particle scales beneath the quark/lepton level. Sub-quark particles (hereafter called preons) are motivated in part by the existence of three fermion generations, and other unexplained relations in the standard model of particle physics (SM), which indicate that quarks and leptons could well be composite. Detailed motivations can be found in, *e.g.*, [8] and references therein. If preons exist, stable compact objects ("preon stars") with densities at least ten orders of magnitude higher than in quark nuggets/stars could exist [9, 10]. See also [11] and [12, 13]. While the microscopic motivation for such objects is still somewhat schematic, and the possibility that they formed in the early universe uncertain, it is by no means impossible [11, 14]. As the consequences of their eventual existence are very interesting and far-reaching, an investigation of their phenomenology seems well-motivated. In the present paper, we briefly discuss some possibilities to observe compact preon dark matter (CPDM), *i.e.*, relic preon stars/nuggets, and how the quark compositeness scale may be linked to astrophysical data. A different scenario where dark matter is related to preons has been suggested in [15].

II. PROPERTIES AND FORMATION

In the mid 1960s it was shown that for solutions to the stellar structure equations, whether Newtonian or relativistic, there is a change in stability whenever the mass reaches an extremum as a function of the central density [16]. The instability in-between white dwarfs and neutron stars, which spans several orders of magnitude of central densities, is an example of this property. Consequently, beyond the density of the maximum mass neutron (or quark/hybrid) star, $\sim 10^{16}$ g/cm^3

[17], configurations are unstable. The order of magnitude for this limiting density is valid also for a hypothetical third class of compact stars [18, 19, 20] and for stars composed of exotic hadron/quark condensates. The instability is therefore generally assumed not to end before the Planck scale, if at all. This assumption, however, is valid only in the context of the SM, where quarks and leptons are elementary. If there is at least one deeper layer of constituents, beneath the particles of the SM, a corresponding class of stable compact objects could exist [9, 10, 11]. The density of such objects cannot be explained within the context of the SM. This "window of opportunity" to new physics is our main motivation for investigating means to observe them. In the following, we briefly describe the relation between the compositeness scale and the properties of such objects.

The characteristic density, size, and mass of a compact object depend on the strength of the interactions between the constituent particles, see, *e.g.*, [21]. Qualitatively, the relation between these quantities can be obtained in a simple way. Under the assumption that the equation of state of matter is everywhere causal it follows that the radius, R, of a stable compact object must exceed 4/3 of its Schwarzschild radius, $R_S = 2GM/c^2$, where M is the mass of the object (without the assumption of causality the factor is not 4/3 but 9/8), a result that follows from the general relativistic stellar structure equations. Simplifying the density to be constant within the object, this leads to an order of magnitude estimate for the relation between the density, ρ, and the mass/radius of the maximum mass configuration

$$M \sim \frac{9c^3}{64}\sqrt{\frac{2}{\pi G^3 \rho}}, \tag{1}$$

$$R \sim \frac{3c}{8}\sqrt{\frac{2}{\pi G \rho}}. \tag{2}$$

For neutron stars with $\rho \sim 10^{15}$ g/cm^3, this estimate yields $M \sim 3$ M$_\odot$ and $R \sim 10$ km, correct order of magnitudes for neutron stars. We assume that the SM is reliable at least up to densities above the onset of the heaviest quark (top), which is of the order $\sim 10^{27}$ g/cm^3 for a charge-neutral fermion gas of six massive quarks and three massive leptons with an MIT bag constant chosen around the traditional value, $B^{1/4} \sim 150$ MeV. The large mass of the top has been assumed to be a consequence of weak binding between preons, see, *e.g.*, [22]. The phase where preons in the top quark can become deconfined should then have a characteristic density

$$\rho \sim \frac{m_t}{4/3\pi(\hbar c/\Lambda)^3} \simeq 9.5 \times 10^{27}\,\mathrm{g/cm^3}\left(\frac{\Lambda}{\mathrm{TeV}}\right)^3, \tag{3}$$

where m_t is the mass of the top quark, $\hbar c/\Lambda$ its "size", and Λ is expected to be of the order of the binding force scale parameter, *i.e.*, Λ gives the compositeness energy scale. Inserting this estimate

in the expressions for the mass and radius of the maximum mass configuration we obtain

$$M \sim \frac{3}{32}\sqrt{\frac{6\hbar^3c^9}{G^3\Lambda^3 m_t}} \simeq 2\times10^{24}\,\mathrm{kg}\left(\frac{\mathrm{TeV}}{\Lambda}\right)^{3/2}, \tag{4}$$

$$R \sim \frac{1}{4}\sqrt{\frac{6\hbar^3c^5}{G\Lambda^3 m_t}} \simeq 3\times10^{-3}\,\mathrm{m}\left(\frac{\mathrm{TeV}}{\Lambda}\right)^{3/2}. \tag{5}$$

Other estimates provided in [9, 10, 11] yield slightly different but qualitatively similar results.

CPDM objects could have been created in a first-order phase transition in the early universe [10, 11], by a mechanism similar to that described in [6]. Under rather general assumptions, this scenario requires that the number of microscopic degrees of freedom is higher during the preon era than during the QCD/quark era [14]. This, perhaps counter-intuitive condition is satisfied by some preon models and can be motivated by the simplicity of the representations and the group structure, rather than an economic number of preons. We do not further speculate about the details of the hypothetical phase transition and the process of CPDM formation, as the main aim here is to explore the possibility to detect such objects, if they exist. We therefore assume that there was a first-order transition from a preon phase to the quark/lepton phase, and that stable preon bubbles formed. What would the characteristic mass of such bubbles be? The density of the radiation background is

$$\rho_R \simeq g_{\mathrm{eff}}\frac{\pi^2}{30}\frac{(k_BT)^4}{\hbar^3c^5}, \tag{6}$$

where g_{eff} is the effective number of microscopic degrees of freedom at temperature T. Inserting (6) in Friedmann's equations for a flat universe (the curvature contribution anyway being negligible at early times) we get an expression for the Hubble expansion parameter

$$H \simeq \left[\frac{8\pi^3G}{90\hbar^3c^5}\,g_{\mathrm{eff}}\right]^{1/2}(k_BT)^2. \tag{7}$$

The maximum size of bubbles is limited by the event horizon, *i.e.*, the Hubble radius, c/H, at the temperature of the phase transition, $T \simeq \Lambda/k_B$. The corresponding maximum mass of a preon bubble is

$$M_H \simeq \frac{4\pi}{3}\left(\frac{c}{H}\right)^3\rho_R \simeq 1.0\times10^{24}\,\mathrm{kg}\,g_{\mathrm{eff}}^{-1/2}\left(\frac{\mathrm{TeV}}{\Lambda}\right)^2, \tag{8}$$

which is less than the maximum mass for stable objects (4). From an observational point of view, M_H is then the maximal mass of CPDM objects, because the number of coalescence events during the lifetime of the universe is negligible, *e.g.*, from (15). In reality, a typical preon bubble could be much smaller than a Hubble radius, depending on the unknown properties of the preon

phase. See [6] for a discussion about formation and evolution of quark bubbles in the QCD phase transition, and [11] for an analogous discussion about preon bubbles. For example, in the QCD phase transition the bubbles should be smaller than the Hubble radius by a factor of at least $\ln[(\hbar c^5/G)^{1/2}/(k_B T_{\rm QCD})]/4$ [23], which is about one order of magnitude for $T_{\rm QCD} \sim 150$ MeV. Except mergers, which in any case should be relatively few and can be neglected from an observational point of view, the mass of CPDM objects should lie in the range $0 \leq M < M_H$. It seems likely that $M \ll M_H$, but a more precise estimate would require further assumptions about the nature of preons and their interactions, which are beyond scope of the present paper. In Fig. 1 the estimates for the theoretical maximum mass (4) and the Hubble mass, M_H (8), are plotted vs. the compositeness scale, Λ. Included in the plot are also the constraints on the mass of compact CDM from gravitational lensing searches, see the next Section. The Large Hadron Collider (LHC) should allow exploration of compositeness scales up to about $\Lambda \sim 40$ TeV, see [24], where future luminosity upgrades of LHC are also discussed.

III. GRAVITATIONAL LENSING

Gravitational lensing is today a well established field of astronomy, with a variety of astrophysical and cosmological applications. Among the many interesting lensing phenomena, there is a possibility to observe low-mass lenses by measuring interference effects between lensed images of narrow astrophysical sources. For lenses with masses in the range $\sim 10^{14}$ kg $< M < 10^{17}$ kg, the time delay induced by the lens would be comparable to the oscillation period of a gamma-ray. It has therefore been suggested [25] that lenses with masses in this range could be observed by gravitational lensing of gamma-ray bursts (GRBs). Because the separation of the images would be in the femto-arcsecond range for lenses and sources at cosmological distances, this phenomenon is called "femtolensing". Femtolenses would produce a characteristic pattern in the spectrum of GRBs [26], which is stable on time scales of 1 s, but might slowly drift on time scales of 10 s due to the relative motion of the lens and source.

No evidence for the existence of femtolenses presently exist, but a number of GRB spectra, see [27] and references therein, have significant features that yet remain to be explained and are similar [28] to those in a femtolensing model spectrum. In particular, the GRB detector aboard the Ginga spacecraft recorded "absorption" features with credible significance near 20 and 40 keV, especially for the burst GRB 880205 [29] and somewhat less convincingly in the burst GRB 870303 [30]. These features were originally interpreted as evidence for cyclotron scattering of electrons in

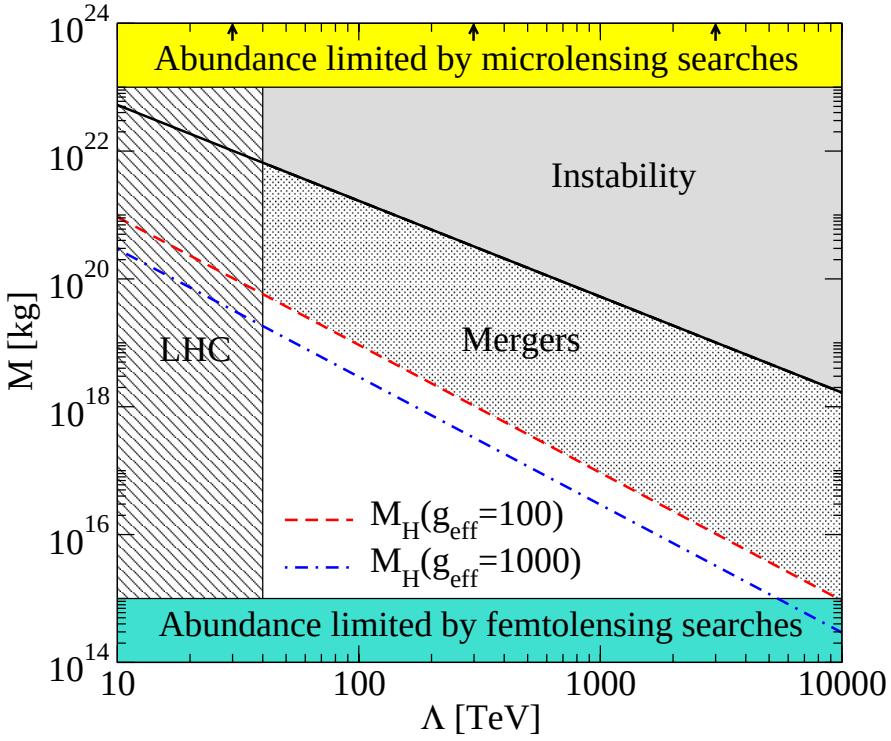

FIG. 1: Constraints on the mass of compact preon dark matter (CPDM) objects vs. the compositeness energy scale, Λ, which is related to the length-scale of a composite top quark by $\hbar c/\Lambda$. The maximum mass, $M_H(\Lambda,\, g_{\rm eff})$, of objects formed in the early universe is the mass within the horizon at the time of the preon phase transition, where $g_{\rm eff}$ is the effective number of degrees of freedom in the preon phase. The relative number of mergers, which could have masses higher than M_H, should be negligible at the present age of the universe. The LHC will probe compositeness scales up to about 40 TeV. The maximal mass of unobserved compact dark matter objects is $\sim 10^{23}$ kg and femtolensing searches rule out $\sim 10^{14} < M < 10^{15}$ kg. No observational technique can presently resolve objects with masses below 10^{14} kg. See the text for details.

a strong magnetic field and, as a consequence, a galactic origin of some GRBs, see, *e.g.*, [27, 31]. More recent observations (afterglows, supernova-GRB connection, etc.) and theoretical models of GRBs falsify this explanation, in particular because these were long GRBs, known to occur at cosmological distances. The origin of the features observed with Ginga is therefore an unsolved mystery. Similar features in the spectra of GRBs have been detected in a number of other missions, notably at 11 and 35 keV in GRB 890306 by Lilas [32], and at 50 and 70 keV in the two peaks of GRB 780325 by HEAO A-4 [33]. Similar features have been detected also by the BATSE

spectroscopy detectors, see [34] and references therein.

For more massive lenses, the energy-dependent spectra from a single GRB detector provide no useful information. Instead, the spatial interference effect needs to be measured. Two spacecrafts separated by a distance that exceeds the radius of the Einstein ring of the lens, $R_E \sim \sqrt{GM/(Hc)} \sim 10^7\text{m} \times \sqrt{M/(10^{15}\text{ kg})}$, could detect lenses with masses in the range $\sim 10^{15}$ kg $< M < 10^{23}$ kg [35]. No present result limits the amount of CPDM with masses in this range [36]. Consequently, refined femto- and picolensing searches could be used to detect CPDM with masses in the range 10^{14} kg $< M < 10^{23}$ kg. A large abundance of CPDM with $M > 10^{23}$ kg is, however, not consistent with observations [7]. This does not preclude the possibility that a small fraction of CDM is in that form, but since the corresponding compositeness scale is within reach of the LHC, see Fig. 1, there is no reason to discuss that possibility here. In the following, we briefly discuss the femtolensing effect on the spectrum of GRBs.

The magnification functions for point and extended sources have been derived in [26]. These functions are not trivial to obtain and have to be calculated numerically. We have therefore provided an on-line tool [37] for calculation of femtolensing magnification functions and model GRB spectra, which implements the model in [26] with some extensions. The magnification function depends on four parameters, the mass and redshift of the lens, the angular separation of the source and lens, and the angular width of the source. The width of the lens is neglected, because it has practically no effect as long as the lenses are smaller than their Einstein ring. We denote the angular diameter distances of the lens and the source from the observer, and of the source from the lens with d_L, d_S, and d_{LS}, respectively. The distance, r_s, between the source and the optical axis is measured in the dimensionless quantity

$$r_s = \frac{\sqrt{\xi^2 + \eta^2}}{d_s \theta_E}, \tag{9}$$

where $\theta_E = \sqrt{4GMd_{LS}/(c^2 d_L d_S)}$ is the angular radius of the Einstein ring and (ξ, η) are the Cartesian coordinates of the source in the source plane. The dimensionless width of the source, σ_s, is defined analogous to r_s, *i.e.*, the actual width is divided by $d_s\theta_E$. Some femtolensing spectra are plotted in Fig. 2, for three different widths of a GRB, which is assumed to have a fixed position relative to the optical axis, $r_s = 0.5$. The model spectrum of the GRB is a assumed to be a power law, with an exponent of -1. The energy scale depends on the redshift, z, and mass, M, of the lens according to

$$E_0 = \frac{hc^3}{4\pi GM(1+z)}$$

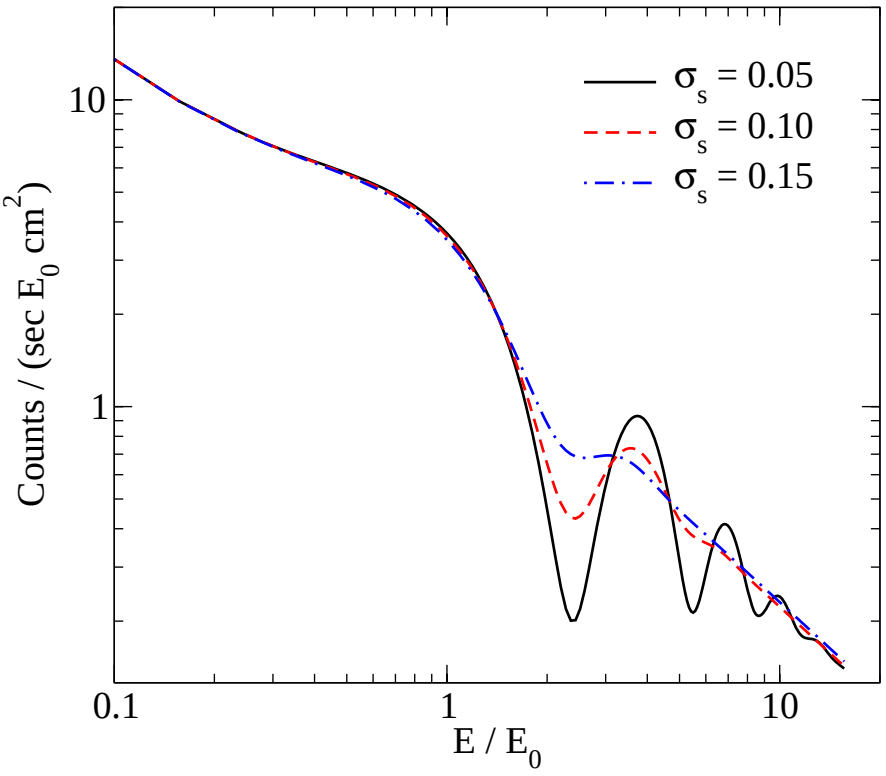

FIG. 2: Femtolensing of a gamma-ray burst (GRB) with model spectrum $(E/E_0)^{-1}$, for three different widths of the source, σ_s. The GRB has a fixed position relative to the optical axis, $r_s = 0.5$, see text. These spectra were calculated with the on-line interface [37].

$$\simeq 1.3 \times 10^3 \,\mathrm{keV} \left(\frac{10^{14}\,\mathrm{kg}}{M}\right)\left(\frac{1}{1+z}\right), \tag{10}$$

for any model spectrum of the GRB. In Fig. 3 a femtolensing spectra is superimposed on the spectral data of GRB 880205 for power law models of the GRB spectrum.

Because the amplitude of the femtolensing magnification function decays with frequency (and the width of the source), detectors that have energy thresholds well below the first minima should be used in femtolensing searches. According to Eq. (15) in [26], the first minimum of the magnification function is located at

$$\begin{aligned} E_1 &\simeq \frac{3\pi E_0}{8 r_s} \\ &\simeq 1.6 \times 10^3 \,\mathrm{keV} \left(\frac{10^{14}\,\mathrm{kg}}{M}\right)\left(\frac{1}{1+z}\right)\left(\frac{1}{r_s}\right). \end{aligned} \tag{11}$$

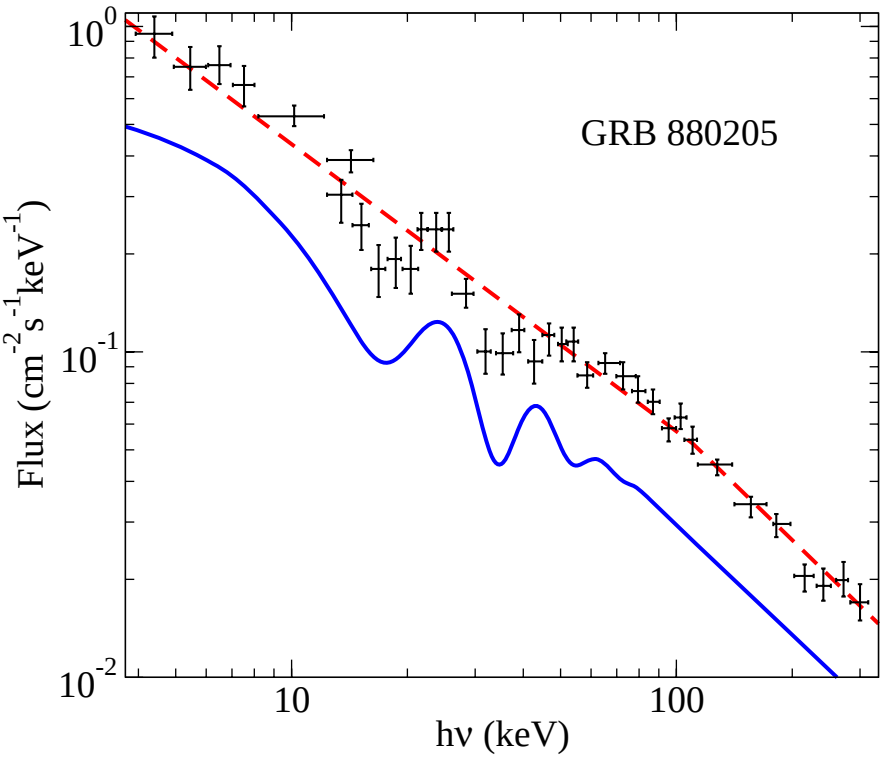

FIG. 3: Ginga spectral data of GRB 880205 for a power law model of the incoming spectrum (dashed line), which is ruled out at more than 99.99% confidence level [27]. The observed spectrum has line features at $h\nu \simeq 20$ and 40 keV, which could be due to gravitational lensing (diffraction) of a Gaussian source by a $\sim 10^{16}$ kg object at redshift $z \sim 1$ (solid line). The spectral data depend on the model used and should not be directly compared to the diffraction spectrum, which therefore has been shifted downwards to enhance viewing [28]. The main concern here is the location of the line features.

Spectra from the Transient Gamma-Ray Spectrometer and the BATSE spectroscopy detectors used in recent searches for absorption line features in GRB spectra were limited to $E > 40$ keV and 20 keV, respectively, see [34, 38] and references therein. Consequently, the advantages of these instruments fall short in searches for femtolenses of high mass due to the relatively high lower-energy thresholds. The absorption features in GRB 870303, GRB 880205, and GRB 890306 observed in earlier missions would appear less significant if observed with these instruments. In particular, the low-energy absorption features in these bursts would not be detected. The limit on the abundance of femtolenses given in [36] should therefore not be taken too seriously for more

massive femtolenses. For masses in the picolensing range, there are presently no limits on the abundance of CPDM (other than $\rho_{\rm CPDM} \leq \rho_{\rm CDM}$). A refined search for femto- and picolensing features in high-resolution spectra of GRBs would therefore provide useful constraints on the abundance of CPDM and similar compact dark matter objects.

IV. GRAVITATIONAL WAVES FROM BINARIES

While gravitational pico- and femtolensing can be used to detect and estimate the mass spectrum of CPDM, these methods provide little information about the actual density of the lenses ($R \lesssim d_L\theta_E$). Consequently, lensing methods alone cannot provide detailed information about the nature of the objects and their constituents. One possibility to constrain the upper limit size of CPDM is to measure high-frequency gravitational wave (GW) radiation emitted from binary systems. In the following, we estimate the properties and expected rate of such events for objects with masses in the range 10^{15} kg $< M < 10^{23}$ kg, which roughly is the range unconstrained by gravitational lensing searches.

Assuming that the objects are distributed randomly in the solar neighbourhood, the probability distribution function for the semi-major axis, a, of binaries is [39]

$$P(a)da = \frac{3}{4}\left(\frac{a}{\bar{x}}\right)^{3/4} \exp\left[-\left(\frac{a}{\bar{x}}\right)^{3/4}\right]\frac{da}{a}, \tag{12}$$

where $\bar{x}$ is the mean separation. Typically, the tidal forces from nearby objects add angular momentum to a binary and head-on collisions are thereby avoided. We assume that the dark halo density in the solar neighbourhood is $0.0079{\rm M}_\odot$ pc^{-3} [40]. For simplicity, we also assume that the bulk of the dark halo is in the form of CPDM of equal masses. The results can readily be generalised to an arbitrary fraction of CPDM. The mean separation is

$$\bar{x} \simeq \left(\frac{0.0079{\rm M}_\odot}{M}\right)^{-1/3} {\rm pc}. \tag{13}$$

The remaining time before coalescence, τ, due to emission of GWs depends on the masses, the semi-major axis, and the eccentricity of the orbit. For small τ the eccentricity can be neglected, as the radiation reaction acts to reduce it. For a circular orbit, the coalescence time is [41]

$$\tau = \frac{5c^5}{512G^3}\frac{a^4}{M^3}. \tag{14}$$

The probability distribution function (12) can be expressed in the coalescence time τ. Consequently, the relative number of coalescence events within a time t is obtained by

$$\int_0^t P(\tau)d\tau \;=\; 1 - \exp\left[-\bar{x}^{-3/4}\left(\kappa t\right)^{3/16}\right], \tag{15}$$

$$\kappa \;=\; \frac{512G^3M^3}{5c^5}, \tag{16}$$

where $\int_0^\infty P(\tau)d\tau = 1$. The exponent in (15) is small for all masses considered here, at any relevant timescale, t. We therefore make the approximation $1-\exp(-x) \simeq x$. The total number of objects, $N(D)$, within a distance D can be expressed in the local dark halo density and the mass of the objects. The number of coalescence events, N_c, within a time t is $N_c = N(D)\int_0^t P(\tau)d\tau$, which yields

$$N_c \simeq 4.9\left(\frac{D}{\mathrm{pc}}\right)^3\left(\frac{10^{15}\,\mathrm{kg}}{M}\right)^{11/16}\left(\frac{t}{\mathrm{yrs}}\right)^{3/16}. \tag{17}$$

This estimate for the coalescence rate scales linearly with the fraction of CPDM, *i.e.*, there is an extra factor $\rho_{\mathrm{CPDM}}/\rho_{\mathrm{CDM}}$ on the right-hand side of (17). In order to obtain a realistic event rate, a detector sensitive enough to detect CPDM coalescence events at a distance of several pc is needed. Next, we estimate the frequency and amplitude of such events.

The frequency of GWs, f_g, emitted from a binary in a circular orbit is twice the Kepler frequency

$$\begin{aligned} f_g \;&=\; \frac{1}{\pi}\left(\frac{2MG}{a^3}\right)^{1/2} \\ &\simeq\; 6.0\times10^{11}\,\mathrm{Hz}\left(\frac{\mathrm{sec}}{\tau}\right)^{3/8}\left(\frac{10^{15}\,\mathrm{kg}}{M}\right)^{5/8}, \end{aligned} \tag{18}$$

because the waves are essentially generated by the quadrupole moment of the binary. The power emitted in GWs is [41]

$$\begin{aligned} L_g \;&=\; \frac{64G^4}{5c^5}\left(\frac{M}{a}\right)^5 \\ &\simeq\; 1.4\times10^{16}\,\mathrm{W}\left(\frac{M}{10^{15}\,\mathrm{kg}}\frac{f_g}{\mathrm{GHz}}\right)^{10/3}, \end{aligned} \tag{19}$$

and the amplitude of the GWs at a distance D from the source is

$$\begin{aligned} h \;&=\; \left(\frac{GL_g}{\pi^2c^3}\right)^{1/2}\frac{1}{f_gD} \\ &\simeq\; 1.9\times10^{-36}\left(\frac{M}{10^{15}\,\mathrm{kg}}\right)^{5/3}\left(\frac{f_g}{\mathrm{GHz}}\right)^{2/3}\left(\frac{\mathrm{pc}}{D}\right). \end{aligned} \tag{20}$$

The frequency dependent amplitude (20) is plotted in Fig. 4 for different masses, M, and distances, D, chosen such that 10 coalescence events per year are expected with at least that amplitude (if the CPDM fraction of CDM is less than one, the number of events per year is lowered by the same factor). Also indicated in the plot are the coalescence time (14), the threshold of the relativistic domain, where the orbital velocity, $v_{orb} = c(R_S/a)^{1/2}$, is 10% of the speed of light, and

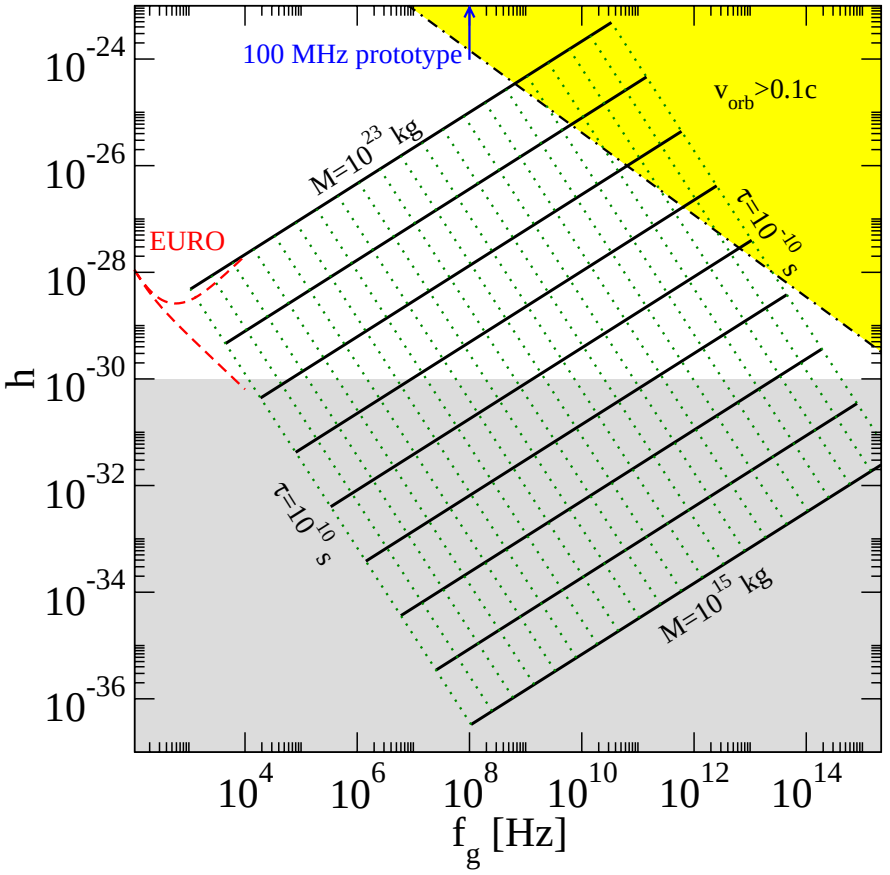

FIG. 4: Amplitude vs. frequency for gravitational waves emitted from an equal-mass binary system in circular orbit. The distance is such that 10 coalescence events per year is expected within that range, *i.e.*, $N_c = 10$ in (17). The solid lines denote the frequency-amplitude relation for different masses, M, of the CPDM objects, in steps of one order of magnitude. The coalescence time (14) is denoted by the dotted lines, also in steps of one order of magnitude. The dash-dotted line corresponds to an orbital velocity of 10% of the speed of light. Dashed lines denote the lower sensitivity curves for an observational time of 5 years with EURO, according to two different design specifications (shot-noise limited antenna with a knee-frequency of 1000 Hz and a xylophone-type interferometer). The sensitivity of the first prototype 100 MHz detector in the UK [43] is presently insufficient to detect CPDM coalescence events. The shaded region, $h < 10^{-30}$, apparently is beyond reach of experiments and could be polluted by the relic gravitational wave background, see [42] and references therein.

an estimate for the sensitivity of future detectors, $h_{\rm min} \sim 10^{-30}$, see [42] and references therein.

Even if this estimate for the sensitivity could be exceeded, coalescence events with significantly lower amplitudes would be difficult to distinguish from the stochastic GW background, created by quantum fluctuations in the early universe. This background exists in most popular cosmological models and, due to the expansion of the universe, the amplitudes of the initial fluctuations are amplified and should approach the $h \sim 10^{-30}$ level [42]. Because $h \propto N_c^{-1/3}$, the amplitudes in Fig. 4 will increase only by a factor two for an order of magnitude decrease of the event rate. We therefore choose $N_c = 10$, to compensate for the simplifying assumption that $\rho_{\rm CPDM}/\rho_{\rm CDM} = 1$.

The planned spectral noise density for the European Gravitational Wave Observatory (EURO) in the range 10-10000 Hz is [44]

$$S_n(f) \;=\; 10^{-50}\left[\left(\frac{f}{245\,\mathrm{Hz}}\right)^{-4} + \left(\frac{f}{360\,\mathrm{Hz}}\right)^{-2} + \left(\frac{f_k}{770\,\mathrm{Hz}}\right)\left(1+\frac{f^2}{f_k^2}\right)\right]\mathrm{Hz}^{-1}, \tag{21}$$

where $f_k = 1000$ Hz is the knee frequency. Alternatively, EURO will be based on a xylophone-type interferometer, which has higher sensitivity at high frequencies. The spectral noise density for the latter choice is described by (21) when the last f_k-dependent term is omitted. The characteristic amplitude of a GW is $h_c = h\sqrt{n}$, where $n = f_g \Delta T$ is the number of cycles during an observational time of ΔT. The wave strength of GWs from a monochromatic source observed with an interferometer is $h_s = h_c/\sqrt{5 f_g}$. Consequently, the minimum amplitude, $h_{\rm min}$, that can be resolved with EURO after an observational time ΔT is $h_{\rm min} = \sqrt{5 S_n(f)/\Delta T}$. This estimate for the sensitivity of EURO is plotted in Fig. 4 for an observational time of five years. High-mass CPDM is marginally within range of the next generation of gravitational wave detectors. However, the semi-major axis of a binary is

$$a \;=\; R_S\left(\frac{c^3}{2\pi G M f_g}\right)^{2/3} \;\simeq\; 1.6\times 10^7 R_S\left(\frac{10^{15}\,\mathrm{kg}}{M}\frac{\mathrm{GHz}}{f_g}\right)^{2/3}, \tag{22}$$

so in order to get useful constraints on the compactness of CPDM, a detector sensitive at higher frequencies is needed. Interestingly, high-frequency GW detectors are laboratory-scale devices that are relatively inexpensive to construct. A first 100 MHz prototype has recently been built in the UK [43]. If the sensitivity of such detectors would approach the estimates given in [42], they would provide useful constraints on CPDM. The range 10^{15} kg $< M \lesssim 10^{18}$ kg would, however, only be accessible by rare nearby events.

V. CONCLUSION & DISCUSSION

If quarks and leptons are composite particles, superdense preon stars (or "nuggets") could exist [9, 10, 11]. While the microscopic motivation for such objects is still somewhat schematic and the exact process of formation uncertain, the consequences of their eventual existence are far-reaching. In the present paper we briefly investigate their phenomenology, assuming that they formed in the early universe and contribute significantly to CDM. Their maximum mass is limited by the horizon at the time of formation, $\sim 10^{24}\,\mathrm{kg}\,g_{\mathrm{eff}}^{-1/2}(\mathrm{TeV}/\Lambda)^2$, where Λ is the quark compositeness energy scale and g_{eff} is the number of microscopic degrees of freedom in the primordial preon phase. This is a factor $\sim 2\sqrt{g_{\mathrm{eff}}\,\Lambda/\mathrm{TeV}}$ lower than the maximum mass for stable hydrostatic configurations. However, the typical mass could be much lower than what is maximally allowed, depending on the properties of the preons and their interactions. Gravitational lensing searches put strong constraints on the abundance of CDM objects with masses in the ranges $M \gtrsim 10^{23}$ kg and $10^{14} \lesssim M \lesssim 10^{15}$ kg. Unexplained features in GRB spectra observed by, *e.g.*, Ginga, Lilas, and HEAO A-4 motivate a continued search for gravitational pico- and femtolenses. This would provide useful constraints on the abundance of compact CDM objects with masses in the range $10^{15} \lesssim M \lesssim 10^{23}$ kg, corresponding to a maximum compositeness energy scale for CPDM of a few thousand TeV. This observational technique, however, provides little information about the nature of the lenses, because their size and density is limited only by the radius of their Einstein ring. Future high-frequency gravitational wave detectors could provide complementary information about the density of compact CPDM binaries, but it is presently unclear whether it is possible to detect the chirp signal of a low-mass binary as the objects coalesce [45]. This would be necessary in order to obtain a useful constraint on the radii and, consequently, a lower-limit for the density of the objects. In an optimistic scenario where the mass of the CPDM objects is comparable to the maximum mass, this method could be useful to indirectly detect compositeness up to a few hundred TeV. Another possibility to detect compact CDM objects and to constrain their density is by seismology, *i.e.*, by measuring the seismic waves generated as they pass through the Earth or the Moon, see [46] and references therein. Unlike the observational methods discussed above, this method is useful in scenarios where the typical mass of the objects is low, as the collision rate increases with the number density of objects. The cross-section of a CPDM object would be at least six orders of magnitude smaller than for a quark nugget of equal mass, making it possible to distinguish them. Should CPDM objects exist, their observational detection may well be the only means, for quite a long time, to discover compositeness beyond the reach of the LHC and other

near-future accelerators. As the observational techniques discussed here are useful also for other purposes, and are already in operation to some extent, they constitute a comparatively simple and inexpensive way to test the CPDM and compositeness hypothesis.

Acknowledgments

F.S. acknowledges support from the Swedish Graduate School of Space Technology and J.H. acknowledges support from Carl Tryggers stiftelse.

[1] J. P. Ostriker & P. J. Steinhardt, Science **300**, 1909 (2003); J. R. Primack, Nucl. Phys. Proc. Suppl. **124**, 3 (2003); New. Astron. Rev. **49**, 25 (2005); G. Bertone, D. Hooper & J. Silk, Phys. Rept. **405**, 279 (2005).

[2] R. Sancisi, Proc. IAU Symposium 220, eds. S. D. Ryder, D. J. Pisano, M. A. Walker & K. C. Freeman, Astron. Soc. Pac. **220** (2004); astro-ph/0311348.

[3] G. Gentile, P. Salucci, U. Klein, D. Vergani & P. Kalberla, Mon. Not. Roy. Astron. Soc. **351**, 903 (2004).

[4] A. Zhitnitsky, Phys. Rev. D **74**, 043515 (2006).

[5] N. A. Bahcall, J. P. Ostriker, S. Perlmutter & P. J. Steinhardt, Science **284**, 1481 (1999); L. M. Wang, R. R. Caldwell, J. P. Ostriker & P. J. Steinhardt, Astrophys. J. **530**, 17 (2000).

[6] E. Witten, Phys. Rev. D **30**, 272 (1984).

[7] R. B. Metcalf & J. Silk; astro-ph/0612253.

[8] J-J. Dugne, S. Fredriksson & J. Hansson, Europhys. Lett. **57**, 188 (2002).

[9] J. Hansson & F. Sandin, Phys. Lett. B **616**, 1 (2005).

[10] F. Sandin, Eur. Phys. J. C bf 40, S15 (2005).

[11] J. E. Horvath, *Constraints on superdense preon stars and their formation scenarios*, accepted for publication in Mod. Phys. Lett. A; ISSN/ISBN: 0217323.

[12] H. Knutsen, Gen. Rel. Grav. **23**, 843 (1991).

[13] G. H. A. Cole & J. Dunning-Davies, Gravitation **4**, 79 (1999) (in Russian).

[14] H. Nishimura & Y. Hayashi, Phys. Rev. D **35**, 3151 (1987).

[15] V. Burdyuzha, O. Lalakulich, Yu. Ponomarev & G. Vereshkov; hep-ph/9907531, astro-ph/9912555.

[16] B. K. Harrison, K. S. Thorne, M. Wakano & J. A. Wheeler, *Gravitation Theory and Gravitational Collapse* (University of Chicago Press, Chicago, 1965).

[17] C. Kettner *et al.*, Phys. Rev. D **51**, 1440 (1995).

[18] U. H. Gerlach, Phys. Rev. **172**, 1325 (1968),
U. H. Gerlach, Ph.D. thesis, Princeton University, 1968.

[19] N. K. Glendenning & C. Kettner, Astron. Astrophys. **353**, L9 (2000).

[20] K. Schertler *et al.*, Nucl. Phys. **A 677**, 463 (2000).

[21] G. Narain, J. Schaffner-Bielich & I. N. Mishustin, Phys. Rev. D, **74**, 063003 (2006).

[22] J. C. Pati, Phys. Rev. D **30**, 1144 (1984).

[23] C. J. Hogan, Phys. Lett. B **133**, 172 (1983).

[24] F. Gianotti, Nucl. Phys. Proc. Suppl., **147**, 23 (2005).

[25] A. Gould, Astrophys. J. **386**, L5 (1992).

[26] K.Z. Stanek, B. Paczyński & J. Goodman, Astrophys. J. **413**, L7 (1993).

[27] E. E. Fenimore *et al.*, Astrophys. J. **335**, L71 (1988).

[28] The observed counts in a gamma-ray detector corresponds to the energy loss spectrum, which is created by the gamma photons as they interact with the medium in the detector, *e.g.*, sodium iodide or germanium. Consequently, it is not certain that the energy of a particular count equals the energy of an incident photon. The spectrum of the light entering the detector can therefore not be deduced from data. Instead, model spectra are used in conjunction with data to calculate the probability that the physical spectrum is/is not explained by a particular model. In this procedure, details about the detector response functions and the original data are needed. We were unable to obtain this information for the detector aboard Ginga and for GRB 880205. A formal detailed comparision with femtolensing spectra has therefore not been done.

[29] T. Murakami *et al.*, Nature **335**, 234 (1998).

[30] P.E. Freeman *et al.*, Astrophys. J. **524**, 753 (1999).

[31] J. C. L. Wang *et al.*, PRL **63**, 1550 (1989).

[32] C. Barat, Astron. Astrophys. Suppl. Ser. **97**, 43 (1993).

[33] G. J. Hueter, Ph.D. Thesis (University of California, San Diego, 1987).

[34] M. S. Briggs *et al.*, Proc. 3rd INTEGRAL workshop, eds. A. Bazzano, C. Winkler & G. Palumbo, Astrophys. Lett. Commun. **38/39** (1999); astro-ph/9901224.

[35] R. J. Nemiroff & A. Gould, Astrophys. J. **452**, L111 (1995).

[36] G. F. Marani *et al.*, Astrophys. J. **512**, L13 (1999).

[37] On-line femtolensing calculator: http://femtolensing.dyndns.org.

[38] P. Kurczynski *et al.*, Astrophys. J. **543**, 77 (2000).

[39] K. Ioka *et al.*, Phys. Rev. D **58**, 063003 (1998).

[40] C. Alcock *et al.*, Astrophys. J. **542**, 281 (2000).

[41] C. W. Misner, K. S. Thorne & J. A. Wheeler, *Gravitation* (W. H. Freeman and Company, San Francisco, 1973).

[42] G. S. Bisnovatyi-Kogan & V. N. Rudenko, Class. Quant. Grav. **21**, 3347 (2004).

[43] A. M. Cruise & R. M. J. Ingley, Class. Quant. Grav. **23**, 6185 (2006).

[44] EURO homepage: http://www.astro.cf.ac.uk/geo/euro.

[45] A. M. Cruise, private communication.

[46] E. T. Herrin, D. C. Rosenbaum & V. L. Teplitz, Phys. Rev. D **73**, 043511 (2006).

Paper VII

The quark core of protoneutron stars in the phase diagram of quark matter

F. Sandin[1,*] and D. Blaschke[2,3,4,†]

[1] *Department of Physics, Luleå University of Technology, SE-97187 Luleå, Sweden*
[2] *Instytut Fizyki Teoretycznej, Uniwersytet Wrocławski, PL-50-204 Wrocław, Poland*
[3] *Bogoliubov Laboratory for Theoretical Physics, JINR Dubna, RU-141980 Dubna, Russia*
[4] *Institut für Physik, Universität Rostock, D-18051 Rostock, Germany*

We study the effect of neutrino trapping in new-born quark stars within a three-flavor Nambu–Jona-Lasinio (NJL) model with self-consistently calculated quark masses. The phase diagrams and equations of state for charge neutral quark matter in β-equilibrium are presented, with and without trapped neutrinos. The compact star sequences for different neutrino untrapping scenarios are investigated and the energy release due to neutrino untrapping is found to be of the order of 10^{53} erg. We find that hot quark stars characterized, *e.g.*, by an entropy per baryon of $1-2$ and a lepton fraction of 0.4, as models for the cores of newborn protoneutron stars are in the two-flavor color superconducting (2SC) state. High temperatures and/or neutrino chemical potentials disfavor configurations with a color-flavor-locked (CFL) phase. Stable quark star solutions with CFL cores exist only at low temperatures and neutrino chemical potentials.

PACS numbers: 12.38.Aw, 12.39.-x, 24.85.+p, 26.60.+c, 97.60.-s

I. INTRODUCTION

The engine of explosive phenomena in astrophysics, such as gamma-ray bursts (GRBs) and type-II supernovæ is presently not fully understood. The generation and propagation of neutrino fluxes, as well as the neutrino interactions in the hot and dense nuclear matter envelope play key roles in models of the evolution of core-collapse supernovæ [1]. Detailed hydrodynamic simulations of the gravitational collapse of a massive star show that the possibility to obtain a successful explosion depends to a large extent on the properties of the protoneutron star (PNS) that forms in the compressed core. About 99% of the gravitational binding energy is released by neutrino emission [2, 3, 4]. The supernova collapse and prompt neutrino production proceeds within milliseconds and the shock-compressed matter is heated up to about $30-50$ MeV. At such high temperature, the neutrino mean free path is much shorter than the radius of a PNS, $R\sim 10$ km, and neutrinos diffuse on a time scale of ~ 10 seconds. During this 'neutrino trapping' regime the number of neutrinos is quasi conserved and the neutrino chemical potential, μ_ν, is of the order 200 MeV [3, 4]. This state lasts until the temperature is low enough for the neutrino mean free path to become comparable to R. The behavior of the neutrino mean free path, which determines the time scale for the untrapping transition and the onset of the 'second shock' of the supernova, depends in a sensitive way on the microphysics of the hot and dense PNS interior. In particular, if superfluid and superconducting phases of hadronic and/or quark matter are created, the transport properties are affected and the consequences for simulations of core-collapse supernovæ could be important.

In a scenario where color superconducting quark matter is the preferred state of matter at high density there are several new aspects to consider, for example:

1. The kinetics of the phase transition, which eventually proceeds with the release of latent heat and requires a nucleation time scale.

2. The possibility that color superconducting phases have large pairing gaps (~ 100 MeV), which affect the transport properties in the PNS core.

3. The possibility that color superconducting phases have a high critical temperature ($\propto$ the gaps) and therefore affect the formation and evolution of PNS.

For recent reviews on dense color superconducting quark matter, see [5, 6, 7, 8, 9, 10, 11, 12] and references therein.

The energy released due to a phase transition to deconfined quark matter in a PNS core can reach the order of 100 bethe ($=10^{53}$ erg) [13, 14, 15], which is the correct order of magnitude for the energy of GRBs. Moreover, the nucleation timescale for a quark matter phase transition could explain the time delay statistics of GRB subpulse structure [16, 17]. It has also been emphasized that in the presence of a strong magnetic field, neutrinos propagating in hot superconducting quark matter can become collimated (beaming) and asymmetric, thus explaining a resulting kick velocity for the PNS [18].

In the present work we consider a microscopic, albeit schematic chiral quark model of NJL type, where the quark masses and pairing gaps are calculated self-consistently at the mean-field level, see [19, 20, 21, 22]. We describe the phase structure of color superconducting three-flavor quark matter for two different strengths of the phenomenological diquark pairing interaction, in systems with and without trapped neutrinos. The corresponding quark star solutions are considered as models

*Electronic address: fredrik.sandin@ltu.se
†Electronic address: blaschke@ift.uni.wroc.pl

for PNS cores and their properties are described. In particular, we are interested in the answers to the following questions:

1. What influence has the neutrino chemical potential on the phase diagram of quark matter?

2. In which regions of the quark matter phase diagram can stable quark stars be found?

3. Can both two-flavor color superconducting (2SC) and three-flavor color-flavor-locked (CFL) phases be realized under PNS conditions?

4. How much energy can be released in the cooling and untrapping evolution for these models of a PNS core?

While the effect of neutrino trapping on the phase structure of color superconducting three-flavor quark matter has been investigated before in Refs. [23] and [24], the focus of our study is on the stability of quark stars for different phase structures and an estimate of the energy release in the cooling and untrapping transitions.

The paper is organized as follows. In Section II we define the NJL-type model that we use to describe color superconducting quark matter with trapped neutrinos. Section III gives a summary of all results, which are discussed in detail in subsections according to the main questions posed in the Introduction. The Conclusions summarize our main findings.

II. MODEL OF HOT QUARK MATTER WITH TRAPPED NEUTRINOS

Due to the high density in compact stars, strange quarks could exist in their interior. We therefore consider a grand canonical ensemble with up, down, and strange quark degrees of freedom. Because strange quarks have a relatively high mass, they should exist only at high density. Therefore, at not too high densities, where matter is in a two-flavor state, there should be an excess of down quarks for matter to be charge neutral. Consequently, the difference between the chemical potentials of the up and down quarks can be sufficiently large for muons to be created by weak interactions, $d \leftrightarrow u + \mu^- + \bar{\nu}_\mu$. It is therefore necessary to include both electron and muon lepton degrees of freedom in the model. The τ lepton is, however, not included, because it is too massive to play a significant role in compact stars. We neglect the influence of neutrino oscillations and therefore omit the τ neutrino as well.

The thermodynamics of the quark matter phase is described with an NJL-type model. The path-integral representation of the quark partition function is [19, 20, 21]

$$Z(T,\hat{\mu}) = \int \mathcal{D}\bar{q}\mathcal{D}q\, e^{\int d^4x(\mathcal{L}_f+\mathcal{L}_{\bar{q}q}+\mathcal{L}_{qq})}, \tag{1a}$$

$$\mathcal{L}_f = \bar{q}(i\partial\!\!\!/ - \hat{m} + \hat{\mu}\gamma^0)q, \tag{1b}$$

$$\mathcal{L}_{\bar{q}q} = G_S \sum_{a=0}^{8} (\bar{q}\tau_a q)^2, \tag{1c}$$

$$\mathcal{L}_{qq} = G_D \sum_{A=2,5,7} (\bar{q}i\gamma_5\tau_A\lambda_A C\bar{q}^T)(q^T iC\gamma_5\tau_A\lambda_A q), \tag{1d}$$

where $\hat{\mu}$ and $\hat{m}$ are the diagonal chemical potential and current quark mass matrices in color and flavor space. For $a = 0$, $\tau_0 = (2/3)^{1/2}\mathbf{1}_f$, otherwise τ_a and λ_a are Gell-Mann matrices acting in flavor and color space, respectively. $C = i\gamma^2\gamma^0$ is the charge conjugation operator and $\bar{q} = q^\dagger\gamma^0$. The coupling constants, G_S and G_D, determine the coupling strengths in the $\bar{q}q$ and qq channels, which represent current-current interactions in the color singlet scalar meson channel and the scalar color antitriplet diquark channel. We follow the argument in [20] concerning the $U_A(1)$ symmetry breaking in the pseudoscalar isoscalar meson sector, which essentially is that the symmetry breaking is dominated by quantum fluctuations, and we therefore omit the 't Hooft determinant interaction. In the following we use the relative coupling strength

$$\eta = G_D/G_S \tag{2}$$

to parametrize the coupling in the diquark channel. In the choice of the four-fermion interaction channels we have omitted the pseudoscalar $\bar{q}q$ terms, which should be present in a chirally symmetric theory. These terms do not contribute to the thermodynamic properties of the deconfined quark matter phase at the mean-field (Hartree) level [22], to which we restrict the discussion in the present paper.

After bosonization using Hubbard-Stratonovich transformations, we obtain an exact transformation of the original partition function (1). The transformed expression constitutes the starting point for approximations, defined as truncations of the Taylor expanded action functional to different orders in the collective boson fields. In the following, we use the mean-field (MF) approximation. This means that the bosonic functional integrals are omitted and the collective fields are fixed at the extremum of the action. The corresponding mean-field thermodynamic potential, from which all thermodynamic

quantities can be derived, is given by

$$\begin{aligned}\Omega_{\rm MF}(T,\hat{\mu},\mu_{L_e},\mu_{L_\mu}) &= -\frac{1}{\beta V}\ln Z_{\rm MF}(T,\hat{\mu}) + \Omega_l(T,\mu_{L_e},\mu_{L_\mu}) \\ &= \sum_{i=u,d,s}\frac{(M_i-m_i)^2}{8G_S} + \frac{\Delta_{ud}^2+\Delta_{us}^2+\Delta_{ds}^2}{4\eta G_S} \\ &- \int\frac{d^3p}{(2\pi)^3}\sum_{a=1}^{18}\left[E_a(p) + 2T\ln\left(1+e^{-E_a(p)/T}\right)\right] \\ &+ \Omega_l(T,\mu_{L_e},\mu_{L_\mu}) - \Omega_0. \end{aligned} \tag{3}$$

Here, $M_i = m_i + \phi_i$ are the renormalized quark masses, m_i are the current quark masses, $E_a(p)$ are the eighteen independent quark quasiparticle dispersion relations, and ϕ_i (Δ_{ij}) are chiral (diquark) gaps, see [20] for details. The gaps, ϕ_i and Δ_{ij}, emerge from the auxiliary boson fields introduced by the Hubbard-Stratonovich transformations and represent collective modes generated by $\bar{q}q$ and qq, respectively. $\Omega_l(T,\mu_{L_e},\mu_{L_\mu})$ is the thermodynamic potential for an ideal gas of neutrinos, electrons ($m_e \simeq 0.511$ MeV), and muons ($m_\mu \simeq 105.66$ MeV)

$$\Omega_l(T,\mu_{L_e},\mu_{L_\mu}) = -\sum_{l=e,\,\mu}\left[\frac{\mu_{\nu_l}^4}{24\pi^2} + \frac{\mu_{\nu_l}^2T^2}{12} + \frac{7\pi^2T^4}{360} + \frac{T}{\pi^2}\sum_{\pm}\int_0^\infty {\rm d}k^2\ln\left(1+e^{-\frac{E_l\pm\mu_l}{T}}\right)\right], \tag{4}$$

where $E_l = \sqrt{p^2+m_l^2}$. Ω_0 is a divergent term that is subtracted in order to get zero pressure and energy density in vacuum (*i.e.*, at $T=\mu=0$)

$$\Omega_0 = \sum_{i=u,d,s}\frac{(\phi_i^0)^2}{8G_S} - 6\int\frac{d^3p}{(2\pi)^3}\sqrt{p^2+(m_i+\phi_i^0)^2}. \tag{5}$$

The model has six conserved charge densities and associated chemical potentials. The $U(3)_f \times SU(3)_c \times U(1)_Q$ symmetry of the quarks is broken in the presence of diquarks. Therefore, there are only four mutually commuting conserved charge densities, *e.g.*, the quark number density

$$n = \langle q^\dagger q\rangle = -\frac{\partial\Omega_{\rm MF}}{\partial\mu}, \tag{6}$$

two color charge densities

$$n_3 = \langle q^\dagger\lambda_3 q\rangle = -\frac{\partial\Omega_{\rm MF}}{\partial\mu_3}, \tag{7a}$$

$$n_8 = \langle q^\dagger\lambda_8 q\rangle = -\frac{\partial\Omega_{\rm MF}}{\partial\mu_8}, \tag{7b}$$

and the electric charge density

$$n_Q = \langle q^\dagger Q q\rangle - n_e - n_\mu = -\frac{\partial\Omega_{\rm MF}}{\partial\mu_Q}. \tag{8}$$

Here, $Q = {\rm diag}_f(\frac{2}{3},-\frac{1}{3},-\frac{1}{3})$ and n_e (n_μ) is the number density of electrons (muons). Consequently, the quark chemical potential matrix, $\hat{\mu}$, is

$$\hat{\mu} = \mu + Q\mu_Q + \lambda_3\mu_3 + \lambda_8\mu_8, \tag{9}$$

where μ is the quark number chemical potential, μ_Q the (positive) electric charge chemical potential, and μ_3 and μ_8 are color charge chemical potentials. The quark number density is related to the baryon number density by

$$n_B = \frac{n}{3}. \tag{10}$$

The remaining two charges are the number densities of the lepton families

$$n_{L_e} = n_e + n_{\nu_e} = -\frac{\partial\Omega_{\rm MF}}{\partial\mu_{L_e}}, \tag{11a}$$

$$n_{L_\mu} = n_\mu + n_{\nu_\mu} = -\frac{\partial\Omega_{\rm MF}}{\partial\mu_{L_\mu}}, \tag{11b}$$

which are conserved when the neutrinos are trapped in the system and oscillations are neglected. Electrons and muons have both electric charge and lepton number, while neutrinos have lepton number only. Therefore

$$\mu_e = \mu_{L_e} - \mu_Q, \tag{12a}$$

$$\mu_\mu = \mu_{L_\mu} - \mu_Q, \tag{12b}$$

$$\mu_{\nu_e} = \mu_{L_e}, \tag{12c}$$

$$\mu_{\nu_\mu} = \mu_{L_\mu}. \tag{12d}$$

The lepton fractions, which represent the relative number of leptons and baryons, are defined as

$$Y_{L_e} \equiv \frac{n_{L_e}}{n_B}, \tag{13a}$$

$$Y_{L_\mu} \equiv \frac{n_{L_\mu}}{n_B}. \tag{13b}$$

Bulk matter in compact stars should be charge neutral. In NJL models there are no gauge fields that neutralize the color charge dynamically, because the gluons are replaced by effective point-like $\bar{q}q$ and qq interactions. Color neutrality must therefore be enforced by solving for the charge chemical potentials, μ_3 and μ_8, such that the corresponding charge densities, $n_a = \langle q^\dagger\lambda_a q\rangle$, are zero. In addition, matter in compact stars should be electrically neutral and in β-equilibrium with respect to weak interactions. The chemical potentials, μ_Q, μ_3, and μ_8 are therefore determined such that the charge densities (7)-(8) vanish

$$\frac{\partial\Omega_{\rm MF}}{\partial\mu_Q} = \frac{\partial\Omega_{\rm MF}}{\partial\mu_3} = \frac{\partial\Omega_{\rm MF}}{\partial\mu_8} = 0. \tag{14}$$

Observe that the definition of the quark chemical potential (9) implies that matter is in β-equilibrium. This holds true also when neutrinos are trapped and $\mu_{L_l} > 0$, because, *e.g.*, $\mu_e + \mu_{\bar{\nu}_e} = (\mu_{L_e} - \mu_Q) + (-\mu_{L_e}) = -\mu_Q$.

The gaps, ϕ_i and Δ_{ij}, are order parameters that are determined by minimization of the mean-field thermodynamic potential (3)

$$\frac{\partial\Omega_{\rm MF}}{\partial\phi_u} = \frac{\partial\Omega_{\rm MF}}{\partial\phi_d} = \frac{\partial\Omega_{\rm MF}}{\partial\phi_s} = 0, \tag{15a}$$

$$\frac{\partial\Omega_{\rm MF}}{\partial\Delta_{ud}} = \frac{\partial\Omega_{\rm MF}}{\partial\Delta_{us}} = \frac{\partial\Omega_{\rm MF}}{\partial\Delta_{ds}} = 0. \tag{15b}$$

Local minima of the thermodynamic potential define competing phases and the global minimum is the physical solution. At the charge neutral global minimum of the thermodynamic potential, the pressure, entropy density, number densities, and energy density are

$$P(T,\mu,\mu_{L_e},\mu_{L_\mu}) = -\Omega_{\rm MF}, \tag{16a}$$

$$s(T,\mu,\mu_{L_e},\mu_{L_\mu}) = -\frac{\partial\Omega_{\rm MF}}{\partial T}, \tag{16b}$$

$$n_a(T,\mu,\mu_{L_e},\mu_{L_\mu}) = -\frac{\partial\Omega_{\rm MF}}{\partial\mu_a}, \tag{16c}$$

$$\epsilon(T,\mu,\mu_{L_e},\mu_{L_\mu}) = -P + Ts + \sum_{a=B,L_e,L_\mu}\mu_a n_a. \tag{16d}$$

The sum in the expression for the energy density should account for all conserved charges in the system. However, because we require that $n_Q = n_3 = n_8 = 0$, only three terms are included.

Once the current quark masses, coupling constants, and momentum regularization method has been fixed, equations (2)-(5), (9), and (14)-(16) define a self-consistent set of equations for the quark matter model.

A. Numerical methods

The quark quasiparticle dispersion relations, $E_a(p)$, in (3) are eigenvalues of Hermitian matrices, see [20] for details. LAPACK is used to calculate the eigenvalues and the corresponding eigenvectors of these matrices. For given values of all parameters, the mean-field thermodynamic potential (3) is calculated with a Gaussian integration quadrature. Observe that the interactions depend only on the magnitude of the three-momentum, so $d^3p \to 4\pi p^2 dp$.

The derivatives of the thermodynamic potential are explicitly calculated using the eigenvectors of the Hermitian matrices. The derivatives are on the form

$$\frac{\partial\Omega_{\rm MF}}{\partial x} = F_1(x) - \int\frac{d^3p}{(2\pi)^3}\sum_{a=1}^{18}F_2\left(\frac{\partial E_a(p)}{\partial x}\right), \tag{17}$$

for some simple functions F_1 and F_2 that depend on the choice of the variable x. The numerical problem therefore is to calculate the derivatives of the quasiparticle dispersion relations, $E_a(p)$, *i.e.*, the derivatives of the eigenvalues of the Hermitian matrices. It is easy to show that

$$\frac{\partial E_a}{\partial x} = \frac{X_a^\dagger\frac{\partial H}{\partial x}X_a}{X_a^\dagger X_a}, \tag{18}$$

where X_a is the eigenvector associated to an eigenvalue E_a of a Hermitian matrix H. The derivatives of the Hermitian matrices are sparse and all derivatives of the thermodynamic potential are therefore obtained practically at the cost of computing the eigenvectors. The integrands of all derivatives and the thermodynamic potential are calculated in parallel and the momentum integrals are evaluated simultaneously to reduce computational redundancy. The gap and charge neutrality equations (14)-(15) are solved with a modified Newton method in multidimensions, *i.e.*, essentially a steepest descent method, for different starting points in parameter space. The solution with the highest pressure is used. The results thereby obtained, and the consequences for the properties of quark stars are discussed in the next Section.

III. RESULTS

We use the same parametrization of the quark matter model as in [20]

$$m_{u,d} = 5.5\text{ MeV}, \tag{19a}$$

$$m_s = 112.0\text{ MeV}, \tag{19b}$$

$$G_S\Lambda^2 = 2.319, \tag{19c}$$

$$\Lambda = 602.3\text{ MeV}. \tag{19d}$$

The relative diquark coupling strength, η, is considered as a free parameter of the model. Here we present results for $\eta = 0.75$ (intermediate coupling), which is the vacuum result obtained by a Fierz transformation, and $\eta = 1.0$ (strong coupling), which is motivated by the phenomenology of compact stars and heavy ion collisions [25]. Quark matter phases are characterized by the order parameters, ϕ_i and Δ_{ij}. In particular, the following phases have been identified in the numerical investigation of the model

2SC phase: $\Delta_{us} = \Delta_{ds} = 0$ and $\Delta_{ud} \neq 0$,
uSC phase: $\Delta_{ds} = 0$ and $\Delta_{ud} \neq 0$, $\Delta_{us} \neq 0$,
dSC phase: $\Delta_{us} = 0$ and $\Delta_{ud} \neq 0$, $\Delta_{ds} \neq 0$,
CFL phase: $\Delta_{ud} \neq 0$, $\Delta_{us} \neq 0$, and $\Delta_{ds} \neq 0$.

In addition, gapless phases exist, which are characterized by the presence of one or more quasiparticle dispersion relations that have no forbidden energy band above the Fermi surface. Such excitations exist when the differences between the Fermi momenta and/or the renormalized masses of the paired quarks are sufficiently large [26]. We denote gapless phases with a leading "g", *e.g.*, g2SC for the gapless 2SC phase.

In the following we present results for two different neutrino untrapping scenarios. In one case the initial state is a hot, $T = 40$ MeV, quark core with trapped neutrinos, $\mu_{\nu_e} = 200$ MeV. The core cools rapidly by neutrino emission and a cold, $T \sim 1$ MeV, configuration with trapped neutrinos, $\mu_\nu = 200$ MeV, forms. The mass defect due to cooling is obtained by comparing the masses of these

two states for configurations of equal baryon number. At low temperature, $T \sim 1$ MeV, the mean-free path of neutrinos increases and becomes comparable to the size of the core/star. The neutrinos therefore escape and the final state is a cold, $T \sim 1$ MeV, star with $\mu_\nu = 0$. The mass defect due to neutrino untrapping is obtained by comparing the masses of $\mu_\nu = 200$ MeV, $T \sim 1$ MeV configurations with the masses of $\mu_\nu = 0$, $T \sim 1$ MeV configurations of equal baryon number. The "final" state will continue to cool for millions of years with practically no effect on its structure, because temperatures below 1 MeV have negligible effects on the quark matter EoS. Phase diagrams for intermediate and strong coupling are provided for matter with trapped and untrapped neutrinos. The second case has a more "conventional" initial state, characterized by a fixed lepton number, $Y_{L_e} = 0.4$, and entropy per baryon, $s/n_B = 1 - 2$.

A. Order parameters at fixed μ

For the calculation of quark matter phase diagrams in the plane of temperature and quark (or baryon) number chemical potential, the gap equations for the order parameters of the model (the masses, M_i, and diquark gaps, Δ_{ij}) are solved selfconsistently. The values of the order parameters characterize the different quark matter phases, as described above. In addition to solving the gap equations, the color and electric charge neutrality conditions are enforced by solving for the corresponding chemical potentials (μ_Q, μ_3, μ_8), for given values of the quark number chemical potential, μ, and temperature, T. In Figs. 1-4, the quark masses (upper row), diquark gaps (second row), chemical potentials (third row) and densities of baryon number, electrons and muons (bottom row) are plotted vs. the temperature for three different values of the quark number chemical potential (columns). The four Figures represent solutions without ($\mu_\nu = 0$) and with ($\mu_\nu = 200$ MeV) trapped neutrinos for intermediate ($\eta = 0.75$) and strong ($\eta = 1.0$) coupling, respectively. Here we use the more compact notation

$$\mu_\nu \equiv \mu_{\nu_e} = \mu_{L_e}, \tag{20}$$

for the electron neutrino chemical potential, because the muon neutrino chemical potential is zero as neutrino oscillations are neglected. Note the gapless constraints, Δ^g_{ij}, that are included in the second row of these Figures. If $\Delta_{ij} \leq \Delta^g_{ij}$, the corresponding quasiparticle has a gapless dispersion relation, *i.e.*, when this condition is met there is no forbidden energy band above the Fermi surface. Typically, the gapless conditions are fulfilled only near the critical temperature ($60 - 70$ MeV for intermediate coupling and $100 - 110$ MeV for strong coupling), where the gaps go to zero in a second order phase transition to a non-superconducting state. Since these temperatures are well above the maximum temperature relevant for PNS, we can neglect gapless phases in our discussion.

B. Order parameters at fixed Y_{L_e} and s/n_B

Next we consider a system with fixed values of the lepton fraction, $Y_{L_e}(T, \mu_\nu) = 0.4$, and the entropy per baryon, $s(T, \mu_\nu)/n_B(T, \mu_\nu) = 1,\ 2$. Consequently, for a given value of the quark number chemical potential, μ, the temperature and electron neutrino chemical potential are determined such that $Y_{L_e} = 0.4$ and $s/n_B = 1$ (or 2). These two equations are solved in parallel with the gap and charge neutrality equations. In Fig. 5 the temperature, constituent quark masses, charge chemical potentials, neutrino chemical potential, gaps, and number densities are plotted vs. the quark number chemical potential for charge neutral quark matter in β-equilibrium at intermediate coupling, $\eta = 0.75$. Fig. 6 shows the same relationships for strong coupling, $\eta = 1$.

C. Equations of state

The equation of state (EoS), $\epsilon(P)$, can be calculated using (16), *e.g.*, for different values of the temperature, T, and lepton number chemical potential, $\mu_{L_e} = \mu_\nu$, or for fixed values of lepton fraction, $Y_{L_e}(T, \mu_{L_e})$, and the entropy per baryon, $s(T, \mu_{L_e})/n_B(T, \mu_{L_e})$, depending on the application. In Figs. 7-8 the EoS for three different pairs of (μ_ν, T) values are plotted for intermediate, $\eta = 0.75$, and strong, $\eta = 1.0$, coupling, respectively. The discontinuities appear at the 2SC-CFL phase transition due to the Maxwell construction, which results in a jump of the energy density at fixed pressure. When increasing T and/or μ_ν, the pressure at the transition increases. Fig. 9 shows the EoS for a fixed lepton fraction, $Y_{L_e}(T, \mu_\nu) = 0.4$, and two values of entropy per baryon, $s(T, \mu_\nu)/n_B(T, \mu_\nu) = 1$ and 2, for intermediate and strong coupling. When increasing the entropy per baryon, the pressure at the transition increases, whereas an increase of the coupling strength lowers it.

D. Quark star sequences

Given an EoS described in the previous Section, the corresponding compact star sequence is calculated by solving the Tolman-Oppenheimer-Volkoff equations for a static spherically symmetric object

$$\frac{dP(r)}{dr} = -\frac{[\epsilon(r) + P(r)][m(r) + 4\pi r^3 P(r)]}{r[r - 2m(r)]}, \tag{21a}$$

$$m(r) = 4\pi \int_0^r \varepsilon(r') r'^2 dr', \tag{21b}$$

for different values of the central pressure. Due to the thermal pressure, the high-temperature EsoS do not extend to zero pressure. The surface of hot configurations is therefore defined to be the point where the (approximate) chiral symmetry is broken by a first order phase transition into the χSB phase.

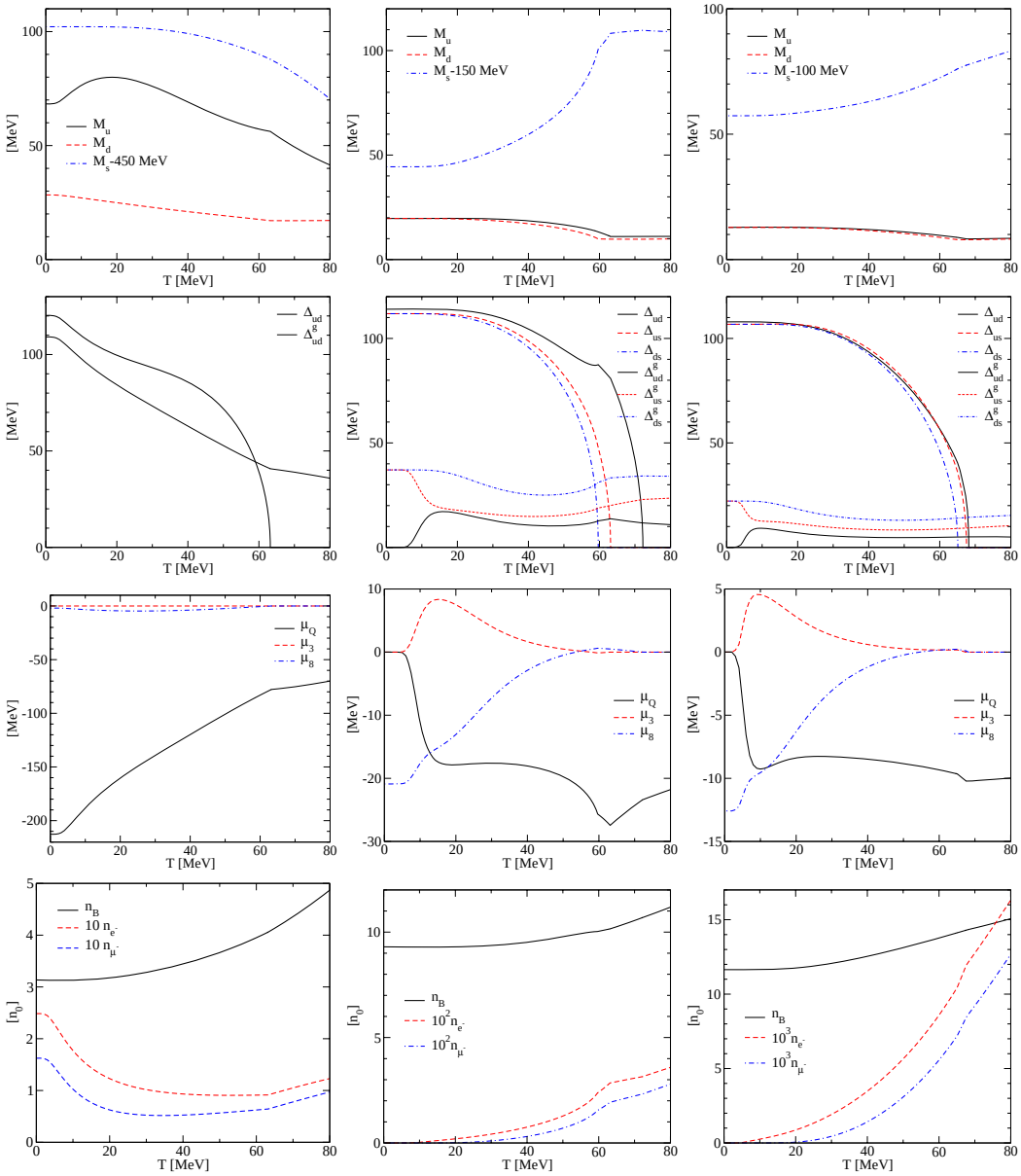

FIG. 1: (Color online) The constituent quark masses, gaps, charge chemical potentials, and number densities of charge neutral quark matter in β-equilibrium with untrapped neutrinos, $\mu_\nu = 0$, at intermediate coupling, $\eta = 0.75$. The three columns (from left to right) represent solutions for $\mu = 400$, 500, and 550 MeV. Δ^g_{ij} are thresholds for the existence of gapless excitations [26], *i.e.*, gapless excitations exist if $\Delta_{ij} \leq \Delta^g_{ij}$.

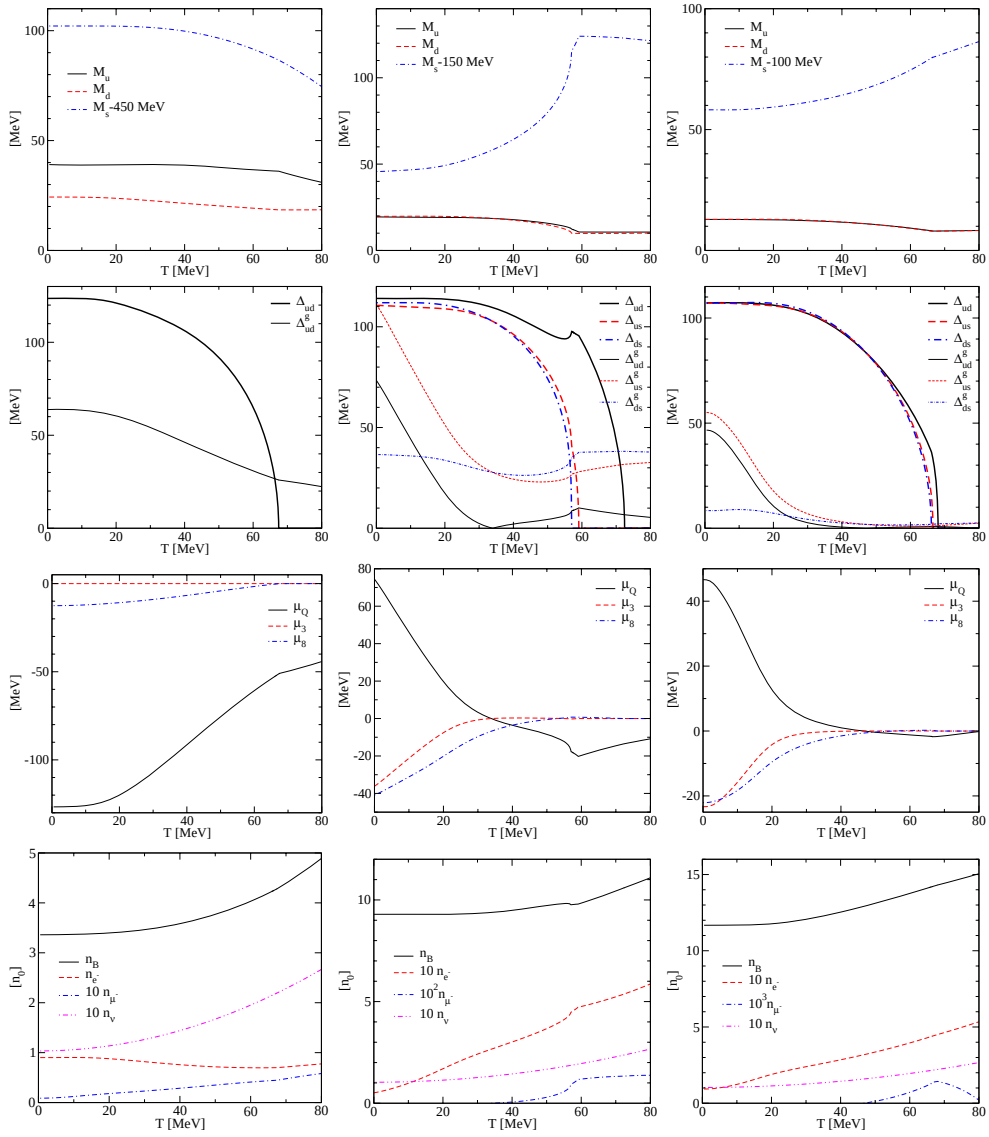

FIG. 2: (Color online) The constituent quark masses, gaps, charge chemical potentials, and number densities of charge neutral quark matter in β-equilibrium with trapped neutrinos, $\mu_\nu = 200$ MeV, at intermediate coupling, $\eta = 0.75$. Line styles as in Fig. 1.

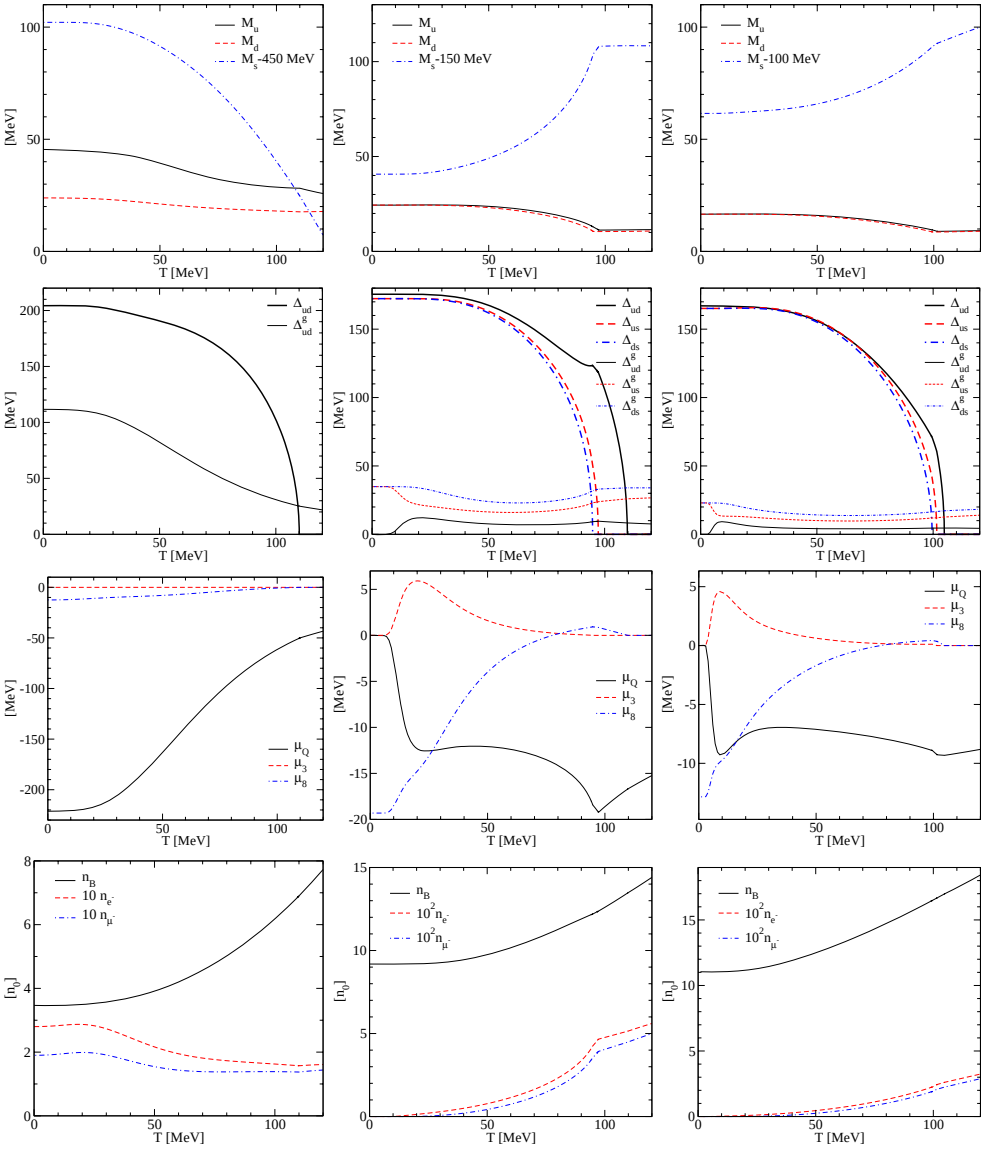

FIG. 3: (Color online) The constituent quark masses, gaps, charge chemical potentials, and number densities of charge neutral quark matter in β-equilibrium with untrapped neutrinos, $\mu_\nu = 0$, at strong coupling, $\eta = 1.0$. Line styles as in Fig. 1.

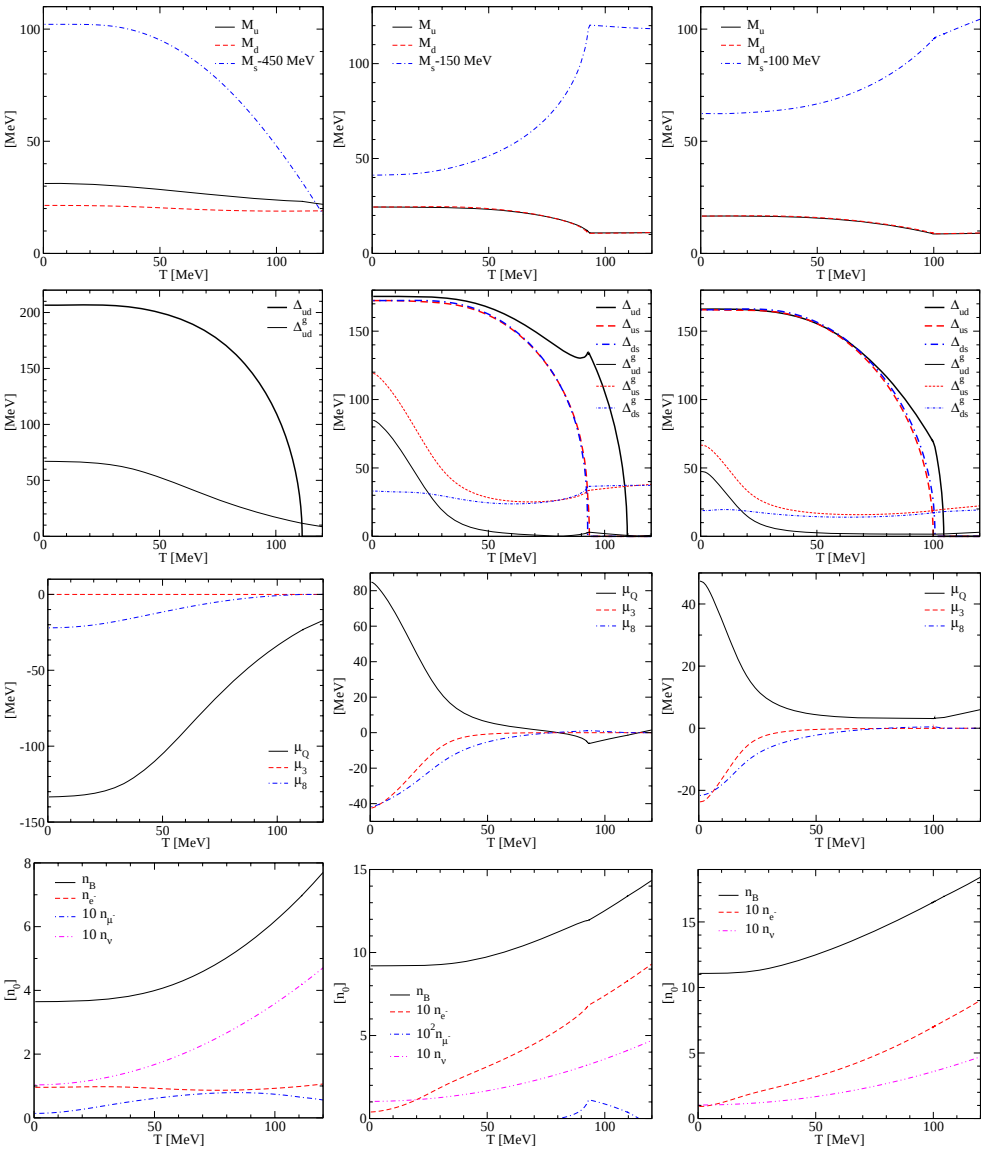

FIG. 4: (Color online) The constituent quark masses, gaps, charge chemical potentials, and number densities of charge neutral quark matter in β-equilibrium with trapped neutrinos, $\mu_\nu = 200$ MeV, at strong coupling, $\eta = 1.0$. Line styles as in Fig. 1.

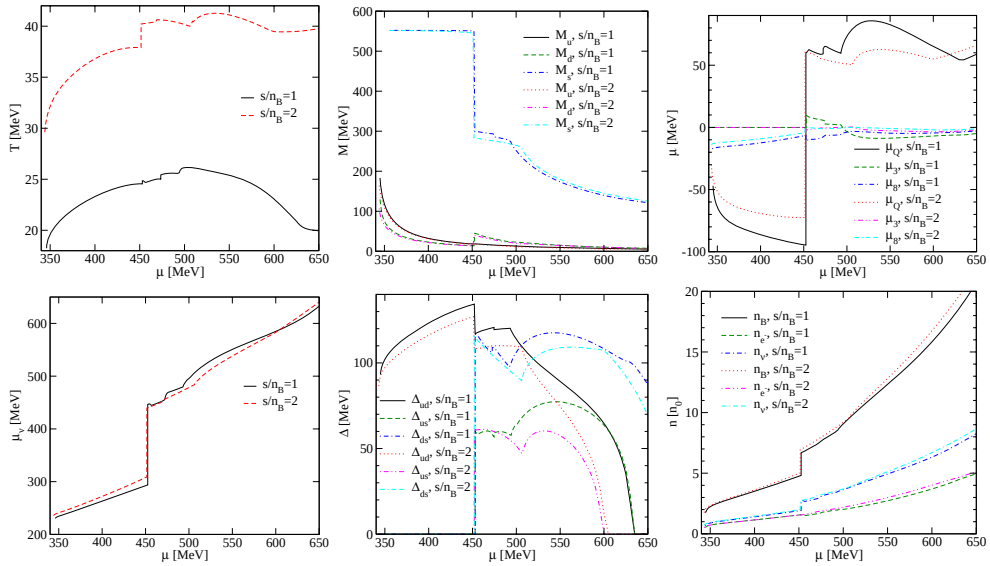

FIG. 5: (Color online) The temperature, constituent quark masses, charge chemical potentials, neutrino chemical potential, gaps, and number densities of charge neutral quark matter in β-equilibrium at intermediate coupling ($\eta = 0.75$) for fixed lepton fraction $Y_{L_e}(T, \mu_\nu) = 0.4$, and two values of the entropy per baryon, $s(T, \mu_\nu)/n_B(T, \mu_\nu) = 1,\ 2$.

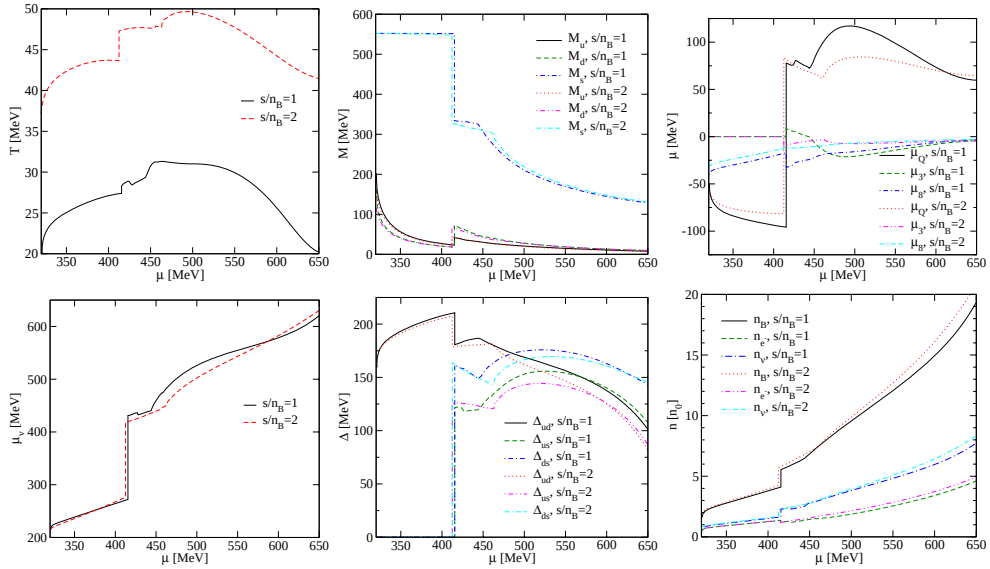

FIG. 6: (Color online) The same as Fig. 5, but at strong coupling, $\eta = 1$.

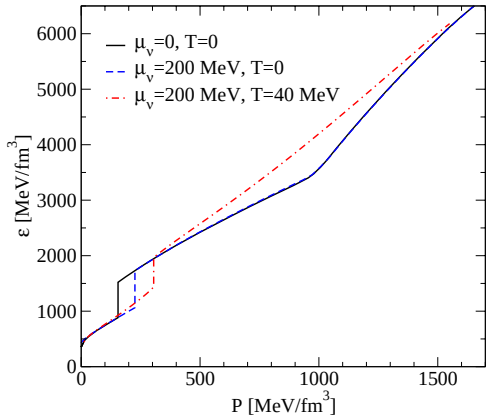

FIG. 7: (Color online) The equation of state for charge neutral quark matter in β-equilibrium at intermediate coupling, $\eta = 0.75$, and fixed values of the temperature and electron neutrino chemical potential. The discontinuities appear at the 2SC-CFL phase transition due to the Maxwell construction, see text.

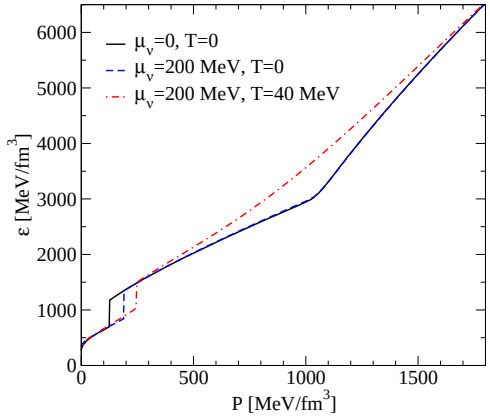

FIG. 8: (Color online) The equation of state for charge neutral quark matter in β-equilibrium at strong coupling, $\eta = 1.0$, and fixed values of the temperature and electron neutrino chemical potential.

In Fig. 10 the quark star sequences for intermediate coupling, $\eta = 0.75$, and fixed (μ_ν, T) values are plotted. The discontinuity at the maximum mass configuration is a consequence of the appearance of CFL matter in the center of the stars. Stars with a CFL core are marginally stable and exist if T and μ_ν are not too high, see Fig. 14 in the following Subsection. Increasing the coupling to $\eta = 1.0$ leads to an interesting situation, shown in Fig. 11. There is a small interval of star masses at $M \sim 1.3$ $M_\odot$ for which mass twins occur: pure 2SC quark stars have

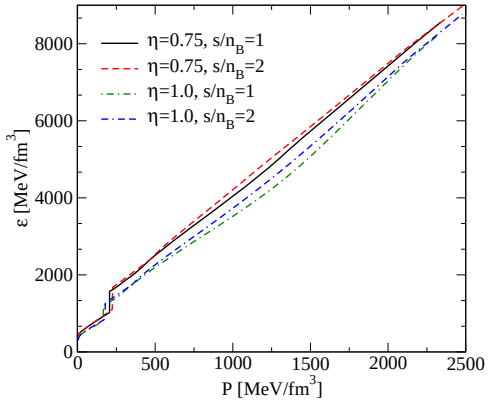

FIG. 9: (Color online) The equation of state for charge neutral quark matter in β-equilibrium for fixed values of the lepton fraction, $Y_{Le}(T, \mu_\nu) = 0.4$, and the entropy per baryon, $s(T, \mu_\nu)/n_B(T, \mu_\nu)$.

stable, high-density mass isomers with a CFL quark core and a smaller radius. Fig. 11 suggests an interesting scenario: upon mass accretion, a 2SC star could undergo a phase transition to its more compact twin with a CFL core, whereby binding energy is released. However, the presence of a hadronic crust could render the twin configurations unstable and this scenario therefore remains to be investigated thoroughly. In Fig. 12 we show the star sequences corresponding to the EsoS in Fig. 9 with fixed entropy per baryon (1 or 2) and fixed lepton fraction $Y_{Le} = 0.4$. While the increase of coupling strength increases the maximum mass and the radius of the stars, both values of the entropy per baryon produce rather similar star sequences. A finite entropy per baryon of $1-2$ correspond to rather high temperatures that do not allow for stable CFL cores. In Fig. 13 the radial dependence of the temperature and baryon number density in PNS are illustrated for fixed values of the lepton fraction and entropy per baryon. These configurations, which resemble realistic PNS formed in the adiabatic compression of the cores in massive stars, have approximately constant temperature and neutrino chemical potential in their interior. Consequently, at the qualitative level the initial state of a PNS can be modelled by a fixed initial temperature, $T(r) = T$, and neutrino chemical potential, $\mu_\nu(r) = \mu_\nu$. This result justifies the alternative neutrino trapping/untrapping scenario considered in this paper.

E. Phase diagrams

Next we present for the first time the central temperatures and quark number chemical potentials of stable quark star solutions in the phase diagrams of quark matter, with and without neutrino trapping. In Figs. 14-

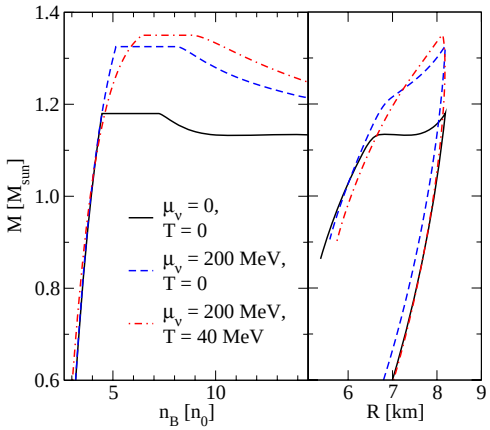

FIG. 10: (Color online) Quark star sequences for intermediate coupling, $\eta = 0.75$, and fixed values of the temperature and electron neutrino chemical potential. The discontinuity at the maximum mass configuration is a consequence of the appearance of CFL matter in the center of the stars. Stars with a CFL core are marginally stable and exist if the temperature and neutrino chemical potential are not too high, see Fig. 14.

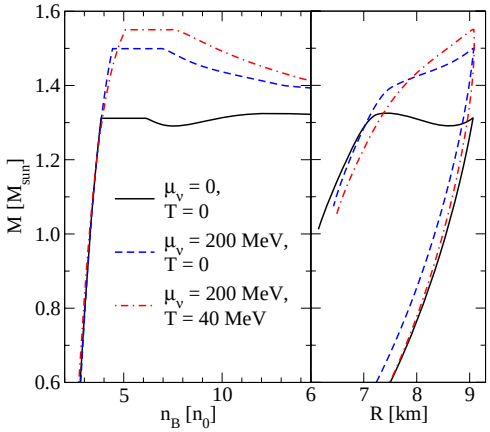

FIG. 11: (Color online) Quark star sequences for the strong coupling, $\eta = 1.0$, and fixed values of the temperature and electron neutrino chemical potential. Stable stars with a CFL core exist if the temperature and neutrino chemical potential are not too high, see Fig. 15.

15 the phase diagrams of charge neutral quark matter in β-equilibrium are shown for intermediate, $\eta = 0.75$, and strong, $\eta = 1$, coupling and for two different values of the electron neutrino chemical potential, $\mu_\nu = 0$ and 200 MeV.

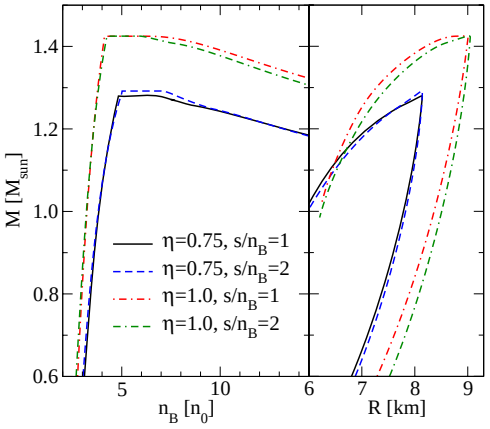

FIG. 12: (Color online) Quark star sequences for fixed values of the lepton fraction, $Y_{L_e}(T, \mu_\nu) = 0.4$, and the entropy per baryon, $s(T, \mu_\nu)/n_B(T, \mu_\nu)$. Stars with a CFL core are unstable (marginally unstable for $\eta = 1$).

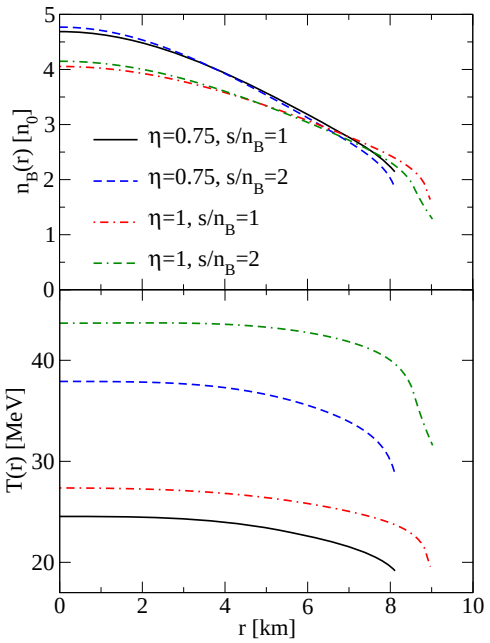

FIG. 13: (Color online) The temperature and baryon number density vs. the coordinate radius of four different quark star solutions, for fixed values of the lepton fraction, $Y_{L_e}(T, \mu_\nu) = 0.4$, and the entropy per baryon, $s(T, \mu_\nu)/n_B(T, \mu_\nu)$. The mass of these quark star solutions is 1.25 $M_\odot$ (1.4 $M_\odot$) for intermediate (strong) coupling.

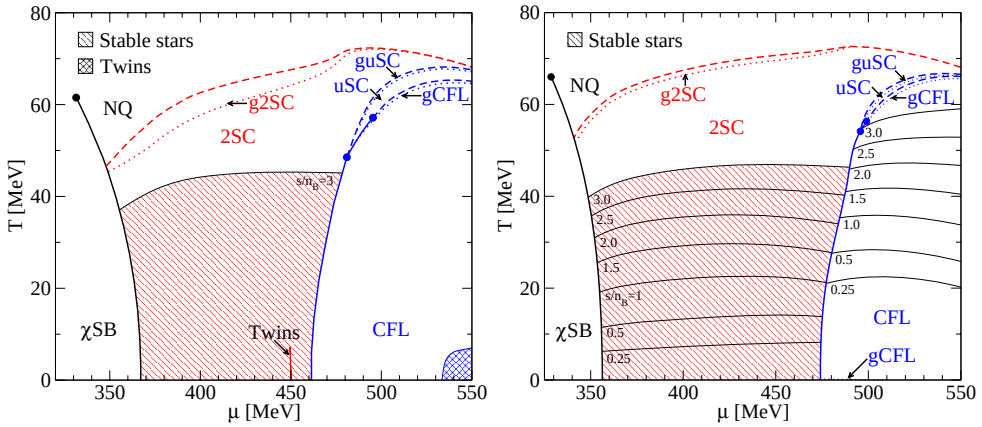

FIG. 14: (Color online) Phase diagrams of charge neutral quark matter in β-equilibrium at intermediate coupling, $\eta = 0.75$, for fixed values of the electron neutrino chemical potential, $\mu_\nu = 0$ (left-hand side) and $\mu_\nu = 200$ MeV (right-hand side). First-order phase transition boundaries are indicated by bold solid lines, while bold dashed lines represent second-order phase boundaries. The dotted lines indicate gapless phase boundaries and the thin solid lines are level curves of constant entropy per baryon. Hatched regions represent stable compact star solutions, with central quark number chemical potential $\mu(r = 0) = \mu$ and temperature $T(r = 0) = T$. The cross-hatched regions correspond to baryon number twins, *i.e.*, for these values of $\mu(r = 0)$ and $T(r = 0)$ there exist stable 2SC stars and 2SC-CFL stars with equal baryon number.

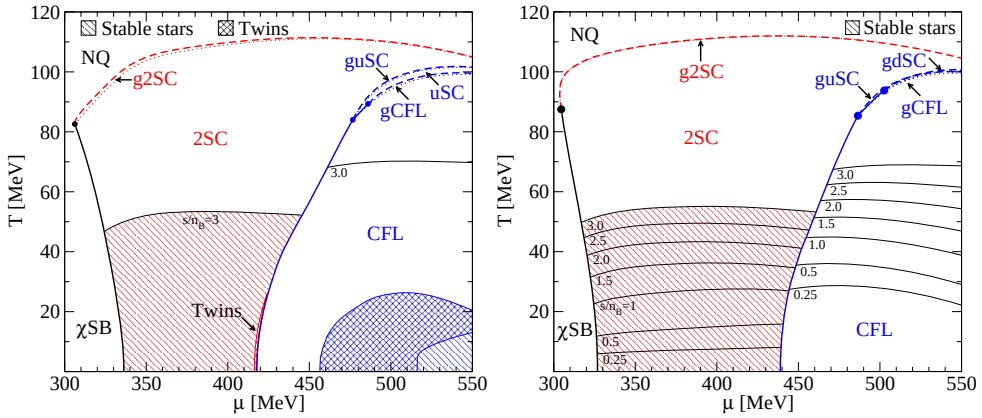

FIG. 15: (Color online) Phase diagrams of charge neutral quark matter in β-equilibrium at strong coupling, $\eta = 1.0$, for fixed values of the electron neutrino chemical potential, $\mu_\nu = 0$ (left-hand side) and $\mu_\nu = 200$ MeV (right-hand side). Line styles as in Fig. 14.

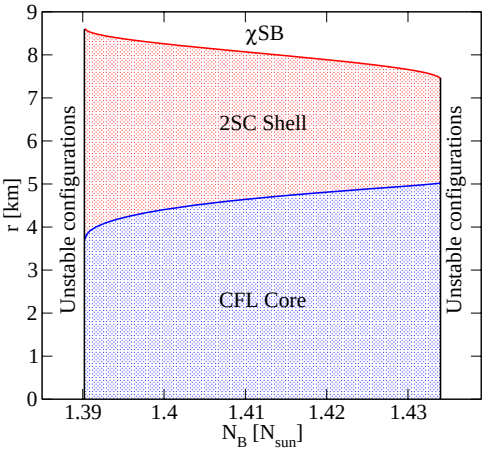

FIG. 16: (Color online) Radial phase structure of final states with CFL cores at strong coupling, $\eta = 1.0$. The $T = 0$, $\mu_\nu = 0$ compact star sequence in Fig. 11 has a branch of stable stars with CFL cores, this Figure shows the radial phase structure of these stars.

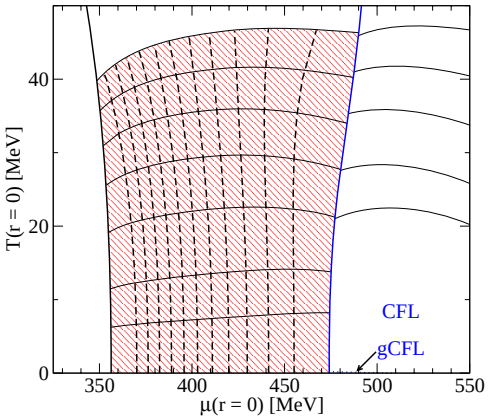

FIG. 17: (Color online) Cooling of PNS with trapped neutrinos, $\mu_\nu = 200$ MeV, at intermediate coupling, $\eta = 0.75$. The dashed lines indicate the central temperature and quark number chemical potential of configurations with fixed baryon number, $N = 0.2,\ 0.3,\ 0.4,\ \ldots, 1.2\ \mathrm{N}_\odot$. Solid lines indicate phase boundaries and level curves of constant entropy per baryon, see Fig. 14.

As an upper limit estimate for the initial core temperatures of quark stars we show the lines corresponding to an entropy per baryon of 3, which in the 2SC phase leads to a maximum temperature of ~ 40 MeV (~ 50 MeV) for intermediate (strong) coupling. For sufficiently high neutrino chemical potentials, quark stars with a CFL core are unstable. In particular, by comparing the left-hand ($\mu_\nu = 0$) and right-hand ($\mu_\nu = 200$ MeV) panels of Fig. 15 it is clear that stars with a CFL core are rendered unstable by the finite neutrino chemical potential. For a typical value of $\mu_\nu = 200$ MeV, which should be realized in the evolution of a PNS core [3, 4], we find no stable CFL cores. Note that the discussion of star temperatures exceeding the neutrino opacity temperature, $T_c \sim 1$ MeV, makes sense only during the PNS era, *i.e.*, when neutrinos are trapped and the neutrino chemical potential is finite. Consequently, the region of stable CFL core stars shown in the panel on the left-hand side of Fig. 15 may not be realized at all during stages of hot PNS (quark star) evolution. We will return to this issue in the next Subsection.

For temperatures below T_c, we find a range of baryon numbers $N_B = 1.39 - 1.43(5)\ \mathrm{N}_\odot$, for which quark stars with a CFL core and a 2SC shell are stable. The phase structure of these stars is illustrated in Fig. 16. Gapless phases of superconducting quark matter exist for both coupling strengths, at temperatures well above those of relevance for the cores of PNS, see Figs. 14-15. The gapless phases can therefore be neglected in the present discussion of PNS evolution [27].

F. Cooling evolution and untrapping transition

In this Subsection we consider a scenario of quark star cooling where the baryon number of the stars is conserved, *i.e.*, we assume that there are no accretion or non-thermal mass loss. In Figs. 17-18 we show the cooling evolution of PNS configurations in the phase diagrams of quark matter with trapped neutrinos, $\mu_\nu = 200$ MeV, for intermediate and strong coupling. The dashed lines indicate the central temperature and quark number chemical potential of configurations with fixed baryon number. The vertical solid lines indicate phase boundaries of the 2SC phase, while the horizontal lines denote curves of constant entropy per baryon. We observe that, as long as the neutrino chemical potential remains fixed, the cooling trajectories that start from stable configurations remain inside the region of stability. The reverse, however, does not hold. Upon heating, a configuration close to the CFL phase border may become unstable at high temperature. See, *e.g.*, the trajectory for $N = 1.6\ \mathrm{N}_\odot$ in Fig. 18.

Another instability occurs during the cooling evolution when a star reaches the neutrino opacity temperature, $T_c \sim 1$ MeV, and neutrinos start leaving the system. In this untrapping transition the neutrino chemical potential goes to zero and the phase diagram and phase structure of the configurations change accordingly. Cooling trajectories that are close to the CFL phase border above T_c continues within the CFL-twin region below it, *i.e.*, conservation of baryon number requires that the phase structure of these stars change near T_c. Leaving aside the details of the untrapping transition itself, we

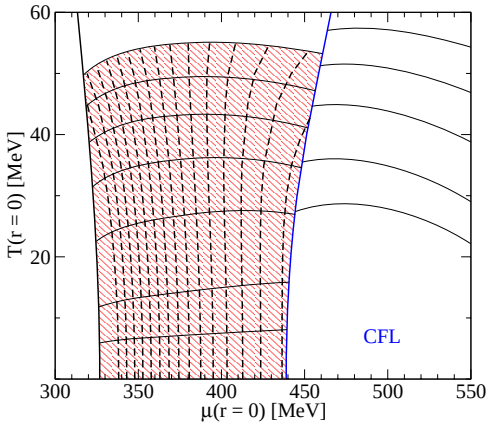

FIG. 18: (Color online) Cooling of PNS with trapped neutrinos, $\mu_\nu = 200$ MeV, at strong coupling, $\eta = 1.0$. The dashed lines indicate the central temperature and quark number chemical potential of configurations with fixed baryon number, $N = 0.2,\ 0.3,\ 0.4,\ \ldots, 1.6\ \mathrm{N}_\odot$. Solid lines indicate phase boundaries and level curves of constant entropy per baryon, see Fig. 15.

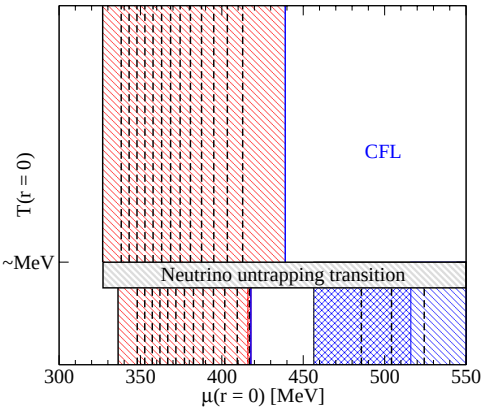

FIG. 19: (Color online) Neutrino untrapping transition at strong coupling, $\eta = 1.0$. The dashed lines in the 2SC phase (See Fig. 15) indicate the central temperature and quark number chemical potential of configurations with fixed baryon number, $N = 0.2,\ 0.3,\ 0.4,\ \ldots, 1.4\ \mathrm{N}_\odot$. Above the critical temperature, $T_c \sim 1$ MeV, of the neutrino untrapping transition the neutrino mean free path is shorter than the size of the stars and μ_ν is therefore fixed at 200 MeV. This corresponds to cold PNS with trapped neutrinos. At T_c the mean free path of the neutrinos is similar to the size of the stars and $\mu_\nu \to 0$. The central baryon number chemical potential of configurations with fixed baryon number increases in the untrapping transition. When the neutrinos have escaped there are stable 2SC stars for $N \lesssim 1.41\ \mathrm{N}_\odot$ and stable stars with a CFL core for $1.39\ \mathrm{N}_\odot \lesssim N \lesssim 1.43\ \mathrm{N}_\odot$. The dashed lines in the CFL phase indicate the central temperature and quark number chemical potential of configurations with fixed baryon number, $N = 1.4,\ 1.41,\ 1.42\ \mathrm{N}_\odot$. The configurations with $N = 1.4$ and $1.41\ \mathrm{N}_\odot$ are CFL baryon number twins, *i.e.*, for these baryon numbers there exist also pure 2SC stars. See Fig. 15 and Fig. 21 for further information.

illustrate this situation in Figs. 19-20 for strong and intermediate coupling, respectively. In these figures, the phase diagram above (below) T_c represents quark matter with trapped (untrapped) neutrinos. We now discuss the strong coupling case illustrated in Fig. 19 in more detail. At T_c the mean free path of the neutrinos is similar to the size of the stars and $\mu_\nu \to 0$. The central quark (or baryon) number chemical potential of configurations with fixed baryon number increases in the untrapping transition. When the neutrinos have escaped there are stable 2SC stars for $N \lesssim 1.41\ \mathrm{N}_\odot$ and stable stars with a CFL core for $1.39\ \mathrm{N}_\odot \lesssim N \lesssim 1.43\ \mathrm{N}_\odot$. The dashed lines in the CFL phase indicate the central temperature and quark number chemical potential of configurations with fixed baryon number, $N = 1.4,\ 1.41,\ 1.42\ \mathrm{N}_\odot$. The configurations with $N = 1.4$ and $1.41\ \mathrm{N}_\odot$ are CFL baryon number twins, *i.e.*, for these baryon numbers there exist also pure 2SC stars.

For intermediate coupling, shown in Fig. 20, there is only a narrow interval of baryon numbers for which a transition to marginally stable CFL baryon number twins is possible during untrapping. These baryon numbers are not shown in that Figure.

G. Mass defects due to cooling and neutrino untrapping

The cooling evolution of a hot PNS from $T \sim 40$ MeV to $T_c \sim 1$ MeV and the subsequent neutrino untrapping transition entail significant changes to the EoS and the structure of the star. This results in a decrease of the gravitational mass. The mass defect, *i.e.*, the difference of the gravitational masses before and after the cooling and/or untrapping transition corresponds to the energy that is released from the star, predominantly by neutrino emission. A fraction of the neutrinos might, however, be converted into photons that give rise to a gamma- or X-ray burst. The PNS cool rapidly by neutrino emission. A few seconds after birth the stars are cold on the nuclear scale ($T \sim 1$ MeV) and further cooling has no direct impact on their structure. However, the neutrino mean-free path is sensitive to the temperature. Below some critical temperature (~MeV) the neutrinos that are trapped in the PNS escape and this has an effect on the structure. In Figs. 21-22 the energy release is estimated from the mass defects due to cooling and neutrino untrapping for strong coupling and two different values of the baryon number.

In Figs. 23-24 the energy release due to cooling and

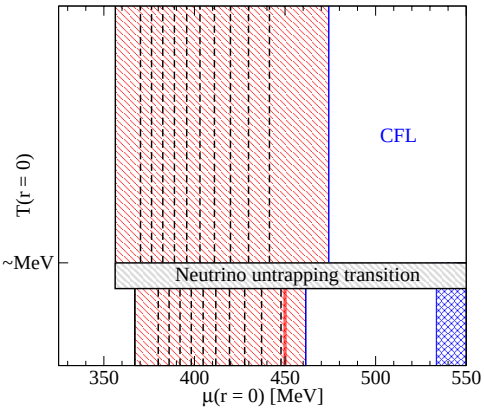

FIG. 20: (Color online) Neutrino untrapping transition at intermediate coupling, $\eta = 0.75$. The dashed lines indicate the central temperature and quark number chemical potential of configurations with fixed baryon number, $N = 0.2,\ 0.3,\ 0.4,\ \ldots, 1.1\ \mathrm{N}_\odot$. CFL baryon number twins are marginally stable and exist only for a narrow interval of baryon numbers. They are therefore omitted. For further information, see Fig. 14 and Fig. 19.

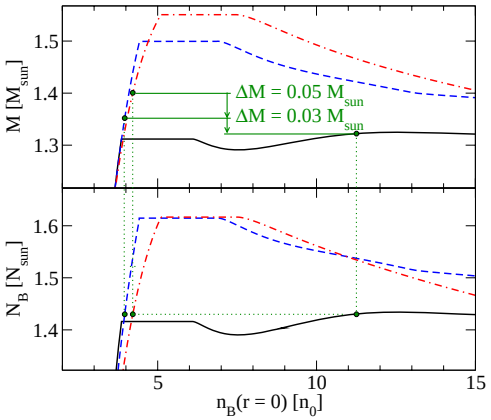

FIG. 21: (Color online) The mass defect due to cooling and neutrino untrapping at strong coupling, $\eta = 1.0$. The dash-dotted line represents the sequence of hot ($T = 40$ MeV) PNS with trapped neutrinos ($\mu_\nu = 200$ MeV). The PNS cool rapidly by neutrino emission. A few seconds after birth the stars are cold on the nuclear scale ($T \sim$ MeV) and further cooling has no direct impact on their structure. However, the neutrino mean-free path is sensitive to the temperature. Below some critical temperature (~MeV) the neutrinos that are trapped in the PNS escape and this has an effect on the structure. The dashed (solid) line represent the sequence of cold stars with trapped (untrapped) neutrinos, *i.e.*, $T = 0$ and $\mu_\nu = 200$ MeV ($\mu_\nu = 0$). When a hot isothermal $1.40\ \mathrm{M}_\odot$ PNS with baryon number $N = 1.43\ \mathrm{N}_\odot$ cools to low temperature by neutrino emission, the mass decreases to $1.35\ \mathrm{M}_\odot$. At low temperature the neutrinos escape from the star and the mass decreases to $1.32\ \mathrm{M}_\odot$. The relative mass defects are 3.5% due to cooling, and 2.1% due to neutrino untrapping.

neutrino untrapping are plotted vs. the initial mass of the PNS, for intermediate and strong coupling, respectively. Fig. 25 shows the net energy release when PNS cool from a given entropy per baryon of 1 or 2 to zero and the neutrinos are untrapped, $Y_{L_e} = 0.4 \to 0$.

IV. CONCLUSIONS

We have studied the effect of finite neutrino chemical potentials on the phase diagram and the finite-temperature EoS of three-flavor quark matter with self-consistently determined quark masses and pairing gaps. We confirm the results of Rüster *et al.* [24] that the phase transition to strange quark matter, such as the CFL phase is shifted to higher densities when neutrinos are trapped in the system, thus making it unlikely that strange matter exist in PNS cores. We find that in the presence of trapped neutrinos, the isospin mismatch induced by the β-equilibrium conditions is reduced and the 2SC phase becomes more favorable. In particular, the onset of the 2SC phase is shifted to lower densities in the presence of trapped neutrinos.

A new result of this study is the systematic analysis of the regions in the quark matter phase diagram that are realised in stable quark star cores. This analysis is carried out for two different strengths of the coupling in the diquark channel and for two different values of the neutrino chemical potential, *i.e.*, with and without neutrino trapping. A remarkable finding is that for the initial evolution of a PNS, when the neutrinos are trapped, all configurations with a CFL core are unstable. In absence of trapped neutrinos there are small, isolated regions in the temperature-density plane where stable configurations with a CFL core exists. A fraction of these 2SC-CFL stars have baryon number twins in the 2SC state. We suspect, however, that the configurations with a CFL core would be unstable when the influence of a hadronic crust is taken into account. See, *e.g.*, Ref. [25] for an analysis of such hybrid star configurations. All 2SC quark star solutions considered in this work are stable, while the phase border in-between the 2SC and CFL phases marks the endpoint of stability for PNS sequences in the plane of central temperature and central quark number chemical potential.

The maximum temperature of PNS are estimated to about 50 MeV for an entropy per baryon of 3, which is an upper limit for the entropy generated in the adiabatic compression of the core during collapse of a massive star. For this value of the entropy per baryon, the temperature in the CFL phase could reach about 65 MeV, but the corresponding PNS configurations are unstable.

When hot PNS cool by neutrino emission and reaches

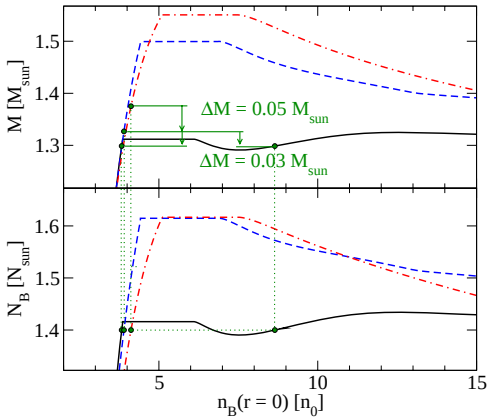

FIG. 22: (Color online) The mass defect due to cooling and neutrino untrapping at strong coupling, $\eta = 1.0$. Line styles as in Fig. 21. When a hot isothermal PNS with baryon number $N = 1.4$ $N_\odot$ cools to low temperature by neutrino emission, the mass decreases from 1.38 $M_\odot$ to 1.33 $M_\odot$. At low temperature the neutrinos escape from the star and the mass decreases to 1.30 $M_\odot$. The final state is either a homogenous 2SC star or a more tightly bound 2SC star with a CFL core. The mass difference between these two final states is 0.01%.

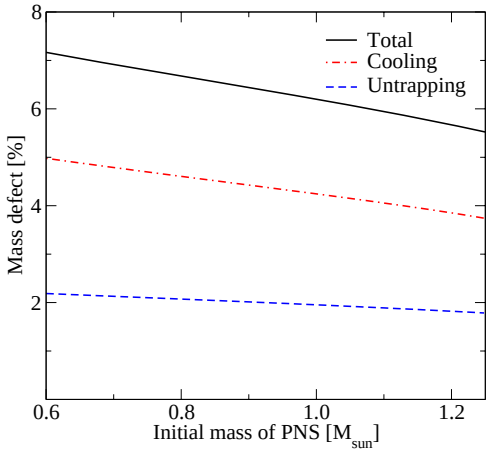

FIG. 23: (Color online) The mass defects due to cooling (T: 40 MeV $\rightarrow$ MeV) and neutrino untrapping (μ_ν: 200 MeV $\rightarrow$ 0) at intermediate coupling, $\eta = 0.75$.

the neutrino opacity temperature, $T_c \sim 1$ MeV, *i.e.*, the temperature where the neutrino mean free path becomes comparable to the size of the quark star core, the neutrinos created by electron capture in the collapse are untrapped. By calculating and comparing the compact star sequences for different neutrino untrapping scenarios we

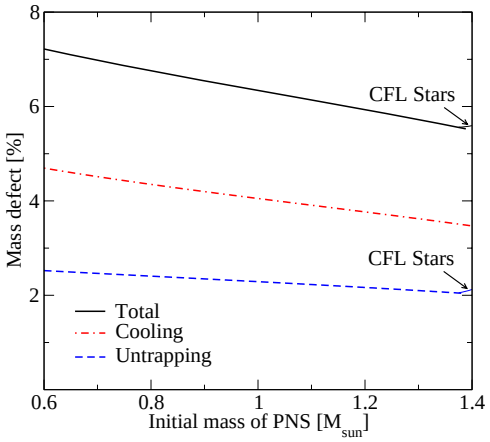

FIG. 24: (Color online) The mass defects due to cooling (T: 40 MeV $\rightarrow$ MeV) and neutrino untrapping (μ_ν: 200 MeV $\rightarrow$ 0) at strong coupling, $\eta = 1.0$.

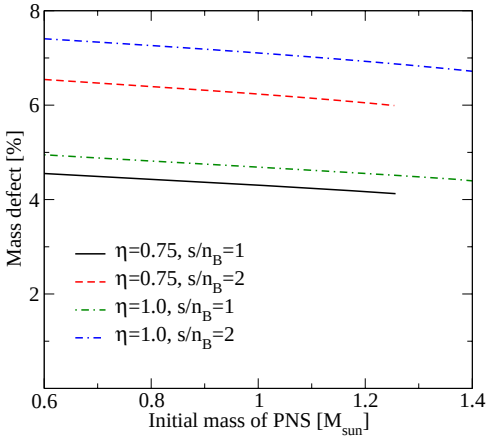

FIG. 25: (Color online) The total mass defects due to cooling ($s(T, \mu_\nu)/n_B(T, \mu_\nu)$: 1 or 2 $\rightarrow$ 0) and neutrino untrapping ($Y_{Le}(T, \mu_\nu)$: 0.4 $\rightarrow$ 0) at intermediate, $\eta = 0.75$, and strong coupling, $\eta = 1.0$.

find that the energy release due to neutrino untrapping (and/or cooling) is of the order of 100 bethe. This process could therefore be important for the inner engine of supernovæ and gamma-ray bursts.

The discussion of superconducting quark matter phases in the present work concerns the stability of PNS configurations with a CFL core and a neutrino heating mechanism for the outer core of newborn PNS due to the fact that the opacity temperature in (superconducting) quark matter exceeds that in nuclear matter. A

detailed study of the neutrino untrapping transition in hybrid stars is beyond scope of the present work and will be given elsewhere.

V. ACKNOWLEDGEMENTS

F.S. acknowledges support from the Swedish Graduate School of Space Technology and the Royal Swedish Academy of Sciences.

[1] H.-Th. Janka, K. Langanke, A. Marek, G. Martínez-Pinedo, B. Müller, arXiv:astro-ph/0612072.
[2] J. M. Lattimer and M. Prakash, arXiv:astro-ph/0612440.
[3] A. Burrows and J. M. Lattimer, Astrophys. J. **307**, 178 (1986).
[4] M. Prakash, I. Bombaci, M. Prakash, P. J. Ellis, J. M. Lattimer and R. Knorren, Phys. Rept. **280**, 1 (1997); [arXiv:nucl-th/9603042].
[5] K. Rajagopal and F. Wilczek, arXiv:hep-ph/0011333.
[6] M. G. Alford, Ann. Rev. Nucl. Part. Sci. **51**, 131 (2001); [arXiv:hep-ph/0102047].
[7] T. Schafer, arXiv:hep-ph/0304281.
[8] D. H. Rischke, Prog. Part. Nucl. Phys. **52**, 197 (2004); [arXiv:nucl-th/0305030].
[9] R. Casalbuoni and G. Nardulli, Rev. Mod. Phys. **76**, 263 (2004); [arXiv:hep-ph/0305069].
[10] M. Buballa, Phys. Rept. **407**, 205 (2005); [arXiv:hep-ph/0402234].
[11] M. Huang, Int. J. Mod. Phys. E **14**, 675 (2005); [arXiv:hep-ph/0409167].
[12] I. A. Shovkovy, Found. Phys. **35**, 1309 (2005); [arXiv:nucl-th/0410091].
[13] I. Bombaci and B. Datta, Astrophys. J. **530**, L69 (2000); [arXiv:astro-ph/0001478].
[14] Z. Berezhiani, I. Bombaci, A. Drago, F. Frontera, and A. Lavagno, Astrophys. J. **586**, 1250 (2003).
[15] D. N. Aguilera, D. Blaschke and H. Grigorian, Astron. & Astrophys. **416**, 991 (2004); [arXiv:astro-ph/0212237].
[16] A. Drago, A. Lavagno and G. Pagliara, Nucl. Phys. A **774**, 823 (2006); [arXiv:astro-ph/0510018].
[17] A. Drago, G. Pagliara and I. Parenti, arXiv:astro-ph/0608224.
[18] J. Berdermann, D. Blaschke, H. Grigorian and D. N. Voskresensky, Prog. Part. Nucl. Phys. **57**, 334 (2006); [arXiv:astro-ph/0512655].
[19] S. B. Rüster, V. Werth, M. Buballa, I. A. Shovkovy and D. H. Rischke, Phys. Rev. D **72**, 034004 (2005); [arXiv:hep-ph/0503184].
[20] D. Blaschke, S. Fredriksson, H. Grigorian, A. M. Öztas and F. Sandin, Phys. Rev. D **72**, 065020 (2005); [arXiv:hep-ph/0503194].
[21] H. Abuki and T. Kunihiro, Nucl. Phys. A **768**, 118 (2006); [arXiv:hep-ph/0509172].
[22] H. J. Warringa, D. Boer and J. O. Andersen, Phys. Rev. D **72**, 014015 (2005); [arXiv:hep-ph/0504177].
[23] A. W. Steiner, S. Reddy and M. Prakash, Phys. Rev. D **66**, 094007 (2002); [arXiv:hep-ph/0205201].
[24] S. B. Rüster, V. Werth, M. Buballa, I. A. Shovkovy and D. H. Rischke, Phys. Rev. D **73**, 034025 (2006); [arXiv:hep-ph/0509073].
[25] T. Klähn *et al.*, arXiv:nucl-th/0609067.
[26] F. Sandin and A. M. Öztas, Phys. Rev. C **73**, 035203 (2006); [arXiv:hep-ph/0512087].
[27] Note that a gapless CFL phase exist at low temperature for intermediate coupling and $\mu_e = 200$ MeV. This is irrelevant for the evolution of PNS for two reasons: (1) at very low T neutrinos are not trapped and (2) the corresponding quark star configurations are unstable. In addition, low-temperature gapless phases suffer from a chromomagnetic instability and are typically unphysical.

Selected
Posters and Awards

Comments

The poster "Compact stars in the standard model – and beyond" was presented at the International School of Subnuclear Physics in Erice, 2004. The title of the course was "How and Where to Go Beyond the Standard Model". The directors of the school were Professors Gerard 't Hooft and Antonino Zichichi.

The award for "An original work in theoretical physics" was designated to the preceding poster and the talk that I gave on the same topic, which were based on the results presented in Paper I. The jury included the directors of the School and other professors from the high-energy physics and astrophysics communities, notably Gabriele Veneziano and Sergio Ferrara. The essence of the talk is presented in Paper II.

Compact Stars in
THE STANDARD MODEL - AND BEYOND

by Fredrik Sandin

Division of Physics, Luleå University of Technology, 971 87 Luleå, Sweden
E-mail: fredrik.sandin@ltu.se

White Dwarfs

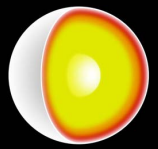

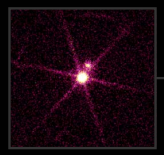

A Chandra X-ray image of the Sirius star system, located 8.6 light years from Earth. The bright source is Sirius B, a white dwarf star with a surface temperature of about 25 000 °C, which produces low-energy X-rays. The dim source is Sirius A, the brightest star in the northern sky.

In white dwarfs, the degeneracy pressure of electrons provides the force counterbalancing gravity. The maximum mass of white dwarfs is ~ 1.4 M_{Sun}, the so-called Chandrasekhar limit. The radius of these objects is ~ 6×10^3 km, and the maximum density is ~ 10^8 g/cm^3.

Neutron Stars, Quark Stars and Hybrid Stars

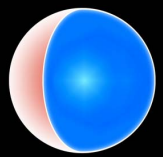

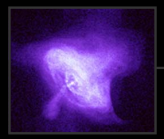

A Chandra X-ray image of the Crab Nebula, located in the constellation Taurus, about 6000 light years from Earth. This is the remnant of a giant explosion, a supernova, which was seen in 1054 AD. At the centre of the bright nebula is a rapidly spinning neutron star, a so-called pulsar.

At roughly seven orders of magnitude higher density than in the limiting-mass white dwarf, nuclei dissolve, and the degeneracy pressure of nucleons (in nuclear matter) and quarks (in quark matter) stabilize the next class of compact stars, the "neutron stars". The maximum mass of this sequence is model dependent and unknown, but not larger than a few solar masses. The characteristic radius is ~ 10 km, and the density is < 10^{16} g/cm^3.

Black Holes

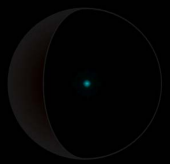

A Spitzer false-colour infrared image of NGC 7331, located at 50 million light-years from Earth, in the constellation Pegasus. NGC 7331 is a spiral galaxy that resembles our own Milky Way. Data indicates the presence of a black hole within the galaxy's central region.

When matter is compressed such that the Schwarzschild radius $R = 2GM/c^2$ is reached, the degeneracy pressure is overcome by gravity and the object collapses to a singularity, or at least to the Planck scale $\rho \sim 10^{93}$ g/cm^3. For stable compact stars the relation is somewhat more restrictive $2GM/Rc^2 < 3/4$.

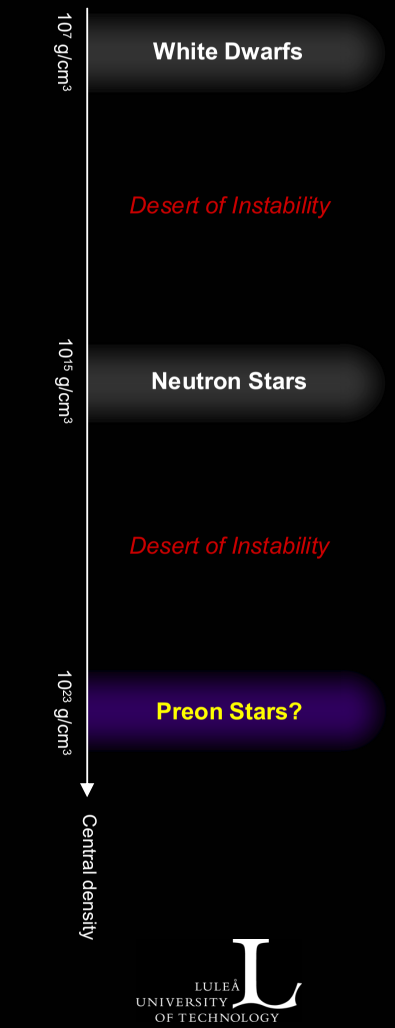

LULEÅ UNIVERSITY OF TECHNOLOGY

The Maximum Density Prophecy

The distinct classes of degenerate compact stars originate directly from the properties of gravity. In-between white dwarfs and neutron stars there is a large interval of central densities where no stable configurations exist.

Also, beyond the density of the limiting-mass neutron star, no stable configurations exist. That is, if quarks and leptons are fundamental entities in our world!

Compact Stars Beyond the Desert

Under the assumption that quarks and leptons are composite particles, built out of more elementary fermions, so-called *preons*, a new class of degenerate compact stars could exist. A simple estimate of the maximum mass of such objects gives ~ 10^2 M_{Earth} ~ 6×10^{26} kg, and a radius of ~ 1 m.

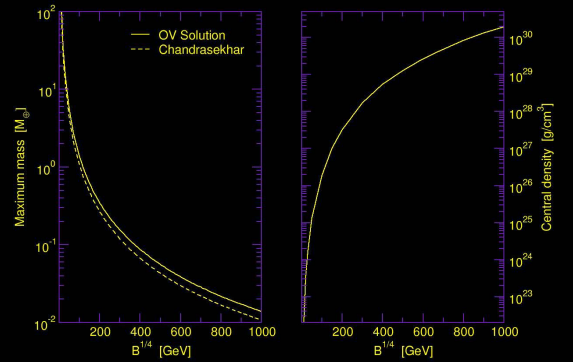

The maximum mass and central density of preon stars vs. the exogenous parameter of the model, the "bag pressure" B. The mass is given in units of the Earth mass ($M_\oplus$).

Formation and Detection

If fermionic preons exist, and configurations of preon matter as small and light as suggested here are stable, preon stars (or "nuggets") might have formed in the early universe.

If preon stars are abundant enough, *e.g.*, a large fraction of the cold dark matter in galaxies, these objects would cause gravitational lensing of gamma-ray bursts (so-called picolensing or femtolensing), which might be observable.

WORLD FEDERATION OF SCIENTISTS

«ETTORE MAJORANA» FOUNDATION AND CENTRE FOR SCIENTIFIC CULTURE

INTERNATIONAL SCHOOL OF SUBNUCLEAR PHYSICS

42nd Course:

How and Where to go beyond the Standard Model

Erice, 29 August - 7 September 2004

"New Talents" Award

for an

ORIGINAL WORK IN THEORETICAL PHYSICS

Jan Fredrik SANDIN

Gerardus 't Hooft and Antonino Zichichi

Directors

Erice, 6 - IX - 2004